



## SUPRAMOLECULAR, PHOTOPHYSICAL AND CATALYTIC PROPERTIES OF ZN(SALPHEN) BASED COMPLEXES AND MATERIALS

Giovanni Salassa

Dipòsit Legal: T. 1430-2013

**ADVERTIMENT.** L'accés als continguts d'aquesta tesi doctoral i la seva utilització ha de respectar els drets de la persona autora. Pot ser utilitzada per a consulta o estudi personal, així com en activitats o materials d'investigació i docència en els termes establerts a l'art. 32 del Text Refós de la Llei de Propietat Intel·lectual (RDL 1/1996). Per altres utilitzacions es requereix l'autorització prèvia i expressa de la persona autora. En qualsevol cas, en la utilització dels seus continguts caldrà indicar de forma clara el nom i cognoms de la persona autora i el títol de la tesi doctoral. No s'autoritza la seva reproducció o altres formes d'explotació efectuades amb finalitats de lucre ni la seva comunicació pública des d'un lloc aliè al servei TDX. Tampoc s'autoritza la presentació del seu contingut en una finestra o marc aliè a TDX (framing). Aquesta reserva de drets afecta tant als continguts de la tesi com als seus resums i índexs.

**ADVERTENCIA.** El acceso a los contenidos de esta tesis doctoral y su utilización debe respetar los derechos de la persona autora. Puede ser utilizada para consulta o estudio personal, así como en actividades o materiales de investigación y docencia en los términos establecidos en el art. 32 del Texto Refundido de la Ley de Propiedad Intelectual (RDL 1/1996). Para otros usos se requiere la autorización previa y expresa de la persona autora. En cualquier caso, en la utilización de sus contenidos se deberá indicar de forma clara el nombre y apellidos de la persona autora y el título de la tesis doctoral. No se autoriza su reproducción u otras formas de explotación efectuadas con fines lucrativos ni su comunicación pública desde un sitio ajeno al servicio TDR. Tampoco se autoriza la presentación de su contenido en una ventana o marco ajeno a TDR (framing). Esta reserva de derechos afecta tanto al contenido de la tesis como a sus resúmenes e índices.

**WARNING.** Access to the contents of this doctoral thesis and its use must respect the rights of the author. It can be used for reference or private study, as well as research and learning activities or materials in the terms established by the 32nd article of the Spanish Consolidated Copyright Act (RDL 1/1996). Express and previous authorization of the author is required for any other uses. In any case, when using its content, full name of the author and title of the thesis must be clearly indicated. Reproduction or other forms of for profit use or public communication from outside TDX service is not allowed. Presentation of its content in a window or frame external to TDX (framing) is not authorized either. These rights affect both the content of the thesis and its abstracts and indexes.

Giovanni Salassa

**Supramolecular, Photophysical and Catalytic  
Properties of Zn(salphen) Based Complexes and  
Materials**

Doctoral Thesis

Supervised by Prof. Arjan W. Kleij

Institut Català d'Investigació Química



UNIVERSITAT ROVIRA I VIRGILI

Tarragona

2013

UNIVERSITAT ROVIRA I VIRGILI

SUPRAMOLECULAR, PHOTOPHYSICAL AND CATALYTIC PROPERTIES OF ZN(SALPHEN) BASED COMPLEXES AND MATERIALS

Giovanni Salassa

Dipòsit Legal: T. 1430-2013



Av. Països Catalans 16  
43007 Tarragona  
Tel: +34 977 920 847  
Email: akleij@iciq.es



UNIVERSITAT  
ROVIRA I VIRGILI

DEPARTAMENT DE QUÍMICA FÍSICA  
I INORGÀNICA

Campus Sescelades  
Marcel·lí Domingo, s/n  
43007 Tarragona  
Tel. +34 977 55 81 37  
Fax +34 977 55 95 63  
[www.quimica.urv.es](http://www.quimica.urv.es)

I STATE that the present study, entitled “Supramolecular, Photophysical and Catalytic Properties of Zn(salphen) Based Complexes and Materials”, presented by Giovanni Salassa for the award of the degree of Doctor, has been carried out under my supervision at the Institut Català d’Investigació Química.

Tarragona, May 25<sup>th</sup>, 2013

Doctoral Thesis Supervisor

Prof. Arjan W. Kleij

UNIVERSITAT ROVIRA I VIRGILI

SUPRAMOLECULAR, PHOTOPHYSICAL AND CATALYTIC PROPERTIES OF ZN(SALPHEN) BASED COMPLEXES AND MATERIALS

Giovanni Salassa

Dipòsit Legal: T. 1430-2013

*Funding Agencies:*



UNIVERSITAT ROVIRA I VIRGILI

SUPRAMOLECULAR, PHOTOPHYSICAL AND CATALYTIC PROPERTIES OF ZN(SALPHEN) BASED COMPLEXES AND MATERIALS

Giovanni Salassa

Dipòsit Legal: T. 1430-2013

*“You can't do anything other than let it happen. You just let it evolve.*

*You don't do anything yourself.*

*All you do is make sure that nothing disturbs this wonderful creation in any way.*

*You are extremely active and at the same time extremely passive.*

*You don't do anything; you just let it evolve.”*

**Sergiu Celibidache**



UNIVERSITAT ROVIRA I VIRGILI

SUPRAMOLECULAR, PHOTOPHYSICAL AND CATALYTIC PROPERTIES OF ZN(SALPHEN) BASED COMPLEXES AND MATERIALS

Giovanni Salassa

Dipòsit Legal: T. 1430-2013

## Table of Contents

### Chapter 1: General Introduction

1.1	Metallosalphen complexes	1
1.2	Synthesis of salphen ligands and complexes	3
1.3	Catalysis with salphen based complexes	6
1.4	Photophysical materials	12
1.5	Functional supramolecules	16
1.6	Aim and outline	22
1.7	References and notes	24

### Chapter 2: Self-Assembly of a Macrocyclic Schiff Base Complex

2.1.	Introduction	29
2.2.	Synthesis of <i>tetra</i> -M(salphen) macrocycles	30
2.3.	Structural information of <i>tetra</i> -Zn(salphen) macrocycle ( <b>3</b> )	32
2.4.	Self-assembly behavior of <i>tetra</i> -Zn(salphen) macrocycle ( <b>3</b> )	32
2.4.1.	<sup>1</sup> H NMR studies	32
2.4.2.	UV-Vis studies	33
2.4.3.	Hyperchromic effects	38
2.4.4.	Mass spectrometry studies	41
2.4.5.	Dilution experiments	41
2.4.6.	TEM analysis	42
2.5.	Conclusions	43
2.6.	Experimental section	44
2.7.	References and notes	48

### Chapter 3: Extremely Strong Self-Assembly of a *bis*-Zn(Salphen) Complex Visualized at the Single-Molecule Level

3.1. Introduction	53
3.2. Synthesis of C <sub>12</sub> -functionalized <i>bis</i> -M(salphen) complexes	56
3.3. STM studies on <i>bis</i> -M(salphen)	57
3.4. Solution-phase behaviour of <i>bis</i> -Zn(salphen) ( <b>1</b> )	61
3.5. Spectroscopic studies on <i>bis</i> -Zn(salphen) ( <b>1</b> )	62
3.6. Modeling and DFT studies on <i>bis</i> -Zn(salphen) ( <b>1</b> )	67
3.7. Conclusions	69
3.8. Experimental section	69
3.9. References and notes	74

### Chapter 4: Photophysical Properties of Zn(Salphenazine) Complexes and their Application in Small Molecule Solar Cells

4.1. Introduction	79
4.2. Synthesis of Zn(salphenazine) complexes	81
4.3. Structural analysis of Zn(salphenazine)s	82
4.4. Photophysical properties of Zn(salphenazine)s	84
4.5. TD-DFT analysis of Zn(salphenazine)s	89
4.6. Thermal stability of Zn(salphenazine)s	92
4.7. Preparation of a smOSC device based on Zn(salphenazine) ( <b>1</b> )	92
4.8. Conclusions	95
4.9. Experimental section	96
4.10. References and notes	104

### Chapter 5: A DFT Study on the Mechanism for the Ring-Expansion Addition Reaction of CO<sub>2</sub> to Epoxides Catalyzed by Zn(salphen) Complexes

5.1. Introduction	109
5.2. The uncatalyzed ring-expansion addition	112
5.3. The Zn(salphen) catalyzed ring-expansion addition	113
5.4. The Zn(salphen)/NBu <sub>4</sub> I catalyzed ring-expansion addition	115

5.5. Ring-closing mechanism	120
5.6. The Zn(salphen)/NBu <sub>4</sub> Br catalyzed ring-expansion addition	121
5.7. Effect of epoxide substituent	121
5.8. Conclusions	127
5.9. Experimental section	128
5.10. References and notes	131
<b>Summary</b>	137
<b>Acknowledgements</b>	143
<b>Curriculum Vitae</b>	147
<b>List of Publications</b>	149

UNIVERSITAT ROVIRA I VIRGILI

SUPRAMOLECULAR, PHOTOPHYSICAL AND CATALYTIC PROPERTIES OF ZN(SALPHEN) BASED COMPLEXES AND MATERIALS

Giovanni Salassa

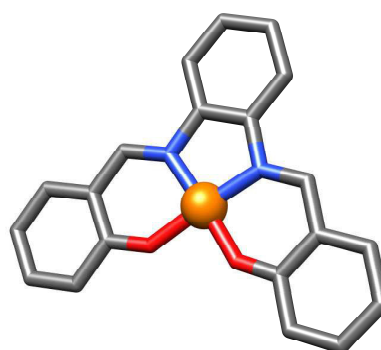
Dipòsit Legal: T. 1430-2013

# Chapter 1

## General Introduction

---

*Schiff bases have long been successfully employed as ligands in combination with various metals to give catalysts capable of realizing a variety of synthetic transformations. The most widely known "salen" ligand has been extensively researched. Recently, there has been increased interest in  $\pi$ -conjugated salens known as "salphen" ligands as a result of the differences in reactivity of their complexes in catalytic applications compared with the salen analogues. Salphen complexes may also display interesting photophysical and supramolecular properties different from salen systems as a result of their  $\pi$ -conjugation; a review of recent developments is given herein together with the focal points of this thesis.*



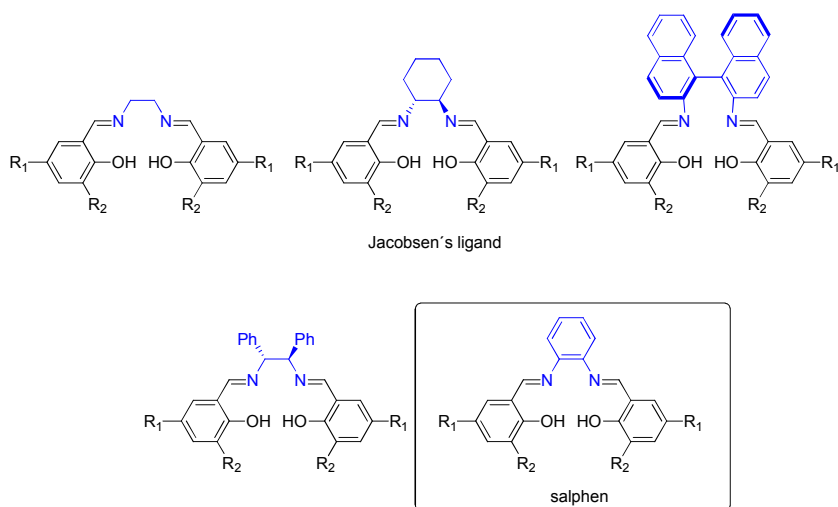
---

Parts of this chapter have been published in an adapted form: C. J. Whiteoak, G. Salassa, A. W. Kleij, *Chem. Soc. Rev.* **2012**, *41*, 622.

### 1.1 Metallosalphen complexes

Salen ligands are rather planar tetradentate,  $N_2O_2$ -coordinating ligand systems which are obtained from the condensation reaction of readily available diamine and (substituted) salicylaldehyde precursors.<sup>[1,2]</sup> The most widely utilized salen based catalyst system is undoubtedly the manganese(III) complex of the salen ligand bearing a chiral cyclohexyl bridging fragment known as Jacobsen's epoxidation catalyst, but other chiral salen systems based on diamino-substituted scaffolds have also been proven to be attractive for a range of catalytic applications (Figure 1). Salen ligated metal complexes

combine typical advantages such as ease of variation in steric and electronic features,<sup>[3]</sup> and the use of modular strategies that enable manipulation of different fragments of the ligand systems.<sup>[4]</sup> Metal-derived salen complexes are versatile and they have proven to be effective catalysts for many asymmetric conversions including (ep)oxidations,<sup>[1,5]</sup> epoxide ring-opening reactions<sup>[6]</sup> and stereo-selective polymerizations.<sup>[7]</sup> Analogous multinuclear metallosalens have also received a great deal of attention since in a number of cases interesting cooperative effects have been observed that can increase overall kinetics of a process and its selectivity.<sup>[8]</sup> Non-chiral salen complexes have received much less attention since their application potential in (homogeneous) catalysis has been considered limited. For instance, phenyl-bridged salen ligands (i.e., “salphens” or “salophens”, Figure 1) and related structures have been neglected for a long time despite the fact that they provide particular advantages over their salen analogues; they represent  $\pi$ -conjugated ligand systems with tunable photophysical properties, and are more cost-effective than the corresponding (chiral) salen ligands. For these reasons, such salphen systems have excellent potential as building blocks in material science amongst other applications.<sup>[9]</sup> It should also be noted that the rigid geometry around the metal center that is dictated by the salphen ligand can be used to manipulate properties such as the Lewis acid character of the metal and therefore can be effectively applied to increase the reactivity of the resulting complex.



**Figure 1.** Structures of the most commonly used salen systems and the family of salphen ligands. In blue are highlighted the different bridging groups.

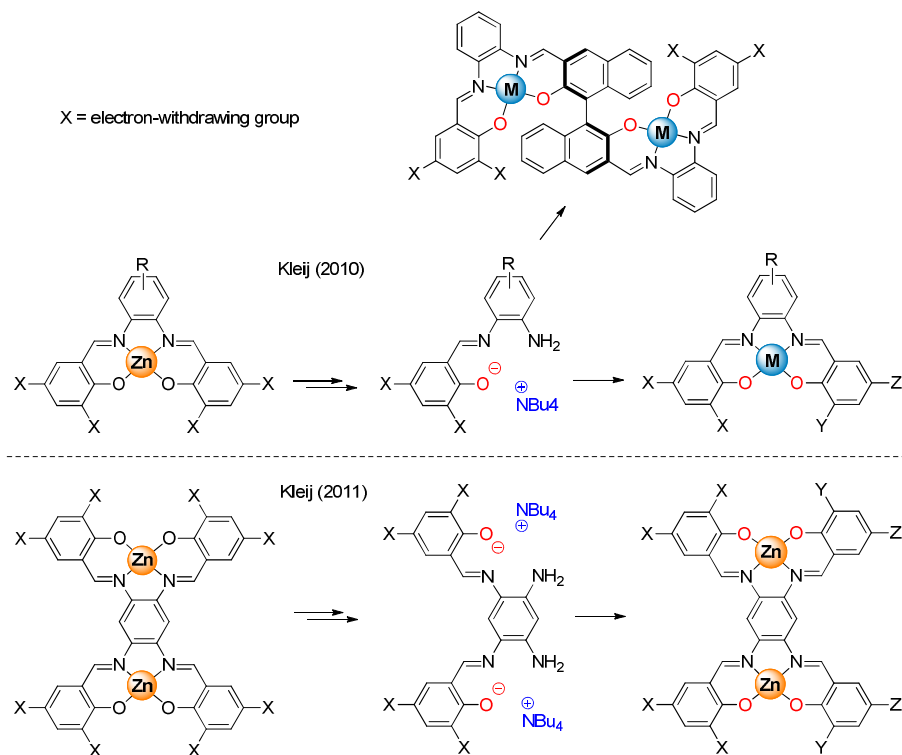
## 1.2 Synthesis of salphen ligands and complexes

The most common way to synthesize salphen ligands is the simple combination of two equivalents of a (substituted) salicylaldehyde with one equivalent of 1,2-phenylenediamine. The scope for producing salphen ligands with various substitutions is wide given that many differently substituted salicylaldehydes and 1,2-phenylenediamines are readily available. The ability to significantly alter the nature of the phenyl group of the ligand backbone gives further potential to vary the intrinsic properties of the salphen scaffold. Metal complexes of salphen ligands are commonly prepared by the simple reaction of the ligand with a metal acetate salt, although variations are known with other anions. The standard combination of two equivalents of salicylaldehyde with 1,2-phenylenediamine gives rise to symmetrical salphen structures. Non-symmetrical ligands would offer further amplified opportunities for tuning of steric and electronic properties and therefore with regard to ligand synthesis, the most recent developments have been in the area of non-symmetrical ligand synthesis.<sup>[10]</sup> Although mono-imine precursors bearing electron donating groups for non-symmetrical salphen ligands can easily be synthesized,<sup>[11]</sup> those containing electron withdrawing groups are synthetically highly challenging.<sup>[12]</sup> Kleij and co-workers have recently developed a simple, metal-templated procedure for the synthesis of non-symmetrical salphen scaffolds (Scheme 1) with various substitution patterns. In this procedure the initial chelated metal (a Zn(II) ion) plays an important role; due to its high Lewis acidity it provokes, in the presence of OH<sup>-</sup> nucleophiles, a selective hydrolysis leading to synthetically useful mono-imine phenolate salts that are easily converted into non-symmetrical (chiral) mono- and *bis*-metallo-salphen products.<sup>[13]</sup> This approach was recently also extended to *bis*-salphen derivatives,<sup>[14]</sup> and the formal desymmetrization of the coordination environment of the salphen units in *bis*-salphen scaffolds could also be readily accomplished.

It is also possible to synthesize more complicated ligand systems bearing the salphen moiety. *Bis*-salphen ligands can for instance be synthesized through the condensation of commercially available 3,3'-diaminobenzidine with four equivalents of a (substituted) salicylaldehyde. By analogy to the mono-salphen ligands, these *bis*-salphen ligands can be easily desymmetrized in each N<sub>2</sub>O<sub>2</sub> unit through prior formation of *bis*-imine/amine



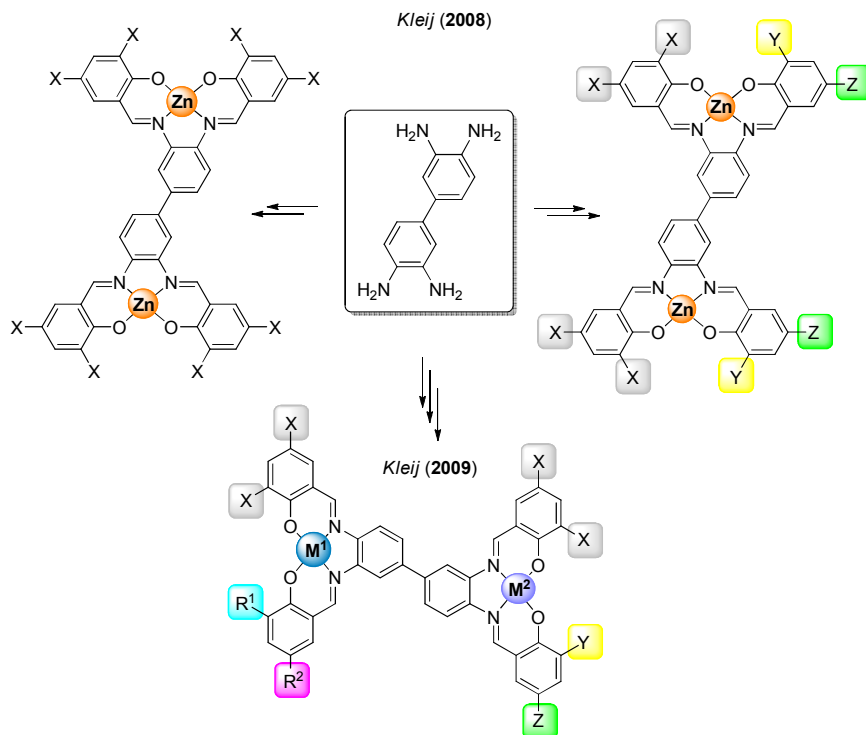
intermediates. Subsequent condensation with a different salicylaldehyde and metalation then yields bimetallic salphen complexes with non-symmetrical salphen pockets (Scheme 2).



**Scheme 1.** Synthesis of non-symmetrical mono- and *bis*-salphen ligands.

Further to this work, Kleij and co-workers have also recently reported a method to synthesize several hetero-bimetallic salphen structures which are of great interest due to the incorporation of two different metal centers within the same molecule.<sup>[4]</sup> In this work the bimetallic salphen structure is synthesized by a stepwise condensation/metalation sequence of 3,3'-diaminobenzidine using metal templation to afford selectively the hetero-bimetallic salphen complex (Scheme 2). It is also possible to synthesize larger macrocyclic ligand systems containing salphen units, of which the most prominent examples are shown in Figure 2. Nabeshima and co-workers reacted 2,3-dihydroxybenzene-1,4-dicarbaldehyde with 1,2-phenylenediamine to give the desired *tri*-salphen macrocycle (denoted as a [3+3] condensation product, Figure 2) in

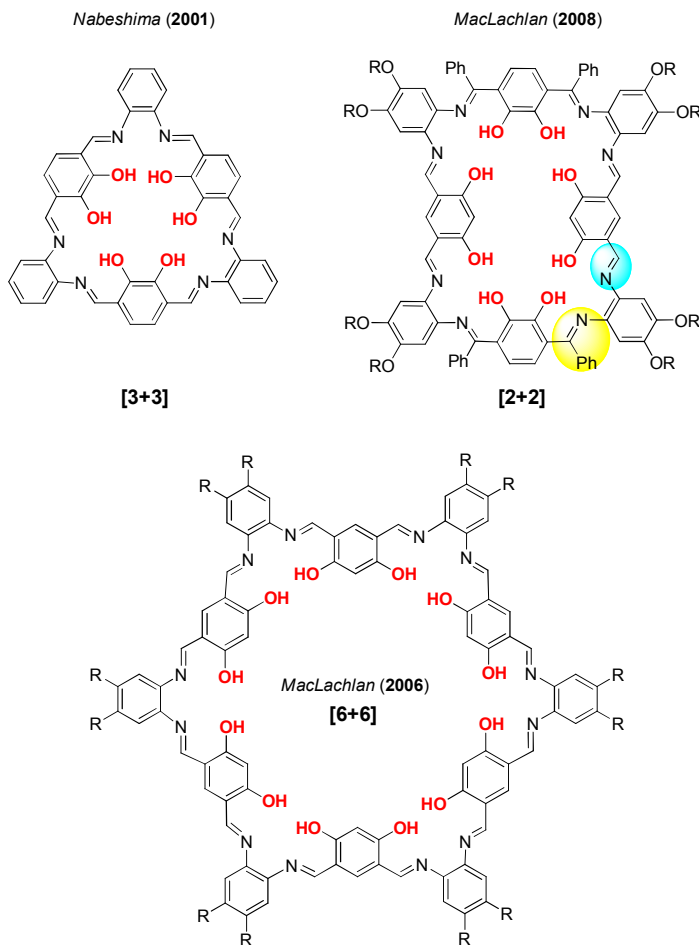
good yield after prolonged stirring.<sup>[15,16]</sup> More recently, MacLachlan and co-workers reported on the formation of various types of *tri*-,<sup>[17]</sup> *tetra*-<sup>[18]</sup> and *hexa*-salphen macrocyclic architectures (Figure 2).<sup>[19]</sup>



**Scheme 2.** Synthesis of non-symmetrical (hetero)bimetallic salphen complexes derived from the 3,3'-diaminobenzidine scaffold.

Interestingly, in the case of the tetra-salphen macrocyclic systems, a stepwise approach was applied and the significant difference in stability between aldimines and ketimines (highlighted in Figure 2) was exploited to construct isomeric macrocyclic structures. This approach is indeed powerful as it allows for access and fine-tuning of these macrocycles, and depending on the directional properties of the building blocks, macrocyclic structures of different dimensions may be simply accessed. More recently, a *tetra*-salphen macrocycle communicated by Kleij and co-workers (see Chapter 2),<sup>[20]</sup> was constructed in a single step thereby providing a system with the salphen coordination pockets orientated “outwards” as opposed to the “inward” nature of the salphen units of the macrocyclic structures presented in Figure 2. The examples of

multi/macrocyclic salphen structures reported in Schemes 1 and 2 and Figure 2 clearly show that the field of multi-salphen scaffold synthesis has tremendously matured over the last few years.



**Figure 2.** Macroscopic systems comprising multi-salphen ligand scaffolds. Note the highlighted section in the [2+2] tetra-salphen macrocycle corresponding to ketimine/aldimine units.

### 1.3 Catalysis with salphen based complexes

Whilst chiral salen ligands (with the chiral information in the bridging fragment) have a proven track record as ligands for complexes in catalysis applications, salphen ligands have only been scarcely used to date. There exist, however, cases where chiral salen ligands are not easily accessible or have proven to be ineffective as mediators for

specific conversions. Here focus is given to those reported cases where the actual M(salphen) unit is involved in the catalytic event rather than being a spectator. Indeed, many groups have reported significant differences between activities of salen catalysts and their salphen analogues in various catalytic reactions. In this section we will give a few examples of contributions involving metal salphen complexes as catalysts for a diverse range of chemical conversions.

Manganese Schiff base complexes have long been investigated as homogeneous catalysts for a variety of (ep)oxidation reactions inspired by the successful and seminal work of Jacobsen and co-workers in the early 1990's.<sup>[21]</sup> Recent developments with Mn(III) Schiff base systems used as oxidation catalysts or antioxidants<sup>[22]</sup> have included the application of Mn(salphen) complexes, and many of these studies have focused on complexes which have been tethered to various supports demonstrating catalysis of reactions which are seemingly not possible in an absolute homogeneous state. Quite often, the immobilization leads to an increased catalyst stability and therefore longevity of the active species, and also enables catalyst recycling.

Mirkhani and co-workers have studied Mn(salen) and Mn(salphen) mediated oxidation of diphenyl sulfide using sodium periodate as the terminal oxidant. The Mn(salphen) complex yields a mixture of sulfoxide and sulfone (4:1 ratio) in 100% conversion under mild conditions.<sup>[23]</sup> This is in strong contrast to the analogous Mn(salen) complex which only led to yields of 18% (ratio sulfoxide/sulfone = 2:1). This Mn(salphen) catalytic system was also successfully applied towards a variety of other sulfides and also furnished 100% yields. Another application of Mn(salphen) complexes in oxidation catalysis has been reported by Nasr-Esfahani and co-workers.<sup>[24]</sup> In this work it has been reported that Mn(salphen)s yield improved catalysts for oxidation of Hantzsch 1,4-dihydropyridines with tetrabutylammonium peroxomonosulfate as the terminal oxidant, compared with the salen analogue (95% *versus* 24% yield). There have been reports of several supported Mn(salphen) complexes employed for catalysis applications. Chitosan-supported Mn(salphen) complexes have been prepared and characterised by Xia and co-workers.<sup>[25]</sup> The complexes were studied as catalysts for oxidation of cyclohexene using oxygen as the terminal oxidant under solvent free conditions. The work shows that the complexes coordinate to the amino groups of the

chitosan support and under mild conditions (343 K, ambient oxygen pressure) are capable of catalyzing the reaction ( $11.0 \times 10^4$  turnover numbers) which is more efficient compared with an equivalent unsupported catalyst which yielded much lower activity ( $0.25 \times 10^4$  turnover numbers). Further work on supported hydroxyl-functionalized Mn(salphen) catalysts by Savavati-Niasari and co-workers using multi-wall carbon nanotubes (MWNTs) as supports has shown their ability to oxidize *para*-xylene.<sup>[26]</sup> The supported catalysts were demonstrated to be recyclable unlike the unsupported catalyst under neat conditions: the latter was only active in the first cycle, and due to decomposition during the catalysis it became inactive in further cycles. Rhenium cluster supported Mn(salphen) complexes have also been reported and were shown to be active in catalysis of epoxidations of a wide range of olefins and the nature of the active species was also probed.<sup>[27]</sup> It has been demonstrated in this work that the nature of the active species is controlled by many factors, including an interesting substrate concentration effect.

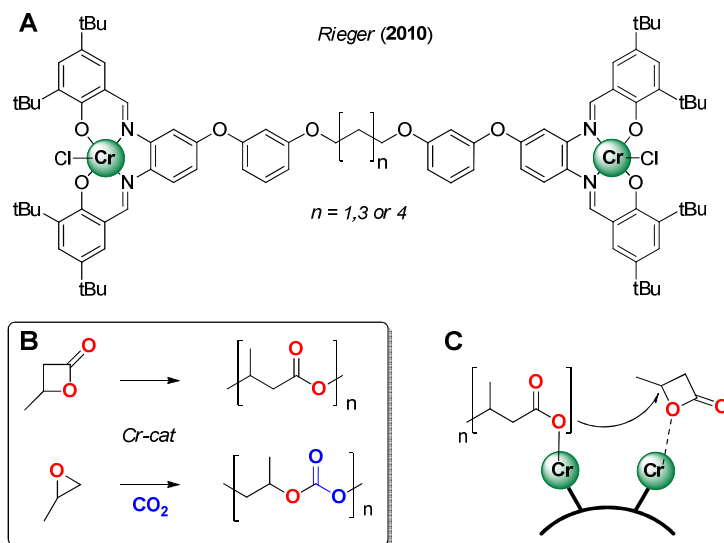
Highly selective catalysts for oxidation of benzyl alcohol to benzaldehyde based on Cr(salphen) complexes using hydrogen peroxide as oxidant have been reported by Wu and co-workers.<sup>[28]</sup> The catalytic activity of the sodium salts of Cr(salphen) complexes have been compared with the same complexes intercalated on a Mg–Al layered-double hydroxide (LDH). The homogeneous catalytic system yielded a mixture of benzaldehyde (77.5%), benzoic acid (15.6%) and benzyl benzoate (6.9%), compared with the sole conversion to benzaldehyde achieved by the LDH supported catalyst. The LDH-bound system also gave better overall yields (66%) compared to the homogeneous system (29%). When compared to the corresponding salen catalyst, the salphen catalyst was also found to give a much better catalytic performance.

Di-iron(III)  $\mu$ -oxo bridged salphen complexes have been shown to be capable of selective oxidation of a variety of alkanes using *m*-CPBA as the terminal oxidant.<sup>[29]</sup> However, these conversions are only possible if the salphen ligand contains bulky groups on the phenolate moiety. If the phenolate moiety is unsubstituted the complex was found to be catalytically inactive. Conte and co-workers have demonstrated that V(salphen) catalysts are capable of catalyzing the epoxidation of alkenes and also the

sulfoxidation of thioethers using hydrogen peroxide as the oxidant in combination with microwave activation in ionic liquids.<sup>[30]</sup>

Investigations using metallosalphen complexes as catalysts for various polymerization reactions have also been reported by several groups. Darensbourg and co-workers have shown that Al- and Sn(salphen) complexes are able to catalyze the ring-opening polymerization of trimethylene carbonate and that the Al(salphen) based catalyst gives higher turnover frequencies (TOF = 72) compared with the corresponding salen analogue (TOF = 60).<sup>[30]</sup> Work by Sugimoto and co-workers has shown that Al(salphen) complexes are able to co-polymerize carbon dioxide and epoxides in the presence of an ammonium salt.<sup>[32]</sup> It was found that, upon comparison with the Al(salen) complexes, the polymer produced using Al(salphen) catalysts gave higher  $M_n$  values (2,900 *versus* 1,400 respectively) and that the cyclic carbonate (i.e., monomer formation) was enhanced in the cases where the catalyst was an Al(salphen) complex.

The Rieger group recently reported an interesting *bis*-Cr(salphen) complex tethered by a diarylether linker (Figure 3).<sup>[33]</sup>



**Figure 3.** A *bis*-Cr(salphen) complex linked by a diarylether spacer (A) active in polymerization catalysis (B). (C) The proposed bimetallic mode of activation.

These flexible bimetallic systems were successfully employed as catalysts for  $\beta$ -butyrolactone polymerization<sup>[34]</sup> and  $\text{CO}_2$ /propylene oxide (PO) copolymerization,<sup>[35]</sup>

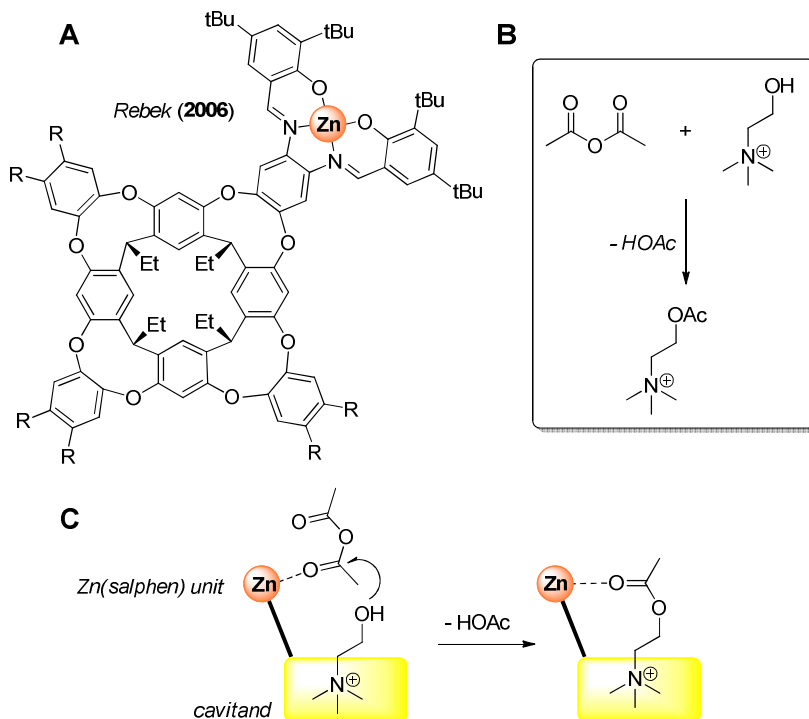
showing that upon comparison with mononuclear Cr(salphen)s, the bimetallic catalysts give rise to much higher activities (per Cr(III) ion) and average molecular weights ( $M_w$ ) in the lactone polymerization reaction. In the CO<sub>2</sub>/PO polymerization reaction, higher rates were particularly observed when the concentration of the catalyst was lowered. The improved catalytic behaviour in both polymerization reactions was associated with a bimetallic reaction pathway, and consequently a cooperative effect was proposed for the *bis*-Cr(salphen) complexes.<sup>[7]</sup> The same group has also published work showing that achiral Cr(salphen) complexes are highly active catalysts for the ring-opening polymerization of  $\beta$ -butyrolactone.

Co(salphen) complexes have been used to catalyze the carbonylation of aniline to N,N'-diphenyl urea.<sup>[36]</sup> The publication shows that the Co(salphen) complex is more active than its salen analogue and the authors suggest that the most likely reason for this enhanced activity is that the salphen ligand is conjugated and therefore reduces the decomposition of the complexes to the Co(III) oxide, which is a known catalyst deactivation route.

Atwood and co-workers have used Al(salphen) bromides to dealkylate organophosphates.<sup>[37]</sup> The results from this work also show that depending upon the substrate, the Al(salphen) shows markedly different behaviour compared with its salen analogue. When catalyzing the dealkylation of trimethyl phosphate the Al(salen) system shows the best activity, but when tributyl phosphate was trialled the Al(salphen) complex was found to be the most active catalyst. When using triethyl phosphate, no discrimination between the two types of catalyst was observed. These differences may be a result of the different steric environments formed around the metal centre by the two different types of ligand.

The synthesis of a sophisticated salphen-based catalyst was reported by the group of Rebek (Figure 4). This contribution constitutes a biomimetic approach towards the acetylation of choline using a resorcinarene-supported Zn(salphen) complex.<sup>[38]</sup> In this salphen structure, the bridging phenyl group is an integrated part of the resorcinarene support. The Lewis acidity of the Zn(II) ion is exploited for binding of acetic anhydride whereas choline forms a host-guest complex. The two reagents are thus brought in close proximity to afford a more efficient process and this was indeed observed upon

comparing the reaction rates of the unsupported Zn(salphen), the cavitant only and the Zn(salphen)/cavitant ensemble.

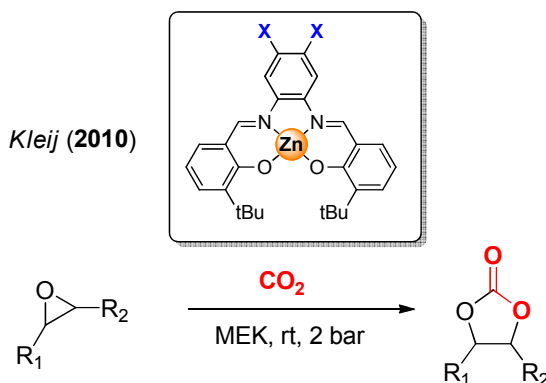


**Figure 4.** A biomimetic cavitant structure comprising a Zn(salphen) catalyst unit (A) active in the acetylation of choline (B). (C) The proposed cooperative catalysis mode.

Kleij and co-workers recently reported on the use of Zn(salphen) complexes as Lewis acid activators in the synthesis of cyclic carbonates from terminal epoxides and carbon dioxide under particular mild conditions (Figure 5, see Chapter 5 for an exhaustive study on the reaction mechanism).<sup>[39]</sup> Interestingly, other Zn(salen) complexes containing ligands having chiral bridging fragments were found to be poor catalysts for this conversion, and the results are explained by the much higher Lewis acidity of the Zn(II) ion in the salphen complexes compared with the corresponding salen systems.<sup>[40]</sup> The Lewis acid behaviour of the Zn(II) ion is a result of the geometry enforced on the complex by the planar ligand system and is a prerequisite for efficient cycloaddition of CO<sub>2</sub> to these epoxides. In the absence of Zn(salphen) catalyst, no conversion was observed. Although initially reasonably mild conditions were employed for the cycloaddition of CO<sub>2</sub> to epoxides (45°C, *p*CO<sub>2</sub> = 10 bar, DCM), at a later stage a



significant improvement of the reaction conditions within the context of sustainability was reported, and it was also shown that various cyclic carbonate structures can be accessed under virtually ambient and green conditions (25°C,  $p\text{CO}_2 = 2$  bar, methylethyl ketone (MEK) as solvent).<sup>[41]</sup> Thus, these Zn(salphen) complexes may now be regarded as (industrially) attractive catalyst systems that are able to convert  $\text{CO}_2$  under very mild conditions; in principle this should open new possibilities for incorporation of  $\text{CO}_2$  into other organic structures among which are oxetanes,<sup>[42]</sup> azidirenes<sup>[43]</sup> and molecules with acidic C–H fragments.<sup>[44]</sup>

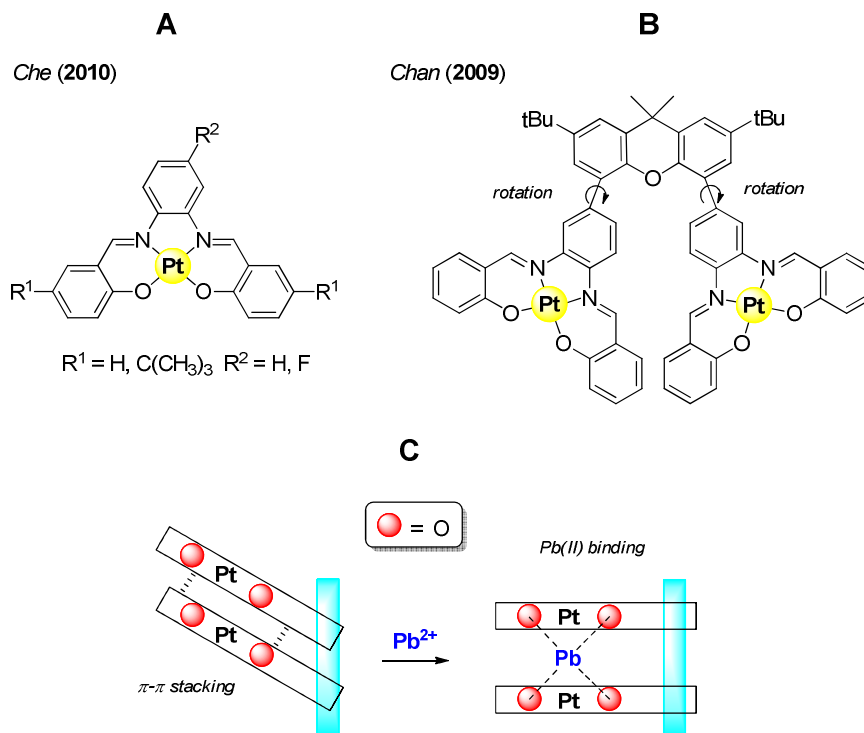


**Figure 5.** Zn(salphen) catalysts for organic carbonate formation under mild reaction conditions.

## 1.4 Photophysical materials

The exploitation of the photophysical properties of Schiff base complexes in the field of functional materials is still a relatively unexplored area of research. One of the first examples in this field was reported by Liu and co-workers, who synthesized a novel blue light-emitting diode (LED) utilizing the electroluminescent properties of a Zn(salen) complex.<sup>[45]</sup> Following this, conjugated polymers containing Zn(II) and Ni(II) Schiff base complexes have also been reported to have organic LED applications.<sup>[46,47]</sup> Further to the salen examples, Che and co-workers have reported the application of Pt(salen) and Pt(salphen) complexes in high-performance organic LED's (Figure 6A).<sup>[48]</sup> In this study, they prepared compounds which exhibit an intense emission in the range of 541–649 nm in acetonitrile, with emission quantum yields of up to 0.27. The authors showed that complexes bearing the salphen scaffold, when employed as a

dopant material for yellow–red organic LED's, have a good device efficiency of  $31 \text{ cd}\cdot\text{A}^{-1}$  and a device lifetime of  $77,000 \text{ h}$  at  $500 \text{ cd}\cdot\text{m}^{-2}$ . This is considerably higher than observed for the corresponding salen analogue.

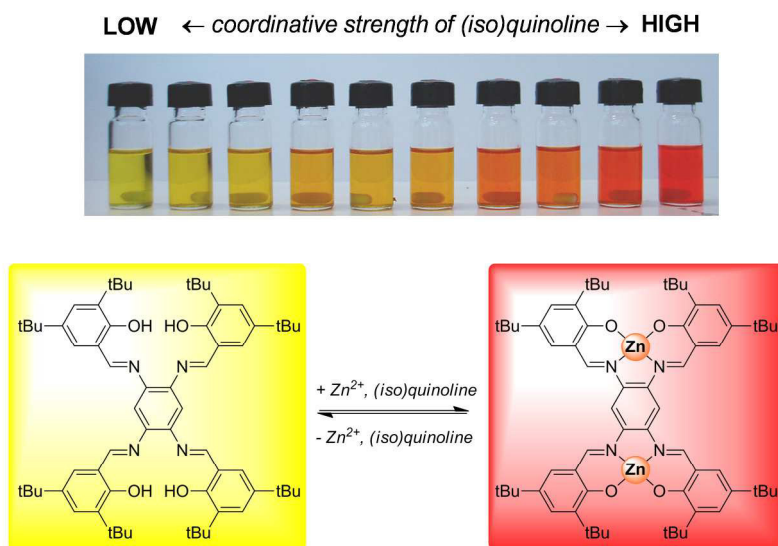


**Figure 6.** (A) Pt(salphen) complexes for use in high-performance organic LED's. (B) Bis-Pt(salphen) complexes as sensors for lead(II) cations. (C) Mode of action upon binding of Pb(II) cations in the interior of the structure presented at (B).

The presence of an aryl bridging group in the salen ligand opens up new possibilities for the design and application of these  $\pi$ -conjugated systems as photo-responsive materials. In this respect, multinuclear salen derivatives designed for sensing of various substrates have been reported recently. For example, Chan and co-workers have described an axially rotating *bis*-Pt(salphen) complex which displays colorimetric and luminescent responses to metal ions (Figure 6B and C).<sup>[49]</sup> In particular, the ability of this *bis*-Pt(salphen) complex to detect Pb(II) by phosphorescence techniques is fascinating since relatively few systems are able to effectively sense this cation. The coordination of the Pb(II) ion causes a rotation along the molecular axis and consequently disrupts the offset  $\pi$ -stacked contacts within the *bis*-Pt(salphen) moiety.

The associated  $\pi$ -stacked emission is therefore transformed by Pb(II) into a blue-shifted ‘monomer-like’ emission from non-interacting Pt(salphen) units. The same authors also reported on phosphorescent conjugated polymers consisting of alternating para-phenyleneethynylene, and ‘para-’ or ‘meta-type’ Pt(salphen) luminophoric units which are potentially useful in metal ion sensing.<sup>[50]</sup>

Other multinuclear salphen systems incorporating Zn(II) have been shown to give a colorimetric response in the presence of N-donor systems based on substituted (iso)quinolines (Figure 7).<sup>[51]</sup> The detection is based on the equilibrium between the complexed and demetalated ligand system under partially aqueous conditions.

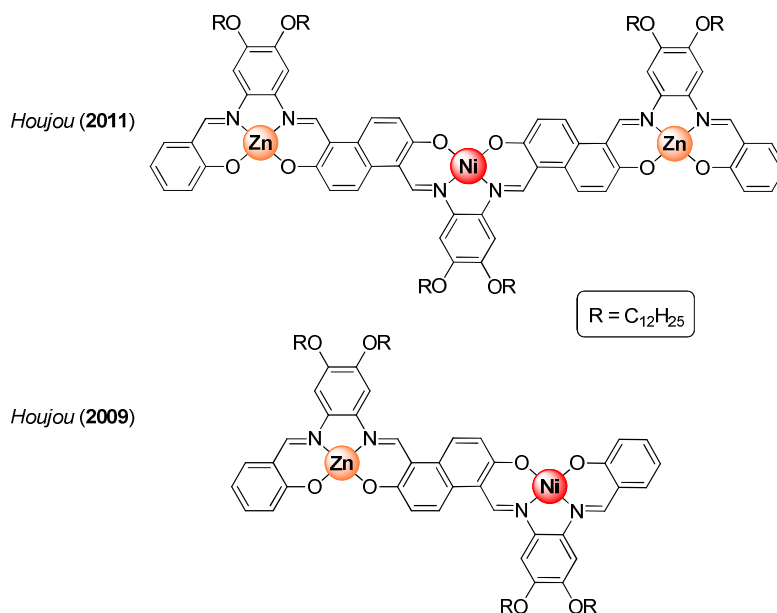


**Figure 7.** A bis-salphen chromophore for discrimination between (iso)quinolines.

This equilibrium is affected by the presence of N-heterocycles in the medium; these donor ligands are able to stabilize the metalated species shifting the equilibrium to the bis-Zn(II) complex. The extent to which the donor ligand can stabilize the Zn(II) ion is expressed in the observed color change which is less pronounced if the N-ligand contains sterically demanding groups in close proximity to the N-atom. If no suitable ligand is present, the equilibrium fully shifts to the side of the demetalated species. This responsive system could be useful for discriminating between rather similarly sized molecules which only differ in steric diversity near the binding site. A similar protocol

has been reported for a series of anions, where protic systems were able to demetallate the *bis*-Zn(salphen) chromophore whereas other anions formed simply coordination complexes.<sup>[52]</sup>

Studies involving highly  $\pi$ -conjugated salphen systems have also been reported by Houjou and co-workers. This work presents a study of interesting homo- and hetero-multinuclear (Zn/Ni) complexes with fully  $\pi$ -conjugated salphen ligands using 2,6-dihydroxynaphthalene-1,5-dicarbaldehyde and 1,2-phenylenediamine as building blocks (Figure 8).<sup>[53,54]</sup> These compounds offer the possibility to understand the effects of an extended  $\pi$ -conjugated system on the absorption properties of salphen complexes. Comparison of the spectroscopic features of these trinuclear complexes with those of analogous dinuclear complexes revealed that the absorption spectra of the trinuclear complexes are composed of a salphen centered absorption band at 400 nm and a naphthalene-centered absorption band around 500-600 nm.



**Figure 8.** Hetero-multinuclear Ni/Zn complexes used to investigate the properties of fully  $\pi$ -conjugated *bis*- and *tris*-salphen systems.

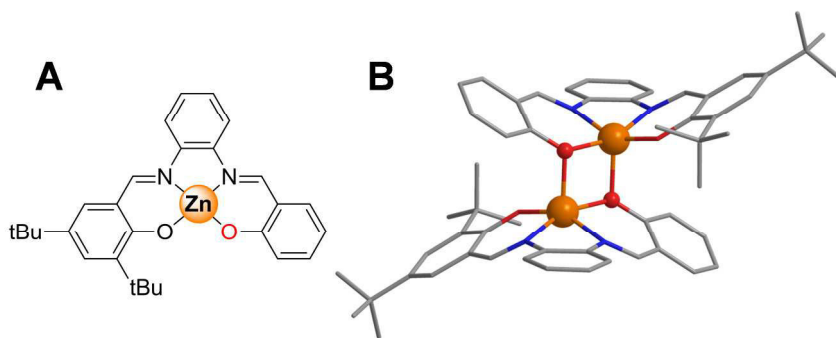
This observation suggests that the electron density of the  $\pi$ -conjugated system is actually more localized, forming several compartments, each of which independently undergoes electronic excitation. Further analysis of the calculated molecular orbitals

reveals that the  $N_2O_2$  metal coordination site effectively breaks the electronic communication by disrupting the  $\pi$ -conjugation, even though the site is bridged by an 1,2-phenylene linkage. These results may demand reconsideration of the molecular design of  $\pi$ -conjugated metallo-polysalen/-salphens; the presence of metal ions may be a useful tool for tuning the degree of  $\pi$ -conjugation as the presence of Zn or Ni ions have been shown to significantly affect the electronic transitions.

Beside the examples mentioned above, U(salphen) complexes have been shown to have unusual photophysical properties, although at this stage further studies are probably required to understand their full potential.<sup>[55]</sup>

### 1.5 Functional supramolecules

Whereas most metal salphen complexes form simple monomeric complexes, it is interesting to note one example where this is not the case. Kleij and co-workers have extensively studied the complexation of Zn(II) ions by salphen ligands. The salphen ligand is a rigid ligand system that imposes an unusual square planar geometry around the Zn(II) ion leaving a vacant, axial coordination site; isolation of such a unique, four-coordinate square planar complex was recently achieved<sup>[56]</sup> and is only possible if there is sufficient steric bulk present near the donor atom of the phenoxide group. If this steric bulk is insufficient then a dimeric species is observed (Figure 9).

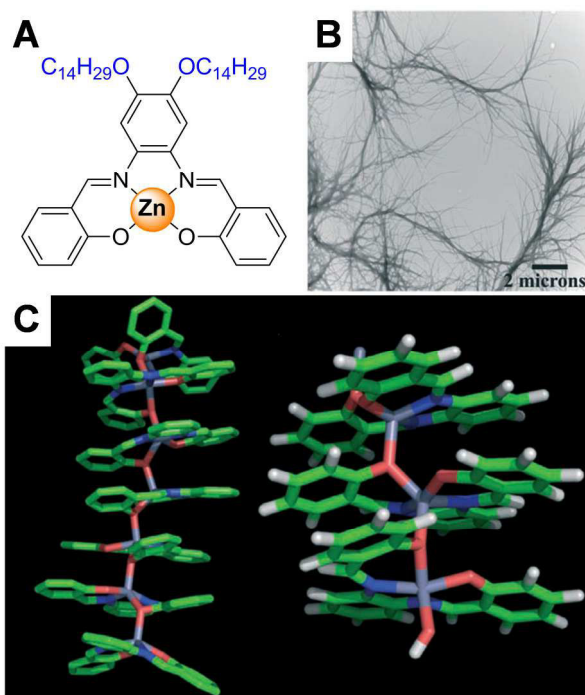


**Figure 9.** Line drawings of a Zn(salphen) complexes (A) and its X-ray crystal structure (B) showing its dimeric nature.

The vacant axial coordination site can thus be potentially used to form interactions with suitable donor ligands or to provide self-assembled structures.<sup>[57]</sup> In particular self-

assembled molecules that provide 1D nanostructures can be an important tool for developing nanoscale technologies and nanomaterials.

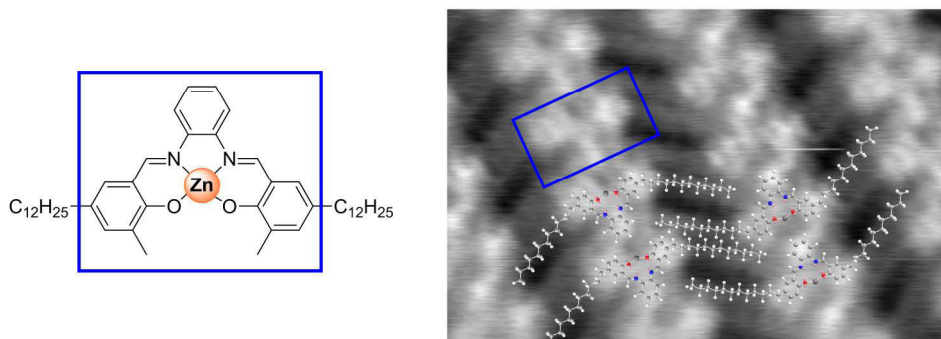
MacLachlan and co-workers reported the first examples of nanofiber formation promoted by  $\text{Zn}\cdots\text{O}$  interactions (i.e.,  $\text{Zn}(\text{salphen})$  dimer formation) between individual salphen complexes.<sup>[58]</sup> They presented a new family of salphen complexes with peripheral linear and branched alkoxy groups (Figure 10A). These complexes are able to form gels and 1D nanofibrils in methanol and in aromatic solvents, such as benzene, toluene and *ortho*-xylene. The transmission electron microscopy (TEM) images illustrated that the obtained fibers are only tens of nanometers in diameter but extend several microns in length (Figure 10B). The authors initially thought that this fiber morphology was due to the hydrophobic alkoxy substituents on the salphen complexes leading the complexes to aggregate in methanol.



**Figure 10.** (A)  $\text{Zn}(\text{salphen})$  complex with peripheral alkoxy groups and (B) TEM micrograph when casted from MeOH. (C) PM3 optimized structure of a helical  $\text{Zn}(\text{salphen})$  oligomer based on  $\text{Zn}-\text{O}$  interactions.

This hypothesis was adjusted upon examination of systems that comprise of hydrophilic glucose and galactose substituents, which showed that the formation of nanofibrils on the TEM grid still occurred. Based on this result, the assumption that the 1D assembly is formed by weak interactions such as H-bonding or  $\pi$ - $\pi$  stacking was subsequently ruled out, and by comparison with the self-assembly behaviour of a series of model compounds, the most likely mode of self-assembly is provided by coordinative Zn–O interactions (i.e. Zn(salphen) dimerization). A computed mode for the self-assembly of these systems is provided in Figure 10C and was separately supported by mass spectrometry analyses.

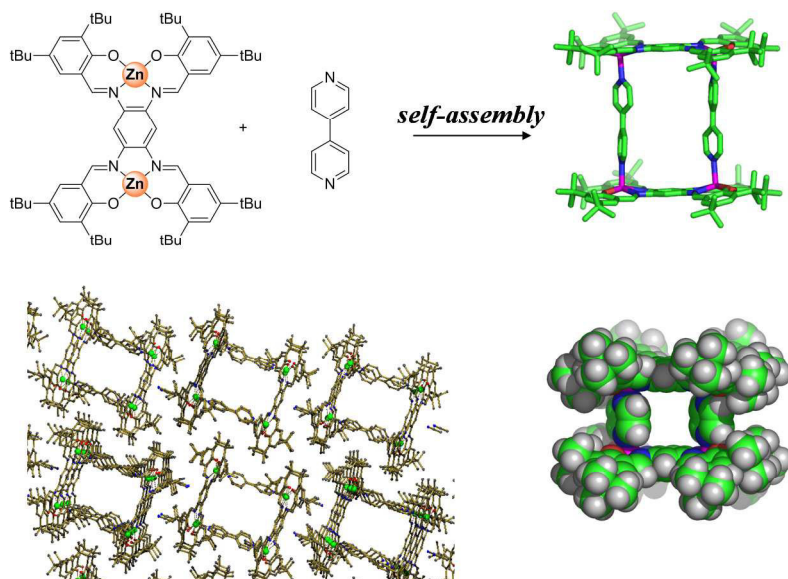
The self-dimerization of mononuclear Zn(salphen)s was recently also visualized at the single-molecule level using Scanning Tunneling Microscopy (STM) techniques (Figure 11).<sup>[59]</sup> These studies provided further unique insight in the stability of these interactions in both the solid-state and solution phase. It turned out that these long-tail Zn(salphen)s showed predominant and unusual bilayer formation on the graphite surface; the self-assembled species was easily disrupted by addition of pyridine donors, giving exclusively mononuclear, pyridine-ligated Zn(salphen)s that assembled as typical monolayers.



**Figure 11.** Scanning tunneling microscopic (STM) analysis of self-assembling Zn(salphen) complexes. Note the highlighted region in the STM image corresponding to the three aromatic groups in the Zn complex.

The ability of the Zn(II) ion, when located in a salphen scaffold, to allow for axial coordination by (external) N-donors, makes such complexes very versatile building blocks in supramolecular chemistry. A recent example was described by Reek and co-

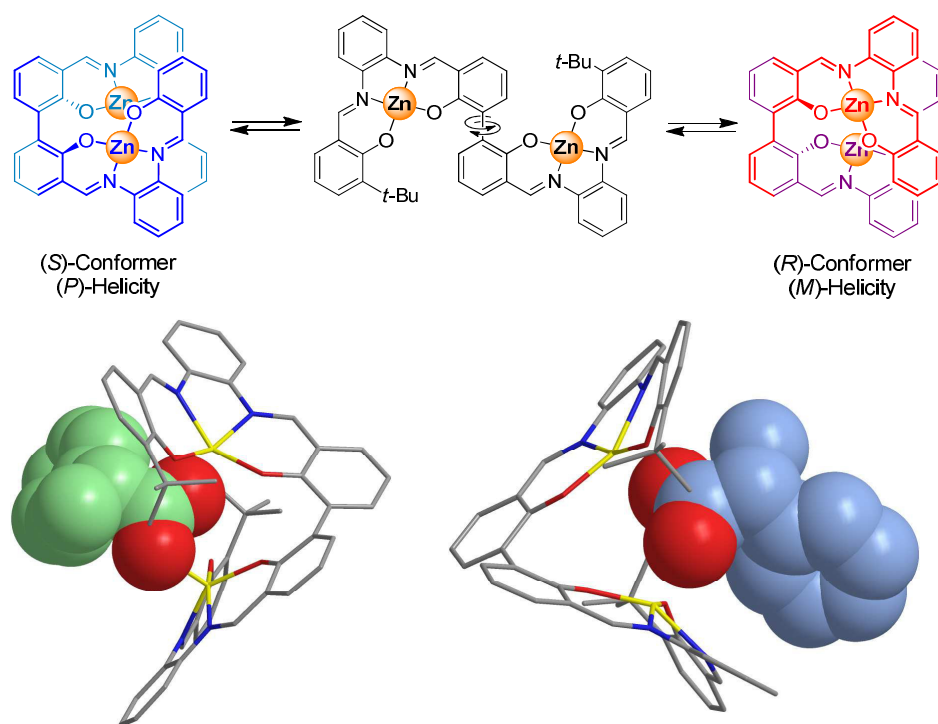
workers (Figure 12)<sup>[60]</sup> where the assembly of supramolecular boxes and coordination polymers based on a rigid *bis*-Zn(salphen) complex in combination with various ditopic nitrogen ligands was studied. The use of the *bis*-Zn(salphen) complex in combination with small ditopic nitrogen ligands leads to coordination polymers both in solution and in the solid state. However, using longer ditopic N-ligands, the authors observed the selective formation of supramolecular boxes that align in the solid state forming porous materials. The size of the pores can easily be modified by changing the length of the dinitrogen spacer giving access to tunable structures with a number of interesting applications in the field of metal organic frameworks (MOFs). More recent work from the same group has also resulted in (supramolecular) templated catalysis brought about by the *bis*-salphen scaffold providing an efficient tool for the asymmetric hydroformylation of styrene.<sup>[61]</sup> Alternatively, Zn(salphen) building blocks may also be exploited as “steric bulk”. Upon combination with suitably modified ligand systems having additional donor fragments that can coordinate to the Zn(II) ions, allows formation of partially encapsulated supramolecular catalysts that show improved Pd-catalysis in the copolymerization of CO and 4-*tert*-butyl-styrene.<sup>[62]</sup>



**Figure 12.** Formation of supramolecular box structures and their solid-state arrangement into porous materials

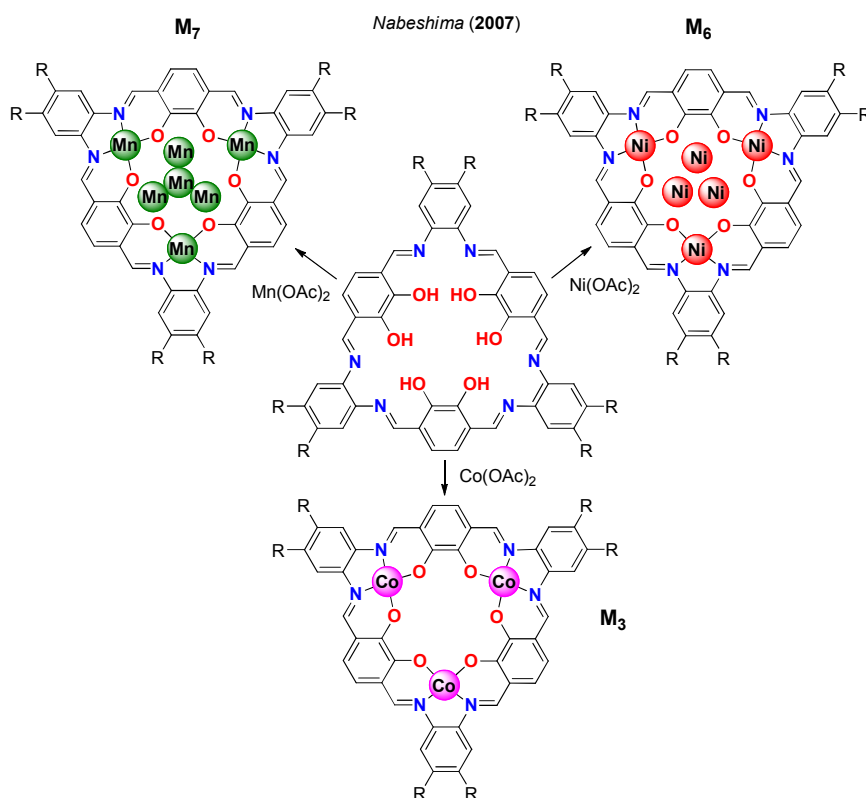


Within the field of supramolecular chemistry, Kleij and co-workers have presented a biphenol-based *bis*-Zn(salphen) complex (Figure 13).<sup>[63]</sup> This complex is in equilibrium between two chiral conformations that interconvert by axial rotation, and form strong host-guest complexes with carboxylic acids. One of the chiral conformations could be effectively induced at ambient temperature and micromolar concentrations, by addition of a chiral acid; no further derivatization of the substrate was required. This transfer of chiral information through supramolecular interactions (chirogenesis) is an appealing field of science inspired by the many examples observed in natural systems (i.e. DNA and proteins). Chirogenesis has also been widely studied for the development of smart, artificial and biomimetic materials. In this synthetic case (Figure 13), the *bis*-salphen system may be a good candidate for the determination of the absolute configuration of chiral carboxylic acid derivatives.



**Figure 13.** Top: schematic view on the interconversion of the two possible conformations of a *bis*-Zn(salphen) host molecule. Below: conformational lock induced by a chiral carboxylic acid in the *bis*-Zn(salphen) host, the pictures represent X-ray crystal structures.

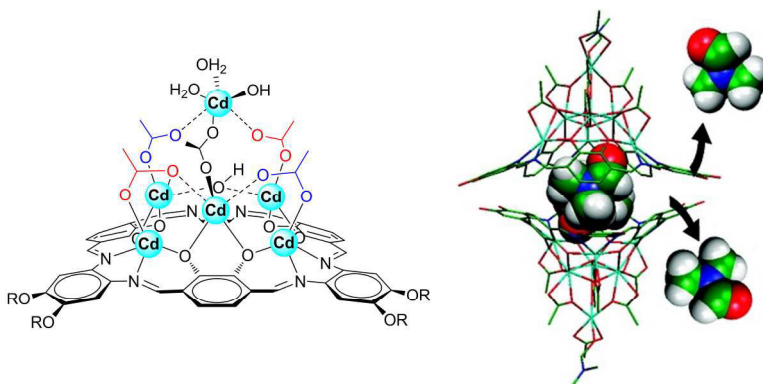
Large multidentate salphen macrocycles have attracted a lot of interest in the last ten years, since Nabeshima's inaugural macrocycle was presented.<sup>[15]</sup> In general an "[X+Y] macrocycle" may be easily synthesized by condensation of X diamine monomers with Y dialdehyde monomers of opposite geometry, giving a single macrocyclic Schiff base as the thermodynamic product. Successful examples of these approaches have been highlighted in Figure 2. These macromolecules show great shape-persistency and are very attractive for a variety of applications. One of the most utilized macrocycle so far is the [3+3] macrocyclic system, which comprises of three salphen units arranged to give a crown ether-like interior. Treatment of this macrocyclic ligand with an excess of various metal acetate leads to the formation of metal cluster complexes with different nuclearities (Figure 14).<sup>[64]</sup>



**Figure 14.** Various multinuclear (cluster) complexes based on a *tri*-salphen macrocycle.

As another example, using  $\text{Cd}(\text{OAc})_2$ , a heptacadmium cluster was also successfully isolated (Figure 15),<sup>[65]</sup> and these metallocavitand complexes adopt a bowl-shaped

structure induced by metal coordination. With this system, interesting host-guest chemistry was observed, where the metallocavitands are able to dimerize yielding supramolecular capsules with vacant coordination and H-bonding sites able to encapsulate one or two molecules of DMF.



**Figure 15.** A cadmium(II) cluster complex capable of host-guest interactions. On the right, the encapsulation of DMF molecules is clearly noted in the X-ray structure of the supramolecular system.

## 1.6 Aim and outline

Salphen-based complexes and materials have been shown to produce properties different from the well-known salen family of structures. Obviously, both the conjugation and the rigidity of the salphen backbone are important structural features that dictate the molecular properties. The recent achievements made in various research fields including homogeneous catalysis and photo- and supramolecular chemistry are a clear testament of the significant potential of these salphen scaffolds. Salphen ligands are also easily synthesised and tuneable, and offer a convenient alternative to synthetically more challenging ligands such as porphyrins, while maintaining similar functionality. Salphen systems therefore may offer amplified opportunities not only as powerful catalysts but also as molecular building blocks. Zn(salphen) building blocks have already demonstrated to be highly useful in supramolecular chemistry and nanotechnology, but their application as catalysts remains to date limited. Beside all the advantageous properties already mentioned, limited information is available about the

effect of the conjugation in the salphen scaffold<sup>[51,52]</sup> on the electrochemical properties of ligated redox-active metals. Furthermore, extended  $\pi$ -systems comprising multiple electronically connected salphen units may be useful for electronic modulation and can allow for selective access to mixed-valence species. The study of these additional properties is still in its infancy,<sup>[66]</sup> but further development thereof may give a boost toward the design of new, functional materials. It is clear that the salphen scaffold (and related conjugated multi-salphen structures) have recently emerged as powerful, complementary systems with excellent building block potential. Further to that, Zn(salphen)s have proven to have easily tuneable properties allowing amplification of their application potential.

The aim of the work described in this thesis is: 1) to further advance the self-assembly properties of multinuclear Zn(salphen) complexes, 2) to study the potential of salphen and related ligands in the formation of new photoactive materials, and 3) to understand the potential and limitations of Zn(salphen)s in catalysis, particularly in the ring-expansion addition of CO<sub>2</sub> to epoxides. Connected to these objectives, the first two chapters (2 and 3) present detailed studies on the self-assembly of different multinuclear Zn(salphen)s focusing on the type and the strength of the interactions involved. These are followed (*Chapter 4*) by application of a new salphen-like scaffold in “small molecule Organic Solar Cells” (smOSC), and a study focusing on the catalytic role of Zn(salphen) catalysts in the formation of organic carbonates derived from CO<sub>2</sub> and epoxides (*Chapter 5*).

*Chapter 2* describes the synthesis and characterization of a *tetra*-Zn(salphen) macrocycle using a metal template approach. The macrocyclic Zn complex shows strong self-assembly mediated by the formation of Zn(salphen) dimer units held together via  $\mu_2$ -phenoxo interactions. The self-assembly mode for *tetra*-Zn(salphen) macrocycle was investigated in detail by comparison of UV-Vis and fluorescence titrations with mononuclear and dinuclear Zn(salphen) model compounds.

*Chapter 3* represents a study on the extremely strong self-assembly of a *bis*-Zn(salphen) complex both in solution as well as at a solid-liquid interface. The self-assembly behavior was investigated in detail by scanning tunneling microscopy (STM), competitive UV-Vis and fluorescence titrations, dynamic light scattering (DLS) and

transmission electron microscopy (TEM). DFT analysis carried out for the *bis*-Zn(salphen) shows that an unusual binding mode is operative, and also rationalizes the very high stability of the self-assembled structures provoked by oligomeric  $(\text{Zn-O})_n$  coordination motifs within the (oligomeric) assembly.

*Chapter 4* reports the synthesis and photophysical properties of novel Zn(salphen) complexes containing a “phenazine” backbone. This new backbone increases the  $\pi$ -conjugation within the ligand scaffold and as a result influences the intensity and the position of the absorption maximum in the UV-Vis spectrum of the complexes. After examination of their photophysical properties (including DFT analysis), these Zn(salphenazine) derivatives were successfully applied in the preparation of Organic Solar Cell devices (smOSC).

*Chapter 5* reports a detailed DFT study of the reaction mechanism of the ring-expansion addition of  $\text{CO}_2$  to epoxides catalyzed by a binary catalyst comprising a Zn(salphen) complex and  $\text{NBu}_4\text{X}$  ( $\text{X} = \text{Br}, \text{I}$ ). The catalytic reaction has been studied in detail describing the three main steps involved: the epoxide ring-opening, the  $\text{CO}_2$  insertion step and a final ring-closure to afford the five-membered cyclic carbonate products. The ring-opening step of the process was examined and the preference for opening at the methylene ( $\text{C}_\beta$ ) or methine carbon ( $\text{C}_\alpha$ ) was established. Also the  $\text{CO}_2$  insertion and the ring-closing steps have been explored for six differently substituted epoxides and proved to be significantly more challenging compared with the ring-opening step. The combined results have helped to explain earlier experimental observations and catalyst limitations.

## 1.7 References and notes

- 
- [1] E. N. Jacobsen, *Acc. Chem. Res.* **2000**, *33*, 421.
  - [2] P. Pfeiffer, E. Brieth, E. Lubbe, T. Tsumaki, *Justus Liebigs Ann. Chem.* **1933**, *503*, 84.
  - [3] M. Palucki, N. S. Finney, P. J. Pospisil, M. L. Güler, T. Ishida, E. N. Jacobsen, *J. Am. Chem. Soc.* **1998**, *120*, 948.
  - [4] A. M. Castilla, S. Curreli, M. Martínez Belmonte, E. C. Escudero-Adán, J. Benet-Buchholz, A. W. Kleij, *Org. Lett.* **2009**, *11*, 5218.

- [5] For a recent example: Y. Sawada, K. Matsumoto, T. Katsuki, *Angew. Chem. Int. Ed.* **2007**, *46*, 4559.
- [6] J. M. Ready, E. N. Jacobsen, *J. Am. Chem. Soc.* **2001**, *123*, 2687.
- [7] W. Hirahata, R. M. Thomas, E. B. Lobkovsky, G. W. Coates, *J. Am. Chem. Soc.* **2008**, *130*, 17658.
- [8] For a recent review on cooperative effects in salen chemistry: R. M. Haak, S. J. Wezenberg, A. W. Kleij, *Chem. Commun.* **2010**, *46*, 2713.
- [9] S. J. Wezenberg, A. W. Kleij, *Angew. Chem. Int. Ed.* **2008**, *47*, 2354.
- [10] A. W. Kleij, *Eur. J. Inorg. Chem.* **2009**, 193.
- [11] For an early example refer to: M.-A. Muñoz-Hernández, T. S. Keizer, S. Parkin, B. Patrick, D. A. Atwood, *Organometallics* **2000**, *19*, 4416.
- [12] A. W. Kleij, D. M. Tooke, M. Kuil, M. Lutz, A. L. Spek, J. N. H. Reek, *Chem. Eur. J.* **2005**, *11*, 4743.
- [13] E. C. Escudero-Adán, M. Martínez Belmonte, J. Benet-Buchholz, A. W. Kleij, *Org. Lett.* **2010**, *12*, 459.
- [14] E. C. Escudero-Adán, M. Martínez Belmonte, E. Martín, G. Salassa, J. Benet-Buchholz, A. W. Kleij, *J. Org. Chem.* **2011**, *76*, 5404.
- [15] S. Akine, T. Taniguchi, T. Nabeshima, *Tetrahedron. Lett.* **2001**, *42*, 8861.
- [16] The Nabeshima group has also reported extensively on oxime-based “salen” type ligands, see for a recent account: S. Akine, T. Nabeshima, *Dalton Trans.* **2009**, 10395.
- [17] J. Jiang, M. J. MacLachlan, *Org. Lett.* **2010**, *12*, 1020.
- [18] P. D. Frischmann, J. Jiang, J. K.-H. Hui, J. J. Grzybowski, M. J. MacLachlan, *Org. Lett.* **2008**, *10*, 1255.
- [19] J. K.-H. Hui, M. J. MacLachlan, *Chem. Commun.* **2006**, 2480.
- [20] G. Salassa, A. M. Castilla, A. W. Kleij, *Dalton Trans.* **2011**, *40*, 5236.
- [21] W. Zhang, J. L. Loebach, S. R. Wilson, E. N. Jacobsen, *J. Am. Chem. Soc.* **1990**, *112*, 2801.
- [22] S. Melov, J. Ravenscroft, S. Malik, M. S. Gill, D. W. Walker, P. E. Clayton, D. C. Wallace, B. Malfroy, S. R. Doctrow, G. J. Lithgow, *Science* **2000**, *289*, 1567.
- [23] V. Mirkhani, S. Tangestaninejad, M. Moghadam, I. P. Mohammadpoor-Baltork, H. Kargar, *J. Mol. Catal. A: Chem.* **2005**, *242*, 251.
- [24] M. Nasr-Esfahani, M. Moghadam, G. Valipour, *Synth. Commun.* **2009**, *39*, 3867.
- [25] J. Tong, Y. Zhang, Z. Li, C. Xia, *J. Mol. Catal. A: Chem.* **2006**, *249*, 47.
- [26] M. Salavati-Niasari, F. Davar, M. Bazarganipour, *Dalton Trans.* **2010**, *39*, 7330.

- [27] S. H. Lee, L. Xu, B. K. Park, Y. V. Mironov, S. H. Kim, Y. J. Song, C. Kim, Y. Kim, S.-J. Kim, *Chem. Eur. J.* **2010**, *16*, 4678.
- [28] G. Wu, X. Wang, J. Li, N. Zhao, W. Wei, Y. Sun, *Catal. Today* **2008**, *131*, 402.
- [29] R. Mayilmurugan, H. Stoeckli-Evans, E. Suresh, M. Palaniandavar, *Dalton Trans.* **2009**, 5101.
- [30] V. Conte, F. Fabbianesi, B. Floris, P. Galloni, D. Sordi, I. W. C. E. Arends, M. Bonchio, D. Rehder, D. Bogdal, *Pure Appl. Chem.* **2009**, *81*, 1265.
- [31] D. J. Darensbourg, P. Ganguly, D. Billodeaux, *Macromolecules* **2005**, *38*, 5406.
- [32] H. Sugimoto, H. Ohtsuka, S. Inoue, *J. Polym. Sci., Part A: Polym. Chem.* **2005**, *43*, 4172.
- [33] S. I. Vagin, R. Reichardt, S. Klaus, B. Rieger, *J. Am. Chem. Soc.* **2010**, *132*, 14367.
- [34] M. Zintl, F. Molnar, T. Urban, V. Bernhart, P. Preishuber-Pflugl, B. Rieger, *Angew. Chem. Int. Ed.* **2008**, *47*, 3458.
- [35] R. Eberhardt, M. Allmendinger, B. Rieger, *Macromol. Rapid Commun.* **2003**, *24*, 194.
- [36] L.-J. Chen, J. Bao, F.-M. Mei, G.-X. Li, *Catal. Commun.* **2008**, *9*, 658.
- [37] A. Mitra, L.-J. DePue, S. Parkin, D. A. Atwood, *J. Am. Chem. Soc.* **2006**, *128*, 1147.
- [38] F. H. Zelder, J. Rebek Jr., *Chem. Commun.* **2006**, 753.
- [39] A. Decortes, M. Martínez Belmonte, J. Benet-Buchholz, A. W. Kleij, *Chem. Commun.* **2010**, *46*, 4580.
- [40] For an early discussion on the Lewis acidity of Zn(salphen)s see: A. W. Kleij, D. M. Tooke, M. Kuil, M. Lutz, A. L. Spek, J. N. H. Reek, *Chem. Eur. J.* **2005**, *11*, 4743.
- [41] A. Decortes, A. W. Kleij, *ChemCatChem.* **2011**, *3*, 831.
- [42] D. J. Darensbourg, A. I. Moncada, W. Choi, J. H. Reibenspies, *J. Am. Chem. Soc.* **2008**, *130*, 6523.
- [43] J. R. Wallace, D. L. Lieberman, M. T. Hancock, A. R. Pinhas, *J. Chem. Educ.* **2005**, *82*, 1229.
- [44] I. I. F. Boogaerts, S. P. Nolan, *J. Am. Chem. Soc.* **2010**, *132*, 8858.
- [45] G. Yu, Y. Liu, Y. Song, X. Wu, D. Zhu, *Synth. Met.* **2001**, *117*, 211.
- [46] O. Lavastre, I. Illitchev, G. Jegou, P. H. Dixneuf, *J. Am. Chem. Soc.* **2002**, *124*, 5278.
- [47] A. C. W. Leung, J. H. Chong, B. O. Patrick, M. J. MacLachlan, *Macromolecules* **2003**, *36*, 5051.
- [48] C.-M. Che, C.-C. Kwok, S.-W. Lai, A. F. Rausch, W. J. Finkenzeller, N. Zhu, H. Yersin, *Chem. Eur. J.* **2010**, *16*, 233.
- [49] Z. Guo, W.-L. Tong, M. C. W. Chan, *Chem. Commun.*, **2009**, 6189.
- [50] S. Sun, W.-L. Tong, M. C. W. Chan, *Macromol. Rapid Commun.* **2010**, *31*, 1965.

- [51] S. J. Wezenberg, E. C. Escudero-Adán, J. Benet-Buchholz, A. W. Kleij, *Org. Lett.* **2008**, *10*, 3311.
- [52] S. J. Wezenberg, E. C. Escudero-Adán, D. Anselmo, J. Benet-Buchholz, A. W. Kleij, *Eur. J. Inorg. Chem.* **2010**, 4611.
- [53] H. Houjou, M. Ito, K. Araki, *Inorg. Chem.* **2009**, *48*, 10703.
- [54] H. Houjou, M. Ito, K. Araki, *Inorg. Chem.* **2011**, *50*, 5298.
- [55] A. E. Vaughn, D. B. Bassil, C. L. Barnes, S. A. Tucker, P. B. Duval, *J. Am. Chem. Soc.* **2006**, *128*, 10656.
- [56] E. C. Escudero-Adán, J. Benet-Buchholz, A. W. Kleij, *Chem. Eur. J.* **2009**, *15*, 4233.
- [57] M. Martínez Belmonte, S. J. Wezenberg, R. M. Haak, D. Anselmo, E. C. Escudero-Adán, J. Benet-Buchholz, A. W. Kleij, *Dalton Trans.* **2010**, *39*, 4541.
- [58] J. K.-H. Hui, Z. Yu, M. J. MacLachlan, *Angew. Chem. Int. Ed.* **2007**, *46*, 7980.
- [59] J. A. A. W. Elemans, S. J. Wezenberg, E. C. Escudero-Adán, J. Benet-Buchholz, D. den Boer, M. J. J. Coenen, S. Speller, A. W. Kleij, S. De Feyter, *Chem. Commun.* **2010**, *46*, 2548.
- [60] M. Kuil, I. Puijk, A. W. Kleij, D. M. Tooke, A. L. Spek, J. N. H. Reek, *Chem. Asian J.* **2009**, *4*, 50.
- [61] M. Kuil, P. E. Goudriaan, P. W. N. M. van Leeuwen, J. N. H. Reek, *Chem. Commun.* **2006**, 4679.
- [62] J. Flapper, J. N. H. Reek, *Angew. Chem. Int. Ed.* **2007**, *46*, 8590.
- [63] S. J. Wezenberg, G. Salassa, E. C. Escudero-Adán, J. Benet-Buchholz, A. W. Kleij, *Angew. Chem. Int. Ed.* **2011**, *50*, 713.
- [64] T. Nabeshima, H. Miyazaki, A. Iwasaki, S. Akine, T. Saiki, C. Ikeda, *Tetrahedron* **2007**, *63*, 3328.
- [65] P. D. Frischmann, G. A. Facey, P. Y. Ghi, A. J. Gallant, D. L. Bryce, F. Lelj, M. J. MacLachlan, *J. Am. Chem. Soc.* **2010**, *132*, 3893.
- [66] For a recent contribution focusing on the electrochemical properties of related salen-metal systems see: Y. Shimazaki, N. Arai, T. J. Dunn, T. Yajima, F. Tani, C. F. Ramogida, T. Storr, *Dalton Trans.* **2011**, *40*, 2469.



UNIVERSITAT ROVIRA I VIRGILI

SUPRAMOLECULAR, PHOTOPHYSICAL AND CATALYTIC PROPERTIES OF ZN(SALPHEN) BASED COMPLEXES AND MATERIALS

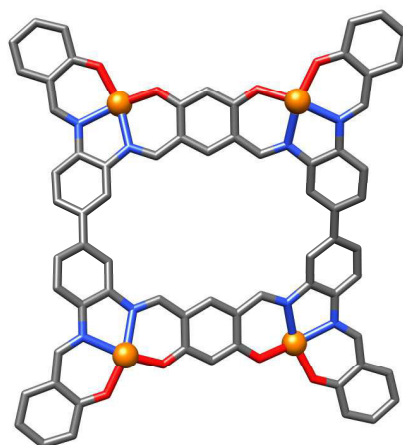
Giovanni Salassa

Dipòsit Legal: T. 1430-2013

# Chapter 2

## Self-Assembly of a Macrocyclic Schiff Base Complex

*A metal template approach affords in high yield and purity, a tetranuclear Zn(salphen) macrocycle (3) which shows strong self-assembly mediated by the formation of Zn(salphen) dimer units held together via  $\mu_2$ -phenoxo interactions. The self-assembly mode for 3 was investigated in detail by comparison of UV-Vis and fluorescence titration data recorded for 3 and respective mononuclear Zn(salphen) and dinuclear bis-Zn(salphen) model compounds. UV-Vis dilution experiments carried out using 3 and its tetra-Pd(salphen) analogue (4), as well as comparative TEM studies involving the same tetranuclear macrocycles further support a strong assembly behavior of 3.*



The work described in this chapter has been published: G. Salassa, A. M. Castilla, A. W. Kleij, *Dalton Trans.* **2010**, 40, 5236.

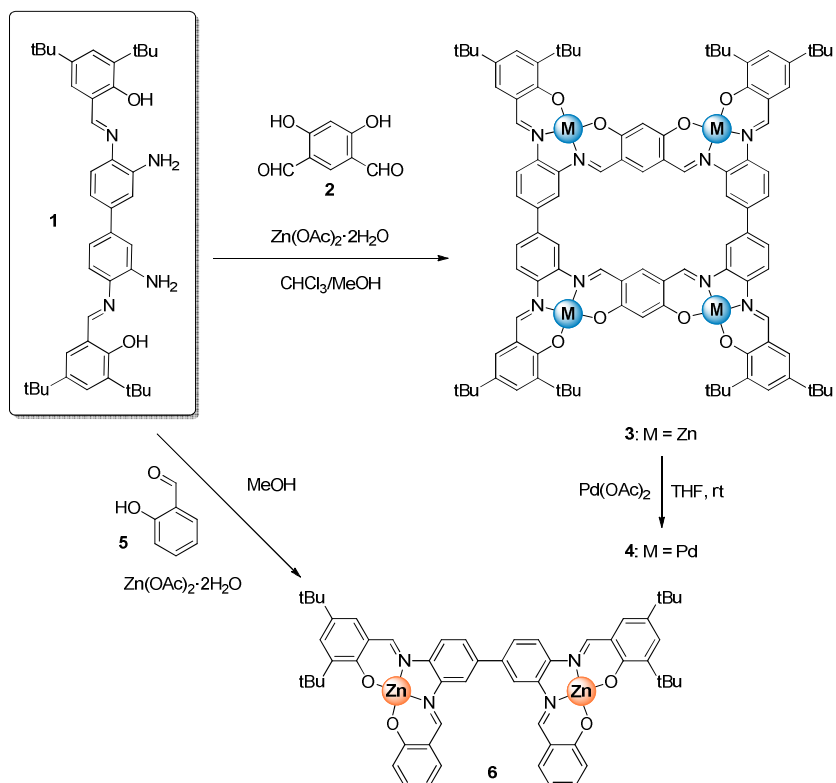
### 2.1 Introduction

Schiff base macrocycles<sup>[1]</sup> have attracted great interest due to their potential in fields such as catalysis,<sup>[2]</sup> host-guest chemistry<sup>[3]</sup> and magnetic materials.<sup>[4]</sup> Their preparation may be challenging, although template synthesis<sup>[5]</sup> has been shown to be a successful strategy that allows for selective formation of Schiff base macrocycles and related structures.<sup>[6,7]</sup> In the absence of a template agent, undesired imine hydrolysis and/or scrambling reactions may take place which complicates product isolation and

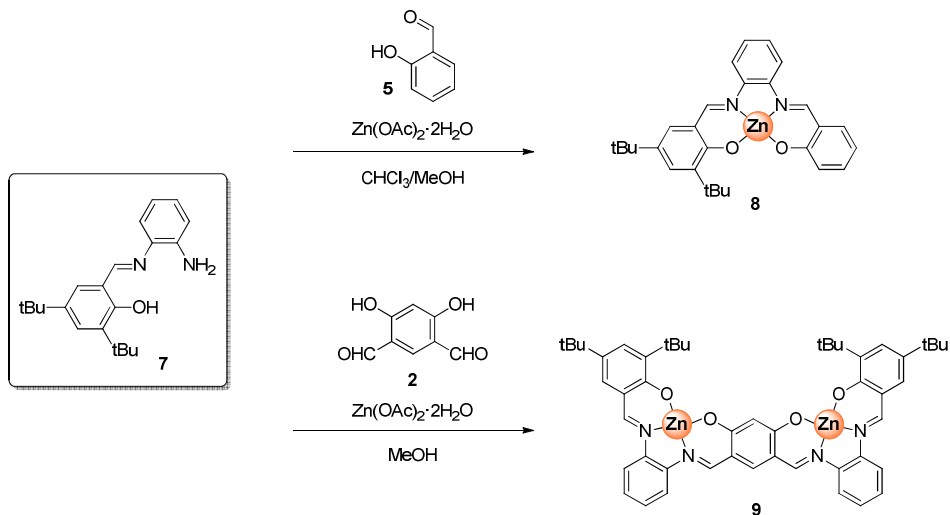
purification. We envisioned that a metal template approach towards salphen macrocycles<sup>[8]</sup> could be effectively achieved by combination of the appropriate building blocks giving rise to new metallo-macrocylic structures (Scheme 1). Furthermore, if successful this would create opportunities for simple fine-tuning of these systems through variation of the peripheral groups of these building blocks, and amplify their electronic properties potentially useful in catalytic and sensing applications.<sup>[9]</sup> Herein is described the formation of a new macrocylic Schiff base complex containing four Zn(salphen) units that shows strong self-assembly compared with a number of reference compounds; the self-assembly is mediated by the formation of intermolecular  $\mu_2$ -phenoxy bridges between adjacent Zn(salphen) units. The presence of multiple Zn(salphen) fragments within the macrocylic framework results in multivalency<sup>[10]</sup> and consequently stronger association behaviour as supported by various titration experiments. Full disruption of the macromolecular aggregation causes a strong hyperchromic effect which, to the best of our knowledge, has not been observed to this extend with other related (macrocylic) systems.<sup>[8c,11]</sup>

## 2.2 Synthesis of *tetra*-M(salphen) macrocycles

The multinuclear Zn(salphen)s used in this study were synthesized using Zn(OAc)<sub>2</sub>·2H<sub>2</sub>O as templating agent. The *tetra*-Zn(salphen) macrocycle **3** was prepared through a one-pot combination of a previously reported di-imine based on the 3,3'-diaminobenzidine scaffold **1**<sup>[12]</sup>, a dialdehyde precursor **2**<sup>[13]</sup> and Zn(OAc)<sub>2</sub>·2H<sub>2</sub>O (see Experimental section, Scheme 1). This procedure affords **3** in a high isolated yield (88%) and purity by a single filtration of the reaction mixture.<sup>[14]</sup> It should be noted that in the absence of the Zn salt, mainly the starting materials were recovered, emphasizing the templating role of the metal reagent. The Zn<sup>2+</sup> ions in **3** can be readily replaced by Pd<sup>2+</sup> ions by means of transmetalation,<sup>[15]</sup> and this furnishes the *tetra*-Pd(salphen) macrocycle **4** (Scheme 1). Further, reaction of precursor **1** with salicylaldehyde **5** affords the nonsymmetrical *bis*-Zn(salphen) **6**, also in high yield and purity. In addition the same one-pot reaction strategy has been applied in the synthesis of *bis*-Zn(salphen) **9** by the combination of previously reported mono-imine **7**, dialdehyde **2** and Zn(OAc)<sub>2</sub>·2H<sub>2</sub>O (see Experimental section, Scheme 2).



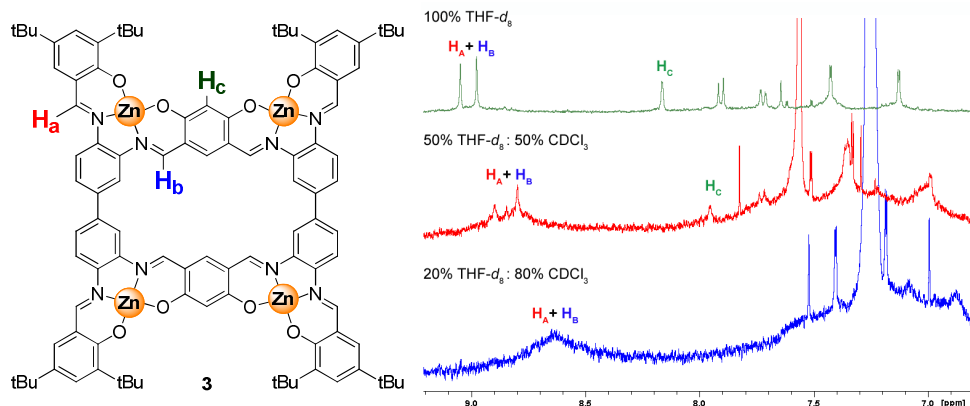
**Scheme 1.** Synthesis of **3**, **4** and **6** from di-imine precursor **1**.



**Scheme 2.** Synthesis of **8** and **9** from the mono-imine precursor **7**.



patterns are observed. Increasing the percentage of coordinating THF- $d_8$ , the signals in the  $^1\text{H}$  NMR spectrum sharpened to a single pattern as in the case of DMSO- $d_6$  (Figure 2). This phenomenon suggests that **3** is able to self-aggregate.

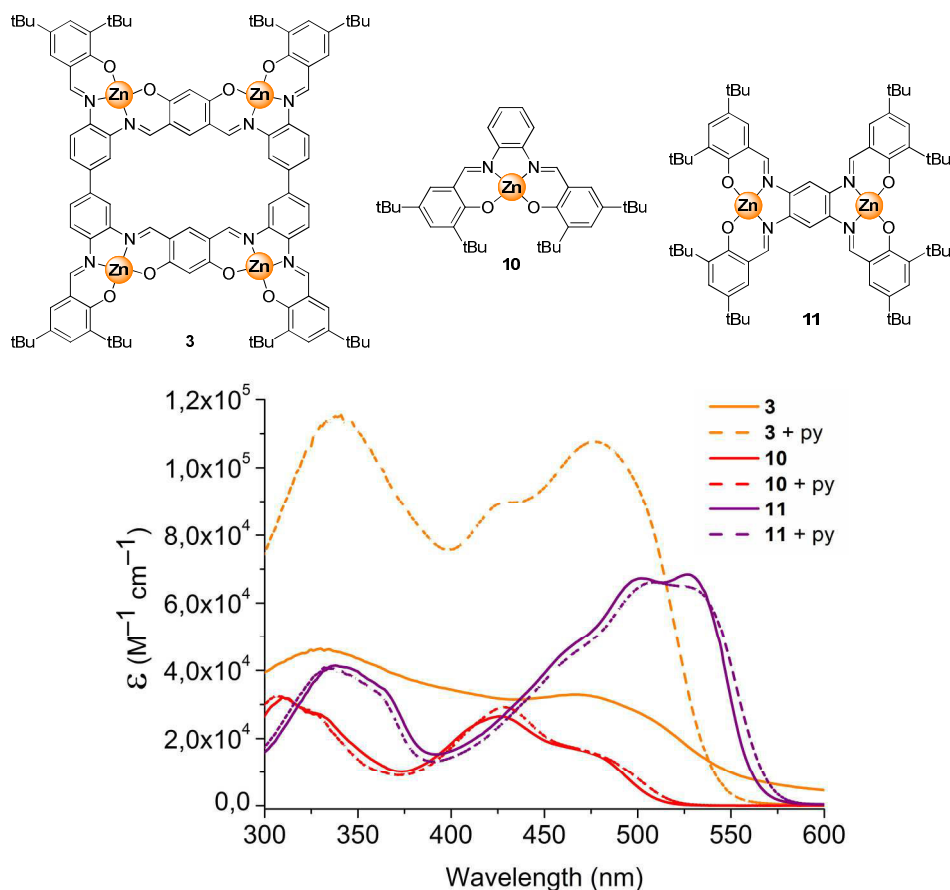


**Figure 2.**  $^1\text{H}$  NMR spectra (aromatic region 6.5-9.0 ppm) of macrocycle **3** using different solvent mixtures.

From the  $^1\text{H}$  NMR studies described above and further solubility tests using a variety of solvents, it is clear that macrocycle **3** has modest solubility in relatively nonpolar solvents such as toluene,  $\text{CH}_2\text{Cl}_2$  and  $\text{CHCl}_3$  but shows much higher solubility in coordinating media including DMSO, THF and pyridine. This axial coordination ability for related Zn(salphen) structures<sup>[17]</sup> has been well documented in the literature and **3** is presumed to exist as a monomeric tetra-solvate in these latter solvents, but seems to be aggregated under relatively nonpolar conditions.

#### 2.4.2 UV-Vis studies

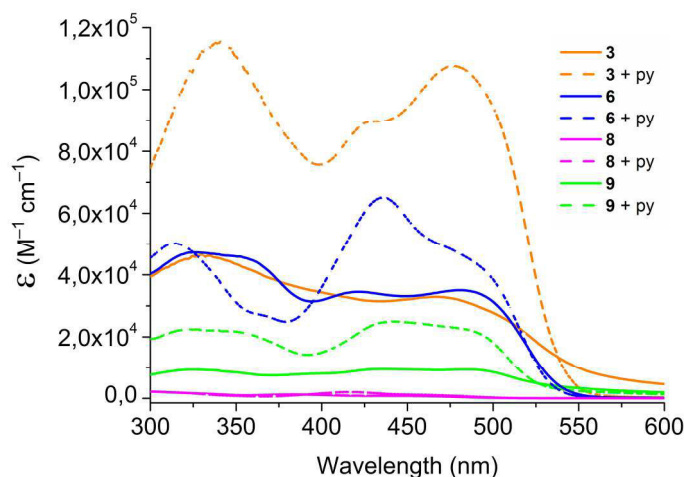
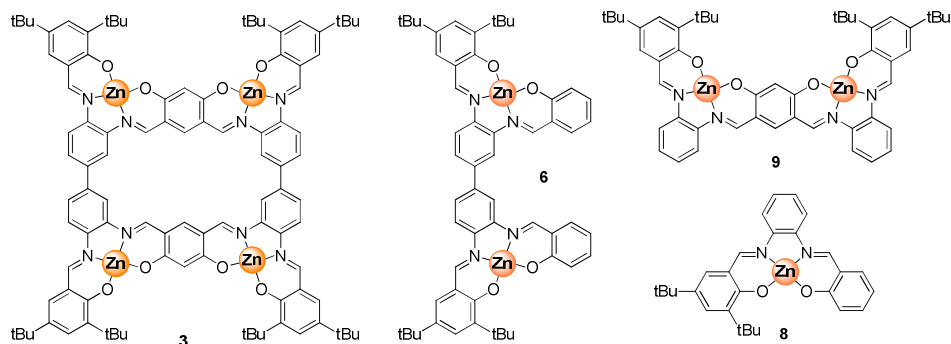
The assembly behaviour of **3** under apolar conditions was then studied in detail by UV-Vis and fluorescence spectroscopy and compared against reference compounds **6**, **8**, **10** and **11** (Figure 3-4). Since Zn(salphen) complexes have a strong tendency to form dimeric structures under relative non-polar conditions,<sup>[8c,11]</sup> the UV-Vis behaviour (toluene) was examined in the absence and presence of an excess of axially coordinating pyridine. Figure 3 shows the UV-Vis traces of macrocycle **3** and complexes **10** and **11**, the dotted lines represent the traces after pyridine addition.



**Figure 3.** UV-Vis comparison between **3**, **10** and **11**. All spectra recorded in toluene at  $4 \times 10^{-5}$  M normalized [Zn(salphen)] units; added pyridine in each case amounts to  $6.2 \times 10^{-4}$  mol.

Interestingly, the UV-Vis spectra of complexes **10** and **11** in the absence/presence of a large excess of pyridine are rather similar, whereas for **3** a remarkable, three-fold increase in absorption (hyperchromic effect) is noted under these conditions. It should be noted that complexes **10** and **11** have large *t*Bu groups at both the 3- and 3'-positions of the salphen ligand which is known to (largely) inhibit the dimerization behaviour (see Chapter 1, section 1.5).<sup>[18]</sup> The UV-Vis features of **3** were also compared with the spectra obtained for **6**, **8** and **9** (Figure 4) as these be considered substructures of the macrocyclic complex. Complexes **3**, **6**, **8** and **9** are all assumed to be able to form dimeric Zn(salphen) stacks *via*  $\mu_2$ -phenoxo bridging.<sup>[19]</sup> For **3** this self-association

behaviour is stronger than for **6**, **8** and **9** since there exist more possibilities for intermolecular dimer formation (*i.e.*, multivalency can occur).



**Figure 4.** UV-Vis comparison between **3**, **6**, **8** and **9**. All spectra were recorded in pre-dried toluene at  $4 \times 10^{-5}$  M normalized [Zn(salphen)] units; added pyridine in each case amounts to  $6.2 \times 10^{-4}$  mol.

This hypothesis was investigated in detail by competitive titrations with pyridine, thereby assessing the amount of pyridine needed to fully break up equimolar amounts of the assembled structures based on **8**, **6** and **3**. A comparison was made for tetranuclear **3**, dinuclear **6** and mononuclear **8** and the inflection points (*i.e.*, the point where the increase in absorption due to coordination by the pyridine starts to level off and full deaggregation occurs) in the titration curves determined. The results of these titration experiments are reported in Figure 5, and Table 1. Interestingly, nearly full deaggregation of mononuclear complex **8** is achieved with 10 equivalents of pyridine in



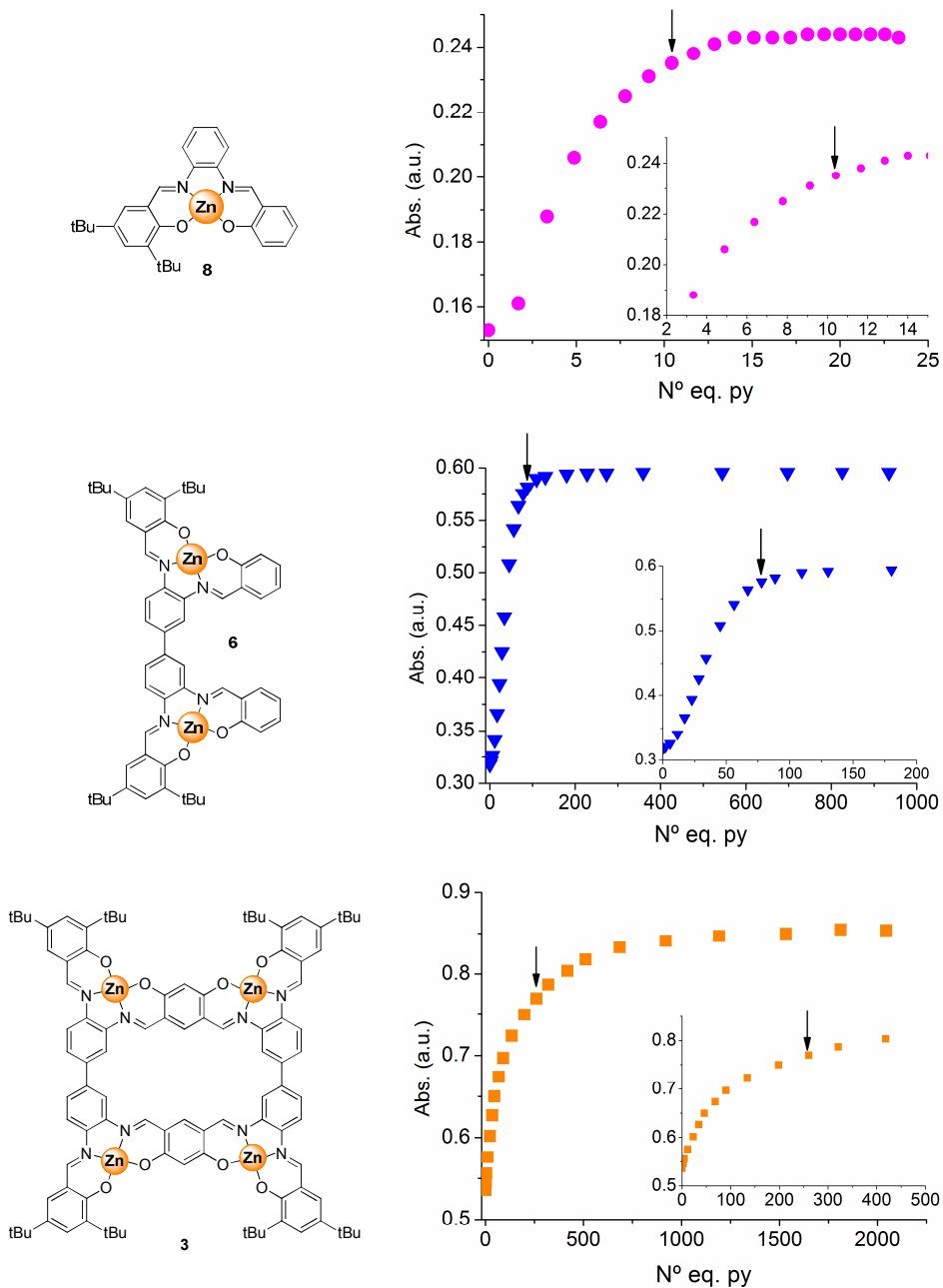
accordance with previously reported works.<sup>[20]</sup> In this work a similar Zn(salphen) complex was described that exhibits very strong self-dimerization with a  $K_{\text{dimer}}$  of  $3.2 \times 10^8 \text{ M}^{-1}$  and only 10-15 eq. of pyridine were needed to fully disrupt the aggregated state. However, upon comparison, the inflection points observed in the titrations of dinuclear **6** (Table 1, at 75 equiv) and tetranuclear **3** (Table 1, at 250 equiv) it is clear that an increasing amount of pyridine is needed to fully convert these assembled species into monomeric, pyridine-ligated complexes. If these numbers are normalized with respect to the number of Zn(salphen) units present in each molecule, then for **8**, **6** and **3** a total of 10, 38 and 63 equivalents of pyridine respectively are required per Zn(salphen) unit to achieve full deaggregation (Table 1).

This increasing amount of pyridine required to disrupt all Zn(salphen) dimer units supports that the molecular assembly process is dictated by the number of Zn(salphen) units (*i.e.*, multivalent binding process).<sup>[10]</sup> The same observations are done when **8**, **6** and **3** were investigated by fluorescence spectroscopy (Figure 6); at similar molar concentrations ( $1.5 \times 10^{-6} \text{ M}$ , toluene), for **3** the highest amount of pyridine was required to reach a maximum fluorescence emission at  $\lambda = 547 \text{ nm}$ .

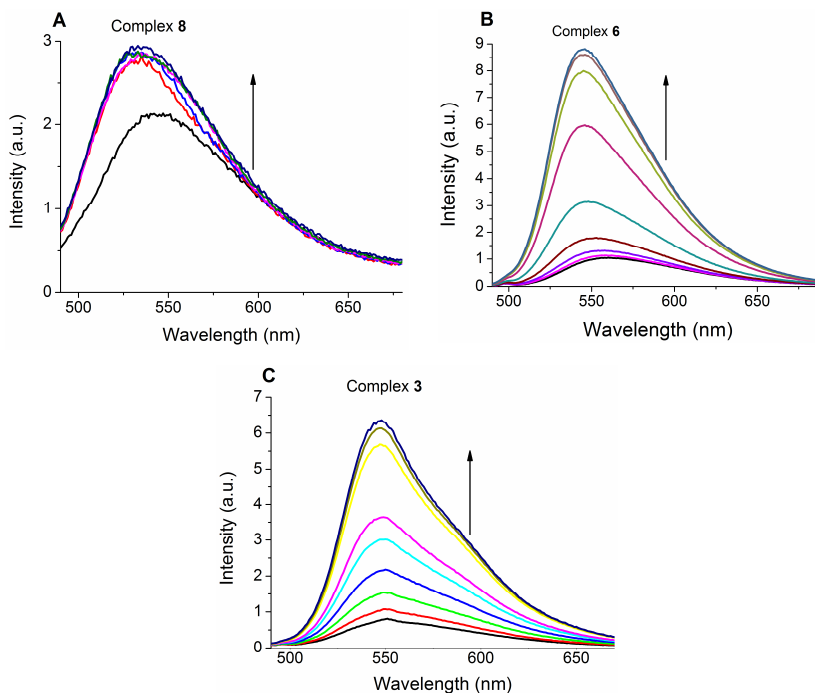
**Table 1.** UV-Vis titration data for complexes **3**, **7** and **9** in toluene at  $1 \times 10^{-5} \text{ M}$  using pyridine as titrant

Complex	Zn centres	IP <sup>a</sup>	Eq. py at $A_{\text{max}}$	Eq. py at IP/Zn <sup>c</sup>
<b>8</b>	1	10	15	10
<b>6</b>	2	75	100	38
<b>3</b>	4	250	750	63

<sup>a</sup> IP inflection point; extrapolated manually. <sup>b</sup> Extrapolated manually  $A_{\text{max}}$  = maximum absorption. <sup>c</sup> Amount of pyridine needed per Zn centre to reach IP.



**Figure 5.** UV-Vis titrations with mononuclear **8** (top), dinuclear **6** (middle) and tetranuclear **3** (bottom) in toluene at equimolar concentrations ( $1 \times 10^{-5}$  M) using pyridine as the titrant. The insets show an enlarged portion of initial part of these curves. The inflection points are marked with an arrow.



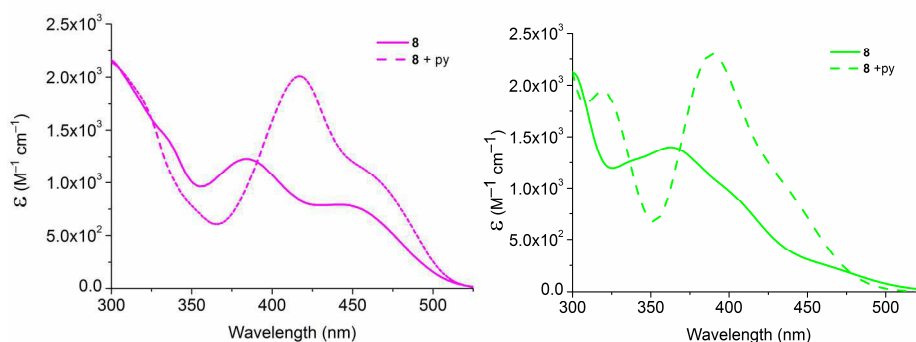
**Figure 6.** Fluorescence titration spectra using mononuclear **8** (A), dinuclear **6** (B) and tetranuclear **3** (C) at  $1.5 \times 10^{-6}$  M in toluene. For Figure 6A amount of pyridine added: 0, 0.03, 0.13, 0.43, 1.3 and 2.8 equiv, respectively; emission maximum located at  $\lambda = 534$  nm. For Figure 6B amount of pyridine added: 0, 12, 20, 30, 59, 112, 209, 320 and 458 equiv, respectively; emission maximum located at  $\lambda = 545$  nm. For Figure 6C amount of pyridine added: 0, 15, 34, 61, 113, 227, 402, 606 and 830 equiv, respectively; emission maximum located at  $\lambda = 547$  nm.

### 2.4.3 Hyperchromic effects

As described in section 2.4.2, the disruption of a Zn(salphen) dimeric unit, resulting from the addition of a pyridine ligand, causes a hyperchromic effect (increase of  $\Delta\varepsilon$ ) in the visible region between 350 nm and 600 nm. Such change in the extinction coefficient is reminiscent of the disruption of double strand DNA into single strand DNA.<sup>[21]</sup> In order to understand this phenomenon in more detail, DFT calculations on complex **8** and its corresponding dimer were performed since they are less computationally demanding than **3**, **6** and **9**. Initially, both the dimeric (**8**)<sub>2</sub> and pyridine-ligated (**8**•py) structures were optimized using DFT at the B3P86 level of theory. Then, excited states were calculated by time-dependent DFT (TD-DFT) and the influence of the solvent (toluene) was considered using the method CPCM (see experimental

section). Figure 7 shows experimental (left) and calculated (right) UV-Vis traces for  $(\mathbf{8})_2$  and  $(\mathbf{8}\cdot\text{py})$ . Calculated UV-Vis spectra are in good agreement with those obtained experimentally, although a blue shift of around 25 nm was observed. Analysis of the absorption response relative to the deaggregation of the dimeric species reveals an increase in intensity for the band at 384 nm (calculated 369 nm) and a red shift to 417 nm (calculated 392 nm).

Examination of TD-DFT singlet-singlet transitions (calculated by TD-DFT) responsible for the lowest-energy absorption band (shoulder included) allows to explain the occurrence of the hyperchromic effect observed experimentally (Table 2). In particular, for  $(\mathbf{8})_2$ , twelve transitions are spread over 101 nm (from 463 nm to 357 nm) and among them only five are allowed (oscillator strength  $f \neq 0$ ). On the contrary, in the case of  $(\mathbf{8}\cdot\text{py})$  the active transitions (which are five as well) are distributed only over 60 nm (from 436 nm to 376 nm), resulting in a narrower and more intense absorption band.



**Figure 7.** Experimental (left) and simulated (right) UV-Vis spectra of complex **7** in toluene: the dashed lines represent the traces after addition of pyridine.

The main transition (at 369 nm) in  $(\mathbf{8})_2$  has a  $\pi\text{-}\pi^*$  character with no contribution from the metal; furthermore no electron density exchange between the two monomeric units is observed (see Table 4 in the Experimental section). For  $(\mathbf{8}\cdot\text{py})$ , the main transition at 392 nm is an intra-ligand charge transfer with a contribution of the coordinated pyridine ligand. Such change in character corresponds to a shift from 369 nm to 392 nm in line with the experimentally obtained red shift (Figure 7).

Taking into account what has previously been described and considering the number of Zn(salphen) fragments in **8** (1), **6** (2), **9** (2) and macrocyclic **3** (4) it is clear that the *tetra*-Zn(salphen) species **3** is likely to provoke the largest hyperchromic effect since the

probability of dimer formation, and thus extended aggregation, is higher. Indeed, the UV-Vis as well as fluorescence titration data (Figure 3, 4 and 6) shows that the hyperchromic effect follows the order **3** >> **6** or **9** >> **8**.

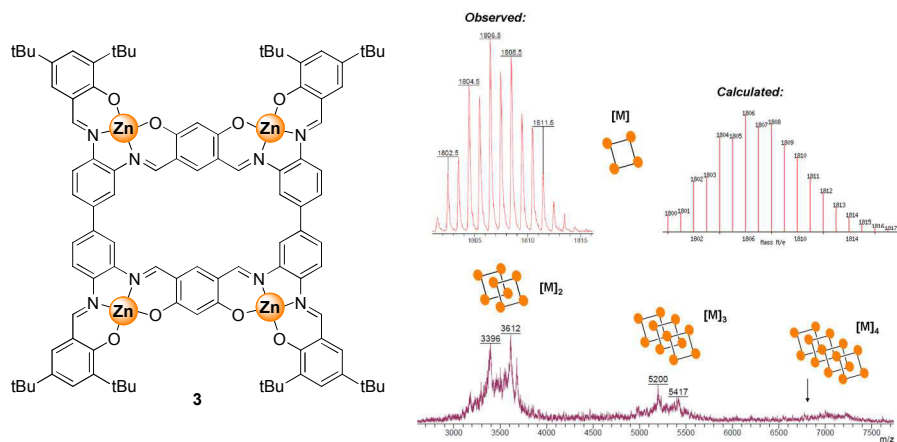
Table 2. Selected calculated singlet excited-state transitions for complex **7** in toluene.

Complex	Transition	Energy <sup>a</sup>	<i>f</i> <sup>b</sup>	Major contributions <sup>c</sup>
<b>(8)<sub>2</sub></b>	1	462	0	HOMO→LUMO (86%)
	2	458	0,10	H-1→LUMO (78%),
	3	452	0,02	HOMO→L+1 (78%)
	4	450	0	H-1→L+1 (88%),
	5	406	0	HOMO→L+2 (49%)
	6	403	0,40	HOMO→L+3 (44%)
	7	388	0	H-1→L+2 (48%),
	8	388	0	H-1→L+3 (52%),
	9	369	0,44	H-2→LUMO (86%)
	10	368	0	H-2→L+1 (49%)
	11	362	0	H-3→LUMO (56%)
	12	357	0,26	H-3→L+1 (90%)
<b>(8•py)</b>	1	436	0,17	HOMO→LUMO (91%)
	2	409	0,07	HOMO→L+1 (56%)
	3	392	0,25	H-1→LUMO (43%),
	4	385	0,08	HOMO→L+2 (78%)
	5	376	0,16	H-1→L+1 (85%)

<sup>a</sup> Related transitions energy values in nm. <sup>b</sup> The oscillator strength values (shown also as vertical bars in the images). <sup>c</sup> Major contributions of the orbital relatively at the transition.

### 2.4.4 Mass spectrometry studies

To further support the proposed Zn(salphen) assembly behaviour, mass spectrometry studies for **3** ( $\text{CH}_2\text{Cl}_2$ , MALDI+),<sup>[22]</sup> and dilution experiments were carried out with both *tetra*-Zn(salphen) and *tetra*-Pd(salphen) macrocycles **3** and **4** in both the absence and the presence of pyridine. Figure 8 shows the mass spectrum of **3**; although the mass spectrum has low quality as a result of the very low solubility of **3** under apolar conditions it further suggests the formation of higher-order, aggregated species  $[\mathbf{3}]_n$ . It particularly shows patterns in those mass regions where the dimer, trimer and tetramer of **3** are expected. It should be noted that these oligomers were not observed in the case of *tetra*-Pd(salphen) macrocycle **4** and that a more accurate mass analysis of **3** under apolar conditions is complicated by the fact that only very small amounts of the oligomeric components can be dissolved in the applied solvent.

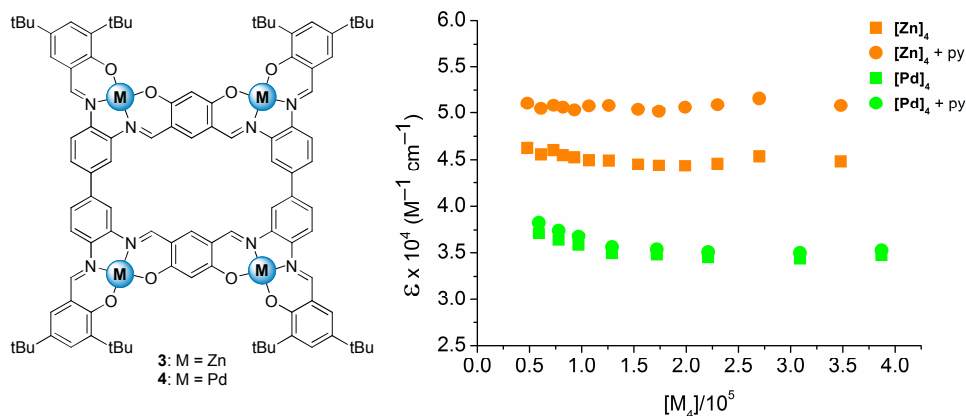


**Figure 8.** MALDI(+)-TOF mass spectrum of **3** (pyrene matrix) showing the molecular ion (top) with the calculated isotopic pattern, and below the higher mass region.  $[\mathbf{3}]$  represents a monomeric unit of **3**.

### 2.4.5 Dilution experiments

The results of dilution experiments (Figure 9) show for this concentration regime a virtually dilution-independent  $\epsilon$  for *tetra*-Pd(salphen) **4** which supports the presence of a single species. Only in the case of the *tetra*-Zn(salphen) macrocycle the presence of pyridine provokes a significant change in  $\epsilon$  that is ascribed to the disruption of the dimeric Zn(salphen) units in **3** and formation of monomeric pyridine ligated *tetra*-

Zn(salphen). For the *tetra-tetra*-Pd(salphen) macrocycle virtually no change is observed upon addition of the pyridine, and probably intermolecular  $\pi$ - $\pi$  stacking plays a minor role in the self-assembly observed for **3**. This is in line with the fact that **4** contains coordinatively saturated metal centers that do not bind axial ligands, and cannot therefore form dimeric structures as observed in the Zn(salphen) examples. The spectroscopic behaviour of **3** emphasizes the unique ability of the Zn(salphen) fragments in **3** to form dimeric structures and thus provide a very strong self-assembly pathway.<sup>[19]</sup>

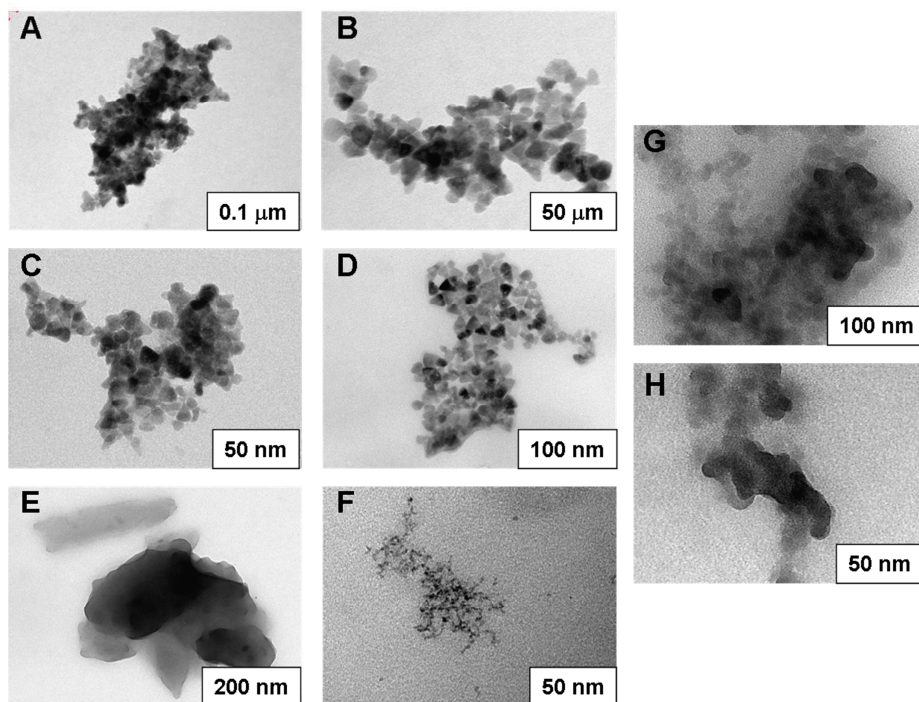


**Figure 9.** UV-Vis dilution experiments ( $\epsilon$ ,  $CHCl_3$ ) carried out for **3** ( $\lambda = 334$  nm) and **4** ( $\lambda = 354$  nm) in the absence/presence of pyridine (200 equiv).  $[M_4]$  concentration of the tetrametallic macrocycles.

#### 2.4.6 TEM analysis

The self-assembly behaviour of *tetra*-Zn(salphen) macrocycle **3** and *tetra*-Pd(salphen) macrocycle **4** was also investigated and compared in the solid state using transmission electron microscopy (TEM, Figure 10). The TEM micrographs show distinct behaviour of **3** and **4**. Whereas for **3** defined triangular-shaped particles are observed (**A–B**, from  $CHCl_3$ ) of around 20 nm, for **4** less defined aggregates are noted (**G–H**, from  $CHCl_3$ ). This difference can be ascribed to the different metal ions in the macrocycle, as observed in solution (*cf.*, Figure 9). The influence of the solvent polarity and the presence of pyridine during the drop-casting procedure were also examined (Figures **C–F**). The presence of pyridine during the deposition of the sample does not seem to have

a large effect (C–D). This can be ascribed to the loss of some pyridine upon drop-casting the sample which favors the re-aggregation of the system. When **3** was dropcasted from a coordinating solvent such as THF (F), a significant effect was noted on the particle size (smaller) and aggregation behaviour (fewer aggregated particles). On the contrary, dropcasting from toluene (E) supports the view of strong association of **3** in non-coordinating media and formation of larger particles.



**Figure 10.** TEM micrographs of **3** (figures A–F) and **4** (figures G–H).

## 2.5 Conclusions

In summary, an effective route towards a new type of macrocyclic Schiff base complex **3** that shows strong self-assembly behaviour through formation of multiple, intermolecular Zn(salphen) dimers has been presented. The switch in aggregation for **3** upon changing solvent polarity or addition of dimer-disrupting donor ligands causes a strong hyperchromic effect which may be a useful instrument for designing responsive materials for detection of molecules that are able to coordinate to the Zn ions of **3**.



Alternatively, since complexes **3** and **4** largely represent shape-persistent molecules, the use of suitable (chiral) diimine reagents (*cf.*, **1** in Scheme 1) and metal ions could pave the way to metallomacrocycles for application in homogeneous catalysis where their relatively large size may be exploited to separate the catalysts from the product/substrate stream by nanofiltration membranes.

## 2.6 Experimental section

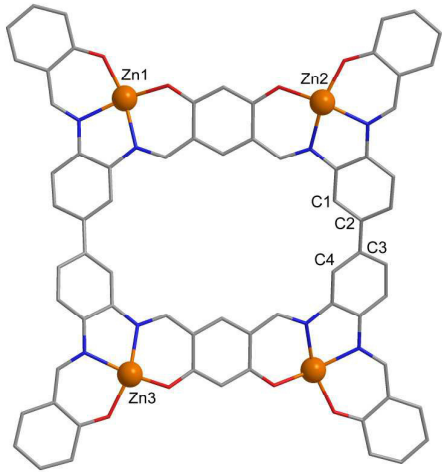
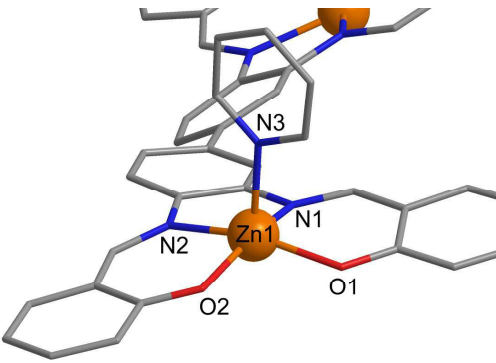
### General methods and materials

All starting materials were purchased from commercial sources and used without further purification. Compounds **10**,<sup>[17b]</sup> **11**,<sup>[17c,23]</sup> **8**<sup>[19b]</sup> and the monoimine based on 3,5-di-*tert*-butylsalicylaldehyde and *o*-phenylenediamine<sup>[24]</sup> were prepared using reported methods. Elemental analyses were performed at the Unidad de Análisis Elemental from the University of Santiago de Compostela (Spain). All NMR measurements were carried out on a Bruker-400 MHz spectrometer at ambient temperature unless stated otherwise, and chemical shifts are given in ppm vs. TMS. Mass spectrometric data was obtained from the Research Support unit of the ICIQ and MALDI-TOF experiments were carried out with pyrene as matrix. UV-Vis spectra were recorded on a Shimadzu UV-1800 spectrophotometer. Transmission electron microscopy (TEM) was performed with a JEOL 1011 microscope operated at 100 keV. All TEM micrographs were collected using a Megaview III camera. Sample solutions were prepared and drop-casted on a copper grid cover by FORMVAR carbon film.

### DFT calculations

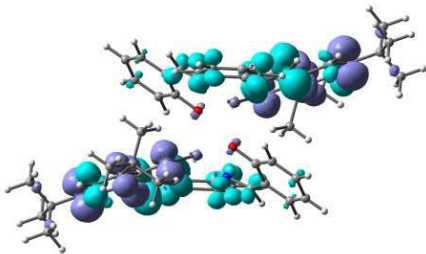
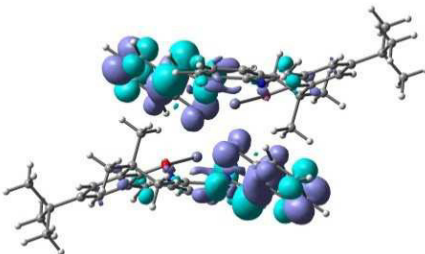
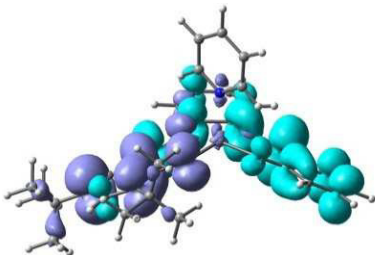
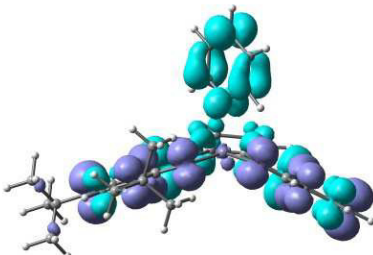
All calculations were performed with the Gaussian 03 (G03) program package<sup>[25]</sup> employing the DFT method with Becke's three parameter hybrid functional<sup>[26]</sup> and Perdew's 86 gradient corrected correlation functional (B3P86).<sup>[27]</sup> The LanL2DZ basis set<sup>[28]</sup> and effective core potential were used for the Zn atom, and the split-valence 6-31G\* basis set<sup>[29]</sup> was applied for all other atoms. Geometry optimizations of complexes **3** and **7** were performed without any constraint, and the nature of all stationary points was confirmed by normal-mode analysis. Non-equilibrium TDDFT<sup>[30]</sup> calculations produced singlet excited states, using the conductor like polarizable continuum model method (CPCM)<sup>[31]</sup> with toluene as solvent. Thirty-two singlet excited states were determined starting from **3** optimized geometry. Electronic distributions and localizations of the singlet excited states were visualized using the electron density difference maps (EDDMs).<sup>[32]</sup> GaussSum 1.05<sup>[33]</sup> was used for singlet EDDMs calculations and for simulation of the electronic spectrum.

**Table 3.** Selected distances and angles for  $3 \cdot (\text{py})_4$  from DFT optimized geometry.

Top view of <b>3</b>	Inset of a Zn(salphen) unit of <b>3</b> <sup>a</sup>
	
Distances (Å)	Angles (deg)
Zn1–Zn2 = 8.407	N1–Zn–O1 = 88.4°
Zn1–Zn3 = 11.683	N1–Zn–N2 = 77.2°
Zn1–N3 = 2.195	O1–Zn–O2 = 98.7°
Zn1–O1 = 1.983	O1–Zn–N3 = 100.1°
Zn1–N1 = 2.155	N1–Zn–N3 = 101.1°
Dihedral Angles (deg)	
C1–C2–C3–C4 = 32.9°	

<sup>a</sup> Note that the substitution of the macrocyclic compound in the Figures is omitted for clarity

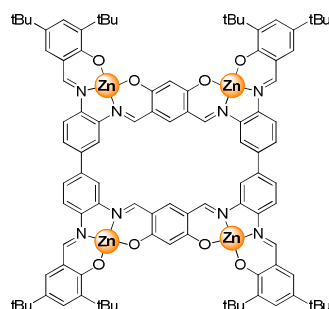
**Table 4.** Electron density difference maps (EDDMs)<sup>a</sup> of the most probable transitions.

<b>(8)<sub>2</sub> complex</b>	
Transition 6	Transition 9
	
Energy = 3,0709 eV (403 nm) $f^b = 0,40$ ; H-1→L+2 (37%), HOMO→L+3 (44%) <sup>c</sup>	Energy = 3,3539 eV (369 nm) $f = 0,44$ ; H-2→LUMO (86%)
<b>(8•py) complex</b>	
Transition 1	Transition 3
	
Energy = 2,8406 eV (436 nm) $f = 0,17$ ; HOMO→LUMO (91%)	Energy = 3,1557 eV (392 nm) $f = 0,25$ ; H-1→LUMO (43%)

<sup>a</sup> The electron density migrates from the violet-coloured lobes to the blue-coloured ones. <sup>b</sup> The oscillator strength values. <sup>c</sup> Major contributions of the orbital relatively at the transition.

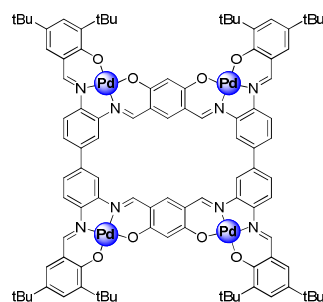
## Synthesis

**tetra-Zn(salphen) complex (3):** A solution of 4,6-dihydroxy-1,3-benzene-dicarboxaldehyde **2** (16.96 mg, 0.102 mmol) in MeOH (10 mL) was added to a solution of diimine **1** (60 mg, 0.0928 mmol) in CHCl<sub>3</sub> (20 ml). Then a solution of Zn(OAc)<sub>2</sub>·2H<sub>2</sub>O (42.8 mg, 0.195 mmol) in MeOH (5 mL) was added. The clear orange reaction mixture was stirred at 60°C for 18 h. Hereafter, the volatiles were evaporated and the solid triturated with MeOH. The precipitate was filtered off and dried to yield macrocycle **3** (73.2 mg, 0.040 mmol, 88%). Complex **3** was recrystallized



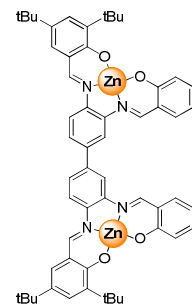
from  $\text{CHCl}_3/\text{MeOH}$ .  $^1\text{H}$  NMR (400 MHz,  $\text{DMSO-}d_6$ ):  $\delta$  = 9.27 (s, 4H; CH=N), 9.01 (s, 4H; CH=N), 8.32 (s, 4H; ArH), 7.98 (d,  $^3J$  = 8.8 Hz, 4H; ArH), 7.89 (s, 4H; ArH), 7.80 (d,  $^3J$  = 8.2 Hz, 4H; ArH), 7.34 (s, 4H; ArH), 7.26 (s, 4H; ArH), 5.84 (s, 2H; ArH), 1.52 (s, 36H;  $\text{C}(\text{CH}_3)_3$ ), 1.30 (s, 36H;  $\text{C}(\text{CH}_3)_3$ ) ppm;  $^{13}\text{C}\{^1\text{H}\}$  NMR (100 MHz;  $\text{DMF-}d_7$ ):  $\delta$  = 178.03, 172.23, 164.09, 163.34, 161.76, 142.04, 141.65, 140.84, 134.65, 130.62, 129.80, 125.58, 119.77, 117.78, 116.44, 114.55, 111.71, 36.31, 31.95, 30.27 ppm; MS (MALDI-TOF+, pyrene)  $m/z$  = 1806.4 ( $\text{M}^+$ ) (calcd. 1806.5); UV-Vis ( $c$  = 0.18 mg in 10 mL, toluene):  $\lambda_{\text{max}}$  ( $\epsilon$ ) = 331 nm ( $46213 \text{ mol}^{-1} \cdot \text{m}^3 \cdot \text{cm}^{-1}$ ),  $\lambda$  ( $\epsilon$ ) = 467 nm ( $32899 \text{ mol}^{-1} \cdot \text{m}^3 \cdot \text{cm}^{-1}$ ); elemental analysis calcd. (%) for  $\text{C}_{100}\text{H}_{104}\text{N}_8\text{O}_8\text{Zn}_4 \cdot \text{CHCl}_3 \cdot 4\text{H}_2\text{O}$ : C 60.69, H 5.70, N 5.61; found: C 60.77, H 5.58, N 5.57.

**tetra-Pd(salphen) complex (4):** A solution of **3** (19.5 mg, 0.0108 mmol) and  $\text{Pd}(\text{OAc})_2$  (9.93 mg, 0.044 mmol) in THF (15 mL) was stirred for 20 h at r.t. The solvent was removed in vacuo and the residue was triturated with MeOH (20 mL) and filtered to give a red-brown solid. Yield: 19.5 mg (0.0099 mmol, 92%).  $^1\text{H}$  NMR (400 MHz,  $\text{DMSO-}d_6$  + pyridine/butylamine as additives):  $\delta$  = 9.13 (s, 4H; CH=N), 8.96 (s, 4H; CH=N), 8.63 (m, J not resolved, Pyr-H), 8.48 (s,



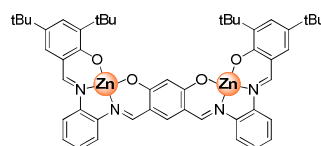
4H; ArH), 8.38 (d,  $^3J$  = 8.5 Hz, 4H; ArH), 7.96 (m, J not resolved; Pyr-H), 7.90 (s, 2H; ArH), 7.77 (d,  $^3J$  = 8.0 Hz, 4H; ArH), 7.62 (m, J not resolved, Pyr-H), 7.57 (s, 4H; ArH), 7.44 (s, 4H; ArH), 5.84 (s, 2H; ArH). MS (MALDI-TOF+, pyrene):  $m/z$  = 1971.4 ( $\text{M}+\text{H}^+$ ) (calcd 1971.4), 1928.4 ( $\text{M} - \text{C}_3\text{H}_6$ )<sup>+</sup> (calcd. 1928.4); HRMS (MALDI+) calcd. for  $[\text{C}_{100}\text{H}_{104}\text{N}_8\text{O}_8\text{Pd}_4]^+$ : 1968.4111; found: 1968.3750; UV-Vis ( $c$  = 0.19 mg in 8 mL, toluene):  $\lambda_{\text{max}}$  ( $\epsilon$ ) = 355 nm ( $101333 \text{ mol}^{-1} \cdot \text{m}^3 \cdot \text{cm}^{-1}$ ),  $\lambda$  ( $\epsilon$ ) = 481 nm ( $74416 \text{ mol}^{-1} \cdot \text{m}^3 \cdot \text{cm}^{-1}$ ),  $\lambda$  ( $\epsilon$ ) = 516 nm ( $59660 \text{ mol}^{-1} \cdot \text{m}^3 \cdot \text{cm}^{-1}$ ).

**bis-Zn(salphen) complex (6):** To a solution of diimine **1** (63.4 mg, 0.098 mmol) in  $\text{CHCl}_3$  (20 mL) was first added a solution of salicylaldehyde **5** (26.4 mg, 0.216 mmol) in MeOH (10 mL). Then a solution of  $\text{Zn}(\text{OAc})_2 \cdot 2\text{H}_2\text{O}$  (49.4 mg, 0.225 mmol) in MeOH (5 mL) was added and a color change occurs from yellow to orange. The reaction mixture was stirred at rt for 18 h. The desired compound was isolated by filtration and dried in vacuo to yield an orange solid (75.3 mg, 0.076 mmol, 85%).  $^1\text{H}$  NMR (400 MHz,  $\text{DMSO-}d_6$ ):  $\delta$  = 9.22 (s, 2H; CH=N), 9.04 (s, 2H; CH=N), 8.29 (s, 2H; ArH), 8.02 (d,  $^3J$  = 8.9 Hz, 2H; ArH), 7.87 (dd,  $^3J$  = 8.9,  $^4J$  = 1.4 Hz, 2H; ArH), 7.50



(dd,  $^3J = 8.0$ ,  $^4J = 1.6$  Hz, 2H; ArH), 7.34 (d,  $^4J = 2.5$  Hz, 2H; ArH), 7.27 (d,  $^4J = 2.4$  Hz, 2H; ArH), 7.24 (d,  $^3J = 7.6$  Hz, 2H; ArH), 6.69 (d,  $^3J = 8.6$  Hz, 2H; ArH), 6.55 (t,  $^3J = 7.3$  Hz, 2H; ArH), 1.51 (s, 18H; C(CH<sub>3</sub>)<sub>3</sub>), 1.30 (s, 18H; C(CH<sub>3</sub>)<sub>3</sub>) ppm;  $^{13}\text{C}\{^1\text{H}\}$  NMR (100 MHz, DMSO-*d*<sub>6</sub>):  $\delta = 172.24$ , 170.53, 163.26, 163.04, 140.72, 139.60, 139.50, 137.74, 136.21, 134.20, 133.38, 129.57, 128.55, 125.65, 123.45, 119.63, 118.30, 116.89, 114.44, 112.86, 35.17, 33.56, 31.35, 29.65 ppm; MS (MALDI-TOF+, pyrene):  $m/z = 981.3$  (M + H)<sup>+</sup> (calcd. 981.3), 967.3 (M + H - CH<sub>3</sub>)<sup>+</sup> (calcd. 967.3); UV-Vis (*c* = 0.18 mg in 8 mL, toluene):  $\lambda_{\text{max}}$  ( $\epsilon$ ) = 324 nm (47369 mol<sup>-1</sup>·m<sup>3</sup>·cm<sup>-1</sup>),  $\lambda$  ( $\epsilon$ ) = 421 nm (34594 mol<sup>-1</sup>·m<sup>3</sup>·cm<sup>-1</sup>),  $\lambda$  ( $\epsilon$ ) = 483 nm (34999 mol<sup>-1</sup>·m<sup>3</sup>·cm<sup>-1</sup>); elemental analysis calcd. (%) for C<sub>56</sub>H<sub>58</sub>N<sub>4</sub>O<sub>4</sub>Zn<sub>2</sub>·3H<sub>2</sub>O: C 64.93, H 6.23, N 5.41; found: C 65.18, H 5.95, N 5.34.

**bis-Zn(salphen) complex (9):** A mixture of 2-[(2-aminophenyl)imino]methyl]-4,6-bis(1,1-dimethylethyl)-phenol[<sup>24</sup>] (94.6 mg, 0.29 mmol), 4,6-dihydroxy-1,3-benzenedicarboxaldehyde **2** (24.2 mg, 0.14 mmol) and



Zn(OAc)<sub>2</sub>·2H<sub>2</sub>O (70.03 mg, 0.30 mmol) was stirred in MeOH (35 mL) for 24 h at rt. A yellow solid was isolated by filtration (69.5 mg, 0.077 mmol, 55%). <sup>1</sup>H NMR (400 MHz, DMSO-*d*<sub>6</sub>):  $\delta = 8.94$  (s, 2H; CH=N), 8.80 (s, 2H; CH=N), 7.84 (dd,  $^3J = 7.5$  Hz,  $^4J = 2.0$  Hz, 2H; ArH), 7.78 (dd,  $^3J = 7.6$ ,  $^4J = 2.0$  Hz, 2H; ArH), 7.63 (s, 1H; ArH), 7.32 (m, 4H; ArH), 7.21 (s, 2H; ArH), 5.75 (s, 1H; ArH), 1.50 (s, 18H; C(CH<sub>3</sub>)<sub>3</sub>), 1.29 (s, 18H; C(CH<sub>3</sub>)<sub>3</sub>) ppm;  $^{13}\text{C}\{^1\text{H}\}$  NMR (100 MHz, DMSO-*d*<sub>6</sub>):  $\delta = 176.17$ , 170.31, 163.21, 159.78, 149.78, 140.60, 139.84, 139.52, 133.20, 129.51, 128.29, 126.63, 126.28, 118.22, 116.30, 115.59, 114.55, 110.40, 35.16, 33.53, 31.35, 29.64 ppm. MS (MALDI-TOF+, pyrene):  $m/z = 1810.6$  (2M<sup>+</sup>) (calcd 1810.5), 906.3 (M+H)<sup>+</sup> (calcd 906.3), 889.3 (M - CH<sub>3</sub>)<sup>+</sup> (calcd. 889.3); UV-Vis (*c* = 0.18 mg in 8 mL, toluene):  $\lambda$  ( $\epsilon$ ) = 326 nm (9320 mol<sup>-1</sup>·m<sup>3</sup>·cm<sup>-1</sup>),  $\lambda_{\text{max}}$  ( $\epsilon$ ) = 436 nm (9480 mol<sup>-1</sup>·m<sup>3</sup>·cm<sup>-1</sup>),  $\lambda$  ( $\epsilon$ ) = 484 nm (9360 mol<sup>-1</sup>·m<sup>3</sup>·cm<sup>-1</sup>); elemental analysis calcd. (%) for C<sub>50</sub>H<sub>54</sub>N<sub>4</sub>O<sub>4</sub>Zn<sub>2</sub>·H<sub>2</sub>O: C 65.01; H 6.11, N 6.07; found: C 64.76, H 5.83, N 5.89.

## 2.7 References and notes

- [1] a) P. A. Vigato, S. Tamburini, *Coord. Chem. Rev.* **2004**, *248*, 1717; b) N. E. Borisova, M. D. Reshetova, Y. A. Ustynyuk, *Chem. Rev.* **2007**, *107*, 46.
- [2] a) J. L. Sessler, E. Tomat, T. D. Mody, V. M. Lynch, J. M. Veauthier, U. Mirsaidov, J. T. Markert, *Inorg. Chem.* **2005**, *44*, 2125; b) S. J. Wezenberg, A. W. Kleij, *Angew.*

- Chem. Int. Ed.* **2008**, *47*, 2354; c) A. Martinez, C. Hemmert, B. Meunier, *J. Cat.* **2005**, *234*, 250; d) A. Martinez, C. Hemmert, C. Loup, G. Barré, B. Meunier, *J. Org. Chem.* **2006**, *71*, 1449; e) K. C. Gupta, A. K. Sutar, *Coord. Chem. Rev.* **2008**, *252*, 1420.
- [3] a) J. Jiang, M. J. MacLachlan, *Chem. Commun.* **2009**, 5695; b) J. L. Sessler, S. Camiolo, P. A. Gale, *Coord. Chem. Rev.* **2003**, *240*, 17; c) M. A. Palacios, R. Nishiyabu, M. Marquez, P. Anzensbacher Jr, *J. Am. Chem. Soc.* **2007**, *129*, 7538; d) G. Givaja, M. Volpe, J. W. Leeland, M. A. Edwards, T. K. Young, S. B. Darby, S. D. Reid, A. J. Blake, C. Wilson, J. Wolowska, E. J. L. McInnes, M. Schröder, J. B. Love, *Chem. Eur. J.* **2007**, *13*, 3707.
- [4] For an example see: S. S. Tandon, S. D. Bunge, L. K. Thompson, *Chem. Commun.* **2007**, 798.
- [5] For an overview of template approaches in salen chemistry: A. W. Kleij, *Chem. Eur. J.* **2008**, *14*, 10520.
- [6] a) V. McKee, W. B. Shepard, *J. Chem. Soc., Chem. Commun.* **1985**, 158; b) Y. Nakamura, M. Yonemura, K. Arimura, N. Usuki, M. Ohba, H. Okawa, *Inorg. Chem.* **2001**, *40*, 3739; For a template approach towards oxime-based metallomacrocycles see: c) S. Tashiro, A. Minoda, M. Yamada, M. Shionoya, *Inorg. Chem.* **2009**, *48*, 10093; d) S. Akine, S. Sunaga, T. Taniguchi, H. Miyazaki, T. Nabeshima, *Inorg. Chem.* **2007**, *46*, 2959; e) S. Akine, S. Kagiya, T. Nabeshima, *Inorg. Chem.* **2007**, *46*, 9525.
- [7] A. M. Castilla, S. Curreli, E. C. Escudero-Adán, M. Martínez Belmonte, J. Benet-Buchholz, A. W. Kleij, *Org. Lett.* **2009**, *11*, 5218.
- [8] For recent examples of salen-based macrocycles see: a) J. K.-H. Hui, M. J. MacLachlan, *Chem. Commun.* **2006**, 2480; b) P. D. Frischmann, J. Jiang, J. K.-H. Hui, J. J. Grzybowski, M. J. MacLachlan, *Org. Lett.* **2008**, *10*, 1255; c) C. T. L. Ma, M. J. MacLachlan, *Angew. Chem. Int. Ed.* **2005**, *44*, 4178; d) A. M. Gallant, M. J. MacLachlan, *Angew. Chem. Int. Ed.* **2003**, *42*, 5307; e) S. Akine, D. Hashimoto, T. Saiki, T. Nabeshima, *Tetrahedron Lett* **2004**, *45*, 4225.
- [9] M. E. Germain, M. J. J. Knapp, *J. Am. Chem. Soc.* **2008**, *130*, 5422.
- [10] The multivalency concept describes a self-assembly pathway where simultaneous interactions take place between complementary functionalities of two or more entities. Here, the four Zn(salphen) units of macrocycle **3** (or in the bimetallic Zn(salphen) complex **9**) interact with those of another molecule of **3**. For some leading references on the multivalency concept: a) A. Mulder, J. Huskens, D. N. Reinhoudt, *Org. Biomol. Chem.* **2004**, *2*, 3409; b) M. Mammen, S.-K. Choi, G. M. Whitesides, *Angew. Chem.*

- Int. Ed.* **1998**, *37*, 2754; c) G. Ercolani, *J. Am. Chem. Soc.* **2003**, *125*, 16097; d) C. A. Hunter, H. L. Anderson, *Angew. Chem. Int. Ed.* **2009**, *48*, 7488.
- [11] a) A. C. W. Leung, M. J. MacLachlan, *J. Mater. Chem.* **2007**, *17*, 1923; b) J. K.-H. Hui, Z. Yu M. J. MacLachlan, *Angew. Chem. Int. Ed.* **2007**, *46*, 7980; c) A. W. Kleij, *Dalton Trans.* **2009**, 4635.
- [12] S. Curreli, E. C. Escudero-Adán, J. Benet-Buchholz, A. W. Kleij, *J. Org. Chem.* **2007**, *72*, 7018.
- [13] L. R. Worden, K. D. Kaufman, P. J. Smith, G. N. Widiger, *J. Chem. Soc. C* **1970**, 227.
- [14] The synthetic procedure was repeated three times with similar results.
- [15] For full details on this transmetalation protocol: E. C. Escudero-Adán, J. Benet-Buchholz, A. W. Kleij, *Inorg. Chem.* **2007**, *46*, 7265.
- [16] E. C. Escudero-Adán, J. Benet-Buchholz, A. W. Kleij, *Eur. J. Inorg. Chem.* **2009**, 3562.
- [17] For recent examples see: a) J. Flapper, J. N. H. Reek, *Angew. Chem. Int. Ed.* **2007**, *46*, 8590; b) A. W. Kleij, D. M. Tooke, M. Kuil, M. Lutz, A. L. Spek, J. N. H. Reek, *Chem. Eur. J.* **2005**, *11*, 4743; c) S. J. Wezenberg, E. C. Escudero-Adán, J. Benet-Buchholz, A. W. Kleij, *Org. Lett.* **2008**, *10*, 3311.
- [18] A. L. Singer, D. A. Atwood, *Inorg. Chim. Acta* **1998**, *277*, 157.
- [19] The self-assembly (or self-dimerization) of Zn(salen)s via  $\mu_2$ -O coordination motifs has been well-documented, see for instance: a) J. K.-H. Hui, Z. Yu, T. Mirfakhrai, M. J. MacLachlan, *Chem. Eur. J.* **2009**, *15*, 13456; b) G. Consiglio, S. Failla, P. Finocchiaro, I. P. Oliveri, R. Purrello, S. Di Bella, *Inorg. Chem.* **2010**, *49*, 5134; See also references 8c, 11, 17 and 19.
- [20] We have reported on the very strong self-association ( $K_{\text{dimer}} = 3.2 \times 10^8 \text{ M}^{-1}$ ) of a comparable mononuclear Zn(salphen) complex. See: a) J. A. A. W. Elemans, S. J. Wezenberg, E. C. Escudero-Adán, J. Benet-Buchholz, D. den Boer, M. J. J. Coenen, S. Speller, A. W. Kleij, S. de Feyter, *Chem. Commun.* **2010**, *46*, 2548; b) M. Martínez Belmonte, S. J. Wezenberg, R. M. Haak, D. Anselmo, E. C. Escudero-Adán, J. Benet-Buchholz, A. W. Kleij, *Dalton Trans* **2010**, *39*, 4541.
- [21] For a recent example of hyperchromic effects with DNA see: C. A. S. A. Minetti, D. P. Remeta and K. J. Breslauer, *Proc. Natl. Acad. Sci. USA.* **2008**, *105*, 70.
- [22] Please note that **3** has low solubility in  $\text{CH}_2\text{Cl}_2$  and that consequently the quality of the mass spectrum obtained is affected.
- [23] a) A. W. Kleij, D. M. Tooke, M. Lutz, A. L. Spek, J. N. H. Reek, *Eur. J. Inorg. Chem.* **2005**, 4626; b) A. W. Kleij, D. M. Tooke, M. Kuil, M. Lutz, A. L. Spek, J. N. H. Reek, *Chem. Eur. J.* **2005**, *11*, 4743.

- [24] M.-A. Muñoz-Hernández, T. S. Keizer, S. Parkin, B. Patrick, D. A. Atwood, *Organometallics* **2000**, *19*, 4416.
- [25] M. J. Frisch, G.W. Trucks, H. B. Schlegel, G. E. Scuseria, M. A. Robb, J. R. Cheeseman, J. A. Montgomery Jr., T. Vreven, K. N. Kudin, J. C. Burant, J. M. Millam, S. S. Iyengar, J. Tomasi, V. Barone, B. Mennucci, M. Cossi, G. Scalmani, N. Rega, G. A. Petersson, H. Nakatsuji, M. Hada, M. Ehara, K. Toyota, R. Fukuda, J. Hasegawa, M. Ishida, T. Nakajima, Y. Honda, O. Kitao, H. Nakai, M. Klene, X. Li, J. E. Knox, H. P. Hratchian, J.B. Cross, C. Adamo, J. Jaramillo, R. Gomperts, R. E. Stratmann, O. Yazyev, A. J. Austin, R. Cammi, C. Pomelli, J. Ochterski, P. Y. Ayala, K. Morokuma, G. A. Voth, P. Salvador, J. J. Dannenberg, V. G. Zakrzewski, S. Dapprich, A. D. Daniels, M. C. Strain, O. Farkas, D. K. Malick, A. D. Rabuck, K. Raghavachari, J. B. Forestman, J. V. Ortiz, Q. Cui, A. G. Baboul, S. Clifford, J. Cioslowski, B. B. Stefanov, G. Liu, A. Liashenko, P. Piskorz, I. Komaromi, R. L. Martin, D. J. Fox, T. Keith, M. A. Al-Laham, C. Y. Peng, A. Nanayakkara, M. Challacombe, P. M. W. Gill, B. Johnson, W. Chen, M. W. Wong, C. Gonzales, J. A. Pople, *Gaussian 03. [revision D.01]* **2004**, Wallingford CT, Gaussian Inc.
- [26] A. D. Becke, *J. Chem. Phys.* **1993**, *98*, 5648.
- [27] J. P. Perdew, *Phys. Rev. B.* **1986**, *33*, 8822.
- [28] P. J. Hay, W. R. Wadt, *J. Chem. Phys.* **1985**, *82*, 270.
- [29] A. D. McLean, G. S. Chandler, *J. Chem. Phys.* **1980**, *72*, 5639.
- [30] a) M. E. Casida, C. Jamorski, K. C. Casida, D. R. Salahub, *J. Chem. Phys.* **1998**, *108*, 4439; b) R. E. Stratmann, G. E. Scuseria, M. J. Frisch, *J. Chem. Phys.* **1998**, *109*, 8218.
- [31] a) M. Cossi, N. Rega, G. Scalmani, V. Barone, *J. Comput. Chem.* **2003**, *24*, 669; b) M. Cossi, V. Barone, *J. Chem. Phys.* **2001**, *115*, 4708.
- [32] W. R. Browne, N. M. O'Boyle, J. J. McGarvey, J. G. Vos, *Chem. Soc. Rev.* **2005**, *34*, 641.
- [33] N. M. O'Boyle and J. G. Vos, *GaussSum 1.0*, Dublin City University, Dublin (Ireland), 2005, available at <http://gausssum.sourceforge.net>.



UNIVERSITAT ROVIRA I VIRGILI

SUPRAMOLECULAR, PHOTOPHYSICAL AND CATALYTIC PROPERTIES OF ZN(SALPHEN) BASED COMPLEXES AND MATERIALS

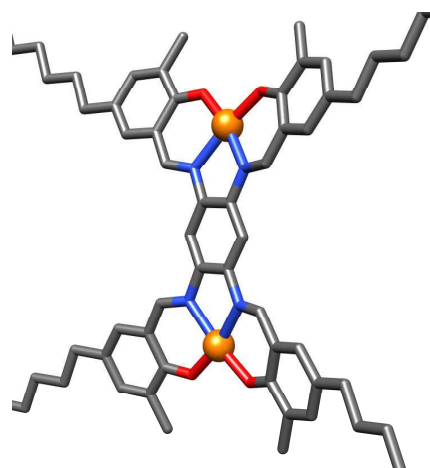
Giovanni Salassa

Dipòsit Legal: T. 1430-2013

# Chapter 3

## Extremely Strong Self-Assembly of a *bis*-Zn(Salphen) Complex Visualized at the Single-Molecule Level

*A bis-Zn(salphen) structure shows extremely strong self-assembly both in solution as well as at the solid-liquid interface as evidenced by scanning tunneling microscopy (STM), competitive UV-Vis and fluorescence titrations, dynamic light scattering (DLS) and transmission electron microscopy (TEM). DFT analysis on the bis-Zn(salphen) rationalizes the most probable binding mode of the self-assembled structures provoked by unusual oligomeric (Zn–O)<sub>n</sub> coordination motifs within the assembly. The high stability of the multinuclear structure therefore holds great promise for the development of stable self-assembled monolayers with potential for new opto-electronic materials.*



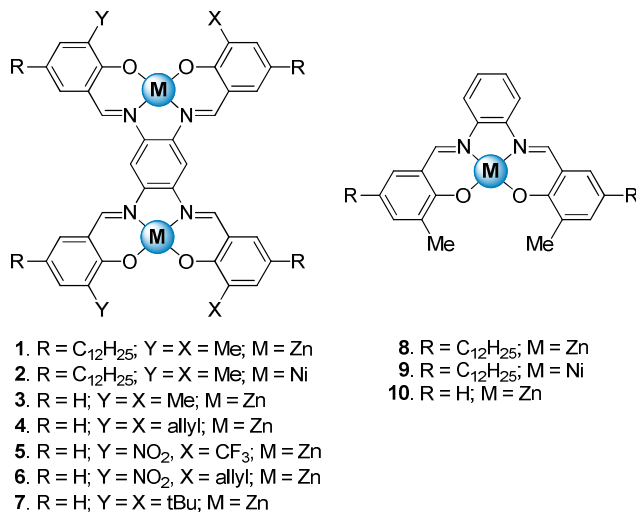
The work described in this chapter has been published: G. Salassa, M. J. J. Coenen, S. J. Wezenberg, B. L. M. Hendriksen, S. Speller, J. A. A. W. Elemans, A. W. Kleij, *J. Am. Chem. Soc.* **2012**, *134*, 7186.

### 3.1 Introduction

Supramolecular aggregation or polymerization<sup>[1]</sup> is a vibrant area of research providing materials that are interesting for nano-fabrication,<sup>[2]</sup> self-healing,<sup>[3]</sup> and electronic<sup>[4]</sup> applications. The use of non-covalent interactions in these polymers allows generally for a reversible assembly process, which is influenced by external stimuli such as

temperature, solvent polarity and additives. Whereas hydrogen bonding has been extensively used for supramolecular oligo- and polymerization of organic monomers,<sup>[5]</sup> metal-coordination driven self-assembly has also been demonstrated to be extremely useful in this area, especially for  $\pi$ -conjugated molecules such as porphyrin-based architectures.<sup>[6]</sup> The formation of highly stable self-assembled monolayers (SAMs) based on  $\pi$ -conjugated systems is particularly attractive in the development of functional patterned surfaces for electronic applications.<sup>[2]</sup> Crucial in these types of materials are the alignment of the molecular components and the overall stability of the system, a combination that is very difficult to control.

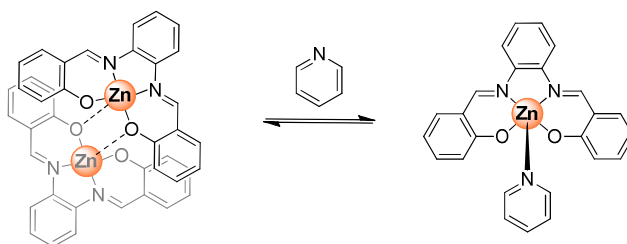
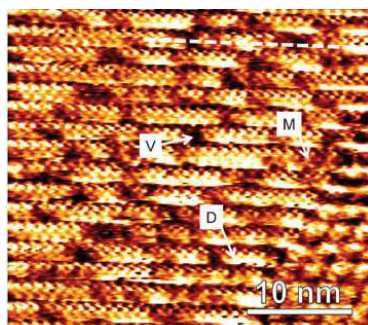
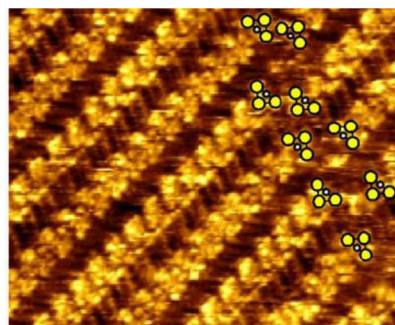
In a previous work from Kleij and co-workers, the self-assembly of mono-nuclear metallosalphen complexes (**8** and **9**; see Scheme 1) has been described at the solid-liquid interface.<sup>[7]</sup> Whereas coordinatively saturated Ni-centered complexes exclusively organize into monolayers, their Zn analogues give unusual bilayers. This is the result of strong dimerization made possible by  $\mu_2$ -phenoxo bridging (see Figure 1A) giving rise to two intermolecular Zn–O coordinative bonds.<sup>[8]</sup>



**Scheme 1.** *bis*-M(salphen)s **1-7** and mononuclear analogues **8-10**.

Furthermore, it has been demonstrated that the addition of small amounts of competitively binding pyridine (py) easily disrupts the Zn(salphen) dimer (Figure 1A). It has been previously observed that a higher nuclearity (i.e., more Zn(salphen) units per

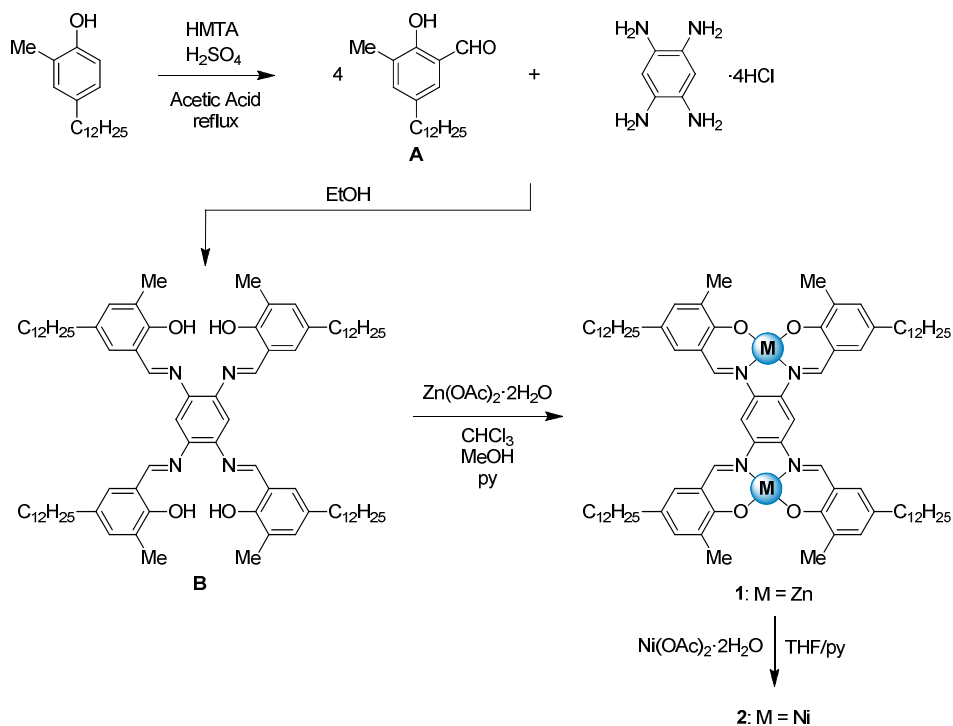
molecule) results in an up to six-fold increase in the overall stability of the formed assemblies (see Chapter 2).<sup>[9]</sup> Herein, we report on the unique self-assembly behavior of *bis*-Zn(salphen) molecules **1** and **3-6** (Scheme 1) into extremely stable oligomeric stacks both in the solution phase as well as at the solid-liquid interface. The aggregation of these dinuclear compounds was investigated by scanning tunneling microscopy (STM), competitive UV-Vis and fluorescence titrations, dynamic light scattering (DLS) and transmission electron microscopy (TEM). Molecular modeling and density functional theory (DFT) analysis have additionally been used to elucidate the most likely coordination mode, which points towards the presence of single Zn–O interactions, where each metal center in the aggregated species is axially coordinated by an oxygen donor from an adjacent *bis*-Zn(salphen) complex.

**A****B****C**

**Figure 1.** (A) Schematic representation of the equilibrium between dimeric and pyridine-ligated complex **1**. (B) STM topography of a self-assembled layer of **8** at the HOPG-TCB (highly oriented pyrolytic graphite - trichlorobenzene) interface; locations of dimeric structure (D), a monomeric structure (M) and vacancy (V) are indicated. (C) STM image of the interface between graphite and a solution of **8** and pyridine in 1-phenyloctane; some molecules are drawn in yellow schematically.

### 3.2 Synthesis of $C_{12}$ -functionalized *bis*-M(salphen) complexes

The synthesis of the *bis*-M(salphen) complexes having long alkyl chains in their 5- and 5'-positions is outlined in Scheme 2. These alkyl tails are generally required for efficient adsorption of the molecules on a graphite surface during the STM experiment. The salicylaldehyde precursor **A** was prepared via a Duff formylation of the commercially available 4-dodecyl-*o*-cresol using hexamethylenetetramine (HMTA) in acetic acid. The presence of substituents in one *ortho*- and the *para*-position of the phenol is fundamental in this reaction, resulting from the potential for addition of more than one aldehyde group. Subsequent reaction of **A** with 1,2,4,5-tetraaminobenzene tetrahydrochloride in EtOH resulted in the formation of a precipitate of **B**, which was isolated by filtration (85% yield). Metalation of ligand precursor **B** was performed using  $Zn(OAc)_2$  in a mixture of  $CHCl_3/MeOH$  and pyridine. The latter was needed to keep the intermediate(s) and product dissolved throughout the entire reaction time.



**Scheme 2.** Synthesis of  $C_{12}$ -functionalized *bis*-M(salphen) complexes **1** and **2**.

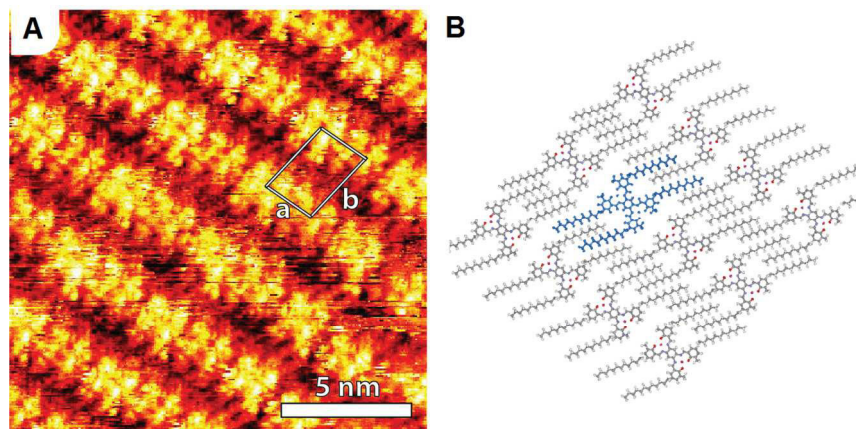
After solvent evaporation followed by trituration with MeOH, the *bis*-Zn(salphen) complex **1** was obtained in excellent yield (89%) and elemental analysis indicated that the final product is free of pyridine.<sup>[10]</sup> If the analogous Ni-centered complex is prepared in the same way, however, a mixture of products is isolated since the Ni-complex does not bind axial ligands and hence the rather insoluble mono-metallated species precipitates before full metalation can occur. *Bis*-Ni(salphen) **2** was therefore prepared in an alternative way involving transmetalation<sup>[11]</sup> of compound **1** using Ni(OAc)<sub>2</sub> in a mixture of THF and pyridine. Subsequent concentration of the solution and trituration of the crude reaction mixture in MeOH gave complex **2** in good yield (81%). Both these *bis*-M(salphen) complexes were found to be highly insoluble, which is most probably due to strong aggregation. This is supported by the increase in solubility of **1** in the presence of solvents that can coordinate to the Zn-center (*i.e.* DMSO, THF, pyridine). The *bis*-Zn(salphen) complexes **3-7**<sup>12</sup> and mononuclear **8-10**<sup>7,8</sup> (Scheme 1) were prepared using reported methods (see Experimental section for details).

### 3.3 STM studies on *bis*-M(salphen)

The aggregation behavior of dinuclear *bis*-Zn(salphen) **1** and *bis*-Ni(salphen) **2** was first studied at the single-molecule level using STM (Figures 2-4). Experiments were carried out in which the *bis*-M(salphen) complexes **1** and **2** were self-assembled at the interface of highly oriented pyrolytic graphite (HOPG) and 1,2,4-trichlorobenzene (TCB). In separate experiments, a droplet of a solution of each of the compounds was brought onto a piece of freshly cleaved graphite, and subsequently topography images were recorded by immersing the STM tip in this droplet. STM images of the monolayer of **2** reveal that the molecules are adsorbed with their extended conjugated surfaces parallel to the graphite surface (Figure 2A).

The unit cell was determined with  $a = (2.1 \pm 0.2)$  nm,  $b = (3.0 \pm 0.2)$  nm, and  $\alpha = (80 \pm 4)^\circ$ . Whilst the conjugated parts of the molecule, which appear bright in the STM image, are submolecularly resolved, the alkyl chains are only partly resolved and situated in the dark regions between the cores of **2**. The square appearance of the bright parts clearly show the internal structure of the *bis*-salphen moieties. A molecular model

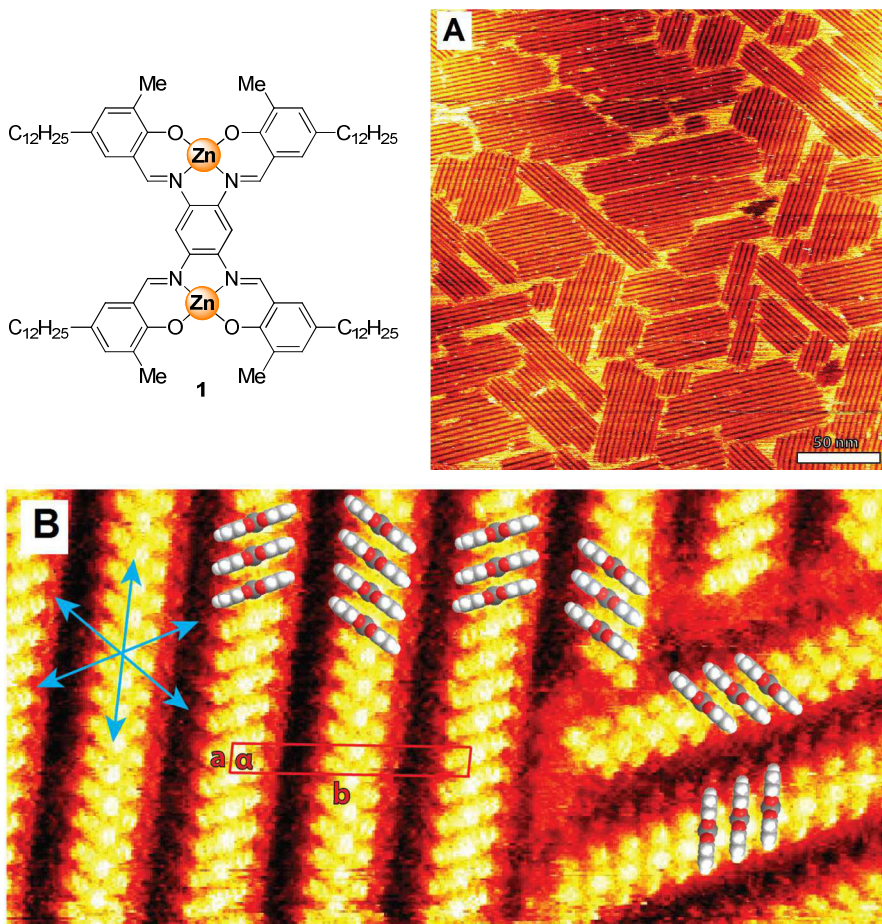
of the proposed organization of **2** at the surface, based on the unit cell parameters, is shown in Figure 2B.



**Figure 2.** (A) STM topography image of a monolayer of *bis*-Ni(salphen) complex **2** at the HOPG/TCB interface,  $V_{\text{bias}} = -550$  mV,  $i_{\text{set}} = 16$  pA, concentration  $2 \sim 10^{-4}$  M; the unit cell is indicated in red. (B) Proposed organization of the molecules of **2** in the monolayer, in which one of the molecules is colored blue for clarity. The conjugated parts of the molecule, which appear bright in the STM image, are submolecularly resolved, and the square shapes of these bright parts clearly show the internal structure of **2**.

In stark contrast to the molecules of **2**, those of *bis*-Zn(salphen) **1** were found to self-assemble exclusively with their extended conjugated surfaces perpendicular to the HOPG-TCB interface (i.e., an edge-on orientation). In the STM images (Figure 3 and Figure 4), extended domains of long lamellar arrays (stacks) of molecules of **1** are visible, which are directed along one of the HOPG symmetry directions. In these arrays, the bright salphen cores are rotated under an angle of  $\pm 60^\circ$  with respect to the lamellar direction, and this rotation is reversed in every other lamella. Both the direction of the arrays and the specific rotation of the salphen planes indicate a significant interaction of the molecules with the underlying graphite lattice. The alkyl tails reside in the dark areas in the STM images and are not well-resolved. Only very occasionally a defect in the form of missing molecules was observed. The unit cell contains two molecules of **1** (Figure 3B). Its parameters have been determined by co-imaging the monolayer together with the underlying graphite lattice, and are  $a = (0.87 \pm 0.04)$  nm,  $b = (6.4 \pm 0.1)$  nm, and  $\alpha = (87.9 \pm 0.9)^\circ$ . The difference in coordination behavior between the penta-coordinate Zn centers in **1** and the coordinatively saturated, tetra-coordinate Ni centers

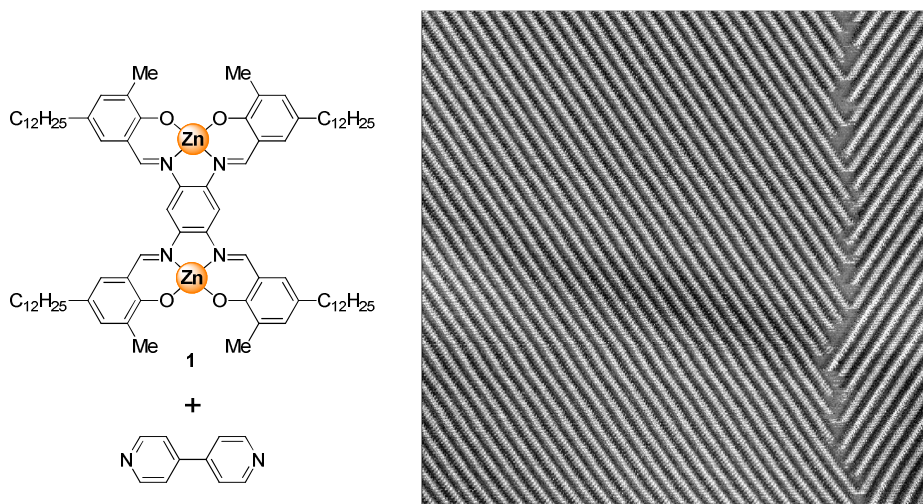
in **2** is clearly reflected in the self-assembly at the surface. The observed stacking behavior of the edge-on-oriented molecules of **1** is not only in complete contrast with the 2D self-assembly of the *bis*-Ni(salphen) **2**, but also with that of previously investigated mononuclear Zn(salphen) complexes, which were found to adsorb exclusively with their aromatic planes face-on at the solid-liquid interface.<sup>[7]</sup> Previous STM studies revealed that stacks of cyclic zinc porphyrin oligomers are also arranged edge-on at the solid/liquid interface in a similar close-packed arrangement as **1**.<sup>[13]</sup>



**Figure 3.** (A) STM topography image overviewing a monolayer of *bis*-Zn(salphen) complex **1** at the HOPG-TCB interface.  $V_{\text{bias}} = -366$  mV,  $i_{\text{set}} = 7$  pA;  $[\mathbf{1}] \approx 10^{-4}$  M. (B) STM topography image of a monolayer of **1** at the interface of HOPG and TCB/THF 95:5 (v/v);  $V_{\text{bias}} = -750$  mV,  $i_{\text{set}} = 19$  pA; some molecular models of **1** are superimposed (alkyl chains have been omitted and the orientation of the aromatic cores is tentatively proposed); in red the unit cell is depicted and the blue arrows indicate the  $\langle -1 \ 0 \ 0 \rangle$  symmetry vectors of the underlying graphite surface.



These stacks could be readily dissociated by adding ~ 10 equivalents of pyridine or 4,4'-bipyridine derivatives, which acted as disruptive axial ligands for the zinc centers. To investigate the stability of the stacked structures of **1**, STM experiments were carried out in which droplets of solutions containing potential axial ligands for the Zn centers were added in situ to the solid/liquid interface. Neither the addition of TCB solutions containing a 100-fold excess of 4,4'-bipyridine (Figure 4), nor the addition of 5% (v/v) of THF (an oxygen-donating axial ligand for **1**) to the TCB solvent (Figure 2B) resulted in any visible dissociation of the stacks with STM or a detectable change in the unit cell parameters. This might be a result of the rigidity of the stacks adsorbed on the surface, which would inhibit penetration of the axial ligands between the individual molecules of **1** due to steric reasons.



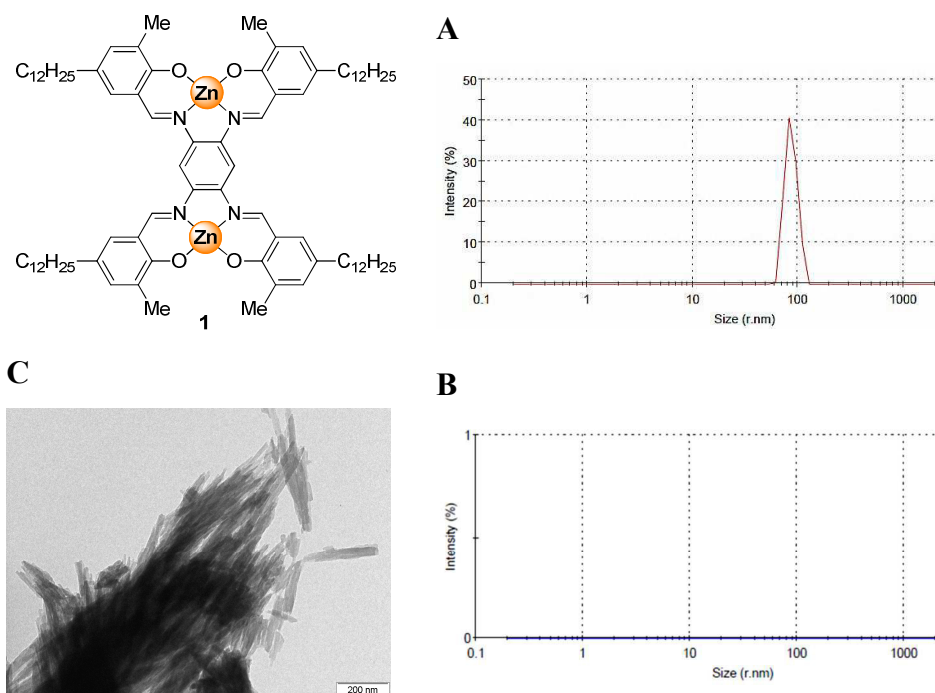
**Figure 4.** STM topography image ( $120 \times 120 \text{ nm}^2$ ) of a monolayer of **1** obtained after adding a droplet of TCB solution containing 100 equiv of 4,4'-bipyridine to the HOPG surface.  $V_{\text{bias}} = -429 \text{ mV}$ ,  $i_{\text{set}} = 12 \text{ pA}$ .

However, when the solutions of **1** and axial ligand were premixed before self-assembly at the surface, identical stacks were observed. Thus, the total inertness towards the addition of axial ligands indicates extremely high stability of these stacks. Moreover, a remarkable feature is displayed in Figure 2A where many domains of self-assembled stacks of **1** are accompanied by relatively stable patches of non-ordered surface areas. This observation indicates the presence of many nucleation sites at the surface and

suggests the absence of lower-order aggregates of **1** (such as dimers) in the solution phase.

### 3.4 Solution-phase behaviour of *bis*-Zn(salphen) (**1**)

To investigate whether the stacks of **1** also exist in the absence of a potentially stabilizing surface, dynamic light scattering (DLS) studies were carried out (Figure 5A–B). Particles in the range of 60–100 nm were observed for a  $1.1 \times 10^{-5}$  M dispersion of **1** in dry toluene; this is in line with the size of particles observed when a dried sample of the solution was analyzed by TEM (Figure 5C).



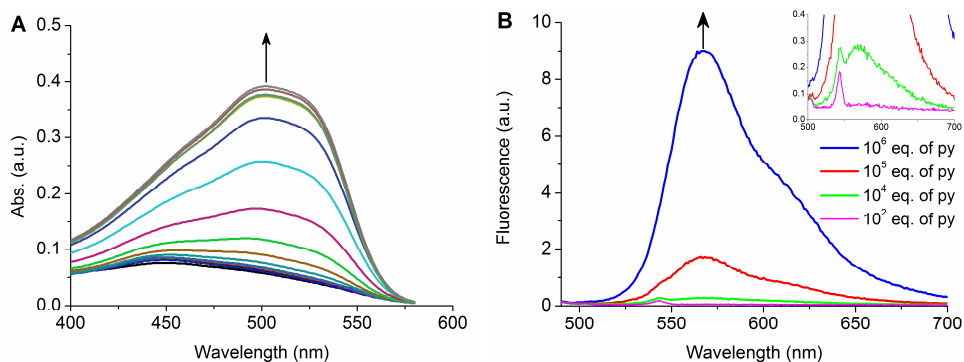
**Figure 5.** (A) Dynamic light scattering analysis of **1** ( $1.1 \times 10^{-5}$  M in dry toluene: 0.16 mg/10 mL). (B) Dynamic light scattering analysis of a mixture **1** ( $1.1 \times 10^{-5}$  M in dry toluene) and pyridine (1.33 mL). (C) Transmission electron microscopic analysis of **1**.

The addition of a very large amount of competitively binding pyridine ( $5 \times 10^5$  equiv) to the analyte solution reduced the observed size to below the DLS detection limit (Figure 5B), indicating the complete disruption of the aggregated state. These results hence indicate that the presence of a potentially stabilizing effect of a graphite surface is not a

decisive element, as highly stable aggregates are also formed when *bis*-Zn(salphen) complex **1** is dispersed in dry toluene.

### 3.5 Spectroscopic studies on *bis*-Zn(salphen) (**1**)

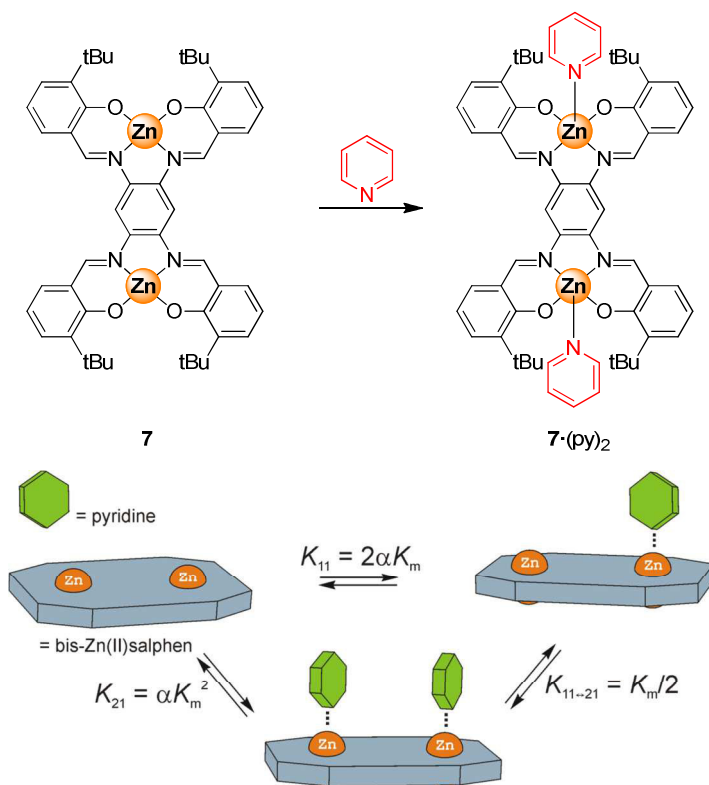
The dissociation of the aggregated state induced by competitive pyridine binding was then monitored in detail by UV-Vis and fluorescence spectroscopy. Addition of pyridine to a solution of **1** in toluene resulted in a very large increase in intensity of the UV-Vis absorption maximum around  $\lambda = 502$  nm (Figure 6A) and also of the fluorescence emission at  $\lambda = 560$  nm (Figure 6B). Similar spectroscopic behavior, although far less pronounced, has been reported for related aggregate-to-monomer transitions (see Chapter 2).<sup>[9,14]</sup> In the case of Zn(salphen) **8**, 10 equivalents of titrant were sufficient to disrupt the aggregated structure (Figure 10 in the Experimental section). For **1** complete de-aggregation could only be realized using a very high amount of 400,000 equivalents of pyridine (Figure 6A), thus its self-assembled state is significantly more stable compared to that of **8**. In order to estimate the stability of these stacked species in solution, the titration data were analysed by fitting to a binding model using Specfit/32<sup>[15]</sup> as described below.



**Figure 6.** Pyridine titration of **1** followed by UV-Vis (A,  $[1] = 0.9 \times 10^{-5}$  M in toluene) and fluorescence (B,  $[1] = 8.8 \times 10^{-7}$  M in toluene) spectroscopy.

A representative binding constant between a *bis*-Zn(salphen) complex and pyridine having a 1:2 stoichiometry was derived from a titration of pyridine to tetra-*tert*-butyl-substituted *bis*-Zn(salphen) complex **7** (Scheme 3). For this complex, aggregation via Zn–O coordination is minimized due to the steric bulk in the 3 and 3'-positions of the

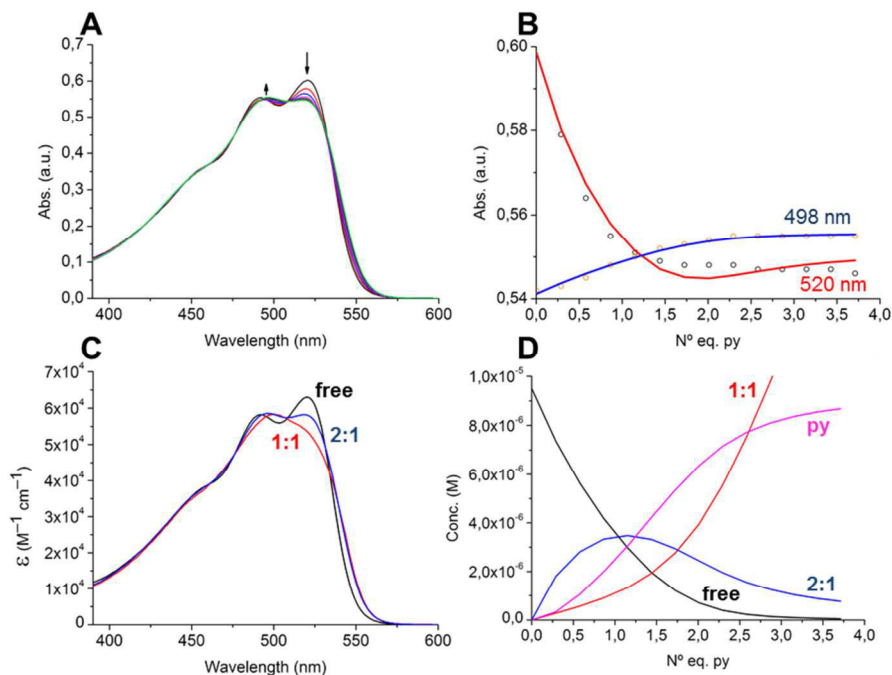
salphen ligand scaffold and hence, the Zn-centers are fully accessible for pyridine coordination.<sup>[8a,16]</sup> Upon addition of pyridine, the absorption maximum at  $\lambda = 520$  nm decreased and a new maximum appeared at  $\lambda = 498$  nm (Figure 7A). These spectral changes are completely different than those observed for complexes **1** and **3-6** without bulky *tert*-butyl groups in the *ortho*-positions and this is attributed to the absence of oligomeric species.



**Scheme 3.** Schematic representation of the species involved in the equilibria of binding pyridine to **7**. The overall binding constants  $K_{11}$  and  $K_{21}$  and stepwise constant  $K_{11 \rightarrow 21}$  are shown and related to  $K_m$  (microscopic binding constant),  $\alpha$  (cooperativity factor) and statistical correction factors.

Furthermore, clear inflection points are observed after the addition of one and two equivalents of the pyridine corresponding to formation of both the 1:1 and 1:2 complexes. The data was analyzed considering three independent colored species (i.e., the “free” *bis*-Zn(salphen), the 1:1 and 1:2 adducts; see Scheme 3) and this yielded an overall stability constant ( $K_{21}$ ) for the  $7 \cdot (\text{py})_2$  complex of  $5.81 \times 10^{11} \text{ M}^{-2}$  (see Table 1

for  $K_{11}$ ,  $K_{11\rightarrow 21}$  and the corrected microscopic constants and Figure 7D for simulated concentration profiles).



**Figure 7.** (A) Spectral changes of complex **7** upon the addition of pyridine carried out in toluene at  $[7] = 0.95 \times 10^{-5}$  M, and (B) the corresponding titration curves and data fits at  $\lambda = 498$  and 520 nm. (C) simulated spectra and (D) simulated concentration profiles for this titration at the specified equilibrium constants.

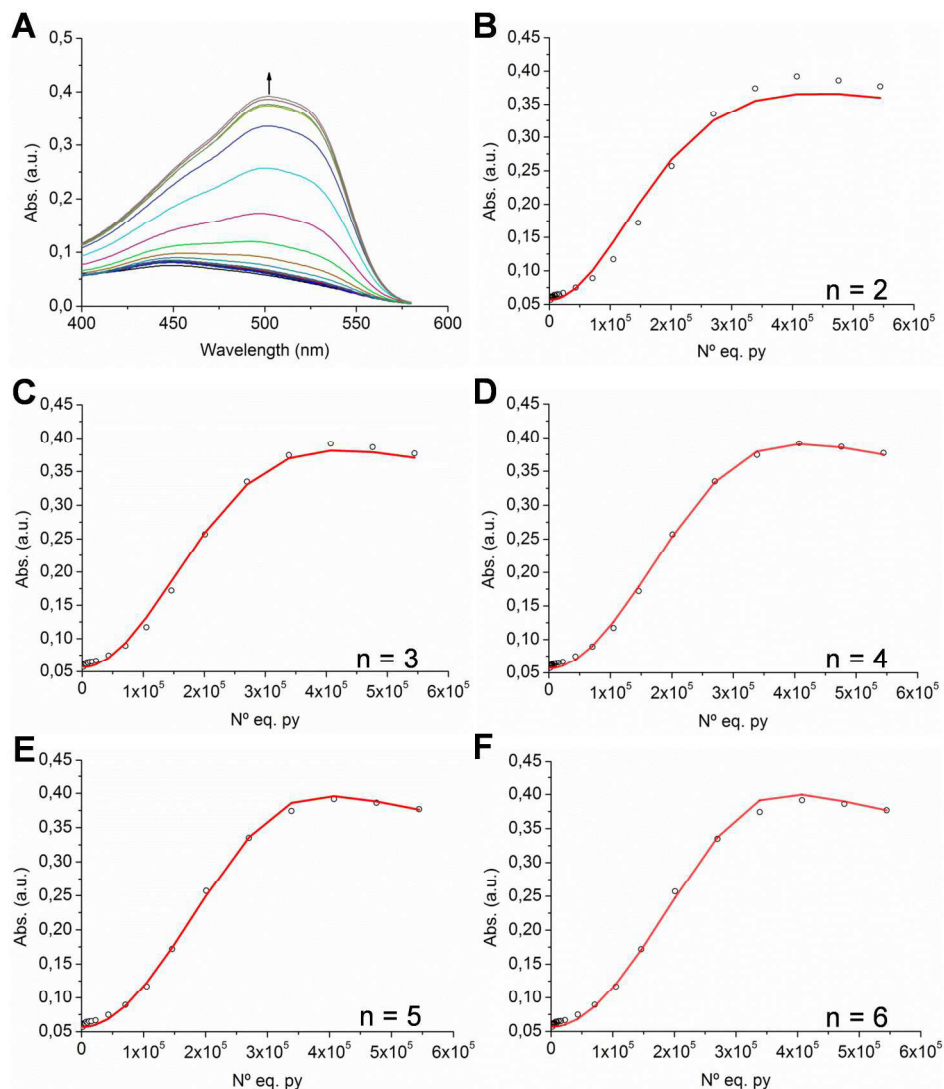
**Table 1.** Macroscopic and microscopic binding constants for the binding of pyridine to **7**.

$K_{11}$ ( $M^{-1}$ )	$K_{11\rightarrow 21}$ ( $M^{-1}$ )	$K_{21}$ ( $M^{-2}$ )	$K_1$ ( $M^{-1}$ ) <sup>a</sup>	$K_2$ ( $M^{-1}$ ) <sup>b</sup>	$\alpha$ <sup>c</sup>
$8.79 \times 10^5$	$6.61 \times 10^5$	$5.81 \times 10^{11}$	$4.40 \times 10^5$	$1.32 \times 10^6$	3.0

<sup>a</sup>  $K_1 = K_{11}/2$ . <sup>b</sup>  $K_2 = 2K_{11\rightarrow 21} = 2K_{21}/K_{11}$ , <sup>c</sup>  $\alpha = K_2/K_1$ ; this observation of cooperativity suggests that, although bulky groups are present in the 3- and 3'-position of the ligand scaffold, a weak intermolecular interaction is present between the *bis*-Zn(salphen) complexes, which is broken up after binding of the first pyridine ligand.

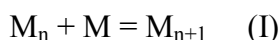
The pyridine titration data for C<sub>12</sub>-containing *bis*-Zn(salphen) complex **1** was analyzed considering the binding model shown in Scheme 4, which includes three coloured species (the “free” monomeric *bis*-Zn(salphen), the 1:2 adduct and the oligomer designated *n*-mer). The presence of a 1:1 py·**1** complex is less likely since the binding of





**Figure 8.** (a) Spectral changes of complex **1** upon the addition of pyridine carried out in toluene at  $[I] = 0.9 \times 10^{-5}$  M and (b-f) the corresponding titration curves and data fits at  $\lambda = 502$  nm for  $n = 2-6$ .

This may result in the poorer data fit for the hexameric assembly. When isodesmic behaviour is assumed, the following equations (I and II) can be considered:



$$K_{n \leftrightarrow n+1} = [M_{n+1}] / [M_n][M] = (K_n)^{1/n-1} \quad (\text{II})$$

From this data we can extrapolate that every addition of monomer to a previously formed oligomer has a remarkably high association constant in the order of about  $10^{20}$   $M^{-1}$ . These oligomers most likely cluster in solution to give the larger particles observed by DLS and TEM.

**Table 2.** Stability constants for the  $n$ -mers based on the competitive pyridine titration of **1**.

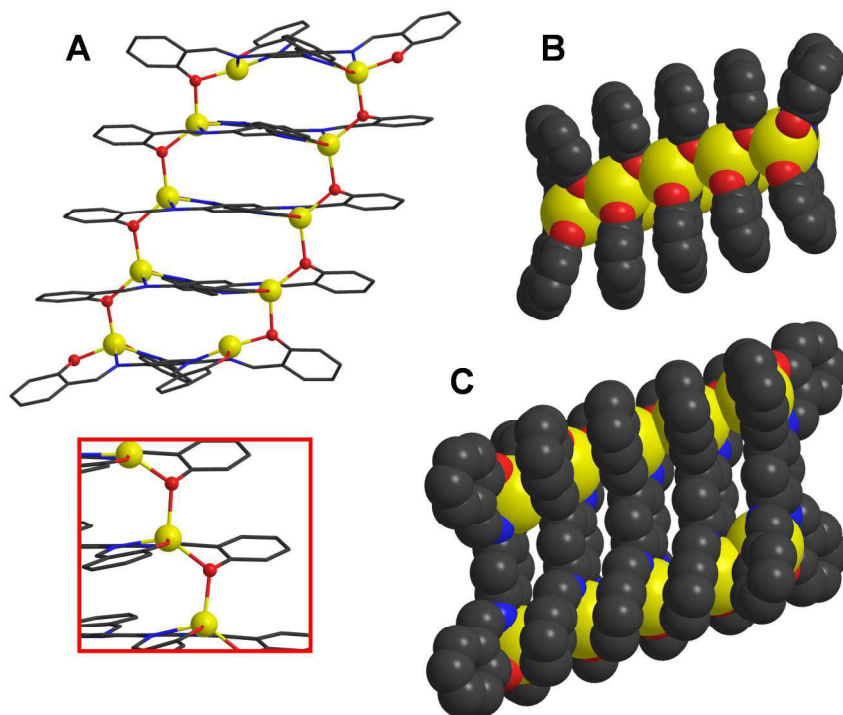
$n$	2	3	4	5	6
$K_n (M^{-(n-1)})$	$2.23 \times 10^{29}$	$5.98 \times 10^{46}$	$1.85 \times 10^{64}$	$6.11 \times 10^{81}$	$2.11 \times 10^{99}$
<b>Error (%)</b>	$\pm 0.087$	$\pm 0.044$	$\pm 0.034$	$\pm 0.034$	$\pm 0.037$

To exclude that the long alkyl chains in the 5- and 5'-positions of the salphen scaffold are the primary cause of aggregation, the same titrations for related mononuclear **10** and dinuclear complexes **3-6** (Scheme 1) were performed. Interestingly, the comparison between **1** and **3-6** gives similar results (Figures 11 in Experimental section). In the case of complexes **3-6**, between 75,000–400,000 equivalents of pyridine were needed to induce full de-aggregation. The size of the substituents in the 3- and 3'-positions of the salphen ligand, on the other hand, proved to be more influential. When bulky *tert*-butyl groups are introduced no observable aggregation is noted (see compound **7**, Figure 7). This, together with the fact that no stacks are observed with STM analysis for complex **2**,<sup>[19]</sup> clearly points to the conclusion that Zn–O interactions are the primary cause of this extremely strong aggregation.

### 3.6 Modeling and DFT studies on *bis*-Zn(salphen) (**1**)

It has been well established that *mono*-Zn(salphen) complexes may dimerize via two  $\mu_2$ -phenoxy interactions leading to the formation of a stable dimeric  $Zn_2O_2$  core unit (Figure 1A).<sup>[7,8]</sup> In order to elucidate the nature of the most likely involved coordination motifs in the self-assembled state of  $(\mathbf{1})_n$ , DFT minimization of the pentamer ( $n = 5$ ) of **1** was performed at the level of B3LYP/6-31G\* using Gaussian 09 (G09) program package<sup>[20]</sup> (Figure 9). In the case of the *bis*-Zn(salphen) complexes (cf., **1** and **3-6**) the same coordination mode (i.e., formation of dimeric  $Zn_2O_2$  units) as observed for *mono*-Zn(salphen) complexes is clearly not feasible as it leads to a heavily distorted  $Zn_2O_2$  unit and an unfavourable geometry around the Zn centers.





**Figure 9.** DFT-minimized structure for the pentameric assembly based on **1** (long tails not included): (A) Ball and stick representation of pentameric **1**, in the red inset an enlargement of the  $(\text{Zn-O})_n$  oligomeric/polymeric chains; (B) and (C) represent space filling models from different angles.

The most efficient coordination mode involves axial coordination by a phenolate O-atom of adjacent molecule forming a ladder-type structure (Figure 9, see also the STM analysis of **1**; Figure 3B). As single Zn-O interactions are prevailing, the formation of larger stacks of molecules leads to electronically more stabilized Zn centers and presumably highly stable  $(\text{Zn-O})_n$  oligomeric/polymeric chains. In this arrangement the length of the calculated Zn-O intermolecular coordinative bonds of 2.12–2.15 Å support the possibility of having strong coordinative interactions between the individual *bis*-salphen scaffolds. This preferred coordination motif in assembled  $(\mathbf{1})_n$  has been rarely observed.<sup>[21]</sup>

### 3.7 Conclusions

In summary, the reported series of *bis*-Zn(salphen) complexes (**1** and **3-6**) show unusually strong self-assembly behaviour through connecting coordination motifs that are fundamentally different from those found for self-assembled mononuclear Zn(salphen)s. All the analytical data support a very strong and rare self-assembly behaviour and the STM imaging represents the first example of visualizing such behaviour at the single molecule level. Since Zn(salphen)s are readily available and easy to modulate synthons, their utilization gives new opportunities for the controlled fabrication of nanostructured materials driven by a tuneable self-assembly process. These versatile structures are potentially useful in the creation of novel electronic and advanced opto-electronic materials.

### 3.8 Experimental section

#### General methods and materials

Complexes **4-7** and **8-10** were prepared using reported methods.<sup>[8a,12a,22]</sup> The precursor 5-dodecyl-2-hydroxy-3-methylbenzaldehyde was prepared following a previously described procedure.<sup>[7a]</sup> All other chemicals were commercial products and were used as received. <sup>1</sup>H NMR and <sup>13</sup>C{<sup>1</sup>H} NMR spectra were recorded on Bruker Avance 400 Ultrashield NMR spectrometers at 297 K. Chemical shifts are reported in ppm relative to tetramethylsilane ( $\delta = 0$  ppm) as an internal standard. Mass analyses were carried out by the Mass Spectrometry Unit at the Institute of Chemical Research of Catalonia (ICIQ), Spain. Elemental analyses were determined by the Elemental Analysis Unit of the University of Santiago de Compostela, Spain. UV-Vis spectra were recorded on a Shimadzu UV-1800 spectrophotometer. Transmission electron microscopy (TEM) was performed with a JEOL 1011 microscope operated at 100 keV. All TEM micrographs were collected using a Megaview III camera. Sample solutions were prepared and drop-casted on a copper grid cover by FORMVAR carbon film. Dynamic Light Scattering (DLS) measurements were performed with **1** in pre-dried toluene in order to determine the aggregate size. A  $1.1 \times 10^{-5}$  M mixture (0,161 mg / 10 ml) of **1** was prepared, which was decanted overnight. Afterward 1 ml of the supernatant was transferred into a glass cuvet and measured at 20°C. A second solution was prepared taking 3 ml of the  $1.1 \times 10^{-5}$  M solution of **1** and to this was added  $1 \times 10^5$  equiv of pyridine. Also this solution was decanted overnight before measuring. For the light scattering measurements a Zetasizer Nano Zs (Malvern Instruments Ltd.) with a 532 nm 'green' laser was used.

### DFT calculations

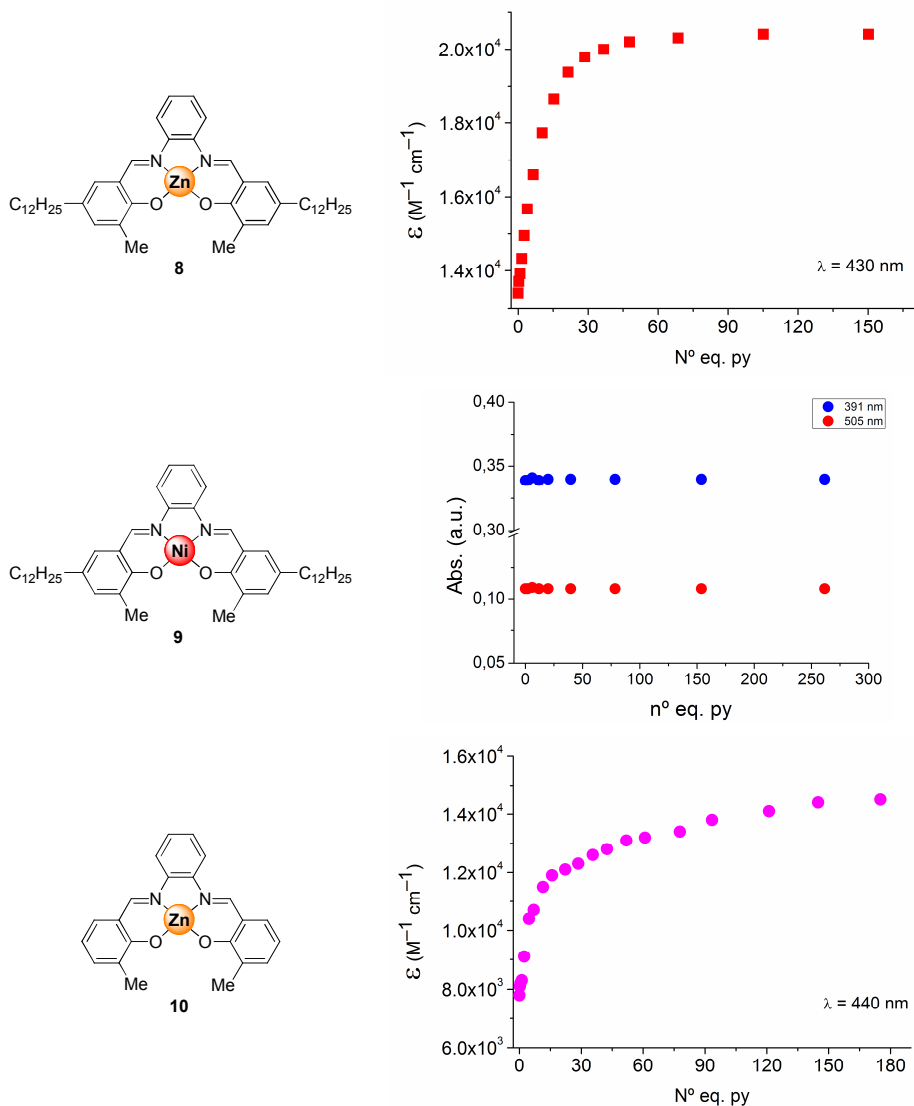
All calculations were performed with the Gaussian 09 (G09) program package<sup>[20]</sup> employing the DFT method with Becke's three parameter hybrid functional<sup>[23]</sup> and Lee–Yang–Parr's gradient-corrected correlation functional (B3LYP).<sup>[24]</sup> The LanL2DZ basis set<sup>[25]</sup> and effective core potential were used for the Zn atom, and the split-valence 6-31G\* basis set<sup>[26]</sup> was applied for all other atoms. Geometry optimizations of the complexes were performed without any constraint, and the nature of all stationary points was confirmed by normal-mode analysis.

### Scanning Tunneling Microscopy (STM)

STM was performed in the constant current mode using a home-built STM setup.<sup>[27]</sup> Tips were mechanically cut from 0.5 mm diameter Pt<sub>0.8</sub>Ir<sub>0.2</sub> wire and freshly cleaved ZYB-grade HOPG (NT-MDT) was used as a substrate. Solvents were used as received. All measurements were performed at solid/liquid interfaces created by the application of a droplet of the solution under investigation between the tip and the substrate. The piezo element of the STM was calibrated in situ by lowering the bias voltage to 100 mV and raising the tunneling current to 50 pA, which allowed imaging of the HOPG surface underneath the molecules. The raw STM data were processed only by the application of a background flattening routine.

### Competitive titrations for compounds 8-10

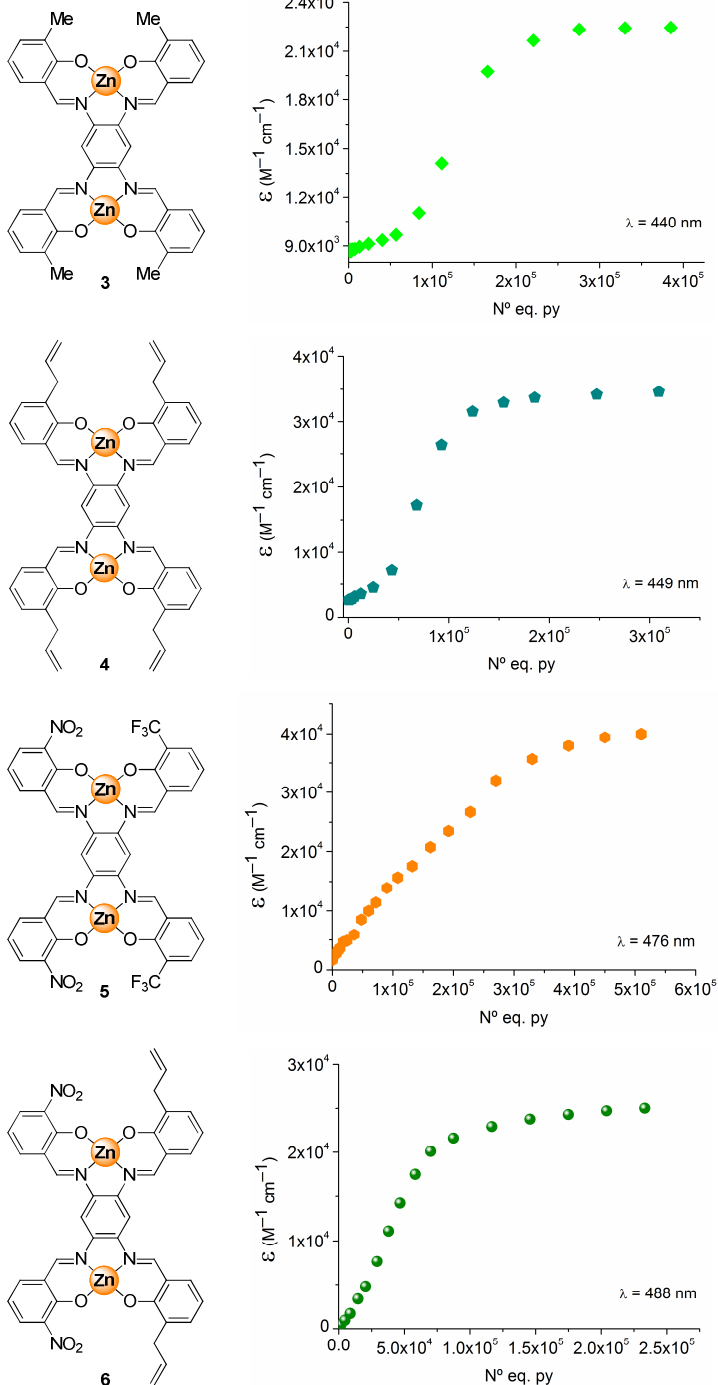
5-50  $\mu$ L aliquots of a pyridine solution in dry toluene ( $[py] = 4 \times 10^{-3}$  M for **8**;  $5 \times 10^{-3}$  M for **10**) were added stepwise to 2 mL of a solution of the guest in dry toluene with  $[8] = 0.97 \times 10^{-5}$  M or  $[10] = 4.16 \times 10^{-5}$  M in a 1 cm quartz cuvette. After each addition a UV-Vis spectrum was acquired. In the case of **9**, a solution of  $[9] = 1 \times 10^{-5}$  M in toluene has been titrated with a pyridine solution  $[py] = 4 \times 10^{-3}$  M. Below, the observed “changes” at two different wavelengths are shown. We attempted to use *bis*-Ni(salphen) complex **2** in titration experiments with pyridine but the complex proved to be virtually insoluble. Therefore, we used **9** instead to show the marked difference in self-assembly between the Ni en Zn complexes. The titration of **9** confirms that here no M–O coordinative interactions occur as the Ni(II) centres are coordinatively saturated.



**Figure 10.** UV-Vis titration curves for complexes 8-10.

### Competitive titration experiments for compounds 3-6

NOTE: all complexes have limited solubility, and in order to start with a clear analyte solution, to all samples an initial amount of 1000 equiv of pyridine was added. Afterwards, 5-50  $\mu$ L aliquots of pure pyridine were added stepwise to 2 mL of a solution of the guest (complexes 3-6) in dry toluene ( $[3] = 1.13 \times 10^{-5}$  M;  $[4] = 1.00 \times 10^{-5}$  M;  $[5] = 1.03 \times 10^{-5}$  M;  $[6] = 1.06 \times 10^{-5}$  M) in a 1 cm quartz cuvet. After each addition a UV-Vis spectrum was acquired.



**Figure 11.** UV-vis titration curves for complexes 3-6.

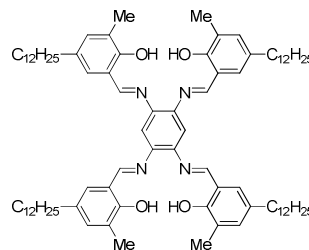
## Synthesis

### Free-base *bis*-salphen (**B**):

1,2,4,5-Tetraaminobenzene tetrahydrochloride (22 mg, 0.08 mmol), dispersed in 2 mL EtOH, was added to a stirred solution of 5-dodecyl-2-hydroxy-3-methylbenzaldehyde (99 mg, 0.33 mmol) in 2 mL EtOH.

The solution was stirred for 16 h and the yellow precipitate was filtered off, washed with EtOH, and air-dried. Yield: 84 mg (0.07 mmol, 85%).  $^1\text{H}$  NMR (400 MHz,  $\text{CDCl}_3$ ):  $\delta$  = 12.90

(s, 4H; OH), 8.69 (s, 4H; CHN), 7.11 (br, 4H; Ar-H), 7.09 (s, 2H; Ar-H), 7.07 (br, 4H; Ar-H), 2.53 (t,  $^3J$  = 7.6 Hz, 8H; Ar- $\text{CH}_2$ ), 2.28 (s, 12H; Ar- $\text{CH}_3$ ), 1.63-1.19 (m, 80H;  $\text{CH}_2$ ), 0.88 (t,  $^3J$  = 6.72 Hz, 12H;  $\text{CH}_3$ ) ppm;  $^{13}\text{C}\{^1\text{H}\}$  NMR (100 MHz,  $\text{CDCl}_3$ ):  $\delta$  = 164.4 (C=N), 157.9 (C-O), 141.7, 135.3, 133.0, 129.6, 126.3, 118.3, 122.0 (Ar-C), 35.1, 32.1, 31.9 ( $\text{CH}_2$ ), 31.1 ( $\text{CH}_3$ ), 29.8 (4), 29.7, 29.5, 29.4, 22.8 ( $\text{CH}_2$ ), 15.7, 14.3 ( $\text{CH}_3$ ) ppm; MALDI(+):  $m/z$  = 1284.1 ( $\text{M}+\text{H}$ ) $^+$ ; elemental analysis calcd. (%) for  $\text{C}_{86}\text{H}_{130}\text{N}_4\text{O}_4 \cdot 1.5\text{H}_2\text{O}$ : C 78.79, H 10.23, N 4.27; found: C 78.78, H 11.15, N 4.46.

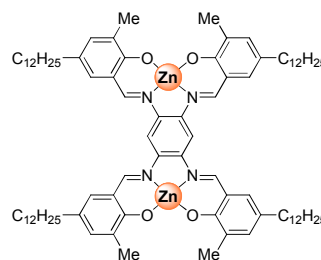


### *bis*-Zn(salphen) complex (**1**):

The free-base ligand **B** (40 mg, 0.031 mmol) was dissolved in 100 mL  $\text{CHCl}_3$ / 50 mL MeOH/ 3 mL pyridine and to the yellow suspension was added, whilst stirring, 21 mg (0.096 mmol)  $\text{Zn}(\text{OAc})_2 \cdot \text{H}_2\text{O}$ .

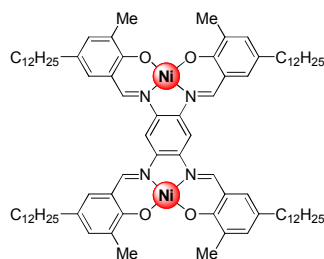
The red solution was stirred for 16 h, concentrated and redispersed in MeOH. The red precipitate was filtered off, washed vigorously with MeOH, and air-dried. Yield: 39 mg

(0.028 mmol, 89%).  $^1\text{H}$  NMR (400 MHz, 10%  $d_5$ -pyridine/ $\text{CDCl}_3$ ):  $\delta$  = 8.78 (s, 4H; CHN), 7.75 (s, 2H; Ar-H), 7.11 (s, 4H; Ar-H), 6.94 (s, 4H; Ar-H), 2.49 (t,  $^3J$  = 7.52 Hz, 8H; Ar- $\text{CH}_2$ ), 2.35 (s, 12H; Ar- $\text{CH}_3$ ), 1.60 (m, 8H;  $\text{CH}_2$ ), 1.38-1.17 (m, 72H;  $\text{CH}_2$ ), 0.87 (t,  $^3J$  = 6.46 Hz, 12H;  $\text{CH}_3$ ) ppm; poor solubility for  $^{13}\text{C}$  NMR measurement; MALDI(+):  $m/z$  = 1406.9 ( $\text{M}$ ) $^+$ ; elemental analysis calcd. (%) for  $\text{C}_{86}\text{H}_{126}\text{N}_4\text{O}_4\text{Zn}_2 \cdot 3\text{H}_2\text{O}$ : C 70.52, H 9.08, N 3.83; found: C 70.08, H 8.98, N 3.78.



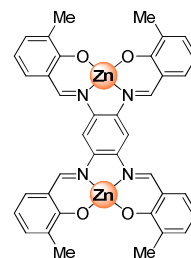
**bis-Ni(salphen) complex (2):** Bis-Zn(salphen) **1** (15 mg, 0.011 mmol) was dissolved in 50 mL THF/ 10 mL pyridine. Then Ni(OAc)<sub>2</sub>·4H<sub>2</sub>O (9 mg, 0.036 mmol) was added and the brown solution was stirred for 16 h, after which the solution was concentrated. The residue was redispersed in MeOH, filtered off, washed with MeOH and air-dried to obtain a dark brown solid. Yield: 12 mg (0.0086 mmol, 81%). <sup>1</sup>H NMR

(400 MHz, *d*<sub>5</sub>-pyridine, T = 400 K): δ = 7.76 (s, 4H; Ar-H), 6.86 (s, 4H; Ar-H), 2.65 (s, 12H; Ar-CH<sub>3</sub>), 2.59 (t, <sup>3</sup>J = 7.30 Hz, 8H; Ar-CH<sub>2</sub>), 1.68 (br, 8H; CH<sub>2</sub>), 1.57-1.22 (m, 64H; CH<sub>2</sub>), 0.96 (br, 20H; CH<sub>2</sub> and CH<sub>3</sub>) ppm, 2 × Ar-H hidden under solvent signal; too insoluble for a <sup>13</sup>C NMR measurement; MALDI(+): *m/z* = 1394.8 (M)<sup>+</sup>, 1338.8 (M-(CH<sub>2</sub>)<sub>3</sub>CH<sub>3</sub>)<sup>+</sup>; elemental analysis calcd. (%) for C<sub>86</sub>H<sub>126</sub>N<sub>4</sub>Ni<sub>2</sub>O<sub>4</sub>·4H<sub>2</sub>O: C 70.30, H 9.19, N 3.81; found: C 70.26, H 8.65, N 4.07.



**bis-Zn(salphen) complex (3):** To a solution of 1,2,4,5-tetra-aminobenzene tetrahydrochloride (306.2 mg, 1.08 mmol) and Zn(OAc)<sub>2</sub>·2H<sub>2</sub>O (1.20 g, 5.47 mmol) in 120 mL THF/ 30 mL MeOH was added a solution of 3-methyl-salicylaldehyde (810.0 mg, 5.95 mmol) in MeOH (20 mL). The reaction mixture was stirred for 4 h and then filtered giving a first fraction of product (red solid, 282.5 mg). After 3 days, the mother liquor was again filtered to give a second fraction of product (344.0 mg). Total yield: 626.5

mg (0.850 mmol, 79%). <sup>1</sup>H NMR (400 MHz, DMSO-*d*<sub>6</sub>): δ = 9.13 (s, 4H, CH=N), 8.30 (s, 2H, ArH), 7.33 (d, <sup>3</sup>J = 7.3 Hz, 4H, ArH), 7.23 (d, <sup>3</sup>J = 6.8 Hz, 4H, ArH), 6.49 (t, <sup>3</sup>J = 7.4 Hz, 4H, ArH), 2.22 (s, 12H, CH<sub>3</sub>). <sup>13</sup>C{<sup>1</sup>H} (100 MHz, DMSO-*d*<sub>6</sub> + 20% DMF-*d*<sub>7</sub>): δ = 171.34, 162.83, 138.95, 134.06, 133.85, 130.63, 118.51, 112.55, 103.92, 16.78. MS (MALDI+, dctb): *m/z* = 737.1 (M + H)<sup>+</sup> (calcd. 737.1). A sample for elemental analyses was prepared by crystallization from pyridine. Anal. calcd. for C<sub>38</sub>H<sub>30</sub>N<sub>4</sub>O<sub>4</sub>Zn<sub>2</sub>·3py·2.5H<sub>2</sub>O: C 59.94, H 4.68, N 8.13; found: C 59.88, H 4.24, N 8.52.



### 3.9 References and notes

- [1] For an essay: T. F. A. de Greef, E. W. Meijer, *Nature* **2008**, 453, 171.
- [2] a) R. van Hameren, A. M. van Buul, M. A. Castriciano, V. Villari, N. Micali, P. Schön, S. Speller, L. Monsù Scolaro, A. E. Rowan, J. A. A. W. Elemans, R. J. M. Nolte, *Nano*

- Lett.* **2008**, *8*, 253; *b*) J. C. Love, L. A. Estroff, J. K. Kriebel, R. G. Nuzzo, G. M. Whitesides, *Chem. Rev.* **2005**, *105*, 1103.
- [3] For some recent examples: *a*) M. Burnworth, L. Tang, J. R. Kumpfer, A. J. Duncan, F. L. Beyer, G. L. Fiore, S. J. Rowan, C. Weder, *Nature* **2011**, *472*, 334; *b*) P. Cordier, F. Tournilhac, C. Soulié-Ziakovic, L. Leibler, *Nature* **2008**, *451*, 977.
- [4] *a*) T. E. O. Screen, J. R. G. Thorne, R. G. Denning, D. G. Bucknall, H. L. Anderson, *J. Am. Chem. Soc.* **2002**, *124*, 9712; *b*) M. Drobizhev, Y. Stepanenko, A. Rebane, C. J. Wilson, T. E. O. Screen, H. L. Anderson, *J. Am. Chem. Soc.* **2006**, *128*, 12432.
- [5] *a*) L. Brunsveld, J. A. J. M. Vekemans, J. H. K. K. Hirschberg, R. R. Sijbesma, E. W. Meijer, *Proc. Natl. Acad. Sci. USA* **2002**, *99*, 4977; *b*) R. P. Sijbesma, F. H. Beijer, L. Brunsveld, B. J. B. Folmer, J. Hirschberg, R. F. M. Lange, J. K. L. Lowe, E. W. Meijer, *Science* **1997**, *278*, 1601. *c*) *Advances in Polymer Science – Hydrogen Bonded Polymers*, vol. 207, ed. W. Binder, Springer, Berlin **2007**.
- [6] *a*) J. K. Sprafke, B. Odell, T. D. W. Claridge, H. L. Anderson, *Angew. Chem. Int. Ed.* **2011**, *50*, 5572; *b*) F. Helmich, C. C. Lee, M. M. L. Nieuwenhuizen, J. C. Gielen, P. C. M. Christianen, A. Larsen, G. Fytas, P. E. L. G. Leclère, A. P. H. J. Schenning, E. W. Meijer, *Angew. Chem. Int. Ed.* **2010**, *49*, 3939; *c*) U. Michelsen, C. A. Hunter, *Angew. Chem. Int. Ed.* **2000**, *39*, 764; *d*) M. C. O’Sullivan, J. K. Sprafke, D. V. Kondratuk, C. Rinfrey, T. D. W. Claridge, A. Saywell, M. O. Blunt, J. N. O’Shea, P. H. Beton, M. Malfois, H. L. Anderson, *Nature* **2011**, *469*, 72; *e*) B. M. J. M. Suijkerbuijk, D. M. Tooke, A. L. Spek, G. van Koten, R. J. M. Klein Gebbink, *Chem. Asian J.* **2007**, *2*, 889; *f*) M. L. Merlau, M. del Pilar Mejia, S. T. Nguyen, J. T. Hupp, *Angew. Chem. Int. Ed.* **2001**, *40*, 4239.
- [7] J. A. A. W. Elemans, S. J. Wezenberg, E. C. Escudero-Adán, J. Benet-Buchholz, D. den Boer, M. J. J. Coenen, S. Speller, A. W. Kleij, S. de Feyter, *Chem. Commun.* **2010**, *46*, 2548.
- [8] *a*) M. Martínez Belmonte, S. J. Wezenberg, R. M. Haak, D. Anselmo, E. C. Escudero-Adán, J. Benet-Buchholz, A. W. Kleij, *Dalton Trans.* **2010**, *39*, 4541; *b*) A. W. Kleij, *Dalton Trans.* **2009**, 4635.
- [9] G. Salassa, A. M. Castilla, A. W. Kleij, *Dalton Trans.* **2011**, *40*, 5236.
- [10] As a result of the deuterated solvent mixture required (10%  $d_5$ -pyridine/ $CDCl_3$ ),  $^1H$  NMR data could not conclusively reveal the presence of coordinated pyridine in **1**.
- [11] E. C. Escudero-Adán, J. Benet-Buchholz, A. W. Kleij, *Inorg. Chem.* **2007**, *46*, 7265



- [12] a) E. C. Escudero-Adán, M. Martínez Belmonte, E. Martín, G. Salassa, J. Benet-Buchholz, A. W. Kleij, *J. Org. Chem.* **2011**, *76*, 5404. b) E. C. Escudero-Adán, J. Benet-Buchholz, A. W. Kleij, *Inorg. Chem.* **2008**, *47*, 4256.
- [13] a) J. A. A. W. Elemans, M. C. Lensen, J. W. Gerritsen, H. van Kempen, S. Speller, R. J. M. Nolte, A. E. Rowan, *Adv. Mater.* **2003**, *15*, 2070; b) M. C. Lensen, J. A. A. W. Elemans, S. J. T. van Dingenen, J. W. Gerritsen, S. Speller, A. E. Rowan, R. J. M. Nolte, *Chem. Eur. J.* **2007**, *13*, 7948.
- [14] a) C. T. L. Ma, M. J. MacLachlan, *Angew. Chem. Int. Ed.* **2005**, *44*, 4178; b) G. Consiglio, S. Failla, P. Finocchiaro, I. P. Oliveri, R. Purello, S. Di Bella, *Inorg. Chem.* **2010**, *49*, 5134; c) A. C. W. Leung, M. J. MacLachlan, *J. Mater. Chem.* **2007**, *17*, 1923. d) G. Consiglio, S. Failla, P. Finocchiaro, I. P. Oliveri, S. Di Bella, *Dalton Trans.* **2012**, *41*, 387.
- [15] *Specfit/32*TM, version 3.0; Spectra Software Associates. *Specfit/32* is a multivariate data analysis program for modeling and fitting multi-wavelength titration data sets giving more reliable parameters than single-wavelength fits. For software details and the related nonlinear algorithms see: a) H. Gampp, M. Maeder, C. J. Meyer, D. A. Zuberbühler, *Talanta* **1985**, *32*, 95; b) H. Gampp, M. Maeder, C. J. Meyer, D. A. Zuberbühler, *Talanta*, **1986**, *33*, 943.
- [16] A. W. Kleij, M. Kuil, M. Lutz, D. M. Tooke, A. L. Spek, P. J. C. Kamer, P. W. N. M. van Leeuwen, J. N. H. Reek, *Inorg. Chim. Acta* **2006**, *359*, 1807.
- [17] *n*-mer: initial UV-Vis spectrum, 1:2 and free complex: final UV-Vis spectrum of the titration data. Note that the free complex will be virtually absent throughout the titration and that its spectrum is thus arbitrary for the data fit. Nevertheless, as can be deduced from titration with *tetra*-*tert*-butyl-substituted complex **7**, it will reasonably equal the absorption spectrum of the 2:1 complex in comparison to the spectrum of the *n*-mer.
- [18] Introduction of multiple *n*-values in the same data fit led to too many free parameters in *Specfit/32* and therefore only a single *n*-value could be chosen in each fitting procedure.
- [19] It is important to note here that mono-Ni complex **9** showed virtually no change in absorption behaviour upon titration with pyridine (Figure 10 in Experimental section), suggesting that this complex is unable to have intermolecular Ni–O interactions.
- [20] *Gaussian 09*, Revision 7.0, M. J. Frisch, G. W. Trucks, H. B. Schlegel, G. E. Scuseria, M. A. Robb, J. R. Cheeseman, G. Scalmani, V. Barone, B. Mennucci, G. A. Petersson, H. Nakatsuji, M. Caricato, X. Li, H. P. Hratchian, A. F. Izmaylov, J. Bloino, G. Zheng, J. L. Sonnenberg, M. Hada, M. Ehara, K. Toyota, R. Fukuda, J. Hasegawa, M. Ishida, T. Nakajima, Y. Honda, O. Kitao, H. Nakai, T. Vreven, J. A. Montgomery, Jr., J. E.

- Peralta, F. Ogliaro, M. Bearpark, J. J. Heyd, E. Brothers, K. N. Kudin, V. N. Staroverov, R. Kobayashi, J. Normand, K. Raghavachari, A. Rendell, J. C. Burant, S. S. Iyengar, J. Tomasi, M. Cossi, N. Rega, J. M. Millam, M. Klene, J. E. Knox, J. B. Cross, V. Bakken, C. Adamo, J. Jaramillo, R. Gomperts, R. E. Stratmann, O. Yazyev, A. J. Austin, R. Cammi, C. Pomelli, J. W. Ochterski, R. L. Martin, K. Morokuma, V. G. Zakrzewski, G. A. Voth, P. Salvador, J. J. Dannenberg, S. Dapprich, A. D. Daniels, Ö. Farkas, J. B. Foresman, J. V. Ortiz, J. Cioslowski, D. J. Fox, Gaussian, Inc., Wallingford CT, **2009**.
- [21] MacLachlan et al. reported on a mono-nuclear Zn(salphen) system able to self-assemble up to a nonamer displaying a coordinative  $[Zn-O]_n$  chain. See: J. K.-H. Hui, Z. Yu, M. J. MacLachlan, *Angew. Chem. Int. Ed.* **2007**, *46*, 7980.
- [22] E. C. Escudero-Adán, J. Benet-Buchholz, A. W. Kleij, *Inorg. Chem.* **2008**, *47*, 4256.
- [23] D. Becke, *J. Chem. Phys.* **1993**, *98*, 5648.
- [24] C. Lee, W. Yang, R. G. Parr, *Phys. Rev. B: Condens. Matter* **1988**, *37*, 785.
- [25] P. J. Hay, W. R. Wadt, *J. Chem. Phys.* **1985**, *82*, 270.
- [26] A. D. McLean, G. S. Chandler, *J. Chem. Phys.* **1980**, *72*, 5639.
- [27] B. Hulsken, R. van Hameren, J. W. Gerritsen, T. Khoury, P. Thordarson, M. J. Crossley, A. E. Rowan, R. J. M. Nolte, J. A. A. W. Elemans, S. Speller, *Nat. Nanotech.* **2007**, *2*, 285.

UNIVERSITAT ROVIRA I VIRGILI

SUPRAMOLECULAR, PHOTOPHYSICAL AND CATALYTIC PROPERTIES OF ZN(SALPHEN) BASED COMPLEXES AND MATERIALS

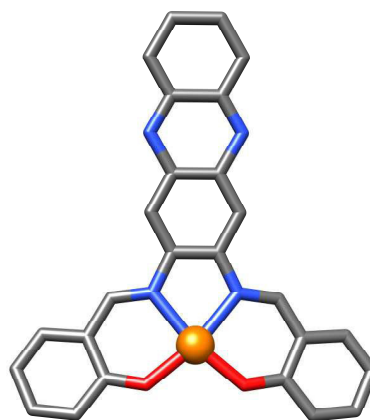
Giovanni Salassa

Dipòsit Legal: T. 1430-2013

# Chapter 4

## Photophysical Properties of Zn(Salphenazine) Complexes and their Application in Small Molecule Solar Cells

*A new family of salphen based complexes, viz. Zn(salphenazine)s, has been prepared and is characterized by a larger  $\pi$ -surface compared to standard Zn-based salphen complexes. The photophysical properties of these Zn(salphenazine)s have been studied in detail using UV-Vis and fluorescence spectroscopy, and further investigated by computational methods. The first application of a Zn(phenazine) complex in a small molecule organic solar cell (smOSC) is presented showing the potential of salphenazine systems in this area.*



The work described in this chapter is in preparation: G. Salassa, J. W. Ryan, E. C. Escudero-Adán, E. Palomares, A. W. Kleij, *to be submitted*.

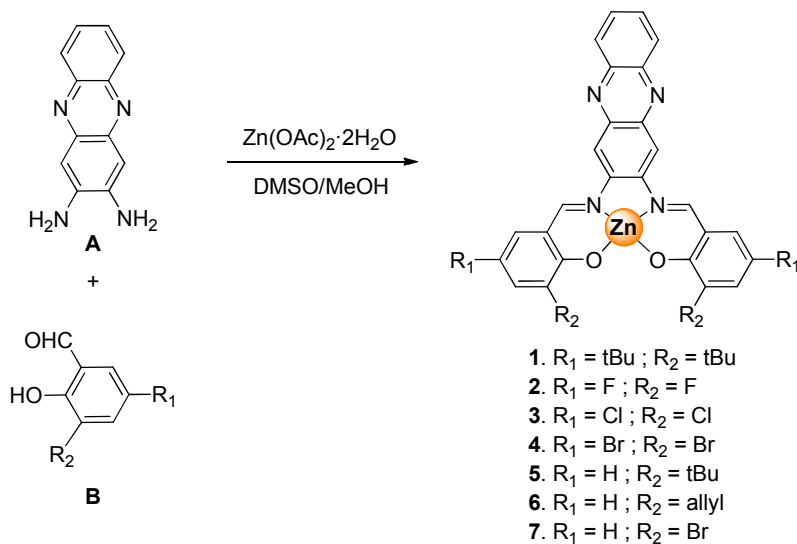
### 4.1 Introduction

Organic photovoltaics (OPVs) or organic solar cells (OSCs) have recently attracted considerable attention as renewable energy sources. These types of solar cells are characterized by a donor-acceptor bulk heterojunction and at this interface electrostatic forces are generated.<sup>[1]</sup> When the donor material absorbs a photon, an excited state is created and confined into the molecules of the material. The excited state can be regarded as an “electron-hole” pair (exciton) bound together by electrostatic interactions. In the photovoltaic cell, excitons are broken up by the effective fields created at the heterojunction with the consequent transmission of the electron from the

excited state of the donor to the excited state of the acceptor molecule. The separated electron moves to the positive electrode and the hole to the negative one, with this process thus generating a current. The first examples of OSCs were employing polymer-based materials<sup>[2]</sup> as donor and were mixed with fullerenes playing the role of acceptors. These types of devices dominated the field until 2007, after which solar cells based on solution-processable small molecules have also demonstrated to give interesting results (*i.e.* power conversion efficiency (PCE) over 7%).<sup>[3]</sup> Small molecules have rapidly evolved as alternatives in this field due to numerous advantages: their straightforward (modular) synthesis and purification, less batch-to-batch variation properties and their intrinsic monodispersity.<sup>[4]</sup> In the exploration of novel suitable small molecule donors, various systems have been examined including oligoacenes,<sup>[5]</sup> oligothiophenes,<sup>[6]</sup> boron dipyrromethenes,<sup>[7]</sup> diketopyrrolopyrroles,<sup>[8]</sup> phthalocyanines,<sup>[9]</sup> merocyanines,<sup>[10]</sup> squaraines<sup>[11]</sup> and porphyrins.<sup>[12]</sup> These latter structures (porphyrins) have shown to have highly interesting photophysical properties due to their unique macrocyclic and conjugated arrangement. Also, considering the fine-tuning of these properties there is a vast amount of literature that shows that a wide range of substituted porphyrins can be accessed with easy variations possible at the *meso* positions of the scaffold. The presence of a metal ion may also be useful to further tune the photophysical behaviour, and additionally the Zn(II) family of porphyrins has been frequently used for the creation of supramolecular structures displaying unusual photochemical features.<sup>[13]</sup>

The application of Schiff base complexes in photovoltaics has been very limited to date,<sup>[14]</sup> even though Schiff base ligands, and more particularly salen systems, are easily prepared and structurally modified; this intrinsic feature has been demonstrated to be useful in the development and optimization of metal catalysts for highly enantio-selective organic transformations.<sup>[15]</sup> Nonetheless, in the last few years an increasing interest has been noted in the photophysical properties of salphen ligands<sup>[16]</sup> and new interesting applications in field of photo-functional materials have appeared.<sup>[17]</sup> Che and co-workers reported the application of Pt(salphen) complexes in high-performance OLEDs, and they have shown the potential of the  $\pi$ -conjugation in these salphens.<sup>[18]</sup> In this study, we present the synthesis and a detailed study of the photophysical properties of a (relatively) new type of Zn(salphen) complex having a phenazine moiety in the

backbone (i.e., a *salphenazine* complex).<sup>[19]</sup> This alternative salen scaffold with a more extensive  $\pi$ -conjugated structure compared to typical salen ligands is shown herein to be an attractive candidate for the development of new sm(O)SC.

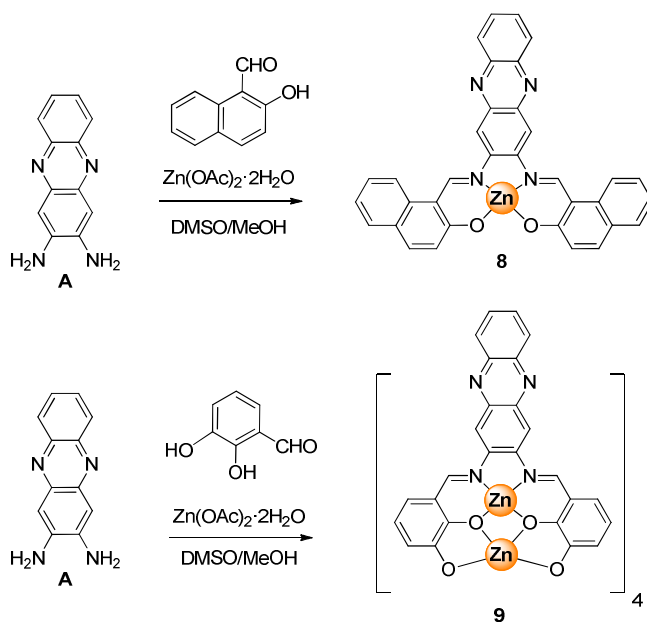


**Scheme 1.** Synthesis of salphenazine complexes **1-7** from precursors **A** and **B**.

## 4.2 Synthesis of Zn(salphenazine) complexes

Zn(salphenazine) complexes **1-7** have been synthesized through a one pot reaction between 2,3-diaminophenazine **A**, substituted salicylaldehydes **B** and  $\text{Zn(OAc)}_2 \cdot 2\text{H}_2\text{O}$  as templating agent (see Experimental section and Scheme 1). Since 2,3-diaminophenazine **A** is relatively insoluble in a wide range of solvents, the reaction was performed in a minimum amount of DMSO at 100°C. This approach allows maintaining all the reagents and intermediates in solution while the product mostly precipitates after a few hours (in some cases addition of MeOH is needed to obtain the precipitate). Subsequent filtration gave salphenazine complexes **1-7** in good yield (60–73%) and purity; in the case of **1** and **5**, however, the isolated yields were lower (10%) as a result of their higher solubility in MeOH. With the aim of preparing a Zn complex with a more extensive  $\pi$ -conjugated structure, the synthesis of complex **8** (Scheme 2) has been successfully achieved by applying the synthetic strategy described above using two

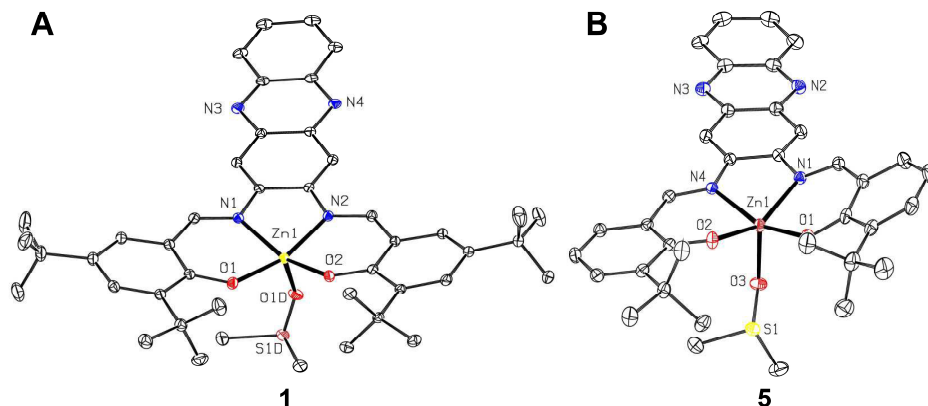
equivalents of 2-hydroxy-1-naphthaldehyde. Furthermore, by using a previously reported methodology<sup>[20]</sup> an octanuclear, Zn<sub>8</sub> cluster complex **9** characterized by the presence of four salphenazine scaffolds has also been prepared (23% yield) using 2,3-dihydroxy-benzaldehyde, 2,3-diaminophenazine **B** and Zn(OAc)<sub>2</sub>·2H<sub>2</sub>O (Scheme 2).



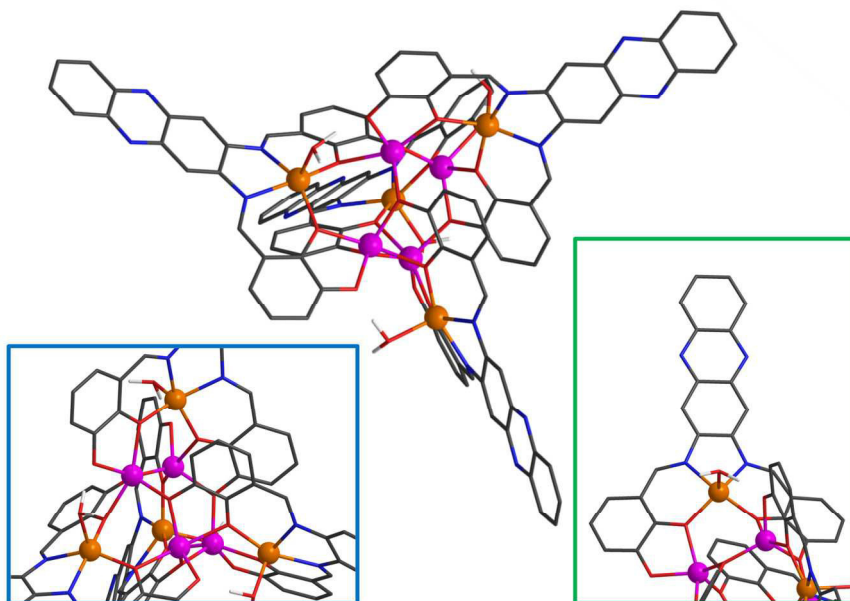
**Scheme 2.** Synthesis of salphenazine complex **8** and the salphenazine cluster complex **9** from precursor **A**.

### 4.3 Structural analysis of Zn(salphenazine)s

Single crystals suitable for X-ray analysis were obtained by dissolving complex **1** and **5** in hot DMSO (Figure 1). Similar to previously reported X-ray structures of Zn(salphen) complexes,<sup>[21]</sup> the Zn ion is slightly tilted from the N<sub>2</sub>O<sub>2</sub> binding pocket of the salphen ligand. The axial coordination site in both structures is occupied by a solvent molecule (DMSO) due to the high Lewis acidity of Zn(salphen)s. In order to get more structural information for the structure of complex **9**, its DFT-minimized structure was computed (see the Experimental Section) using previously reported X-ray structures of similar Zn(salphen) clusters as a starting point.<sup>[20]</sup> The computed structure (Figure 2) shows the assembly of four salphenazine units positioned in a *pseudo* tetrahedral structure with every vertex ending with a phenazine moiety: the latter are thus outward.



**Figure 1.** Displacement ellipsoid plots at 50% probability level of complex **1** and **5**. Selected bond lengths and angles for **1**: N(1)-Zn(1) = 2.0928 Å, N(2)-Zn(1) = 2.0537 Å, O(1)-Zn(1) = 1.9788 Å, O(2)-Zn(1) = 1.9570 Å, Zn(1)-O(1D) = 2.0862 Å, O(2)-Zn(1)-N(1) = 153.48°, O(1)-Zn(1)-N(1) = 89.13°, O(2)-Zn(1)-O(1D) = 103.47°; for **5**: N(1)-Zn(1) = 2.0717 Å, N(4)-Zn(1) = 2.0765 Å, O(1)-Zn(1) = 1.9554 Å, O(2)-Zn(1) = 1.9807 Å, Zn(1)-O(3) = 2.0658 Å, O(2)-Zn(1)-N(4) = 158.04°, O(2)-Zn(1)-N(4) = 88.22°, O(1)-Zn(1)-O(3) = 102.45°.



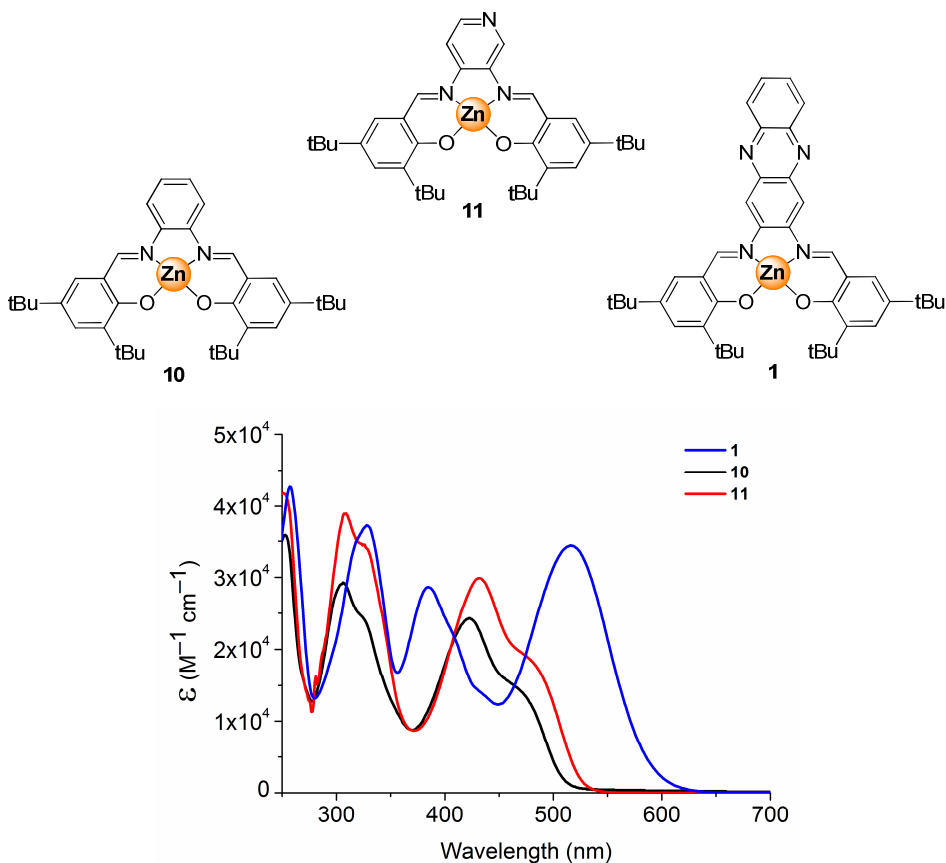
**Figure 2.** DFT calculated structure for **9**·(H<sub>2</sub>O)<sub>4</sub>, the orange and the purple spheres represent the Zn ions respectively inside the N<sub>2</sub>O<sub>2</sub> and the O<sub>4</sub> coordination pockets. In the blue square an enlargement of Zn<sub>8</sub> cluster is shown; in the green square an enlargement of a salphenazine unit is given.



Four of the in total eight Zn ions are situated in the N<sub>2</sub>O<sub>2</sub> pockets (represented in orange in Figure 2) having an axial H<sub>2</sub>O ligand associated. The other four “internal” Zn ions (represented in purple in Figure 3) are surrounded by five O-atom donors, two of which belong to the same salphenazine unit and the other three form μ<sub>2</sub>-phenoxo bridges between two Zn ions of adjacent salphenazine units.

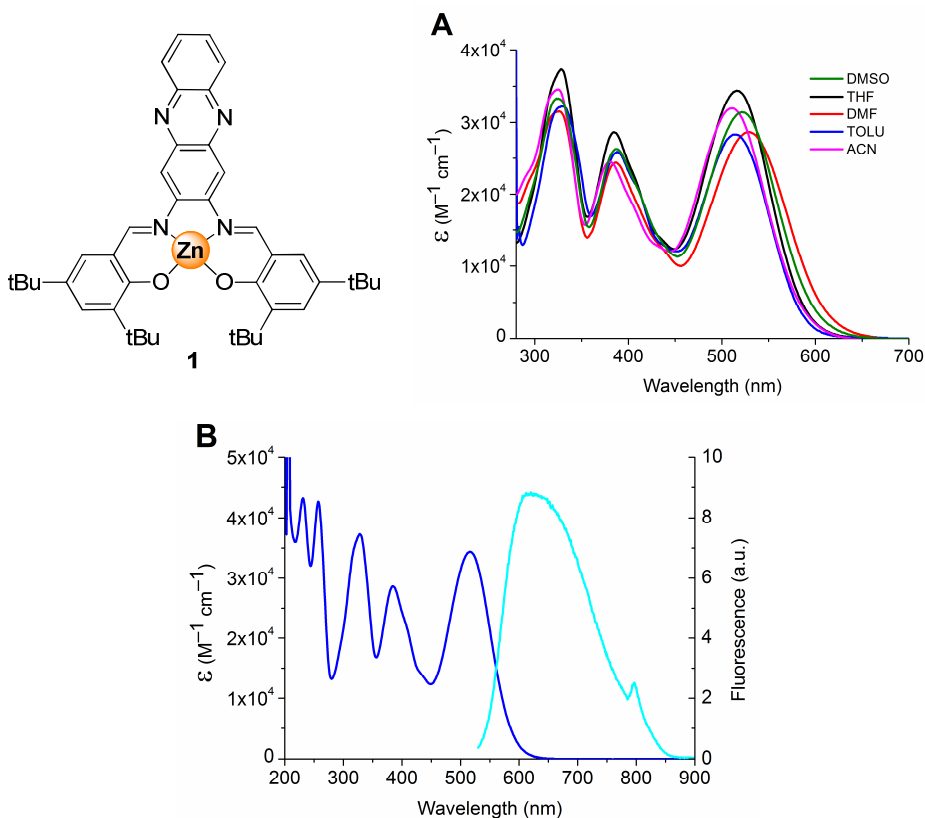
#### 4.4 Photophysical properties of Zn(salphenazine)s

Typical Zn(salphen)s are generally characterized by two absorption bands in their UV-Vis spectra (200-600 nm region), a first one around 400 nm and a second one around 300 nm (*i.e.*, black trace of compound **10** in Figure 3).



**Figure 3.** UV-Vis comparison between Zn(salphen) derivative **10**, Zn(salpyr) complex **11** and Zn(salphenazine) **1** in THF at a concentration of 1×10<sup>-5</sup> M.

These two bands are influenced by the substituents present in the salphen scaffold; especially the role of the phenyl ring in backbone of the salphen ligand is important. When the latter is substituted with a pyridine ring (designated as “salpyr” complex **11**), for example, an increase in the extinction coefficient  $\epsilon$  occurs combined with a slight red-shift (see red trace in Figure 3). Inspired by this characteristic change in the UV-Vis, a further modification of the backbone motif was realized and a phenazine scaffold was then selected for its presence in many natural dyes.<sup>[22]</sup> As shown in Figure 3, the phenazine contribution to the electronic properties of complex **1** results in a red-shift of 100 nm and a 50% increase of the  $\epsilon$  of the lower energy band compared to salphen complex **10**.



**Figure 4.** (A) Comparison between absorption spectra of **1** in different solvents at a concentration of  $1 \times 10^{-5}$  M. (B) Absorption and emission spectra of **1** in dry THF at  $1.76 \times 10^{-5}$  M.

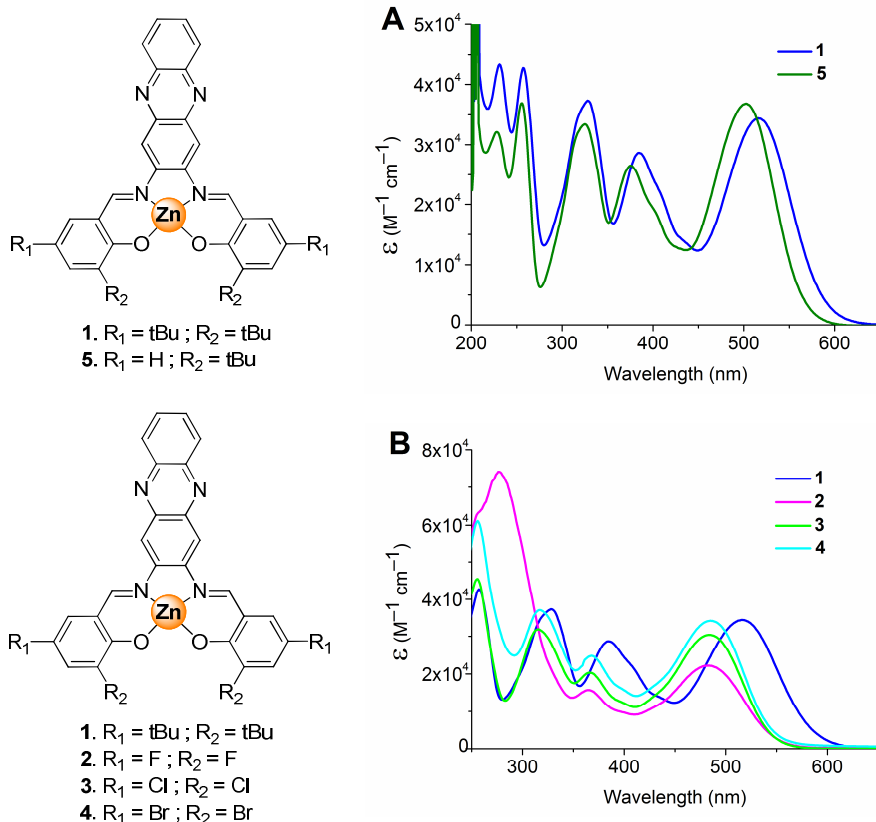
A detailed study toward the photophysical properties of Zn(salphenazine) complexes has been carried out using Zn(salphenazine) **1** as model compound due to its higher solubility compared to **2-9**. Furthermore, the presence of four *tert*-butyl groups highly reduces the possibility of formation of dimeric species, which can affect the absorption and emission properties (see Chapter 2.4.3). The UV-Vis spectra of **1** slightly changes upon variation of the solvent (Figure 4A), and this suggest that the type of electronic transitions that are involved have  $\pi\text{-}\pi^*$  rather than charge transfer (CT) character.

Figure 4B shows the UV-Vis absorption and emission spectra of **1** in THF, which provides the highest  $\epsilon$  value among all the solvents tested. In the absorption spectra five main bands are observed, two in the visible region ( $\lambda = 384$  nm and  $\lambda = 516$  nm) and three in the near-UV ( $\lambda_{\text{max}} = 231$  nm,  $\lambda_{\text{max}} = 257$  nm and  $\lambda_{\text{max}} = 328$  nm). Upon excitation of the lowest energy band ( $\lambda = 516$  nm), an intense emission band at  $\lambda = 624$  nm is observed.

Comparing all the UV-Vis spectra of complexes **1-9**, the role of the substituents in the salphenazine ligand has been evaluated. In the case of tetra-substituted **1**, the two bands in the visible region are at slightly lower energy ( $\Delta\lambda = 15$  nm) compared to ones from the di-substituted complex **5** (Figure 5A). The two additional *tert*-butyl groups in the 5- and 5'-positions of the salphenazine scaffold bring about an additional positive inductive effect that would destabilize more the  $\pi$  ground state in **1**. Halogens are controversial substituents, since they produce a negative inducting effect and a positive resonance effect. As suggested by TD-DFT calculations (see section 4.5) the resonance effect seems to have a stronger influence on the salphenazine scaffold causing a destabilization of the  $\pi^*$  excited states. This results in a blue-shift of around 31 nm for **2-4** (Figure 5B). Complexes **5-7**, due to the presence of only two substituents (3- and 3'-position in the ligand backbone), are less influenced by the electron-donating and electron-withdrawing groups but show similar effects (see Figure 12 in the Experimental section).

In order to obtain systems with increased absorbance towards the near IR, two modified synthetic strategies were applied (see 4.2). The preparation of a Zn(salphenazine) complex with a more extended  $\pi$ -conjugated system compared to salphenazine complex **1** (i.e, Zn(salphenazine) **8**) was carried out; instead of having two

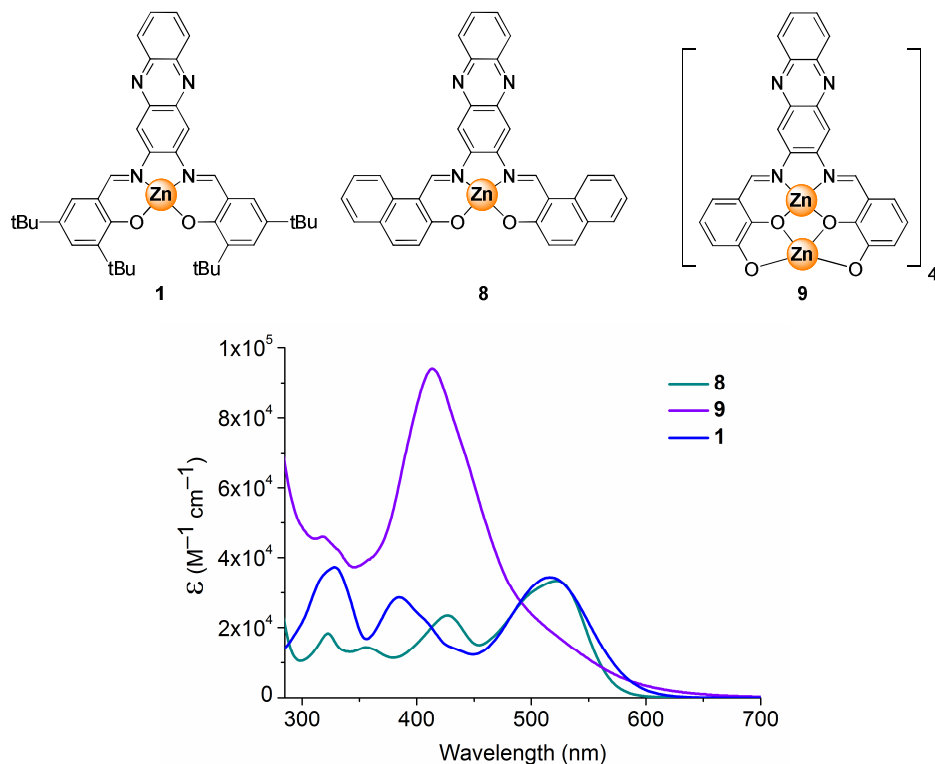
substituted phenyl rings (derived from the salicylaldehyde precursor), complex **8** is characterized by the presence of two naphthyl groups.



**Figure 5.** UV-Vis comparisons: (A) between di-substituted **5** and tetra-substituted **1**; (B) comparison between tetra-substituted complexes **1-4**. All UV-Vis spectra were recorded in THF at a concentration of  $1 \times 10^{-5}$  M.

The enhancement of the  $\pi$ -conjugation, however, results only in a small improvement of the absorption properties (Figure 6); a slight red-shift of 8 nm was observed while maintaining a similar value of  $\epsilon$  compared to complex **1**. This suggests that simple extension of the  $\pi$ -conjugation (change from phenyl to naphthyl side groups) does not substantially improve the photophysical properties required for an effective application thereof in OSC. Thus, in order to obtain good smOSC candidates the attention should better focus on Zn(salen)s with heteroaryl bridging groups such as present in

Zn(salphenazines) as also heterocyclic synthons have shown interesting results in heterojunction solar cells.<sup>[23]</sup>

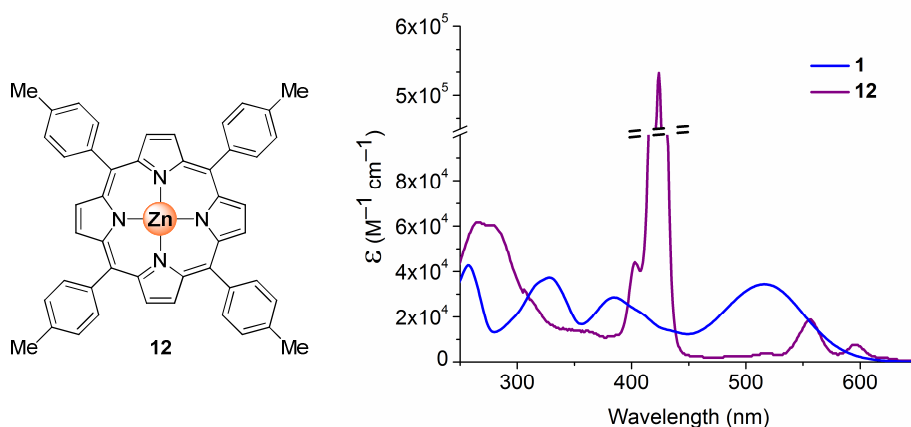


**Figure 6.** UV-Vis comparison between Zn(salphenazine) complexes **1**, **8** and **9** in THF at a concentration of  $1 \times 10^{-5}$  M.

A second synthetic strategy was considered in order to interconnect multiple chromophores; this was successfully achieved in the preparation of the octanuclear Zn-cluster **9** incorporating four Zn(salphenazine) units. As shown in Figure 6, the absorption spectra of **9**, in comparison with **1**, is characterized by a 70% increase of the  $\epsilon$  value for the band in the range of the visible. However, the absorption maximum located at 413 nm (100 nm towards the blue with respect to complex **1**) does not make complex **9** suitable for OSC.

As mentioned in the introduction (section 4.1), porphyrins and their metal complexes have demonstrated to be good candidates in the preparation of devices for

DSC and OSC. Therefore, a comparison between the newly developed Zn(salphenazine) systems and a Zn(porphyrin) would be useful. In Figure 7 the comparison between Zn(salphenazine) complex **1** and Zn(porphyrin) complex **12** is reported. Porphyrin **12** shows a typical Soret band (424 nm) with a  $\epsilon$  value of an order of magnitude higher than **1**. On the contrary, complex **1** has an absorption spectrum that covers a wider range of accessible wavelengths. These photophysical properties combined with the easy synthesis/functionalization demonstrate that the salphenazine scaffold could be a potential alternative to porphyrins and its derivatives.



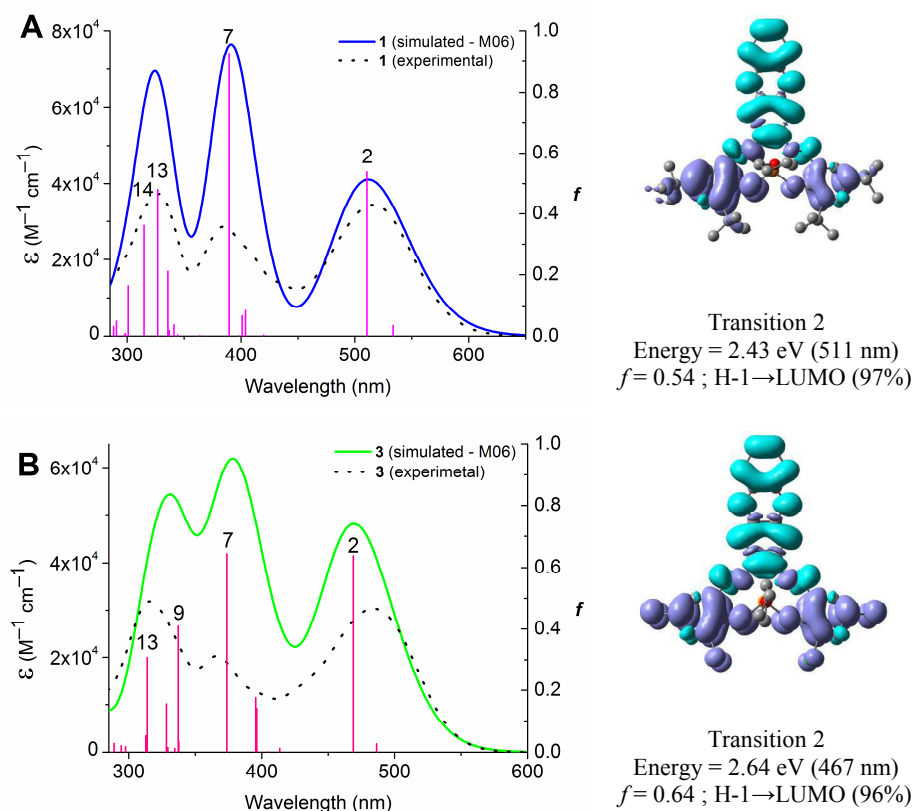
**Figure 7.** UV-Vis comparison between salphenazine complex **1** and porphyrin **12** in THF at a concentration of  $1 \times 10^{-5}$  M.

#### 4.5 TD-DFT analysis of Zn(salphenazine)s

TD-DFT was employed for calculating 80 singlet excited states starting from the gas-phase optimized geometry of **1** and **3** with a THF molecule coordinated in the axial position. Experimental and theoretical absorption spectra of complex **1** and **3** in THF are reported in Figure 8 together with the electron density difference maps (EDDMs)<sup>[24]</sup> of the major electronic transitions of the lowest energy band. The solvent effect was taken into account with the CPCM method.

A very good agreement between the experimental and simulated UV-Vis spectra has been observed for **1**; the three bands shown in the experimental spectrum are blue-shifted only by 5 nm in the DFT calculated UV-Vis trace. Despite this good agreement,

TD-DFT significantly the extinction coefficient of the two highest energy bands. The lowest energy band is formed by two electronic transitions: the first one at 534 nm (2.32 eV) with small oscillator strength (0.035) and the second one at 511 nm (2.43 eV) with oscillator strength of 0.54. Both transitions are shown to have a  $\pi$ - $\pi^*$  character with no contribution from the metal center, in particular the electron density migrates from the two salicylaldehyde moieties towards the salphenazine backbone as represented in the EDDM of the major transition 2 (Figure 8A, right).

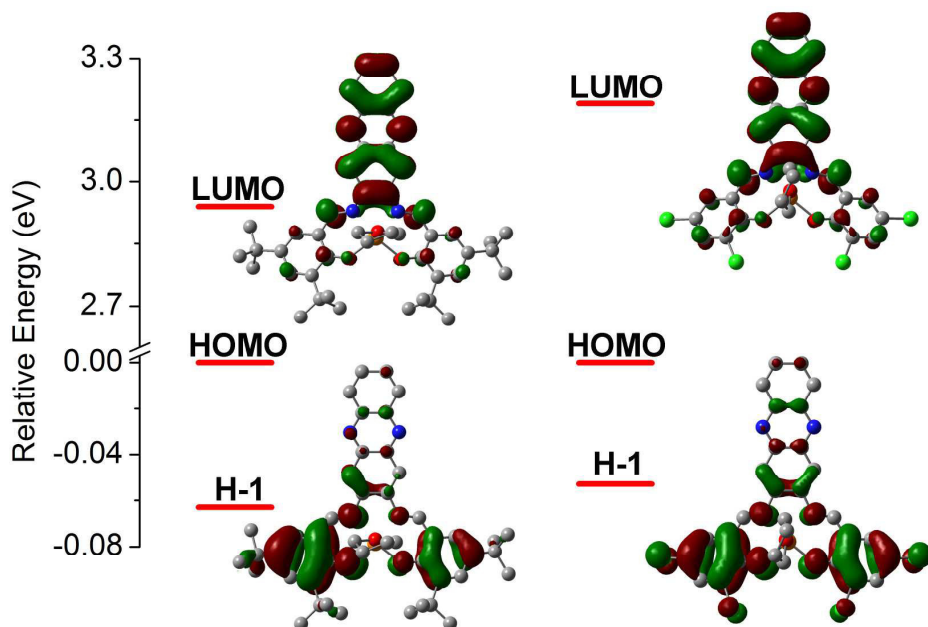


**Figure 8.** Calculated (blue and green lines) and experimental (black dotted lines) absorption spectra of **1** (A) and **3** (B) in THF. The excited states are shown as vertical bars and the transition 2 of **1** (A) and **3** (B) is represented with electron density difference maps on the right (EDDMs, the electron density migrates from the violet to the blue lobes). Energy values, oscillator strength values and major orbital contributions are reported below the EDDMs.

The other two bands at higher energy (389 nm and 326 nm, respectively) are also based on  $\pi$ - $\pi^*$  transitions (see EDDMs of transition 7, 13 and 14 in Table 2, Experimental

section), and this is in line with the observations done in the UV-Vis experiments in different solvents (see Figure 4A).

In the case of Zn(salphenazine) complex **3** the computed spectrum is in reasonable agreement with the experimental one, and a blue-shift of 15 nm of the lowest energy band is now observed. Through analysis of the type of transition involved in the UV-Vis spectrum of **3**, similar  $\pi$ - $\pi^*$  excited states were found as observed for Zn(salphenazine) complex **1** (EDDMs in Figure 8B, see also Tables 2 and 3 in the Experimental section). In order to understand the 44 nm blue-shift of the lowest energy band caused by the substitution of the four *tert*-butyl groups in **1** with four Cl atoms present in **3**, frontier molecular orbital (FMO) analysis has been carried out. Figure 9 shows that the Cl substituents significantly destabilize the lowest unoccupied molecular orbital (LUMO) in **3** and also cause a slight destabilization of the H-1. This behavior may be ascribed to the resonance effect of the ion pairs of the chlorine atoms which destabilize the frontier MO donating more electron density. The latter results in the enhancement of the energy difference between H-1 and LUMO of **3** and thus a relative shift towards the blue of the lowest energy band compared with complex **1**.



**Figure 9.** Relative energy diagram of the frontier molecular orbitals for **1** and **3**. The zero is set on the HOMO energy. Note that the Cl-atoms in complex **3** are shown in light green.



## 4.6 Thermal stability of Zn(salphenazine)s

The thermal stability of Zn(salphenazine) complexes **1-7** has been examined by thermogravimetric analysis (TGA) under a nitrogen atmosphere (Table 1). All complexes show high thermal stability, the decomposition temperature ranges from 410°C (**4**) to 520°C (**2**). Comparing the di-substituted complexes **5** and **7** with the tetra-substituted **1** and **4**, a higher thermal stability for the di-substituted systems was observed. In the case of complexes **1-4** (tetra-substituted ones), replacing the R<sub>1</sub> and R<sub>2</sub> substituent from Br to tBu, Cl or F leads to a significant increase in the decomposition temperature (T<sub>d</sub>) from 410°C to 520°C. No glass transition temperature (T<sub>g</sub>) was observed in the differential scanning calorimetric experiments (DSC) done for **1-7**.

**Table 1.** Thermal degradation (T<sub>d</sub>) for complexes **1-7**

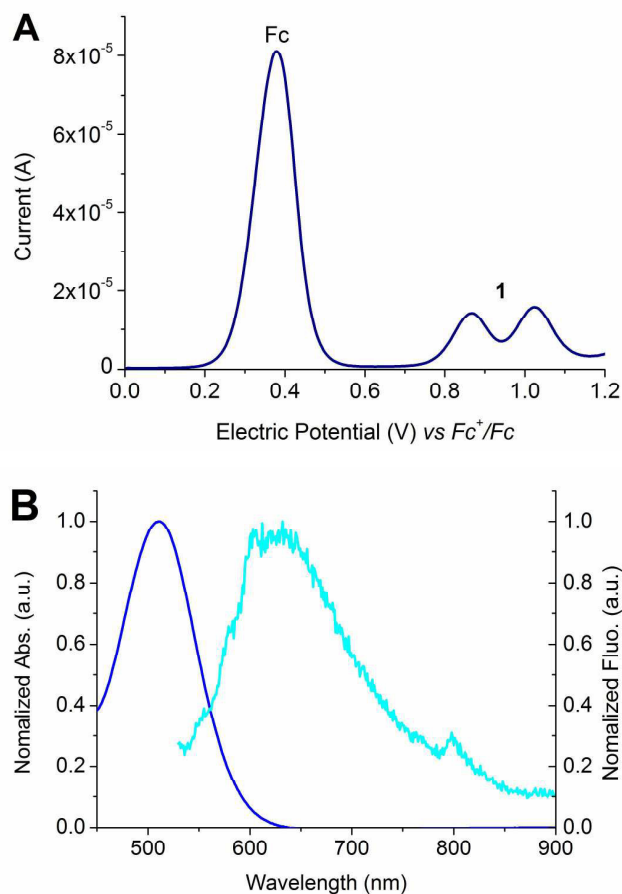
Complex	<b>1</b>	<b>2</b>	<b>3</b>	<b>4</b>	<b>5</b>	<b>6</b>	<b>7</b>
T <sub>d</sub> (°C)	470°	520°	480°	410°	440°	480°	440°

## 4.7 Preparation of a smOSC device based on Zn(salphenazine) **1**

Zn(salphenazine) **1** shows to have the highest solubility among all the compounds reported herein and has relative good thermal stability (see section 4.6). At the same time, the photophysical properties of **1** display optimal characteristics to be donors in the production of relatively efficient smOSC and therefore this complex was selected for the preparation of a photovoltaic device.

One of the most important requisites for the correct operation of an OSC and the production of a photocurrent is the establishment of an adequate energy gap between the LUMO of the donor (i.e, salphenazine complex **1**) and the acceptor (C<sub>60</sub>) LUMO. The photogenerated electron-hole pair (exciton) is bound by a Coulombic force, which is of the order of 0.3 eV.<sup>[25]</sup> In order to successfully separate the charges, the general process requires excitons to travel to the donor-acceptor interface where the difference in donor and acceptor LUMO levels must exceed the Coulombic attraction force ( $\Delta E_{\text{LUMO}} > 0.3$  eV). Energy values of the HOMO and LUMO for complex **1** have thus been calculated using differential pulse voltammetry (DPV), and absorption and emission spectroscopy. DVP of **1** was recorded in degassed acetonitrile (ACN) with 0.1 M tetrabutylammonium

hexafluorophosphate (TBAP) as supporting electrolyte and all the potentials were referenced to the ferrocenyl-ferrocene ( $Fc^+/Fc$ ) couple. Two reversible, anodic waves (confirmed by cyclic voltammetry, see Experimental section) with  $E^{ox}$  at 0.852 V and 1.01 V were observed; both of them are attributed to the oxidation of the salphenazine ligand (Figure 10A).



**Figure 10.** (A) Differential pulse voltammetry for **1** vs  $Fc^+/Fc$  recorded in degassed ACN. (B) Normalized absorption (blue) and emission (light blue) spectra in ACN.

To determine the energy level of the HOMO, the following formulae<sup>[26]</sup> was used:

$$E_{\text{HOMO}} = -(1.4 \pm 0.1) \times (qV_{\text{CV}}) - (4.6 \pm 0.08) \text{ eV} \quad (1)$$

where  $V_{\text{CV}}$  corresponds to  $E^{\text{OX}}$  of complex **1**. The HOMO level of **1** was estimated to be  $-5.27 \text{ eV}$ .

From the intersection point between the normalized absorption and emission curves it is possible to extract the energy gap between HOMO and LUMO and consequently obtain the LUMO energy value of complex **1**. Figure 10B shows that the intersection point is at 560 nm, which corresponds to 2.21 eV (in good agreement with the DFT calculated value, see section 4.5) and the LUMO level is  $-3.05 \text{ eV}$ . By comparison with the LUMO value of  $\text{C}_{60}$ ,  $-3.5 \text{ eV}$ ,<sup>[27]</sup> an OSC device based on complex **1** would display an acceptable  $\Delta E_{\text{LUMO}}$  between donor and acceptor.

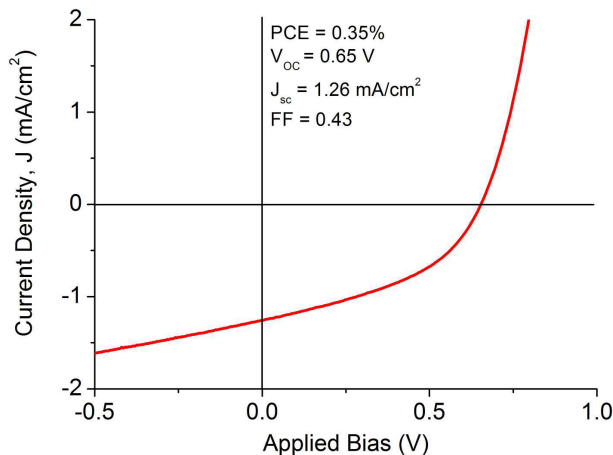
The devices were fabricated by spin coating of a 1 mg/ml solution of Zn(salphenazine) **1** directly onto UV/O<sub>3</sub> treated indium tin oxide (ITO) (2000 rpm, 1 min,  $\sim 13 \text{ nm}$  thick),<sup>[28]</sup> followed by the evaporation of  $\text{C}_{60}$  (40 nm), BCP (10 nm), and Al (100 nm), with devices having an active area of  $0.09 \text{ cm}^2$ . The device has been studied under standard conditions (A.M 1.5 G solar spectrum,  $100 \text{ mW cm}^{-2}$ ), and the current-voltage curve (J-V curve) relative to the **1**: $\text{C}_{60}$  device is reported in Figure 11. The power conversion efficiency (PCE) is calculated using the following formula:

$$\text{PCE} = \frac{V_{\text{OC}} \times J_{\text{SC}} \times FF}{P_{\text{in}}} \quad (2)$$

where,  $V_{\text{OC}}$  is the open-circuit voltage,  $J_{\text{SC}}$  is the current density at a short-circuit,  $FF$  is the fill factor (measure of squareness of curve in the fourth quadrant of the J-V curve) and  $P_{\text{in}}$  is the incident power of the lamp. At the standard conditions the device has an efficiency of 0.35% (PCE), which is not competitive compared to known systems,<sup>[5-12]</sup> nonetheless it demonstrates the potential of this new class of compound. In particular, the  $V_{\text{OC}}$  of the device was 0.65 V, which is suitable and allows for improvement by modification of the HOMO level of donor **1**. On the contrary the fill factor was small

due to the insufficient uniformity in the morphology of the donor layer. In order to improve the  $FF$  a direct evaporation of **1** could be a good strategy compared with solution-process approaches. The current density  $J_{SC}$  was also low; the reason for this behavior is the modest extinction coefficient  $\epsilon$  value of **1**. A possible strategy would be the production of devices with a thicker donor layer (higher absorption) but due to transport issues (low  $FF$  value) a correct charge migration to the electrodes would not be feasible. Thus a better design at the molecular level is need to reduce the overlap between donor and acceptor (extend  $\pi$ -conjugation) and to increase the  $\epsilon$  value of the donor molecules.

An approach to improve the photocurrent and the relative efficiency of the device would be using a bulk heterojunction architecture<sup>[12a]</sup> which maximises the interfacial area between donor and acceptor (investigation is currently underway in this respect). A possible advantage of Zn(salphen) complexes in this regard is their ability to self-assemble creating well-ordered large domains which could easily mix with an acceptor matrix.<sup>[29]</sup>



**Figure 11.** J-V curve for the devices comprising of ITO/1/C<sub>60</sub>/BCP/Al.

## 4.8 Conclusions

In summary, a new class of Zn(II) Schiff base complexes incorporating a phenazine unit in the backbone has been developed. Salphenazine complexes show interesting photophysical properties compared to typical salen and salphen complexes while

remaining easily synthesized and tunable. From the experimental and theoretical UV-Vis data the absorption bands have been assigned to  $\pi$ - $\pi^*$  transitions which are directly influenced by the type of substituents present in the salphenazine scaffold. Therefore, by a judicious choice of these groups, it is possible to obtain systems with desired photophysical properties.

Zn(salphenazine) complexes have also shown to have potential application in smOSCs due to their high stability and adequate electronic properties against the acceptor C<sub>60</sub>. Even though the efficiency of the device is not competitive yet, Zn(salphenazine)s show the synthetic potential for significant improvement based on the modular construction of these photo-active complexes.

## 4.9 Experimental section

### General methods and materials

All chemicals were commercial available and were used as received. <sup>1</sup>H NMR and <sup>13</sup>C{<sup>1</sup>H} NMR spectra were recorded on Bruker Avance 400 MHz Ultrashield NMR spectrometers at 297 K. Chemical shifts are reported in ppm relative to tetramethylsilane ( $\delta = 0$  ppm) as an internal standard. Mass analyses were carried out by the Mass Spectrometry Unit at the Institute of Chemical Research of Catalonia (ICIQ), Spain. X-ray analyses were also performed at ICIQ by the X-ray crystallographic unit. Elemental analyses were determined by the Elemental Analysis Unit of the University of Santiago de Compostela, Spain. UV-Vis spectra were acquired on a Shimadzu UV-1800 spectrophotometer. Fluorescence spectroscopy was performed on an AMINCO Bowman series 2 luminescence spectrometer. Acetonitrile, N,N-dimethylformamide, tetrahydrofuran and toluene used for UV-Vis and the DPV experiment were dried by using a solvent purification system (SPS) from Innovative Technology.

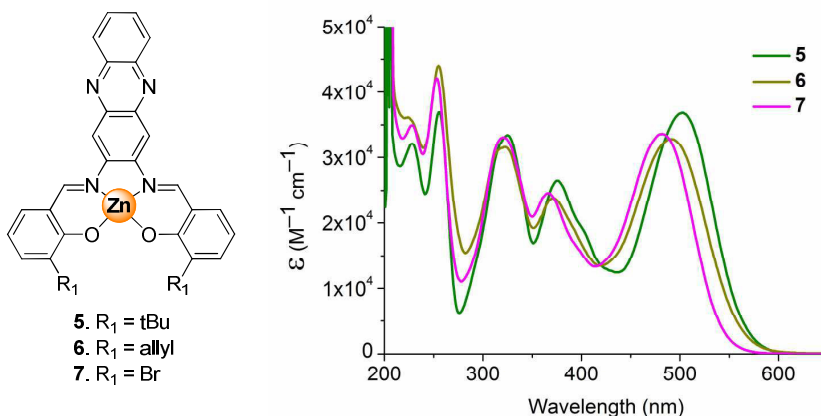
### DFT calculations

All calculations were performed with the Gaussian 09 (G09) program package<sup>[30]</sup> employing the DFT method with Becke's three parameter hybrid functional<sup>[31]</sup> and Lee-Yang-Parr's gradient-corrected correlation functional (B3LYP).<sup>[32]</sup> The LanL2DZ basis set<sup>[33]</sup> and effective core potential were used for the Zn atom, and the split-valence 6-311G\*\* basis set<sup>[34]</sup> was applied for all other atoms. Geometry optimizations of the complexes were performed without any constraint, and the nature of all stationary points was confirmed by normal-mode analysis. Non-equilibrium TDDFT<sup>[35]</sup> calculations produced singlet excited states employing the DFT method with the

hybrid functional of Truhlar and Zhao (M06),<sup>[36]</sup> using the conductor like polarizable continuum model method (CPCM)<sup>[37]</sup> with THF as solvent. Eighty singlet excited states were determined starting from optimized geometries of **1** and **3**. Electronic distributions and localizations of the singlet excited states were visualized using the electron density difference maps (EDDMs).<sup>[38]</sup> GaussSum 2.25<sup>[39]</sup> was used for singlet EDDMs calculations and for simulation of the electronic spectrum.

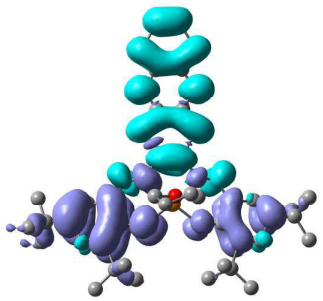
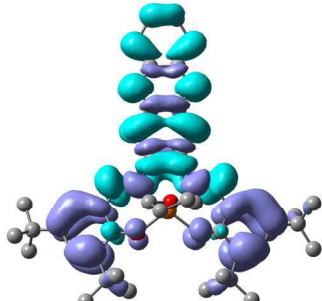
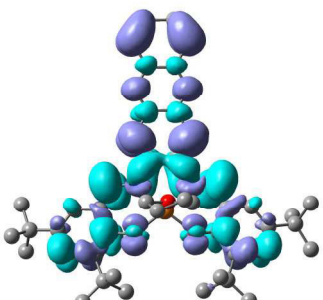
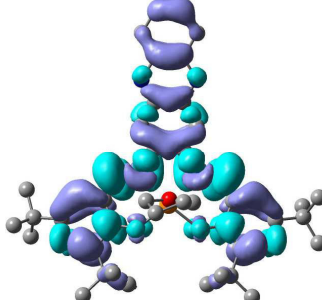
### Differential Pulse Voltammetry

Differential pulse voltammetry (DPV) experiments were carried out using a CH Instruments 660c Electrochemical Workstation, with a standard three-electrode setup utilizing a Pt disc working electrode, Pt wire working electrode and SCE reference electrode. A 0.1 M solution of tetrabutylammonium phosphate in DMSO was used as the background electrolyte.



**Figure 12.** UV-Vis comparisons: between di-substituted **5-7**. All UV-Vis spectra were recorded in THF at a concentration of  $1 \times 10^{-5}$  M.

**Table 2.** Selected calculated singlet excited-state transitions for **1**•THF in THF.

Transition 2	Transition 7
	
Energy = 2.43 eV (511 nm) $f = 0.54$ ; H-1→LUMO (97%)	Energy = 3.18 eV (389 nm) $f = 0.92$ ; H-3→LUMO (69%)
Transition 13	Transition 14
	
Energy = 3.79 eV (327 nm) $f = 0.48$ ; H-2→L+1 (75%)	Energy = 3.94 eV (315 nm) $f = 0.36$ ; H-3→L+1 (75%)

Top: calculated (blue line) and experimental (black line) absorption spectra of **1** in THF. The excited states are shown as vertical bars. Bottom: selected transition represented with electron density maps (EDDMs, the electron density migrates from the violet to the blue lobes). Energy values, oscillator strength values and major orbital contributions are reported below the EDMs.

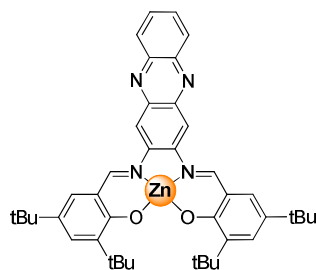
### Device fabrication

Devices were prepared on ITO substrates (5 ohm/square, Psiotech Ltd. U.K.). The substrates were cleaned by sonicating in acetone and 2-propanol, followed by 20 min exposure to UV/O<sub>3</sub>. Thin films of the Zn(salphenazine) **1** donor were prepared by spin-coating a 1 mg/ml solution in CHCl<sub>3</sub> of the respective donor and filtered using a 0.2 mm cellulose acetate membrane. The spin-coating conditions employed were 2000 rpm/minute. Subsequently, the films were allowed to dry for 30

min under ambient conditions before transferring them to a nitrogen rich glove box, where they were annealed at a temperature of 100°C for 15 min in an attempt to remove any residual water. Finally the substrates were placed in the evaporator where the C<sub>60</sub> (40 nm, MER Corp., 99.9%), bathocuproine BCP (8 nm, Sigma Aldrich), and Al (100 nm, Sigma Aldrich) were deposited at a base pressure of  $1 \times 10^{-6}$  mbar. Device J-V curves were recorded using a 150 W solar simulator (Abet Technologies) at 1 sun conditions (AM 1.5, 100 mW/cm<sup>2</sup>). Incident to photon current efficiency (IPCE) studies were carried out using a home-built system utilizing a 150 W Oriol Xenon lamp as the light source.

### Synthesis

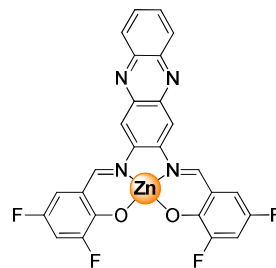
**Zn(salphenazine) complex (1):** 2,3-diaminophenazine (103 mg, 0.49 mmol) was dissolved in DMSO (2 mL) and the mixture was heated to 95°C in order to dissolve the reagent. While stirring, to the heated solution was added a methanol solution (2 mL) of 3,5-*tert*-butyl-2-hydroxybenzaldehyde (230 mg, 0.75 mmol) and a methanol solution (1 mL) of Zn(OAc)<sub>2</sub>·H<sub>2</sub>O (88 mg, 0.40 mmol). The solution was stirred overnight at 95 °C, subsequently cooled to room temperature



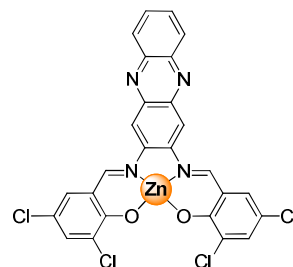
and the precipitate which formed was filtered off, washed with methanol and dried under vacuum to yield a dark brown powder (44 mg, 12 %). <sup>1</sup>H NMR (400 MHz, DMSO-*d*<sub>6</sub>): δ = 9.41 (s, 2H; CH=N), 8.64 (s, 2H; Ar-H), 8.20-8.18 (m, 2H; Ar-H), 7.93-7.87 (m, 2H; Ar-H), 7.41 (d, 2H, <sup>4</sup>J<sub>HH</sub> = 2.7 Hz; Ar-H), 7.39 (d, 2H, <sup>4</sup>J<sub>HH</sub> = 2.7 Hz; Ar-H), 1.51 (s, 9H; *t*Bu), 1.32 (s, 9H; *t*Bu); Due to the low solubility of **1** a proper <sup>13</sup>C NMR analysis was not possible; MALDI(+): *m/z* = 704.5 [M]<sup>+</sup> (calcd. 704.31); UV-Vis (*c* = 0.25 mg in 20 mL, THF): λ<sub>max</sub> (ε) = 231 nm (43107 mol<sup>-1</sup>·m<sup>3</sup>·cm<sup>-1</sup>), λ<sub>max</sub> (ε) = 257 nm (42508 mol<sup>-1</sup>·m<sup>3</sup>·cm<sup>-1</sup>), λ<sub>max</sub> (ε) = 328 nm (37445 mol<sup>-1</sup>·m<sup>3</sup>·cm<sup>-1</sup>), λ (ε) = 384 nm (28709 mol<sup>-1</sup>·m<sup>3</sup>·cm<sup>-1</sup>), λ (ε) = 516 nm (34357 mol<sup>-1</sup>·m<sup>3</sup>·cm<sup>-1</sup>); elemental analysis calcd. (%) for C<sub>42</sub>H<sub>48</sub>N<sub>4</sub>O<sub>2</sub>Zn·2MeOH: C 68.60, H 7.33, N 7.27; found: C 68.82, H 7.27, N 7.55. The presence of MeOH was also supported by <sup>1</sup>H NMR of the microanalysis sample.



**Zn(salphenazine) complex (2):** This compound was prepared in a similar manner to complex **1** using 2,3-diaminophenazine (108 mg, 0.51 mmol), 3,5-difluorosalicylaldehyde (162 mg, 1.03 mmol) and Zn(OAc)<sub>2</sub>·H<sub>2</sub>O (116 mg, 0.53 mmol). After cooling to room temperature the complex was precipitated by further addition of methanol to yield a red powder (185 mg, 66 %). <sup>1</sup>H NMR (400 MHz, DMSO-*d*<sub>6</sub>): δ = 9.37 (s, 2H; CH=N), 8.66 (s, 2H; Ar-H), 8.25-8.23 (m, 2H; Ar-H), 7.98-7.96 (m, 2H; Ar-H), 7.40-7.34 (m, 2H; Ar-H), 7.27-7.24 (m, 2H; Ar-H); <sup>19</sup>F NMR (400 MHz, DMSO-*d*<sub>6</sub>): δ = -129.96 (d, 2F, <sup>3</sup>J<sub>HF</sub> = 11.4 Hz; Ar-F), -130.66 (dd, 2F, <sup>3</sup>J<sub>HF</sub> = 8.8 Hz, <sup>3</sup>J<sub>HF</sub> = 8.8 Hz; Ar-F); Due to the low solubility of **2** a proper <sup>13</sup>C NMR analysis was not possible; MALDI(+): *m/z* = 552.1 [M]<sup>+</sup> (calcd. 552.02), 1108.2 [2M]<sup>+</sup> (calcd. 1108.3); UV-Vis (*c* = 0.25 mg in 20 mL, THF): λ<sub>max</sub> (ε) = 277 nm (74112 mol<sup>-1</sup>·m<sup>3</sup>·cm<sup>-1</sup>), λ<sub>max</sub> (ε) = 365 nm (15685 mol<sup>-1</sup>·m<sup>3</sup>·cm<sup>-1</sup>), λ<sub>max</sub> (ε) = 483 nm (22177 mol<sup>-1</sup>·m<sup>3</sup>·cm<sup>-1</sup>); elemental analysis calcd. (%) for C<sub>26</sub>H<sub>12</sub>F<sub>4</sub>N<sub>4</sub>O<sub>2</sub>Zn·MeOH·2/3DMSO: C 52.37, H 2.82, N 9.05, S 3.45; found: C 52.29, H 2.94, N 8.90, S 3.47. The presence of DMSO and MeOH in the microanalysis sample was also supported by <sup>1</sup>H NMR.



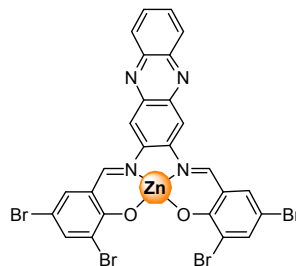
**Zn(salphenazine) complex (3):** This compound was prepared in a similar manner to complex **1** using 2,3-diaminophenazine (93.4 mg, 0.44 mmol), 3,5-dichlorosalicylaldehyde (178 mg, 0.93 mmol) and Zn(OAc)<sub>2</sub>·H<sub>2</sub>O (109 mg, 0.5 mmol). After cooling to room temperature the complex was precipitated by addition of extra methanol to yield an orange powder (200 mg, 73 %). <sup>1</sup>H NMR (400 MHz, DMSO-*d*<sub>6</sub>): δ = 9.34 (s, 2H; CH=N) 8.64 (s, 2H; Ar-H), 8.25-8.23 (m, 2H; Ar-H), 7.98-7.95 (m, 2H; Ar-H), 7.64 (d, 2H, <sup>4</sup>J<sub>HH</sub> = 2.9 Hz; Ar-H), 7.62 (d, 2H, <sup>4</sup>J<sub>HH</sub> = 2.9 Hz; Ar-H); Complex **3** was too insoluble for a proper <sup>13</sup>C NMR analysis; MALDI(+): *m/z* = 617.8 [M]<sup>+</sup> (calcd. 617.9), 1237.6 [2M]<sup>+</sup> (calcd. 1237.79); UV-Vis (*c* = 0.25 mg in 20 mL, THF): λ<sub>max</sub> (ε) = 256 nm (45424 mol<sup>-1</sup>·m<sup>3</sup>·cm<sup>-1</sup>), λ<sub>max</sub> (ε) = 316 nm (31863 mol<sup>-1</sup>·m<sup>3</sup>·cm<sup>-1</sup>), λ<sub>max</sub> (ε) = 366 nm (20328 mol<sup>-1</sup>·m<sup>3</sup>·cm<sup>-1</sup>), λ (ε) = 484 nm (30383 mol<sup>-1</sup>·m<sup>3</sup>·cm<sup>-1</sup>); elemental analysis calcd. (%) for C<sub>42</sub>H<sub>48</sub>N<sub>4</sub>O<sub>2</sub>Zn·H<sub>2</sub>O·DMSO: C 46.99, H 2.82, N 7.83; found: C 46.40, H 2.27, N 7.50. The presence of DMSO in the microanalysis sample was also supported by <sup>1</sup>H NMR analysis.



**Zn(salphenazine) complex (4):**

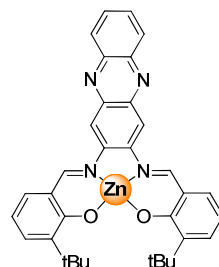
This compound was prepared in a similar manner to **1** using 2,3-diaminophenazine (107 mg, 0.51 mmol), 3,5-dibromosalicylaldehyde (285 mg, 1.02 mmol) and Zn(OAc)<sub>2</sub>·H<sub>2</sub>O (132 mg, 0.60 mmol). After cooling to room temperature the complex was precipitated by addition of extra methanol to yield a dark orange powder (295 mg, 73 %). <sup>1</sup>H

NMR (400 MHz, DMSO-*d*<sub>6</sub>): δ = 9.32 (s, 2H; CH=N), 8.63 (s, 2H; Ar-H), 8.25-8.22 (m, 2H; Ar-H), 7.97-7.95 (m, 2H; Ar-H), 7.84 (d, 2H, <sup>4</sup>J<sub>HH</sub> = 2.5 Hz; Ar-H), 7.62 (d, 2H, <sup>4</sup>J<sub>HH</sub> = 2.5 Hz; Ar-H); Complex **4** was too insoluble for a proper <sup>13</sup>C NMR analysis; MALDI(+): *m/z* = 797.8 [M]<sup>+</sup> (calcd. 797.69), 1595.4 [2M]<sup>+</sup> (calcd. 1595.38); UV-Vis (*c* = 0.25 mg in 20 mL, THF): λ<sub>max</sub> (ε) = 233 nm (47110 mol<sup>-1</sup>·m<sup>3</sup>·cm<sup>-1</sup>), λ<sub>max</sub> (ε) = 256 nm (61100 mol<sup>-1</sup>·m<sup>3</sup>·cm<sup>-1</sup>), λ<sub>max</sub> (ε) = 317 nm (37110 mol<sup>-1</sup>·m<sup>3</sup>·cm<sup>-1</sup>), λ (ε) = 368 nm (24770 mol<sup>-1</sup>·m<sup>3</sup>·cm<sup>-1</sup>), λ (ε) = 485 nm (34220 mol<sup>-1</sup>·m<sup>3</sup>·cm<sup>-1</sup>); elemental analysis calcd. (%) for C<sub>26</sub>H<sub>12</sub>Br<sub>4</sub>N<sub>4</sub>O<sub>2</sub>Zn: C 39.16, H 1.52, N 7.03; found: C 39.19, H 1.74, N 6.93.

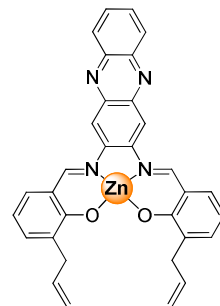
**Zn(salphenazine) complex (5):**

This compound was prepared in a similar manner to complex **1** using 2,3-diaminophenazine (108 mg, 0.51 mmol), 3-*tert*-butyl-2-hydroxybenzaldehyde (183 mg, 1.03 mmol) and Zn(OAc)<sub>2</sub>·H<sub>2</sub>O (114 mg, 0.52 mmol). After cooling to room temperature the complex was precipitated by further addition of methanol to yield a dark brown powder (62 mg, 20 %). <sup>1</sup>H NMR (400

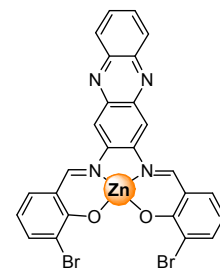
MHz, DMSO-*d*<sub>6</sub>): δ = 9.35 (s, 2H; CH=N), 8.61 (s, 2H; Ar-H), 8.22-8.20 (m, 2H; Ar-H), 7.94-7.92 (m, 2H; Ar-H), 7.42 (dd, 2H, <sup>3</sup>J<sub>HH</sub> = 7.8 Hz, <sup>4</sup>J<sub>HH</sub> = 1.7 Hz; Ar-H), 7.30 (dd, 2H, <sup>3</sup>J<sub>HH</sub> = 7.8 Hz, <sup>4</sup>J<sub>HH</sub> = 1.7 Hz; Ar-H), 6.52 (dd, 2H, <sup>3</sup>J<sub>HH</sub> = 7.8, <sup>3</sup>J<sub>HH</sub> = 7.8 Hz, Ar-H), 1.49 (s, 9H; *t*Bu); Complex **5** was too insoluble for a proper <sup>13</sup>C NMR analysis; MALDI(+): *m/z* = 592.3 [M]<sup>+</sup> (calcd. 592.18); UV-Vis (*c* = 0.22 mg in 20 mL, THF): λ<sub>max</sub> (ε) = 228 nm (32067 mol<sup>-1</sup>·m<sup>3</sup>·cm<sup>-1</sup>), λ<sub>max</sub> (ε) = 255 nm (36994 mol<sup>-1</sup>·m<sup>3</sup>·cm<sup>-1</sup>), λ<sub>max</sub> (ε) = 326 nm (33442 mol<sup>-1</sup>·m<sup>3</sup>·cm<sup>-1</sup>), λ (ε) = 375 nm (26488 mol<sup>-1</sup>·m<sup>3</sup>·cm<sup>-1</sup>), λ (ε) = 501 nm (36820 mol<sup>-1</sup>·m<sup>3</sup>·cm<sup>-1</sup>); elemental analysis calcd. (%) for C<sub>34</sub>H<sub>32</sub>N<sub>4</sub>O<sub>2</sub>Zn·½DMSO·H<sub>2</sub>O: C 64.10, H 5.54, N 8.79; found: C 64.07, H 5.56, N 8.78. The presence of DMSO in the microanalysis sample was also supported by <sup>1</sup>H NMR.



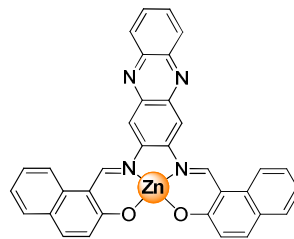
**Zn(salphenazine) complex (6):** This compound was prepared in a similar manner to complex **1** using 2,3-diaminophenazine (146 mg, 0.69 mmol), 3-allyl-salicylaldehyde (236 mg, 1.46 mmol) and Zn(OAc)<sub>2</sub>·H<sub>2</sub>O (156 mg, 0.71 mmol). After cooling to room temperature the complex was precipitated by addition of methanol to yield a reddish brown powder (233 mg, 60 %). <sup>1</sup>H NMR (500 MHz, DMSO-*d*<sub>6</sub>): δ = 9.28 (s, 2H; CH=N), 8.56 (s, 2H; Ar-H), 8.22-8.19 (m, 2H; Ar-H), 7.94-7.91 (m, 2H; Ar-H), 7.42 (dd, 2H, <sup>3</sup>J<sub>HH</sub> = 8.0 Hz, <sup>4</sup>J<sub>HH</sub> = 1.7 Hz; Ar-H), 7.23 (dd, 2H, <sup>3</sup>J<sub>HH</sub> = 7.0 Hz, <sup>4</sup>J<sub>HH</sub> = 1.8 Hz; Ar-H), 6.52 (dd, 2H, <sup>3</sup>J<sub>HH</sub> = 7.0, <sup>3</sup>J<sub>HH</sub> = 8.0 Hz; Ar-H), 6.22-6.14 (m, 2H; Allyl-H), 5.18-5.13 (m, 2H; Allyl-H), 5.03-5.01 (m, 2H; Allyl-H), 3.44 (d, 4H, <sup>3</sup>J<sub>HH</sub> = 6.8 Hz; CH<sub>2</sub>); Complex **6** was too insoluble for a proper <sup>13</sup>C NMR analysis; MALDI(+): *m/z* = 560.1 [M]<sup>+</sup> (calcd. 560.12), 1124.2 [2M]<sup>+</sup> (calcd. 1124.23); UV-Vis (*c* = 0.25 mg in 20 mL, THF): λ<sub>max</sub> (ε) = 224 nm (36150 mol<sup>-1</sup>·m<sup>3</sup>·cm<sup>-1</sup>), λ<sub>max</sub> (ε) = 255 nm (44000 mol<sup>-1</sup>·m<sup>3</sup>·cm<sup>-1</sup>), λ<sub>max</sub> (ε) = 322 nm (31584 mol<sup>-1</sup>·m<sup>3</sup>·cm<sup>-1</sup>), λ (ε) = 371 nm (23811 mol<sup>-1</sup>·m<sup>3</sup>·cm<sup>-1</sup>), λ (ε) = 491 nm (32830 mol<sup>-1</sup>·m<sup>3</sup>·cm<sup>-1</sup>); elemental analysis calcd. (%) for C<sub>32</sub>H<sub>24</sub>N<sub>4</sub>O<sub>2</sub>Zn·2H<sub>2</sub>O: C 64.27, H 4.72, N 9.37; found: C 64.87, H 4.73, N 9.40.



**Zn(salphenazine) complex (7):** This compound was prepared in a similar manner to complex **1** using 2,3-diaminophenazine (107 mg, 0.51 mmol), 3-bromo-salicylaldehyde (215 mg, 1.07 mmol) and Zn(OAc)<sub>2</sub>·H<sub>2</sub>O (132 mg, 0.60 mmol). After cooling to room temperature the complex was precipitated by further addition of methanol to yield an orange powder (146 mg, 45 %). <sup>1</sup>H NMR (400 MHz, DMSO-*d*<sub>6</sub>): δ = 9.36 (s, 2H; CH=N), 8.66 (s, 2H; Ar-H), 8.25-8.22 (m, 2H; Ar-H), 7.97-7.95 (m, 2H; Ar-H), 7.75 (dd, 2H, <sup>3</sup>J<sub>HH</sub> = 7.6 Hz, <sup>4</sup>J<sub>HH</sub> = 1.8 Hz; Ar-H), 7.61 (dd, 2H, <sup>3</sup>J<sub>HH</sub> = 7.6 Hz, <sup>4</sup>J<sub>HH</sub> = 1.8 Hz; Ar-H), 6.53 (dd, 2H, <sup>3</sup>J<sub>HH</sub> = 7.6, <sup>3</sup>J<sub>HH</sub> = 7.6 Hz; Ar-H); Complex **7** was too insoluble for a proper <sup>13</sup>C NMR analysis; MALDI(+): *m/z* = 639.9 [M]<sup>+</sup> (calcd. 639.87), 1279.8 [2M]<sup>+</sup> (calcd. 1279.75); UV-Vis (*c* = 0.25 mg in 20 mL, THF): λ<sub>max</sub> (ε) = 234 nm (34887 mol<sup>-1</sup>·m<sup>3</sup>·cm<sup>-1</sup>), λ<sub>max</sub> (ε) = 253 nm (42152 mol<sup>-1</sup>·m<sup>3</sup>·cm<sup>-1</sup>), λ<sub>max</sub> (ε) = 321 nm (33094 mol<sup>-1</sup>·m<sup>3</sup>·cm<sup>-1</sup>), λ (ε) = 367 nm (24573 mol<sup>-1</sup>·m<sup>3</sup>·cm<sup>-1</sup>), λ (ε) = 482 nm (33632 mol<sup>-1</sup>·m<sup>3</sup>·cm<sup>-1</sup>); elemental analysis calcd. (%) for C<sub>26</sub>H<sub>14</sub>Br<sub>2</sub>N<sub>4</sub>O<sub>2</sub>Zn·H<sub>2</sub>O: C 47.49, H 2.45, N 8.52; found: C 47.59, H 2.36, N 8.22.

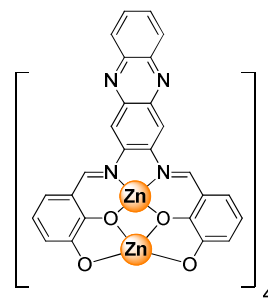


**Zn(salphenazine) complex (8):** This compound was prepared in a similar manner to complex **1** using 2,3-diaminophenazine (109 mg, 0.52 mmol), 2-hydroxy-1-naphthaldehyde (187 mg, 1.04 mmol) and Zn(OAc)<sub>2</sub>·H<sub>2</sub>O (119 mg, 0.54 mmol). After cooling to room temperature the precipitate which formed, was filtered off and washed with methanol to yield a brown powder



(164 mg, 54 %). <sup>1</sup>H NMR (500 MHz, DMSO-*d*<sub>6</sub>): δ = 10.05 (s, 2H; Ar-H), 8.76 (s, 2H; CH=N), 8.64 (d, 2H, <sup>3</sup>J<sub>HH</sub> = 8.5 Hz; CH<sub>2</sub>), 8.24-8.22 (m, 2H; Ar-H), 7.94-7.92 (m, 2H; Ar-H), 7.88 (d, 2H, <sup>3</sup>J<sub>HH</sub> = 9.3 Hz; CH<sub>2</sub>), 7.74 (d, 2H, <sup>3</sup>J<sub>HH</sub> = 7.9 Hz, <sup>4</sup>J<sub>HH</sub> = 1.1 Hz; Ar-H), 7.54 (dd, 2H, <sup>3</sup>J<sub>HH</sub> = 7.9 Hz, <sup>4</sup>J<sub>HH</sub> = 1.2 Hz; Ar-H), 7.30 (dd, 2H, <sup>3</sup>J<sub>HH</sub> = 7.4, <sup>3</sup>J<sub>HH</sub> = 1.1 Hz; Ar-H), 7.02 (d, 2H, <sup>3</sup>J<sub>HH</sub> = 9.1 Hz; CH<sub>2</sub>); Complex **8** was too insoluble for a proper <sup>13</sup>C NMR analysis; MALDI(+): *m/z* = 580.3 [M]<sup>+</sup> (calcd. 580.09); UV-Vis (*c* = 0.20 mg in 20 mL, THF): λ<sub>max</sub> (ε) = 248 nm (56802 mol<sup>-1</sup>·m<sup>3</sup>·cm<sup>-1</sup>), λ<sub>max</sub> (ε) = 322 nm (18520 mol<sup>-1</sup>·m<sup>3</sup>·cm<sup>-1</sup>), λ<sub>max</sub> (ε) = 356 nm (14414 mol<sup>-1</sup>·m<sup>3</sup>·cm<sup>-1</sup>), λ (ε) = 428 nm (23622 mol<sup>-1</sup>·m<sup>3</sup>·cm<sup>-1</sup>), λ (ε) = 522 nm (33424 mol<sup>-1</sup>·m<sup>3</sup>·cm<sup>-1</sup>); elemental analysis calcd. (%) for C<sub>34</sub>H<sub>20</sub>N<sub>4</sub>O<sub>2</sub>Zn·H<sub>2</sub>O·½DMSO: C 65.34, H 3.71, N 9.01; found: C 65.61, H 3.73, N 9.48. The presence of DMSO in the microanalysis sample was supported by <sup>1</sup>H NMR.

**Zn(salphenazine) complex (9):** 2,3-diaminophenazine (90 mg, 0.42 mmol) was dissolved in DMSO (1.5 mL) and the mixture was heated to 100°C in order to dissolve the reagent. While stirring, to the heated solution was added a DMSO solution (1 mL) of 2,3-dihydroxy-benzaldehyde (130 mg, 0.94 mmol) and a methanol solution (1 mL) of Zn(OAc)<sub>2</sub>·H<sub>2</sub>O (193 mg, 0.87 mmol). The reaction mixture was stirred for 2 h at 100°C, and subsequently cooled to room temperature. A further amount of methanol was



added and the precipitate which formed was filtered off. The solid that was obtained was recrystallized from hot DMF to yield a brown powder (59 mg, 23 %). <sup>1</sup>H NMR (400 MHz, DMSO-*d*<sub>6</sub>): δ = 9.50 (s, 4H; CH=N), δ = 9.10 (s, 4H; CH=N), 8.87 (s, 4H; Ar-H), 8.62 (s, 4H; Ar-H), 8.27-8.24 (m, 8H; Ar-H), 8.10-7.94 (m, 8H; Ar-H), 6.97 (d, 4H, <sup>3</sup>J<sub>HH</sub> = 7.3 Hz; Ar-H), 6.68 (d, 4H, <sup>3</sup>J<sub>HH</sub> = 7.7 Hz; Ar-H), 6.59-6.55 (m, 8H; Ar-H), 6.43 (d, 4H, <sup>3</sup>J<sub>HH</sub> = 7.6 Hz; Ar-H), 6.02-5.96 (m, 4H; Ar-H); Complex **9** was too insoluble for a proper <sup>13</sup>C NMR analysis; MALDI(+): *m/z* = 2308.1 [M]<sup>+</sup> (calcd. 2308.83); UV-Vis (*c* = 0.65 mg in 20 mL, THF): λ<sub>max</sub> (ε) = 413 nm (94263 mol<sup>-1</sup>·m<sup>3</sup>·cm<sup>-1</sup>); elemental analysis calcd. (%) for C<sub>104</sub>H<sub>56</sub>N<sub>16</sub>O<sub>16</sub>Zn<sub>8</sub>·3py·4H<sub>2</sub>O: C 54.59, H 3.04, N 10.17; found: C 55.01, H 3.62, N 10.11. The presence of pyridine in the microanalysis

sample was supported by  $^1\text{H}$  NMR.

## 4.10 References and notes

- 
- [1] *Organic Photovoltaics. Concept and Realization*, C. Brabec (ed.), V. Dyakonov, J. Parisi, N. S. Saritiftci, Springer Verlag, Berlin, **2003**.
- [2] G. Yu, J. Gao, J. C. Hummelen, F. Wudl, A. J. Heeger, *Science* **1995**, *270*, 1789.
- [3] a) Y. Sun, G. C. Welch, W. L. Leong, C. J. Takacs, G. C. Bazan, A. J. Heeger, *Nat. Mater.* **2012**, *11*, 659; b) Y.-H. Chen, L.-Y. Lin, C.-W. Lu, F. Lin, Z.-Y. Huang, H.-W. Lin, P.-H. Wang, Y.-H. Liu, K.-T. Wong, J. Wen, D. J. Miller, S. B. Darling, *J. Am. Chem. Soc.* **2012**, *134*, 13616.
- [4] a) J. Roncali, *Acc. Chem. Res.* **2009**, *42*, 1719; b) B. Walker, C. Kim, T.-Q. Nguyen, *Chem. Mater.* **2011**, *23*, 470.
- [5] a) M. T. Lloyd, A. C. Mayer, S. Subramanian, D. A. Mourey, D. J. Herman, A. V. Bapat, J. E. Anthony, G. G. Malliaras, *J. Am. Chem. Soc.* **2007**, *129*, 9144; b) F. Silvestri, A. Marrocchi, M. Seri, C. Kim, T. J. Marks, A. Facchetti, A. Taticchi, *J. Am. Chem. Soc.* **2010**, *132*, 6108; c) K. N. Winzenberg, P. Kemppinen, G. Fanchini, M. Bown, G. E. Collis, C. M. Forsyth, K. Hegedus, T. B. Singh, S. E. Watkins, *Chem. Mater.* **2009**, *21*, 5701.
- [6] a) J. Roncali, P. Frère, P. Blanchard, R. de Bettignies, M. Turbiez, S. Roquet, P. Leriche, Y. Nicolas, *Thin Solid Films* **2006**, *511*, 567; b) X. Sun, Y. Zhou, W. Wu, Y. Liu, W. Tian, G. Yu, W. Qiu, S. Chen, D. Zhu, *J. Phys. Chem. B* **2006**, *110*, 7702; c) N. Kopidakis, W. J. Mitchell, J. van de Lagemaat, D. S. Ginley, G. Rumbles, S. E. Shaheen, W. L. Rance, *Appl. Phys. Lett.* **2006**, *89*, 103524; d) C.-Q. Ma, M. Fonrodona, M. C. Schikora, M. M. Wienk, R. A. J. Janssen, P. Bäuerle, *Adv. Funct. Mater.* **2008**, *18*, 3323.
- [7] T. Rousseau, A. Cravino, E. Ripaud, P. Leriche, S. Rihn, A. de Nicola, R. Ziessel, J. Roncali, *Chem. Commun.* **2010**, *46*, 5082.
- [8] a) A. B. Tamayo, B. Walker, T.-Q. Nguyen, *J. Phys. Chem. C* **2008**, *112*, 11545; b) A. B. Tamayo, X.-D. Dang, B. Walker, J. H. Seo, T. Kent, T.-Q. Nguyen, *Appl. Phys. Lett.* **2009**, *94*, 103301; c) B. Walker, A. B. Tamayo, X.-D. Dang, P. Zalar, J. H. Seo, A. Garcia, M. Tantiwiwat, T.-Q. Nguyen, *Adv. Funct. Mater.* **2009**, *19*, 3063; d) S. Loser, C. J. Bruns, H. Miyauchi, R. P. Ortiz, A. Facchetti, S. I. Stupp, T. J. Marks, *J. Am. Chem. Soc.* **2011**, *133*, 8142.

- [9] a) M. K. R. Fischer, I. López-Duarte, M. M. Wienk, M. V. Martínez-Díaz, R. A. J. Janssen, P. Bäuerle, T. Torres, *J. Am. Chem. Soc.* **2009**, *131*, 8669; b) G. Bottari, G. de la Torre, D. M. Guldi, T. Torres, *Chem. Rev.* **2010**, *110*, 676.
- [10] H. Bürckstümmer, E. V. Tulyakova, M. Deppisch, M. R. Lenze, N. M. Kronenberg, M. Gsänger, M. Stolte, K. Meerholz, F. Würthner, *Angew. Chem. Int. Ed.* **2011**, *50*, 11628.
- [11] a) D. Bagnis, L. Beverina, H. Huang, F. Silvestri, Y. Yao, H. Yan, G. A. Pagani, T. J. Marks, A. Facchetti, *J. Am. Chem. Soc.* **2010**, *132*, 4074; b) G. Wei, S. Wang, K. Sun, M. E. Thompson, S. R. Forrest, *Adv. Energy Mater.* **2011**, *1*, 184.
- [12] a) Y. Matsuo, Y. Sato, T. Niinomi, I. Soga, H. Tanaka, E. Nakamura, *J. Am. Chem. Soc.* **2009**, *131*, 16048; b) J. Hatano, N. Obata, S. Yamaguchi, T. Yasuda, Y. Matsuo, *J. Mater. Chem.* **2012**, *22*, 19258.
- [13] For an overview of supramolecular porphyrin structures: a) F. D'Souza, O. Ito, *Coord. Chem. Rev.* **2005**, *249*, 1410; b) H. Imahori, T. Umeyama, K. Kurotobi, Y. Takano, *Chem. Commun.* **2012**, *48*, 4032; c) T. Umeyama, H. Imahori, *J. Phys. Chem. C* **2013**, *117*, 3195.
- [14] S. Yang, H. Kou, H. Wang, K. Cheng, J. Wanga, *New J. Chem.* **2010**, *34*, 313.
- [15] a) E. N. Jacobsen, *Acc. Chem. Res.* **2000**, *33*, 421; b) P. Pfeiffer, E. Brieth, E. Lubbe, T. Tsumaki, *Justus Liebigs Ann. Chem.* **1933**, *503*, 84; c) M. Palucki, N. S. Finney, P. J. Pospisil, M. L. Güler, T. Ishida, E. N. Jacobsen, *J. Am. Chem. Soc.* **1998**, *120*, 948.
- [16] a) H. Houjou, M. Ito, K. Araki, *Inorg. Chem.* **2009**, *48*, 10703; b) H. Houjou, M. Ito, K. Araki, *Inorg. Chem.* **2011**, *50*, 5298.
- [17] a) A. C. W. Leung, J. H. Chong, B. O. Patrick, M. J. MacLachlan, *Macromolecules.* **2003**, *36*, 5051; b) Z. Guo, W.-L. Tong, M. C. W. Chan, *Chem. Commun.*, **2009**, 6189; c) S. Sun, W.-L. Tong, M. C. W. Chan, *Macromol. Rapid Commun.* **2010**, *31*, 1965; d) S. J. Wezenberg, E. C. Escudero-Adán, J. Benet-Buchholz, A. W. Kleij, *Org. Lett.* **2008**, *10*, 3311; e) S. J. Wezenberg, E. C. Escudero-Adán, D. Anselmo, J. Benet-Buchholz, A. W. Kleij, *Eur. J. Inorg. Chem.* **2010**, 4611.
- [18] C.-M. Che, C.-C. Kwok, S.-W. Lai, A. F. Rausch, W. J. Finkenzeller, N. Zhu, H. Yersin, *Chem. Eur. J.* **2010**, *16*, 233.
- [19] Zn(salphenazine)s have been reported but not characterized in great detail, see: A. Abdolmaleki, S. Malek-Ahmadi, *Can. J. Chem.* **2011**, *89*, 1202.
- [20] a) R. M. Haak, A. Decortes, E. C. Escudero-Adán, M. Martínez Belmonte, E. Martín, J. Benet-Buchholz, A. W. Kleij, *Inorg. Chem.* **2011**, *50*, 7934; b) E. C. Escudero-Adán, N. Kielland, M. Martínez Belmonte, Arjan W. Kleij, *Dalton Trans.* **2013**, *42*, 1427.

- [21] a) A. W. Kleij, D. M. Tooke, M. Kuil, M. Lutz, A. L. Spek, J. N. H. Reek, *Chem. Eur. J.* **2005**, *11*, 4743; b) A. L. Singer, D. A. Atwood, *Inorg. Chim. Acta.* **1998**, *277*, 157.
- [22] a) M. Mentel, E. G. Ahuja, D. V. Mavrodi, R. Breinbauer, L. S. Thomashow, W. Blankenfeldt, *ChemBioChem* **2009**, *10*, 2295; b) A. K. Jana, *J. Photochem. Photobiol., A.* **2000**, *132*, 1.
- [23] B. Walker, C. Kim, T.-Q. Nguyen, *Chem. Mater.* **2011**, *23*, 470.
- [24] For more information on EDDM see Experimental section.
- [25] J.-L. Brédas, J. E. Norton, J. Cornil, V. Coropceanu, *Acc. Chem. Res.* **2009**, *42*, 1691.
- [26] B. W. D'Andrade, S. Datta, S. R. Forrest, P. Djurovich, E. Polikarpov, M. E. Thompson, *Org. Electron.* **2005**, *6*, 11.
- [27] R. Schwedhelm, L. Kipp, A. Dallmeyer, M. Skibowski, *Phys. Rev. B* **1998**, *58*, 13176.
- [28] S. Schumann, R. A. Hatton, T. S. Jones, *J. Phys. Chem. C* **2011**, *115*, 4916.
- [29] G. Salassa, M. J. J. Coenen, S. J. Wezenberg, B. L. M. Hendriksen, S. Speller, J. A. A. W. Elemans, A. W. Kleij, *J. Am. Chem. Soc.* **2012**, *134*, 7186.
- [30] *Gaussian 09*, Revision 7.0, M. J. Frisch, G. W. Trucks, H. B. Schlegel, G. E. Scuseria, M. A. Robb, J. R. Cheeseman, G. Scalmani, V. Barone, B. Mennucci, G. A. Petersson, H. Nakatsuji, M. Caricato, X. Li, H. P. Hratchian, A. F. Izmaylov, J. Bloino, G. Zheng, J. L. Sonnenberg, M. Hada, M. Ehara, K. Toyota, R. Fukuda, J. Hasegawa, M. Ishida, T. Nakajima, Y. Honda, O. Kitao, H. Nakai, T. Vreven, J. A. Montgomery, Jr., J. E. Peralta, F. Ogliaro, M. Bearpark, J. J. Heyd, E. Brothers, K. N. Kudin, V. N. Staroverov, R. Kobayashi, J. Normand, K. Raghavachari, A. Rendell, J. C. Burant, S. S. Iyengar, J. Tomasi, M. Cossi, N. Rega, J. M. Millam, M. Klene, J. E. Knox, J. B. Cross, V. Bakken, C. Adamo, J. Jaramillo, R. Gomperts, R. E. Stratmann, O. Yazyev, A. J. Austin, R. Cammi, C. Pomelli, J. W. Ochterski, R. L. Martin, K. Morokuma, V. G. Zakrzewski, G. A. Voth, P. Salvador, J. J. Dannenberg, S. Dapprich, A. D. Daniels, Ö. Farkas, J. B. Foresman, J. V. Ortiz, J. Cioslowski, D. J. Fox, Gaussian, Inc., Wallingford CT, **2009**.
- [31] D. Becke, *J. Chem. Phys.* **1993**, *98*, 5648.
- [32] C. Lee, W. Yang, R. G. Parr, *Phys. Rev. B: Condens. Matter* **1988**, *37*, 785.
- [33] P. J. Hay, W. R. Wadt, *J. Chem. Phys.* **1985**, *82*, 270.
- [34] A. D. McLean, G. S. Chandler, *J. Chem. Phys.* **1980**, *72*, 5639.
- [35] a) M. E. Casida, C. Jamorski, K. C. Casida, D. R. Salahub, *J. Chem. Phys.* **1998**, *108*, 4439; b) R. E. Stratmann, G. E. Scuseria, M. J. Frisch, *J. Chem. Phys.* **1998**, *109*, 8218.
- [36] Y. Zhao and D. G. Truhlar, *Theor. Chem. Acc.* **2008**, *120*, 215.

- [37] a) M. Cossi, N. Rega, G. Scalmani, V. Barone, *J. Comput. Chem.* **2003**, *24*, 669; b) M. Cossi, V. Barone, *J. Chem. Phys.* **2001**, *115*, 4708.
- [38] W. R. Browne, N. M. O'Boyle, J. J. McGarvey, J. G. Vos, *Chem. Soc. Rev.* **2005**, *34*, 641.
- [39] *Gausssum 2.25*: N. M. O'Boyle, A. L. Tenderholt, K. M. Langner, *J. Comput. Chem.* **2008**, *29*, 839.



UNIVERSITAT ROVIRA I VIRGILI

SUPRAMOLECULAR, PHOTOPHYSICAL AND CATALYTIC PROPERTIES OF ZN(SALPHEN) BASED COMPLEXES AND MATERIALS

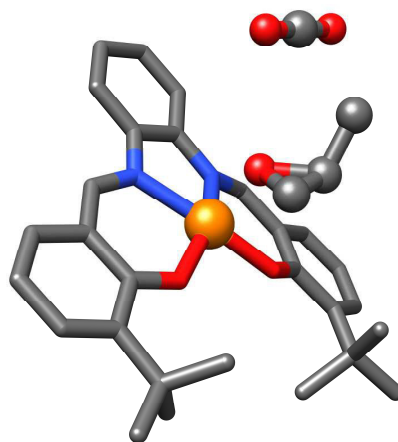
Giovanni Salassa

Dipòsit Legal: T. 1430-2013

# Chapter 5

## A DFT Study on the Mechanism for the Ring-Expansion Addition Reaction of CO<sub>2</sub> to Epoxides Catalyzed by Zn(salphen) Complexes

*The reaction mechanism for the Zn(salphen)/NBu<sub>4</sub>X (X = Br, I) mediated ring-expansion addition of CO<sub>2</sub> to a series of epoxides, affording cyclic carbonate products has been investigated in detail using DFT. The ring-opening step of the process was examined and the preference for opening at the methylene (C<sub>β</sub>) or methine carbon (C<sub>α</sub>) was established. Furthermore, calculations were performed to clarify the reasons for the lethargic behaviour of internal epoxides in the presence of the binary catalyst. Also the CO<sub>2</sub> insertion and the ring-closing steps have been explored for six differently substituted epoxides and these proved to be significantly more challenging compared with the ring-opening step.*



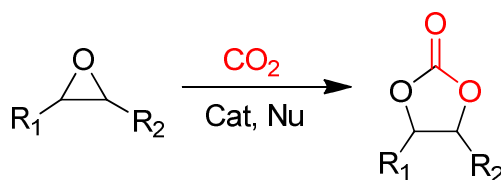
The work described in this chapter has been published: F. Castro-Gómez, G. Salassa, A. W. Kleij, C. Bo, *Chem. Eur. J.* **2013**, *19*, 6289.

### 5.1 Introduction

The growing concerns about climate change and the need to find suitable alternatives for our depleting fossil fuel based feedstocks have resulted in extensive research to find new renewable carbon sources. Carbon dioxide (CO<sub>2</sub>) may indeed be considered an abundant and renewable carbon source. In light of this, it has become a popular building

block from a sustainability point of view<sup>[1]</sup> and can thus be seen as an interesting starting point for the synthesis of various organic molecules.<sup>[2]</sup> One reaction that utilizes CO<sub>2</sub> as a carbon source and which is currently attracting a great deal of interest is the atom-efficient ring-expansion addition of CO<sub>2</sub> to epoxides, resulting in useful cyclic carbonate products (Scheme 1).<sup>[3]</sup> The conventional industrial way of organic carbonate formation uses phosgene as a (toxic) reagent and results in hazardous waste streams.<sup>[4]</sup> Therefore, new and greener methodologies able to mediate this transformation have become increasingly interesting. Cyclic carbonates are employed as polar aprotic solvents and electrolytes in rechargeable batteries, intermediates for organic polycarbonate synthesis, and in the production of pharmaceuticals and fine chemicals.<sup>[1,5]</sup>

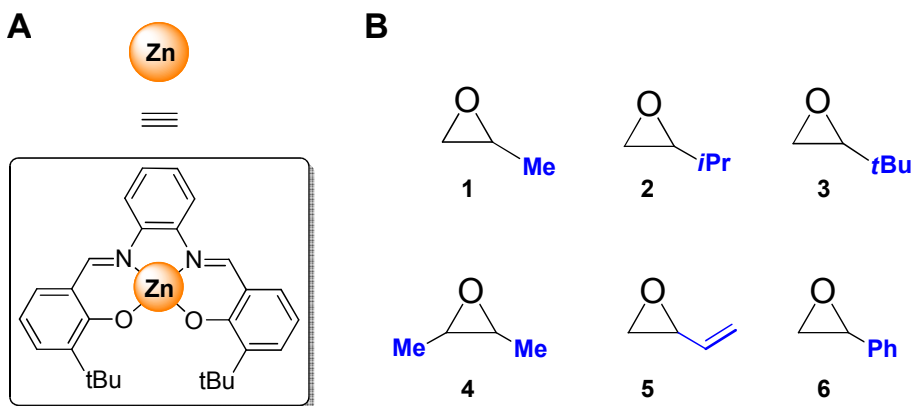
The ring-expansion addition reaction has been widely studied and can be catalyzed by a variety of catalyst types such as quaternary ammonium salts,<sup>[6]</sup> alkali metal halides,<sup>[7]</sup> ionic liquids,<sup>[8]</sup> functional polymers<sup>[9]</sup> and transition metal complexes.<sup>[10]</sup> However, there are still disadvantages to overcome upon using these catalyst systems such as low catalyst reactivity/stability, use of high pressures and/or temperatures, high catalyst loadings required for efficient turnover, toxicity issues, cost effectiveness and availability of the catalyst system, or a combination of these features. Hence, it is crucial to know how the performance of any given catalyst can be improved, and mechanistic understanding provides a means to unravel the obstacles associated with the observation of low reactivity and/or selectivity.



**Scheme 1.** The ring-expansion addition reaction of CO<sub>2</sub> with epoxides generating five-membered cyclic carbonates using a Lewis acidic metal catalyst (Cat) and a co-catalyst (Nu; nucleophile).

To date, a limited series of theoretical studies on the mechanism for the catalytic ring-expansion addition of CO<sub>2</sub> to epoxides have been reported involving either heterobimetallic Ru-Mn complexes<sup>[11]</sup>, ionic liquids,<sup>[12]</sup> N-heterocyclic carbenes<sup>[13]</sup>, polyoxometalates,<sup>[14]</sup> polyphenolic compounds<sup>[15]</sup> or carboxylate-tagged biopolymers.<sup>[16]</sup>

Zhang and co-workers<sup>[17]</sup> thoroughly elucidated the mechanism of conversion of ethylene oxide with CO<sub>2</sub> catalyzed by quaternary ammonium salts. In these studies, they obtained structural and energetic information concerning each step of the catalytic cycle and also evaluated the effect of the N-alkyl chain length and the type of anion. In addition, Han and co-workers<sup>[18]</sup> studied in detail the KI catalyzed ring-expansion addition of CO<sub>2</sub> to propylene oxide, and also investigated the (co)catalytic role of glycerol and propylene glycol.



**Scheme 2.** (A) Schematic drawing of the Zn(salphen) catalyst; (B) substrates 1-6 used in this investigation.

Kleij and co-workers recently reported on the use of Zn(salphen) complexes (Scheme 2A) in conjunction with NBu<sub>4</sub>I as efficient binary catalysts for the formation of cyclic carbonates under mild reaction conditions ( $p\text{CO}_2 = 2\text{-}10$  bar;  $T = 25\text{-}45^\circ\text{C}$ ).<sup>[19]</sup> From these previous studies it has become clear that terminal epoxides are conveniently converted into their carbonates in high yield, whereas the same binary catalyst system proved to be rather ineffective for the conversion of internal and more sterically congested substrates. At a later stage, Kleij and co-workers found that more efficient catalysis of these latter substrates can be achieved when working under solvent-free, supercritical CO<sub>2</sub> conditions,<sup>[20]</sup> giving highly improved conversion levels in much shorter time frames. As reported extensively in literature, there are a variety of well-defined binary catalytic systems based on metallosalens<sup>[21]</sup> and halide salts which provide efficient CO<sub>2</sub>/epoxide ring-expansion addition catalysts under mild reaction conditions. Thus, the metallosalen family of catalysts could be regarded as privileged

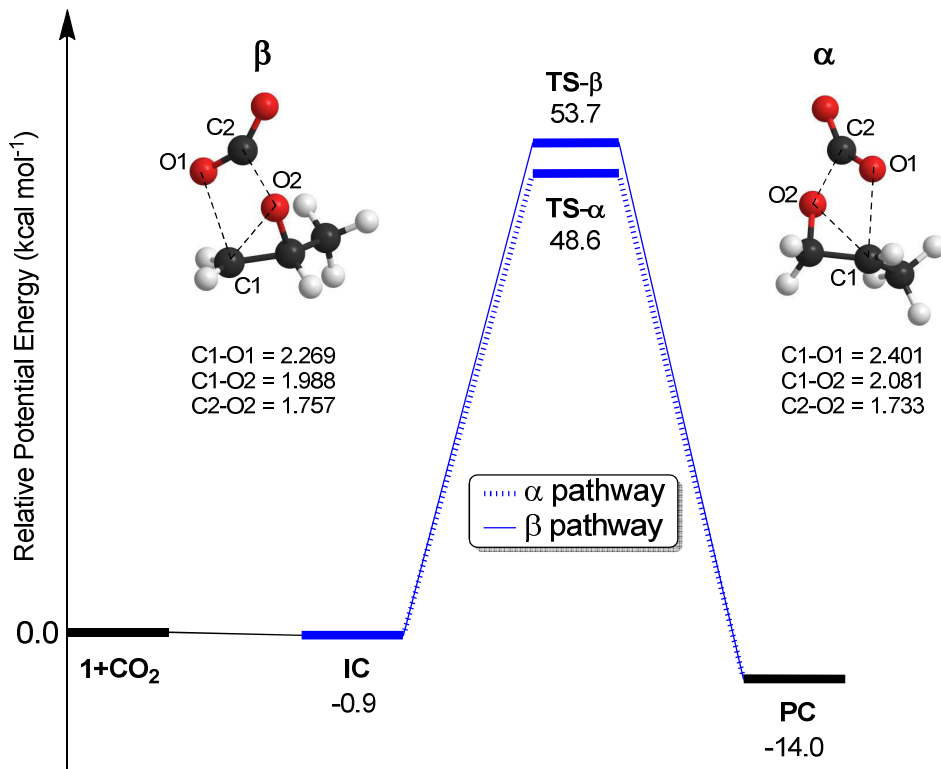
systems in the context of (cyclic) organic carbonate formation. Though various mechanistic proposals have been put forward throughout the years and in some cases even verified by experimental data,<sup>[22]</sup> there is surprisingly limited information available regarding the major obstacles associated with the use of relatively more challenging substrates including those based on sterically congested oxiranes and internal epoxides. This in combination with our previous findings<sup>[19,20]</sup> using Zn(salphen)s as catalyst systems prompted us to investigate these challenging conversions in more detail using computational methods. Herein, a detailed DFT study on the mechanism of the ring-expansion addition reaction with a series of epoxides (Scheme 2B, compounds **1-6**) catalyzed by the binary system Zn(salphen)/NBu<sub>4</sub>X (X = Br, I) is reported. We have calculated the full energy profiles for various substrates and particularly focused on those aspects that help to explain the lower reactivities found for the more challenging substrates, providing new insights that are potentially useful for the development of more powerful catalyst systems.

## 5.2 The uncatalyzed ring-expansion addition

Ring-expansion addition of CO<sub>2</sub> to propylene oxide **1** can be achieved through a single step, leading to the formation of propylene carbonate (**PC**). The reaction in the absence of catalyst proceeds *via* nucleophilic attack from an oxygen atom of CO<sub>2</sub> on the  $\alpha$  carbon (most substituted carbon) or the  $\beta$  carbon (least substituted carbon) atom of **1**. The two calculated reaction pathways are shown in Figure 1, together with the optimized structures of the two transition states (**TS**). The unique imaginary vibrational frequencies of TS- $\alpha$  and TS- $\beta$  correspond to the simultaneous breaking of the C <sub>$\alpha$</sub> -O or C <sub>$\beta$</sub> -O bond of the epoxide and the simultaneous formation of two new C-O bonds which originate from the insertion of CO<sub>2</sub>.

High energy barriers of 48.6 ( $\alpha$  pathway) and 53.7 kcal·mol<sup>-1</sup> ( $\beta$  pathway) are involved to form the cyclic carbonate product. The  $\alpha$  pathway is favoured by 5.1 kcal·mol<sup>-1</sup> compared to  $\beta$  pathway. Previous DFT calculations reported by Zhang and co-workers<sup>[12a]</sup> showed somewhat higher energy barriers of 53.4 kcal·mol<sup>-1</sup> for  $\alpha$  pathway and 58.1 kcal·mol<sup>-1</sup> for the  $\beta$  pathway. Similar to the work from Zhang, Han

and co-workers<sup>[18]</sup> reported energy barriers of 55.3 and 61.4 kcal·mol<sup>-1</sup> for the  $\alpha$  and  $\beta$  pathways, respectively.

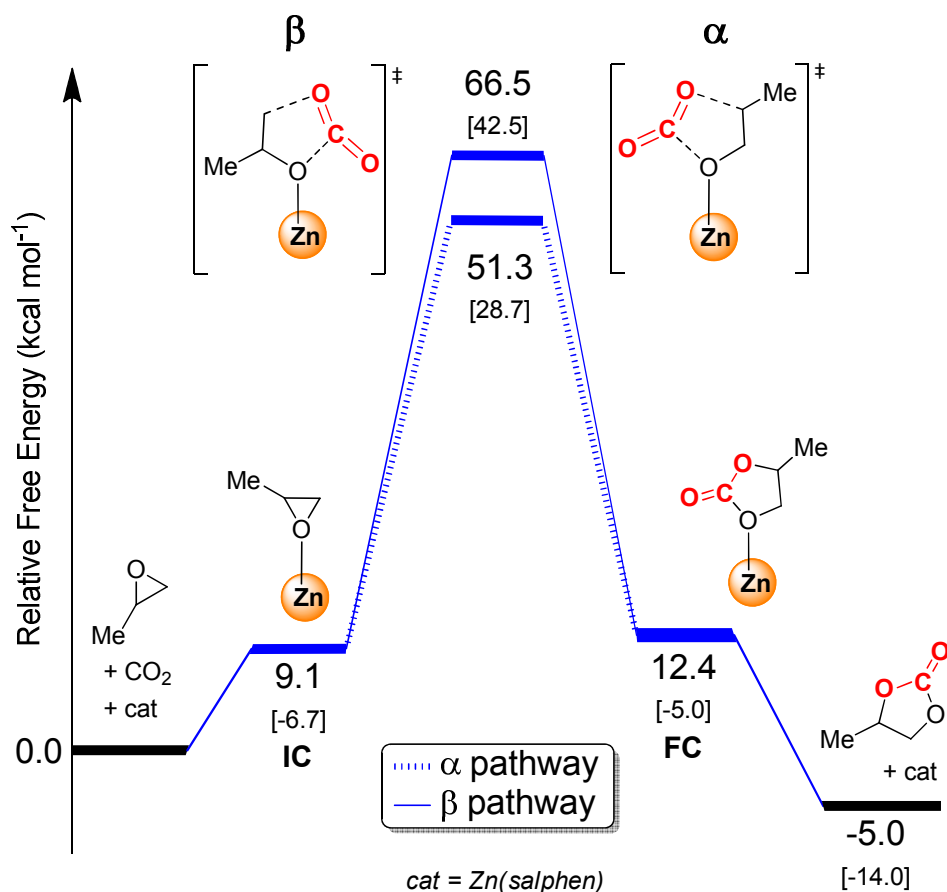


**Figure 1.** Potential energy profile for the uncatalyzed ring-expansion addition of CO<sub>2</sub> with propylene oxide **1** to give propylene carbonate (**PC**). **IC** stands for initial complex formation. Note that potential energy is here used to make a comparison possible with the literature data.

### 5.3 The Zn(salphen) catalyzed ring-expansion addition

Similar to the uncatalyzed reaction, the ring-expansion addition reaction of CO<sub>2</sub> to propylene oxide **1** catalyzed by the Zn(salphen) complex of Scheme 2 can involve two possible reaction pathways. The relative free energy profile of the  $\alpha$  and  $\beta$  pathways are depicted in Figure 2, where the sum of energies of the isolated reactants (**1** + CO<sub>2</sub>) and Zn(salphen) was set to zero. The initial step is the coordination of the epoxide to the Zn(salphen) complex forming an initial complex (**IC**) followed by a concerted ring-opening and CO<sub>2</sub> insertion step. For both pathways the only transition state relates to the simultaneous stretching/breaking of the C <sub>$\alpha$</sub> -O or C <sub>$\beta$</sub> -O bond of the epoxide, and

the bending of the CO<sub>2</sub> molecule leading to the formation of two new C–O bonds. Once the coordinated cyclic carbonate is formed (**FC**) it is released from the Zn(salphen) complex allowing for further epoxide turnover. The calculated barriers for the exothermic reaction show that the  $\alpha$  pathway is favored by 15.2 kcal·mol<sup>-1</sup> compared to the  $\beta$  pathway. The relative potential energy barrier for the Zn(salphen) catalyzed ring-expansion addition (Figure 2, energy values in brackets) is reduced by 19.9 kcal·mol<sup>-1</sup> compared to the uncatalyzed reaction likely as a result of the formation of a Zn(salphen)/epoxide complex polarizing the C–O bond of the substrate and thus playing an important role in its activation.



**Figure 2.** Free energy profile for the Zn(salphen) catalyzed ring-expansion addition of CO<sub>2</sub> to propylene oxide **1**; the relative potential energy values are reported in brackets. **IC** stands for initial complex formation; **FC** stands for the final complex having the carbonate product coordinated.

## 5.4 The Zn(salphen)/NBu<sub>4</sub>I catalyzed ring-expansion addition

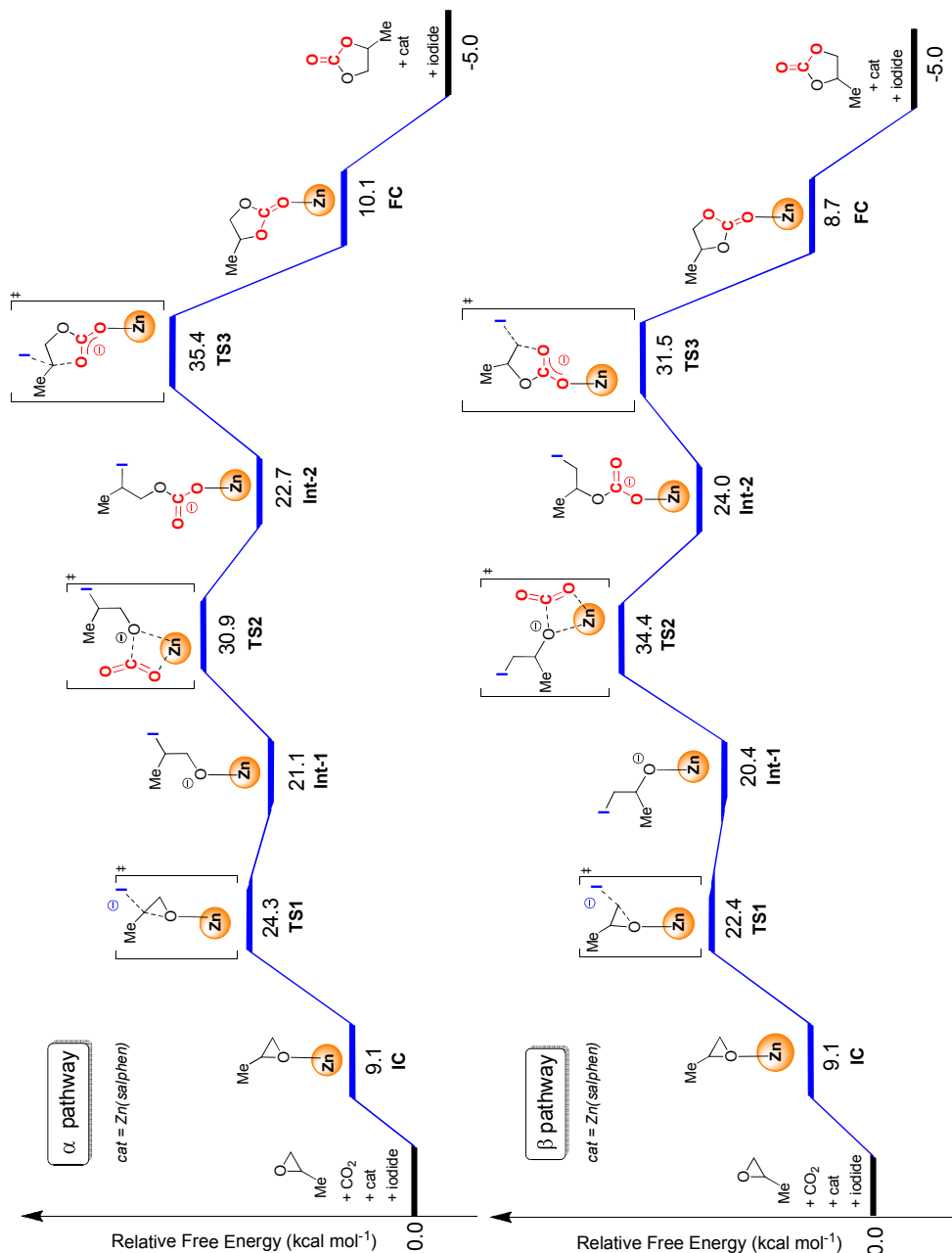
In the previous discussion, the investigation of the uncatalyzed and the Zn(salphen) catalyzed mechanisms highlight that the ring-opening step is initiated by CO<sub>2</sub> leading to the direct formation of the cyclic carbonate. The high energy barriers found for this ring-opening process suggest that these reactions can thus only occur under harsh reaction conditions, i.e. high temperatures and/or pressures. As reported extensively in the literature,<sup>[21]</sup> generally a binary catalytic system is needed in order to obtain good conversions/yields under mild reaction conditions. The binary catalytic system usually combine a Lewis acid and a suitable nucleophile (most often a halide) that make the ring-opening procedure less energetically demanding and the subsequent CO<sub>2</sub> insertion easier. It should be noted that the nucleophiles themselves are able to catalyze the CO<sub>2</sub> addition to epoxides.<sup>[6a,15,17,18]</sup> The most relevant result to the present study is the KI catalyzed ring-opening of propylene oxide reported by Han<sup>[18]</sup> showing gas phase barriers in the range 36.3–37.6 kcal·mol<sup>-1</sup> depending on the reaction pathway. Kleij and co-workers found a fairly similar barrier (38.9 kcal·mol<sup>-1</sup>) when using NBu<sub>4</sub>I as catalyst.<sup>[3g]</sup> Thus, halide nucleophiles are able to significantly lower the transition state related to ring-opening of the epoxide (cf., values reported for the uncatalyzed reaction in Figure 1).

Zn(salphen) complexes have recently been shown to efficiently catalyze the ring-expansion addition reaction under mild reaction conditions, using quaternary ammonium halide salts as nucleophiles.<sup>[19,20]</sup> Next we evaluated computationally the effect of combining both the Zn(salphen) as well as halide nucleophile (NBu<sub>4</sub>X; X = Br, I) in the DFT analysis. Upon evaluation of this binary system the potential for two different catalytic pathways ( $\alpha$  or  $\beta$  attack on the epoxide) was identified similar to the uncatalyzed and Zn(salphen) catalyzed ring-expansion addition reaction (Figures 1 and 2). DFT calculations were performed in the first instance on the simplest substrate, propylene oxide **1**. It should be noted that for the envisioned mechanisms we have only considered penta-coordinated rather than hexa-coordinated reaction intermediates. Hexa-coordinated species have been frequently observed and proposed for other metallosalen catalysts comprising of Al,<sup>[23]</sup> Mn,<sup>[24]</sup> Co,<sup>[25]</sup> and Cr<sup>[26]</sup> metal ions, and in some of these cases (preliminary) mechanistic work has revealed that bimetallic pathways lead to



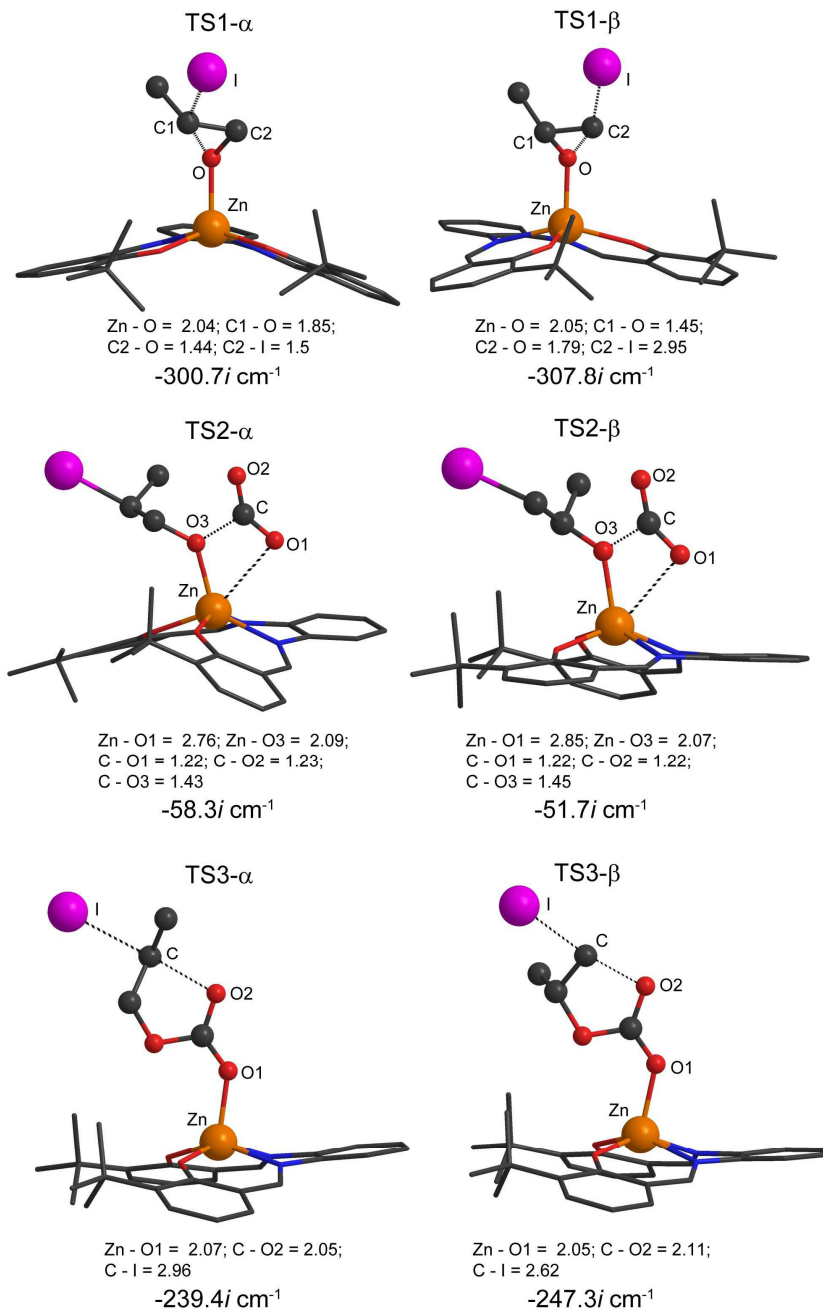
more efficient catalytic processes. However, in the case of Zn(salphen)s, hexa-coordination is an extremely rare phenomenon and is only observed in condensed solid phases.<sup>[27]</sup> Furthermore, we<sup>[28]</sup> and others<sup>[29]</sup> have clearly demonstrated that penta-coordination in Zn(salphen)s is highly favoured both in the solid state as well as in solution phases as supported by crystallographic evidence, UV-Vis titration data, Job plot analyses and fitting 1:1 complex–ligand binding models using multivariate data analysis.<sup>[30]</sup> Therefore, the consideration of penta-coordination in the Zn(salphen) case seems to give a reasonable starting point in the mechanisms discussed below.

The resulting energy profiles<sup>[31]</sup> of the  $\alpha$  and  $\beta$  pathways are shown in Figures 3 with schematic representations of the involved intermediates and transitions states; in both cases the first step involves the coordination of **1** (**IC**) to the Zn(salphen) which, as mentioned before, polarizes the C–O epoxide bond thereby facilitating the ring-opening step. It should be noted that the higher free energy for **IC** compared with the separate components is mainly due to an entropic cost for bringing together the Zn(salphen) and the epoxide. The C–O bond polarization is supported by charge analysis of the carbon atoms of the epoxide revealing that both  $C_\alpha$  and  $C_\beta$  become more electron-deficient (Table 2 in the Experimental section) compared with a non-coordinated epoxide. After initial coordination of the epoxide to the Zn(salphen) complex (cf., **IC**), the ring-opening step occurs *via* nucleophilic attack of the iodide. The first transition state (**TS1**) is characterized by the breaking of  $C_{\alpha\beta}$ –O bond and the simultaneous formation of a  $C_{\alpha\beta}$ –I bond as confirmed by the unique imaginary frequency for the attack at  $C_\alpha$  and for  $C_\beta$  (Figure 4). In the case of  $\beta$  pathway, the epoxide ring-opening is energetically more favourable by almost 2 kcal·mol<sup>-1</sup> compared with the  $\alpha$  pathway. In the subsequent step, a molecule of CO<sub>2</sub> reacts with the negatively charged oxygen atom (insertion) of the intermediate **Int-1** leading to the formation of linear carbonate **Int-2**. The second transition state **TS2** involves the formation of new C–O and Zn–O bonds that involve the CO<sub>2</sub> molecule as shown in the relative imaginary frequencies at 58.3i cm<sup>-1</sup> for the  $\alpha$  pathway and 51.7i cm<sup>-1</sup> for the  $\beta$  route (Figure 4). In the pathway related to the  $\beta$  attack, this step is rate-determining with an energy value of 34.4 kcal·mol<sup>-1</sup>, in the  $\alpha$  pathway this step has an energy of 30.9 kcal·mol<sup>-1</sup> and is thus more facile.



**Figure 3.** Free energy profile for the ring-expansion addition of CO<sub>2</sub> to propylene oxide 1 catalyzed by Zn(salphen)/NBu<sub>4</sub>I considering the α and β pathway. IC stands for initial complex formation; FC stands for the final complex having the carbonate product coordinated.

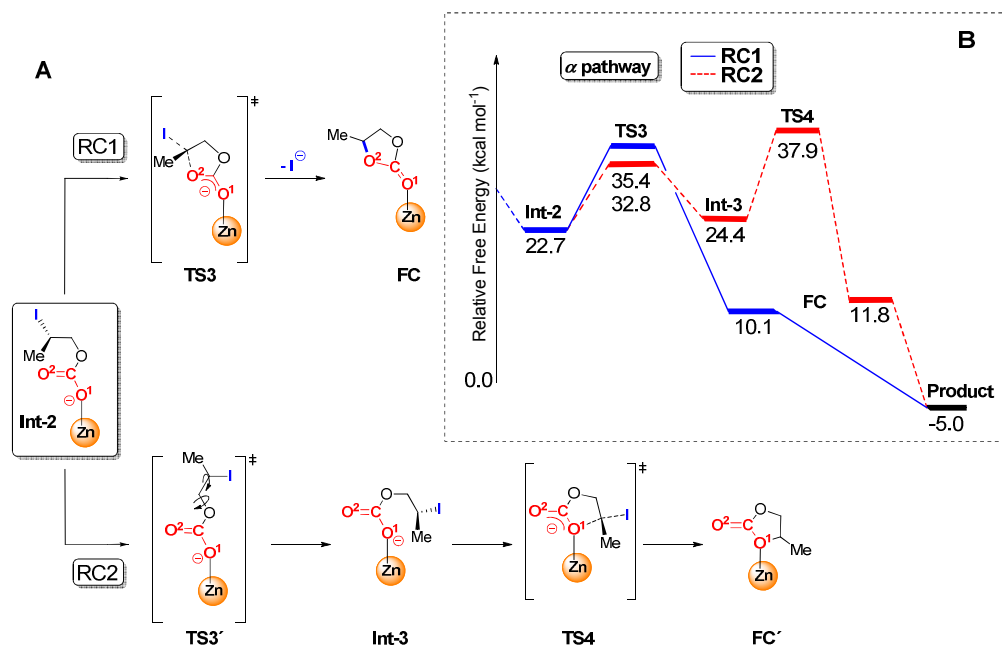
The reason for this difference between the two pathways has mainly a steric origin; the position of the methyl group in the  $\beta$  pathway is closer to the O-atom of the epoxide making the insertion of CO<sub>2</sub> more difficult (see Figure 4). The linear carbonate intermediate **Int-2** undergoes an intramolecular ring-closing with the concomitant release of the iodide nucleophile and formation of the **FC**. In this latter step the carbon atom bound to the iodide binds to the nearest oxygen atom forming a new C–O bond; at the same time, the iodide bond elongates until it breaks (Figure 4). The ring-closing step is found to be the rate-determining step in the  $\alpha$  pathway with an energy of 35.4 kcal·mol<sup>-1</sup>. Similar to the CO<sub>2</sub> insertion step, the methyl group on the C <sub>$\alpha$</sub>  makes the ring-closing step more difficult in the  $\alpha$  pathway, whereas in the  $\beta$  pathway the intermediate linear carbonate is in a more suitable conformation for the ring-closing event. Once formed, the cyclic carbonate is released from the Zn(salphen) complex allowing further epoxide turnover. The overall reaction is exergonic with a release of 5.0 kcal·mol<sup>-1</sup>. The synergistic effect of the binary Zn(salphen)/NBu<sub>4</sub>I catalyst system makes the synthesis of the cyclic carbonate much more accessible. In particular, the high Lewis acidity of the Zn(salphen) complex<sup>[32]</sup> strongly reduces the energy barrier for the ring-opening step through a polarization of the epoxide carbon atoms (48.6 kcal·mol<sup>-1</sup> for the uncatalyzed reaction to 7.03 kcal·mol<sup>-1</sup> for the binary catalyst; both energy values refer to potential energy, see the Experimental section), allowing the nucleophile to attack more easily. As shown in the energetic profiles in Figures 3 there are some important differences between the  $\alpha$  and  $\beta$  pathway using propylene oxide **1** as substrate. First, in the ring-opening step, in contrast with the non-catalyzed reaction, the attack at the  $\beta$  carbon is favoured. Second, the rate-determining steps of the  $\alpha$  and  $\beta$  pathways are at different points during the catalytic cycle; the ring-closing step in the  $\alpha$  pathway and the CO<sub>2</sub> insertion step in the  $\beta$  pathway. This is a consequence of the different position in which the methyl substituent is located during the two possible pathways.



**Figure 4.** Optimized structures for the transition states **TS1–TS3** for both the  $\alpha$  and  $\beta$  pathway together with the most relevant calculated distances (in Å) and value of the negative (imaginary) vibrational frequencies using propylene oxide **1** as substrate.

## 5.5 Ring-closing mechanism

As already shown in Figures 3, the ring-closing step involves the formation of a new C–O bond in both pathways, but when considering the linear intermediate **Int-2** there are two possible routes leading to the cyclic carbonate product through either O–atom of the carbonate (Figure 5a, O1 and O2). In order to establish which ring-closing mechanism is more preferred, the energy profiles for both possible intramolecular nucleophilic pathways were calculated. It can be seen in Figure 5a that when ring-closing occurs *via* the non-coordinating O-atom O2 (**RC1**) only one step is required evolving through **TS3** giving the final intermediate **FC**. When the nucleophilic attack is made by O1 (i.e., through pathway **RC2**), a multi-step mechanism would be operative going first through **TS3'** that after skeletal rearrangement affords **Int-3** followed by ring-closing in **TS4** giving **FC'**. The distinction between complexes **FC** and **FC'** is a consequence of which O–atom (O1 or O2) takes part in the ring closing step.



**Figure 5.** (A) Two possible ring-closing pathways (**RC1** and **RC2**) for the intermediate **Int-2** involving different O–atoms of the carbonate fragment (O1 and O2) in the formation of propylene carbonate. (B) Free energy profile for the ring-closing step in the  $\alpha$  pathway for the conversion of propylene oxide **1** catalyzed by the binary Zn(salphen)/NBu<sub>4</sub>I catalyst.

The comparison between the two pathways indicates that **RC1** is favoured over **RC2** as a result of the fewer steps required and also the lower energy requirement for the rate-determining step (35.4 kcal·mol<sup>-1</sup> for **RC1** compared to 37.9 kcal·mol<sup>-1</sup> for **RC2**). The energy profiles for the two possible ring-closing events in the  $\alpha$  pathway are shown in Figure 5b and similar behaviour is observed for the  $\beta$  pathway (see Figure 9 in the Experimental section).

## 5.6 The Zn(salphen)/NBu<sub>4</sub>Br catalyzed ring-expansion addition

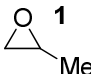
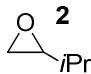
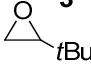
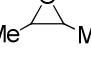
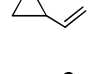
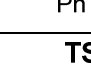

From our initial results<sup>[19a]</sup> we observed that NBu<sub>4</sub>I proved to be a better co-catalyst than NBu<sub>4</sub>Br giving higher conversion levels when using 1,2-epoxyhexane as substrate. Therefore, the effect of using bromide as the nucleophile instead of iodide was evaluated for both the  $\alpha$  and  $\beta$  pathway during the ring-expansion addition of CO<sub>2</sub> to propylene oxide **1**. The first two entries of Table 1 show that the  $\alpha$  pathway is less energetically demanding compared to  $\beta$  pathway and the rate-determining step in the latter is, as calculated for the same pathway using iodide as nucleophile (Figure 3), the CO<sub>2</sub> insertion step (36.5 kcal·mol<sup>-1</sup>). In the ring-opening step, bromide favours the nucleophilic attack at the  $\beta$  carbon by 2.6 kcal·mol<sup>-1</sup> compared with the  $\alpha$ -carbon. When comparing both nucleophiles in the  $\beta$  pathway, the use of bromide (19.6 kcal·mol<sup>-1</sup>) thus lowers the barrier for the ring-opening (**TS1**) of propylene oxide compared to iodide (22.4 kcal·mol<sup>-1</sup>) but higher barriers are found for the other two steps, i.e. **TS2** and **TS3**. Thus, these results are in line with the experimental data obtained for the binary catalyst Zn(salphen)/NBu<sub>4</sub>X (X = Br, I) showing generally somewhat higher activity when iodide is used as nucleophile, and in particular in the conversion of terminal epoxides through the  $\beta$  pathway that shows less dependency on the steric requirements of the catalyst.<sup>[19,20]</sup>

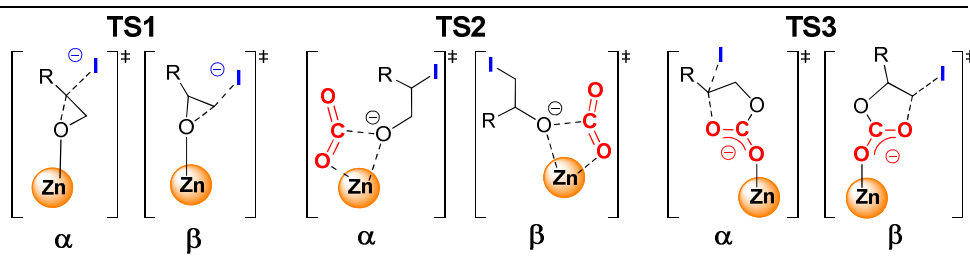
## 5.7 Effect of epoxide substituent

So far focus has been on the ring-expansion addition of CO<sub>2</sub> using propylene oxide **1** as substrate. In order to study the influence of the steric bulk/substitution pattern in the epoxide, further substrates **2-6** (Scheme 2) were considered. When the steric bulk of the C <sub>$\alpha$</sub>  substituent is increased (methyl  $\rightarrow$  isopropyl  $\rightarrow$  *tert*-butyl), the barriers related to the

transition states **TS1–TS3** significantly increase and thus reveal that conversion of more sterically encumbered substrates is more difficult in line with our previous experimental findings using Zn(salphen)s as catalysts.<sup>[19,20]</sup>

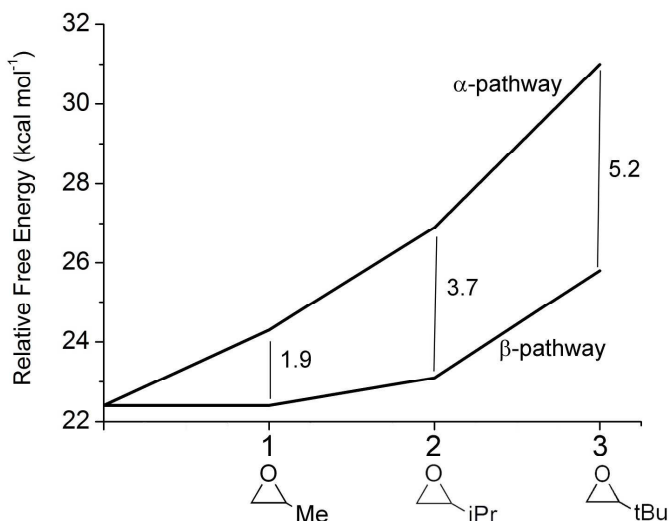
**Table 1.** Calculated free energy values for the three transition states in the ring-expansion addition of CO<sub>2</sub> to epoxides **1–6** at 25°C.<sup>a</sup>

Substrate <sup>[b]</sup>	Nucleophile	TS1 <sup>[c]</sup>	TS2 <sup>[c]</sup>	TS3 <sup>[c]</sup>	
		[kcal·mol <sup>-1</sup> ]	[kcal·mol <sup>-1</sup> ]	[kcal·mol <sup>-1</sup> ]	
	<b>1α</b>	Br	22.2	33.5	33.9
	<b>1β</b>	Br	19.6	36.5	32.0
	<b>1α</b>	I	24.3	30.9	35.4
	<b>1β</b>	I	22.4	34.4	31.5
	<b>2α</b>	I	26.9	31.2	33.7
	<b>2β</b>	I	23.1	38.4	34.5
	<b>3α</b>	I	31.0	41.1	41.2
	<b>3β</b>	I	25.8	44.4	36.3
	<b>4</b>	I	29.5	38.5	40.0
	<b>5α</b>	I	20.0	35.1	32.2
	<b>5β</b>	I	23.5	37.1	35.7
	<b>6α</b>	I	26.0	36.0	36.3
	<b>6β</b>	I	27.5	42.9	40.0



<sup>a</sup> Transition states: **TS1** refers to the ring-opening of the epoxide, **TS2** to the CO<sub>2</sub> insertion step and **TS3** to the energetically most favoured ring-closing pathway. <sup>b</sup> The α and β designations relate to their respective pathways. <sup>c</sup> The energies indicate a system in which the CO<sub>2</sub> pressure is 10 bar as previously used.<sup>[19]</sup>

Furthermore, for the ring-opening of the epoxides **1-3** a clear increase in the difference in energy for **TS1** can be noted when comparing the  $\alpha$  and  $\beta$  pathway in the series **1**→**2**→**3** (Figure 6), and overall the  $\beta$  pathway becomes more favourable. Similar to the calculated mechanism of **1** (Figures 3) we observe that with epoxides **2** and **3** the rate-limiting step does not change and remains the CO<sub>2</sub> insertion for the  $\beta$  pathway and the ring-closing step for the  $\alpha$  pathway.



**Figure 6.** Free energy difference between  $\alpha$  pathway and  $\beta$  pathway in the ring-opening step for epoxides **1**, **2** and **3**

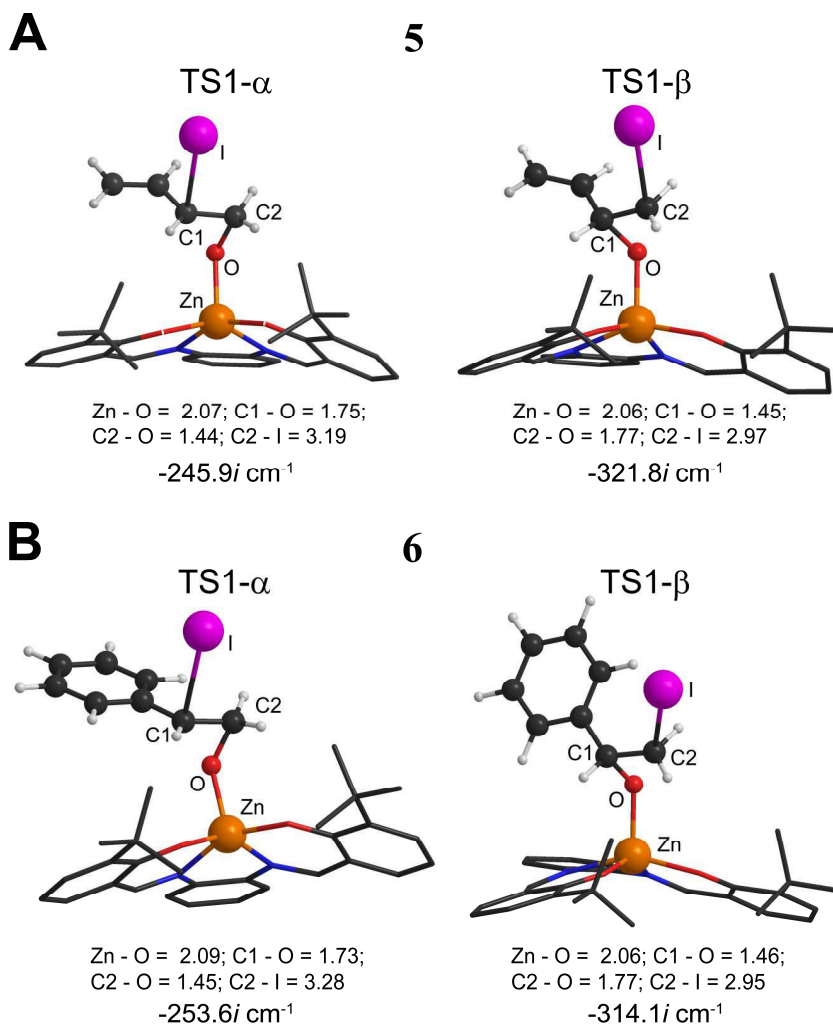
As an example of an internal epoxide, the reaction mechanism of *trans*-2,3-epoxybutane **4** has also been calculated as, experimentally, **4** has been shown to be a significantly less reactive substrate<sup>[19]</sup> and as a result it was necessary to employ much harsher reaction conditions (i.e., higher temperatures and pressures) for successful conversion compared with terminal epoxides.<sup>[20]</sup> As reported in Table 1, all the transition states of **4** have a relatively high energy compared with propylene oxide **1**, and thus the presence of two methyl substituents creates significant steric hindrance in the epoxide to raise the energy barriers for all three steps. These barriers could be overcome by using supercritical CO<sub>2</sub> (conditions used: 80°C,  $p$ CO<sub>2</sub> = 80 bar) as reaction medium<sup>[20]</sup> allowing for good conversion of **4** using Zn(salphen)/NBu<sub>4</sub>Br as a binary catalyst. From the computational data presented thus far, it seems reasonable to assume that for



epoxide substrates **1-4** steric effects are dominant and electronic effects play a less important role. Whereas most terminal epoxides are easily converted into their respective cyclic carbonates, in general substrates **5** and **6** (Scheme 2) are slightly more sluggish and show lower conversion levels with various catalyst systems. Therefore, also the conversion of these substrates with the binary Zn(salphen)/NBu<sub>4</sub>I catalyst was investigated in detail using DFT calculations (Table 1). In the case of 2-vinyloxirane **5** (Scheme 2), the presence of the vinyl functionality makes the ring-opening step more favourable on C<sub>α</sub> unlike the clear preference for C<sub>β</sub> observed with epoxides **1-3**. This is a result of a larger stabilization of **TS1** through delocalization of the charge in the linear alkoxide through the vinyl fragment; this is likely also the case in **Int-1** making the coordinated alkoxide less nucleophilic. In line with the lower reactivity is the higher barrier found for the CO<sub>2</sub> insertion step (**TS2**, 35.1 kcal·mol<sup>-1</sup>) compared to 30.9 kcal·mol<sup>-1</sup> using **1** as substrate. Figure 7a shows the difference in the first transition states **TS1** for both pathways using epoxide **5**. In the α pathway the four carbon atoms are lying in the same plane allowing for π-conjugation and consequently higher stabilization of the system. In contrast with the trend seen for substrates **1-3**, for **5** the α pathway is more favourable compared with the β pathway and the CO<sub>2</sub> insertion step is rate-limiting.

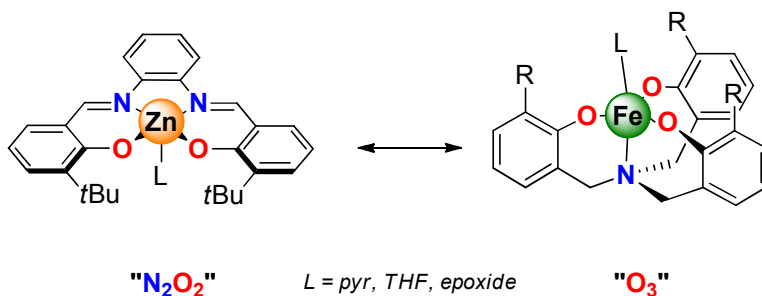
For styrene oxide **6** (Figure 7b) the presence of the phenyl substituent also favours the α pathway, and in particular the transition state **TS2** related to the CO<sub>2</sub> insertion step is markedly lower (36.0 kcal·mol<sup>-1</sup>) compared to the β pathway (42.6 kcal·mol<sup>-1</sup>) but again higher than observed with propylene oxide **1** (33.5 kcal·mol<sup>-1</sup>). In the first transition state **TS1** similar to **5** a planar conformation allows the aromatic ring to stabilize the charge in the coordinated alkoxide. In the transition state describing the ring-closing step again the inductive effect of the phenyl group is responsible for stabilization of the charge resulting from the release of iodide. Experimental data with the binary Zn(salphen)/NBu<sub>4</sub>I catalyst system<sup>[19]</sup> are fully in line with these computational findings for substrates **5** and **6** and have shown that these latter epoxides have lower conversion levels compared to other terminal epoxides such as propylene oxide **1**. For **6** both **TS2** (CO<sub>2</sub> insertion) and **TS3** (ring-closing step) have similar (rate-determining) barriers of around 36 kcal·mol<sup>-1</sup>. The preference for ring-opening at C<sub>α</sub> in

both **5** as well as **6** (i.e., the methine carbon) follows the observations from Darensbourg, Lu and co-workers who studied the Co<sup>III</sup>-salen catalysed formation of polycarbonates based on CO<sub>2</sub> and epichlorohydrin<sup>[33]</sup> or styrene carbonate;<sup>[34]</sup> in these cases a higher preference for the  $\alpha$  pathway in these epoxides with electron-withdrawing groups was noted compared to propylene oxide **1**.



**Figure 7.** Optimized structures of TS1 in  $\alpha$  and  $\beta$  pathways for epoxides (A) **5** and (B) **6** together with the most relevant calculated bond distances (in Å), and value of the negative (imaginary) vibrational frequencies.

The DFT analyses suggest that for catalyst improvement, and specifically for those substrates that are sterically more demanding such as internal epoxides, metallosalen systems having a planar coordination environment cannot be effective mediators under mild reaction conditions. In order to create more space to facilitate both the sterically demanding CO<sub>2</sub> insertion and ring-closing steps (which have shown to be more challenging than the ring-opening of the epoxide, see Table 1) other ligand geometries (Figure 8) should be considered such as metal complexes comprising of a trigonal bipyrimidal (TBP) coordination environment. Recent work from Kleij and co-workers concentrating on Fe<sup>III</sup>-based amino triphenolate complexes <sup>[3c,35]</sup> with these NO<sub>3</sub>-chelating ligands in combination with an external ligand such as pyridine, THF or an epoxide (Figure 8) provide a TBP coordination arrangement; these complexes have indeed proven to be more effective catalyst systems with lower metal loadings (0.1-0.5 mol% Fe versus 2.5 mol% Zn) and able to convert internal epoxides and oxetanes. Furthermore, whereas the Zn(salphen) complexes were hardly effective for conversion of internal epoxides except when using very high pressures and elevated temperatures (i.e., using sc-CO<sub>2</sub> as medium),<sup>[20]</sup> these Fe-amino triphenolate complexes (using 0.5 mol% Fe) showed good conversion levels and yields for several internal epoxides using much lower pressures (*p*CO<sub>2</sub> = 10 bar) and similar temperatures (80°C). Thus, the presence of less donor atoms in the plane of the metal centre (O<sub>3</sub>) compared to the family of metallosalens (N<sub>2</sub>O<sub>2</sub>) seems to be beneficial in the creation of more powerful catalyst systems for the formation of cyclic carbonates and possibly also for the synthesis of polycarbonates.



**Figure 8.** Schematic representation and comparison of the coordination geometry in the plane of the metal centres in Zn(salphen) complexes and Fe-based amino triphenolates.

## 5.8 Conclusions

The mechanism for the ring-expansion addition of CO<sub>2</sub> to epoxides catalyzed by the binary Zn(salphen)/NBu<sub>4</sub>X (X = Br, I) catalyst system has been investigated and elucidated in detail by DFT methods. Computational studies clearly explain the reasons why the ring-expansion addition of CO<sub>2</sub> to the benchmark substrate propylene oxide **1** proceeds in a much easier way in presence of Zn(salphen)/NBu<sub>4</sub>I compared to the uncatalyzed or Zn(salphen) catalyzed route. More importantly, this work has also revealed a number of interesting and important observations that may help to design better and more broadly applicable catalysts for organic carbonate formation.

For alkyl-substituted terminal epoxides **1–4** the reaction is predominantly controlled by steric factors, whereas for the vinyloxirane **5** and styrene oxide **6** electronic factors are more dominant. For substrates **1–3** ring-opening at the unsubstituted carbon atom ( $\beta$  pathway) is favored and this preference becomes more pronounced upon increasing the steric bulk at C <sub>$\alpha$</sub> . In general the  $\beta$  pathway is favored and the rate-limiting step for these substrates is the CO<sub>2</sub> insertion step in the coordinated linear alkoxide complex. In contrast to **1–3**, for substrates **5** and **6** the  $\alpha$  pathway is favored with the CO<sub>2</sub> insertion step also being rate-determining. The current results also explain why internal epoxides such as *trans*-2,3-epoxybutane **4** are more sluggish as all the involved calculated transition states (**TS1–TS3**) are significantly higher compared to those computed for propylene oxide **1**. In summary, we believe that this comprehensive study based on the ring-expansion addition of CO<sub>2</sub> to various epoxides gives useful insights in the limitations of a very important family of catalysts (metalloalens)<sup>[21]</sup> and provides a deeper understanding of this well-known CO<sub>2</sub> fixation reaction. Based on recent promising findings with other types of binary catalyst systems (amino trisphenolate complexes)<sup>[3c,35]</sup> having different coordination environments around the active metal center, the development of more active/selective catalysts for organic carbonate synthesis from epoxides and carbon dioxide should be feasible.

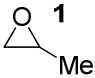
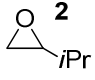
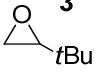
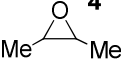

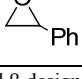
## 5.9 Experimental section

### DFT calculations

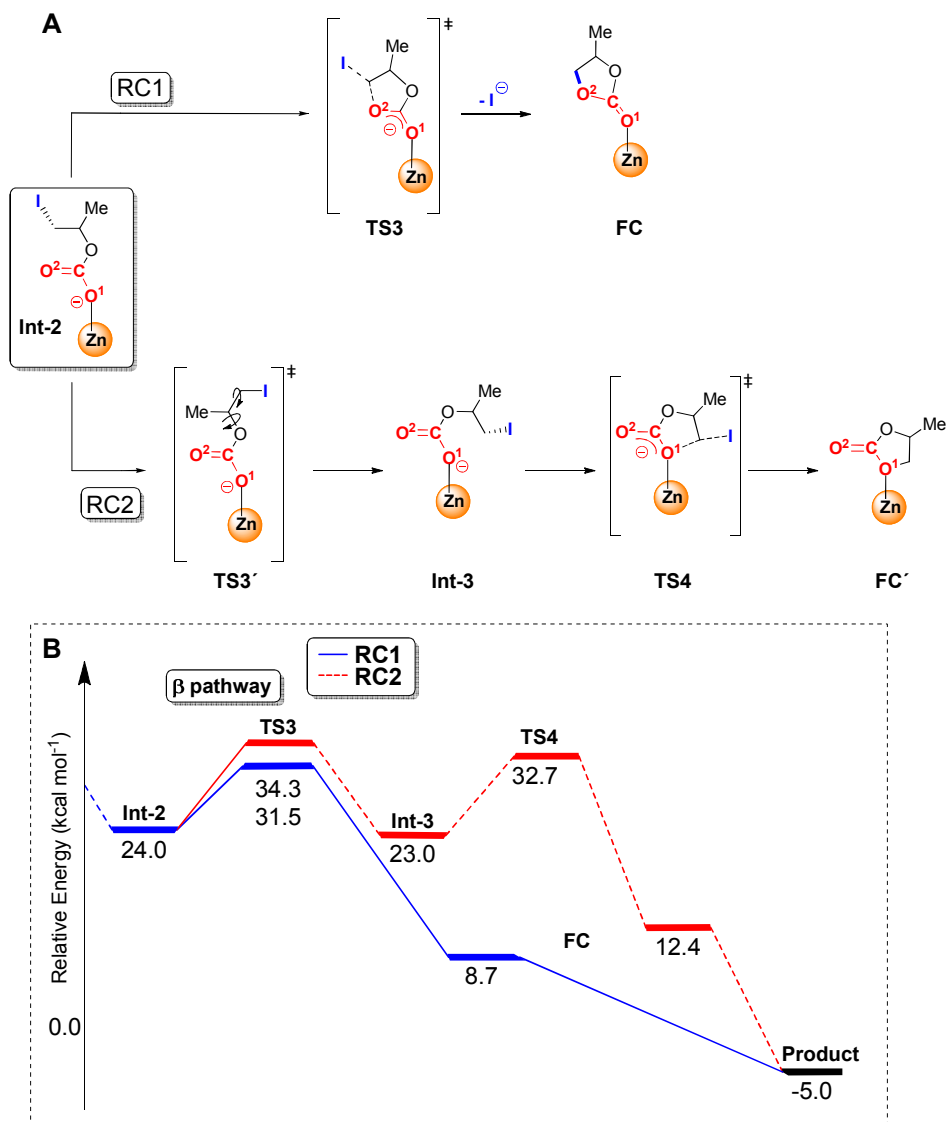
All calculations were carried out by using the Amsterdam Density Functional (ADF v2010.01) package.<sup>[36]</sup> DFT-based methods was employed at the generalized-gradient-approximation (GGA) level, with the Becke exchange<sup>[37]</sup> and the Perdew correlation<sup>[38]</sup> functionals (BP86). A triple- $\xi$  plus polarization Slater basis set was used on all atoms. Relativistic corrections were introduced by scalar-relativistic zero-order regular approximation (ZORA).<sup>[39]</sup> Full geometry optimizations were performed without constraints, and the nature of the stationary points in the potential energy hypersurface, were characterized either as minima or transition states by means of harmonic vibrational frequencies analysis. In order to match with the experimental conditions reported previously,<sup>[19]</sup> standard corrections to Gibbs free energy were evaluated at 298 K and pressure of 10 bar, according to the expression of an ideal gas  $G_m(p) = G_m^\circ + RT \ln \frac{p}{p^\circ}$ .<sup>[40]</sup> Solvent effects were introduced by using the continuous solvent model COSMO.<sup>[41]</sup>

### Mulliken populations for epoxides 1-6

**Table 2.** Calculated Mulliken populations for free and epoxides 1-6 coordinating to Zn(salphen).

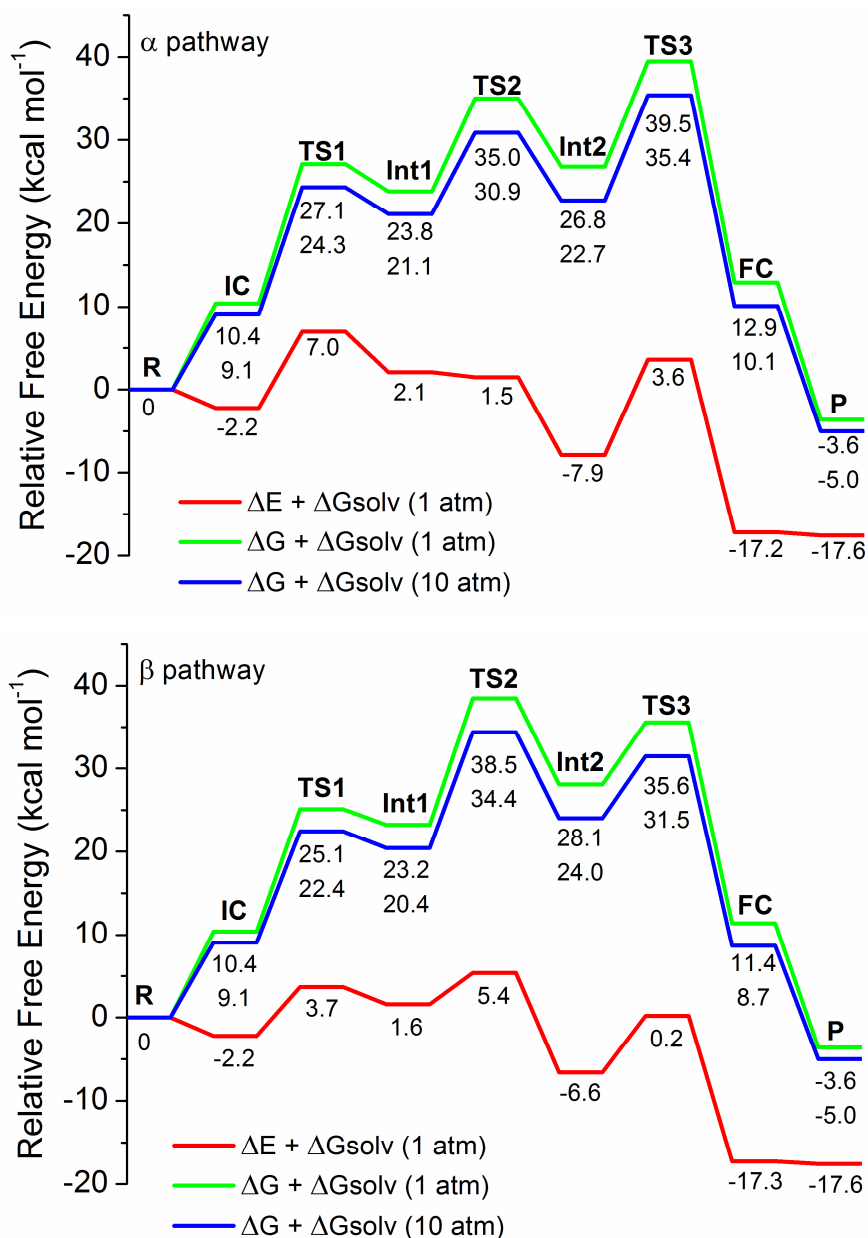
Substrate <sup>a</sup>		Epoxide <sup>b</sup>	Epoxide-Zn(salphen)
	1 C $_{\alpha}$	0.4731	0.5162
	1 C $_{\beta}$	0.5016	0.5303
	2 C $_{\alpha}$	0.5162	0.5660
	2 C $_{\beta}$	0.4963	0.5297
	3 C $_{\alpha}$	0.5501	0.6002
	3 C $_{\beta}$	0.4889	0.5254
	4 C $_{\alpha}$	0.4771	0.4600
	4 C $_{\beta}$	0.4776	0.5135
	5 C $_{\alpha}$	0.4442	0.4779
	5 C $_{\beta}$	0.4928	0.5401
	6 C $_{\alpha}$	0.4032	0.4334
	6 C $_{\beta}$	0.4851	0.5311

<sup>a</sup> The  $\alpha$  and  $\beta$  designations relate to their respective carbon atoms. <sup>b</sup> Mulliken population in electronic charge.

Energy profiles for ring-closing mechanism in  $\beta$  pathway for **1**.

**Figure 9.** (A) Two possible ring-closing pathways (**RC1** and **RC2**) for the intermediate **Int-1** involving different O-atoms of the carbonate fragment (O1 and O2) in the formation of propylene carbonate. (B) Free energy profile for the ring-closing step in the  $\beta$  pathway for the conversion of propylene oxide **1** catalyzed by the binary Zn(salphen)/NBu<sub>4</sub>I catalyst.

Energy profiles for propylene oxide (1).



**Figure 10.** The potential energy profiles for epoxide **1** including the  $\Delta G$  of solvation (in red). The relative free energy profiles for epoxide **1** including the  $\Delta G$  of solvation (in green at 1 bar and in blue at 10 bar).

## 5.10 References and notes

- [1] a) *Carbon Dioxide as Chemical Feedstock*, M. Aresta (ed), Wiley-VCH, Weinheim **2010**; b) P. Markewitz, W. Kuckshinrichs, W. Leitner, J. Linssen, P. Zapp, R. Bongartz, A. Schreiber, T. E. Müller, *Energy Environ. Sci.* **2012**, *5*, 7281; c) T. Sakakura, J. C. Choi, H. Yasuda, *Chem. Rev.* **2007**, *107*, 2365.
- [2] a) R. Martín, A. W. Kleij, *ChemSusChem* **2011**, *4*, 1259; b) M. Peters, B. Köhler, W. Kuckshinrichs, W. Leitner, P. Markewitz, T. E. Müller, *ChemSusChem* **2011**, *4*, 1216; c) M. Cokoja, C. Bruckmeier, B. Rieger, W. A. Herrmann, F. E. Kühn, *Angew. Chem. Int. Ed.* **2011**, *50*, 8510.
- [3] For recent original contributions: a) M. North, C. Young, *Catal. Sci. Technol.* **2011**, *1*, 93; b) A. Coletti, C. J. Whiteoak, V. Conte, A. W. Kleij, *ChemCatChem* **2012**, *4*, 1190; c) C. J. Whiteoak, E. Martin, M. Martínez Belmonte, J. Benet-Buchholz, A. W. Kleij, *Adv. Synth. Catal.* **2012**, *354*, 469; d) T. Ohshima, J. Okudac, K. Mashima, *Catal. Sci. Technol.* **2012**, *2*, 509; e) T. Ema, Y. Miyazaki, S. Koyama, Y. Yano, T. Sakai, *Chem. Commun.* **2012**, *48*, 4489; f) J. Qu, C.-Y. Cao, Z.-F. Dou, H. Liu, Y. Yu, P. Li, W.-G. Song, *ChemSusChem* **2012**, *5*, 652; g) C. J. Whiteoak, A. Nova, F. Maseras, A. W. Kleij, *ChemSusChem* **2012**, *5*, 2032; h) Q.-W. Song, L.-N. He, J.-Q. Wang, H. Yasuda, T. Sakakura, *Green Chem.* **2013**, *15*, 110; i) C. Qi, J. Ye, W. Zeng, H. Jiang, *Adv. Synth. Catal.* **2010**, *352*, 1925; j) J. Sun, L. Han, W. Cheng, J. Wang, X. Zhang, S. Zhang, *ChemSusChem* **2011**, *4*, 502.
- [4] For a biography on phosgene and its derivatives see: a) D. D. Berolzheimer, *Ind. Eng. Chem.* **1919**, *11*, 263; b) A.-A. G. Shaikh, S. Sivaram, *Chem. Rev.* **1996**, *96*, 951.
- [5] a) T. Sakakura, K. Kohno, *Chem. Commun.* **2009**, 1312; b) A. A. G. Shaikh, S. Sivaram, *Chem. Rev.* **1996**, *96*, 951; c) B. Schäffner, F. Schäffner, S. P. Verevkin, A. Börner, *Chem. Rev.* **2010**, *110*, 4554; d) D. J. Darensbourg, S. J. Wilson, *Green Chem.* **2012**, *14*, 2665.
- [6] a) V. Caló, A. Nacci, A. Monopoli, A. Fanizzi, *Org. Lett.* **2002**, *4*, 2561; b) B. R. Buckley, A. P. Patel, K. G. Wijayantha, *Chem. Commun.* **2011**, *47*, 11888.
- [7] a) N. Kihara, N. Hara, T. Endo, *J. Org. Chem.* **1993**, *58*, 6198; b) L. Guo, C. Wang, X. Luo, G. Cui, H. Li, *Chem. Commun.* **2010**, *46*, 5960; c) M. Aresta, A. Dibenedetto, *J. Mol. Catal. A.: Chem.* **2002**, *182-183*, 399.
- [8] a) J. J. Peng, Y. Q. Deng, *New J. Chem.* **2001**, *25*, 639; b) H. Yang, Y. Gu, Y. Deng, F. Shi, *Chem. Commun.* **2002**, 274; c) H. Kawanami, A. Sasaki, K. Matsui, Y. Ikushima,



- Chem. Commun.* **2003**, 896; d) J. Sun, S. Fujita, M. Arai, *J. Organomet. Chem.* **2005**, 690, 3490.
- [9] a) Y. Xie, Z. Zhang, T. Jiang, J. He, B. Han, T. Wu, K. L. Ding, *Angew. Chem. Int. Ed.* **2007**, 46, 7255; b) Y. B. Xiong, H. Wang, R. M. Wang, Y. F. Yan, B. Zheng, Y. P. Wang, *Chem. Commun.* **2010**, 46, 3399.
- [10] a) W. J. Kruper, D. V. Dellar, *J. Org. Chem.* **1995**, 60, 725; b) F. W. Li, C. G. Xia, L. W. Xu, W. Sun, G. X. Chen, *Chem. Commun.* **2003**, 2042; c) W. Clegg, R. W. Harrington, M. North, R. Pasquale, *Chem. Eur. J.* **2010**, 16, 6828; d) R. L. Paddock, S. T. Nguyen, *Chem. Commun.* **2004**, 1622.
- [11] M. L. Man, K. C. Lam, W. N. Sit, S. M. Ng, Z. Zhou, Z. Lin, C. P. Lau, *Chem. Eur. J.* **2006**, 12, 1004.
- [12] a) H. Sun, D. Zhang, *J. Phys. Chem. A* **2007**, 111, 8036; b) Y. Ren, T. T. Meng, J. Jia, H. S. Wu, *Comput. Theor. Chem.* **2011**, 978, 47; c) Z.-Z. Yang, Y.-N. Zhao, L.-N. He, J. Gao, Z.-S. Yin, *Green Chem.* **2012**, 14, 519; d) R. A. Watile, D. B. Bagal, K. M. Deshmukh, K. P. Dhake, B. M. Bhanage, *J. Mol. Catal. A: Chem.* **2011**, 351, 196; e) Z.-Z. Yang, L.-N. He, C.-X. Miao, S. Chanfreau, *Adv. Synth. Catal.* **2010**, 352, 2233.
- [13] M. J. Ajitha, C. H. Suresh, *Tetrahedron Lett.* **2011**, 52, 5403.
- [14] F. Chen, X. Li, B. Wang, T. Xu, S. L. Chen, P. Liu, C. Hu, *Chem. Eur. J.* **2012**, 18, 9870.
- [15] J.-Q. Wang, J. Sun, W.-G. Cheng, K. Dong, X.-P. Zhang, S.-J. Zhang, *Phys. Chem. Chem. Phys.* **2012**, 14, 11021.
- [16] K. Roshith Roshan, G. Mathai, J. Kim, J. Tharun, G.-A. Park, D.-W. Park, *Green Chem.* **2012**, 14, 2933.
- [17] J.-Q. Wang, K. Dong, W.-G. Cheng, J. Sun, S. J. Zhang, *Catal. Sci. Technol.* **2012**, 2, 1480.
- [18] J. Ma, J. Liu, Z. Zhang, B. Han, *Green Chem.* **2012**, 14, 2410.
- [19] a) A. Decortes, M. Martínez Belmonte, J. Benet-Buchholz, A. W. Kleij, *Chem. Commun.* **2010**, 46, 4580; b) A. Decortes, A. W. Kleij, *ChemCatChem* **2011**, 3, 831.
- [20] M. Taherimehr, A. Decortes, S. M. Al-Amsyar, W. Lueangchaichaweng, C. J. Whiteoak, E. C. Escudero-Adàn, A. W. Kleij, P. P. Pescarmona, *Catal. Sci. Technol.* **2012**, 2, 2231.
- [21] a) A. Decortes, A. M. Castilla, A. W. Kleij, *Angew. Chem. Int. Ed.* **2010**, 49, 9822. For some other reviews see: b) P. P. Pescarmona, M. Taherimehr, *Catal. Sci. Technol.* **2012**, 2, 2169; c) M. North, R. Pasquale, C. Young, *Green Chem.* **2010**, 12, 1514. For a

- computational review on CO<sub>2</sub> conversion see: *d*) M. Drees, M. Cokoja, F. E. Kühn, *ChemCatChem* **2012**, *4*, 1703.
- [22] A detailed study on the mechanism using bimetallic Al(salen) complexes was reported by North and co-workers: M. North, R. Pasquale, *Angew. Chem. Int. Ed.* **2009**, *48*, 2946.
- [23] D. Tian, B. Liu, Q. Gan, H. Li, D. J. Darensbourg, *ACS Catal.* **2012**, *2*, 2029. See also reference 22.
- [24] F. Jutz, J.-D. Grunwaldt, A. Baiker, *J. Mol. Catal. A: Chem.* **2008**, *279*, 94.
- [25] X.-B. Lu, B. Liang, Y.-J. Zhang, Y.-Z. Tian, Y.-M. Wang, C.-X. Bai, H. Wang, R. Zhang, *J. Am. Chem. Soc.* **2004**, *126*, 3732.
- [26] D. J. Darensbourg, A. I. Moncada, W. Choi, J. H. Reibenspies, *J. Am. Chem. Soc.* **2008**, *130*, 6523.
- [27] S. J. Wezenberg, G. A. Metselaar, E. C. Escudero-Adán, J. Benet-Buchholz, A. W. Kleij, *Inorg. Chim. Acta* **2009**, *362*, 1053.
- [28] For illustrative examples see: *a*) R. M. Haak, A. Decortes, E. C. Escudero-Adán, M. Martínez Belmonte, E. Martín, J. Benet-Buchholz, A. W. Kleij, *Inorg. Chem.* **2011**, *50*, 7934; *b*) J. A. A. W. Elemans, S. J. Wezenberg, E. C. Escudero-Adán, J. Benet-Buchholz, D. den Boer, M. J. J. Coenen, S. Speller, A. W. Kleij, S. De Feyter, *Chem. Commun.* **2010**, *46*, 2548; *c*) E. C. Escudero-Adán, J. Benet-Buchholz, A. W. Kleij, *Chem. Eur. J.* **2009**, *15*, 4233; *d*) S. J. Wezenberg, E. C. Escudero-Adán, J. Benet-Buchholz, A. W. Kleij, *Chem. Eur. J.* **2009**, *15*, 5695; *e*) E. C. Escudero-Adán, J. Benet-Buchholz, A. W. Kleij, *Eur. J. Inorg. Chem.* **2009**, *15*, 3562. See also reference 31.
- [29] For some examples: *a*) A. L. Singer, D. A. Atwood, *Inorg. Chim. Acta* **1998**, *277*, 157; *b*) P.D. Frischmann, A. J. Gallant, J.H. Chong, M. J. MacLachlan, *Inorg. Chem.* **2008**, *47*, 101; *c*) M. Kuil, P. E. Goudriaan, A. W. Kleij, D. M. Tooke, A. L. Spek, P. W. N. M. van Leeuwen, J. N. H. Reek, *Dalton Trans.* **2007**, 2311. See also: *d*) C. J. Whiteoak, G. Salassa, A. W. Kleij, *Chem. Soc. Rev.* **2012**, *41*, 622.
- [30] E. C. Escudero-Adán, J. Benet-Buchholz, A. W. Kleij, *Inorg. Chem.* **2008**, *47*, 4256. See also references 28b and 31c.
- [31] We also computed the  $\alpha$  and  $\beta$  pathways for propylene oxide **1** catalyzed by the Zn(salphen)/NBu<sub>4</sub>I binary couple using the M06 level of theory by the meta-hybrid GGA M06 DFT method (see Supporting Information for details). The relative energies of the different TS proved to lower and markedly different (comparing **TS1** with **TS2/TS3**), though the **TS1** (i.e., ring-opening step) showed to be relatively more

demanding. Closer inspection of the **TS1** conformation showed that the M06 method favors the iodide attacking the coordinated epoxide from the side where the tBu groups of the Zn(salphen) are located ( $\alpha$  pathway). In the  $\beta$  pathway this observation is less pronounced. Thus, the use of M06 favors the steric bulk of the Zn(salphen), the coordinated epoxide and the incoming (large) iodide nucleophile to reside in the same area of space. Previous coordination studies carried out by us using substituted pyridines and Zn(salphen)s revealed a preferred positioning of the ligand both in the solid state (X-ray data) and in solution (NMR experiments) supported by data consistent with the pyridine-ortho groups pointing away from the tBu fragments of the Zn(salphen) complex. See: *a*) E. C. Escudero-Adán, J. Benet-Buchholz, A. W. Kleij, *Eur. J. Inorg. Chem.* **2009**, 3562; *b*) see also reference 30. We then carried out coordination studies with propylene oxide (PO **1**) and the Zn(salphen) complex, and evaluated the chemical shift changes upon complexation. Interestingly, upon coordination the epoxide hydrogens all undergo a downfield shift (inductive effect) except for the epoxide-Me group which shows a small upfield shift (Supporting Information). This seems to indicate that also in this case the coordinated ligand (epoxide) may have a preferred positioning to release steric strain. Therefore, some caution may be needed with the M06 computational data.

- [32] The high Lewis acidity is provoked by the rigid, planar coordination environment around the Zn metal center. See for applications: *a*) A. W. Kleij, D. M. Tooke, M. Kuil, M. Lutz, A. L. Spek J. N. H. Reek, *Chem. Eur. J.* **2005**, *11*, 4743; *b*) S. J. Wezenberg, G. Salassa, E. C. Escudero-Adán, J. Benet-Buchholz, A. W. Kleij, *Angew. Chem. Int. Ed.* **2011**, *50*, 713; *c*) G. Salassa, M. J. J. Coenen, S. J. Wezenberg, B. L. M. Hendriksen, S. Speller, J. A. A. W. Elemans, A. W. Kleij, *J. Am. Chem. Soc.* **2012**, *134*, 7186. See also reference 29.
- [33] G.-P. Wu, S.-H. Wei, W.-M. Ren, X.-B. Lu, T.-Q. Xu, D. J. Darensbourg, *J. Am. Chem. Soc.* **2011**, *133*, 15191.
- [34] *a*) G.-P. Wu, S.-H. Wei, W.-M. Ren, X.-B. Lu, B. Li, Y.-P. Zua, D. J. Darensbourg, *Energy Environ. Sci.* **2011**, *4*, 5084; *b*) G.-P. Wu, S.-H. Wei, X.-B. Lu, W.-M. Ren, D. J. Darensbourg, *Macromolecules* **2010**, *43*, 9202.
- [35] C. J. Whiteoak, B. Gjoka, E. Martin, M. Martínez Belmonte, E. C. Escudero-Adán, C. Zonta, G. Licini, A. W. Kleij, *Inorg. Chem.* **2012**, *51*, 10639.
- [36] ADF2010, SCM, Theoretical Chemistry, Vrije Universiteit, Amsterdam, The Netherlands, <http://www.scm.com>; E. J. Baerends, T. Ziegler, J. Autschbach, D. Bashford, A. Bérces, F. M. Bickelhaupt, C. Bo, P. M. Boerrigter, L. Cavallo, D. P.

Chong, L. Deng, R. M. Dickson, D. E. Ellis, M. van Faassen, L. Fan, T. H. Fischer, C. Fonseca Guerra, A. Ghysels, A. Giammona, S. J. A. van Gisbergen, A. W. Götz, J. A. Groeneveld, O. V. Gritsenko, M. Grüning, S. Gusarov, F. E. Harris, P. van den Hoek, C. R. Jacob, H. Jacobsen, L. Jensen, J.W. Kaminski, G. van Kessel, F. Kootstra, A. Kovalenko, M. V. Krykunov, E. van Lenthe, D. A. McCormack, A. Michalak, M. Mitoraj, J. Neugebauer, V. P. Nicu, L. Noodleman, V. P. Osinga, S. Patchkovskii, P. H. T. Philipsen, D. Post, C. C. Pye, W. Ravenek, J. I. Rodríguez, P. Ros, P. R. T. Schipper, G. Schreckenbach, J. S. Seldenthuis, M. Seth, J. G. Snijders, M. Solà, M. Swart, D. Swerhone, G. te Velde, P. Vernooijs, L. Versluis, L. Visscher, O. Visser, F. Wang, T. A. Wesolowski, E. M. van Wezenbeek, G. Wiesenekker, S. K. Wolff, T. K. Woo, A. L. Yakovlev.

[37] A. D. Becke, *Phys. Rev. A* **1988**, *38*, 3098.

[38] a) J. P. Perdew, *Phys. Rev. B* **1986**, *33*, 8822; b) J. P. Perdew, *Phys. Rev. B* **1986**, *34*, 7406.

[39] a) E. van Lenthe, E. J. Baerends, J. G. Snijders, *J. Chem. Phys.* **1993**, *99*, 4597; b) E. van Lenthe, E. J. Baerends, J. G. Snijders, *J. Chem. Phys.* **1994**, *101*, 9783.

[40] *Atkins' Physical Chemistry*, Eds. P. Atkins, J. de Paula, 8<sup>th</sup> edition, Oxford University Press, Oxford UK **2006**, pp. 108-109.

[41] A. Klamt, *J. Phys. Chem.* **1995**, *99*, 2224.

UNIVERSITAT ROVIRA I VIRGILI

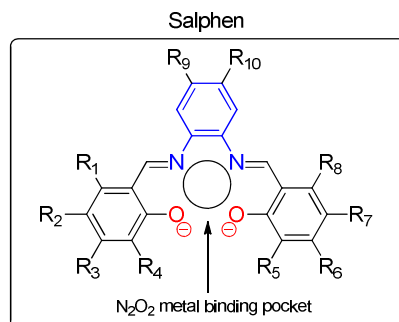
SUPRAMOLECULAR, PHOTOPHYSICAL AND CATALYTIC PROPERTIES OF ZN(SALPHEN) BASED COMPLEXES AND MATERIALS

Giovanni Salassa

Dipòsit Legal: T. 1430-2013

## Summary

“Salen” ligands are relatively planar tetradentate,  $N_2O_2$ -coordinating ligand systems which are obtained by the condensation reaction of readily available diamine and (substituted) salicylaldehyde precursors. Metallosalen complexes combine a number of advantages such as ease of variation in steric and electronic features, and the use of modular strategies that enable manipulation of different fragments of the ligand systems. Metal-derived salen complexes are versatile and they have proven to be effective catalysts for many asymmetric conversions including (ep)oxidations, epoxide ring-opening reactions and stereo-selective polymerizations. Lately, phenyl-bridged salen ligands (designated as “salphens” or “salophens”, Scheme 1) and related structures have started to raise the attention of the scientific community due to their particular advantages over their salen analogues; they represent  $\pi$ -conjugated ligand systems with tuneable photophysical properties, and are more cost-effective than the corresponding (chiral) salen ligands. For these reasons, such salphen systems have excellent potential as building blocks in material science amongst other applications.

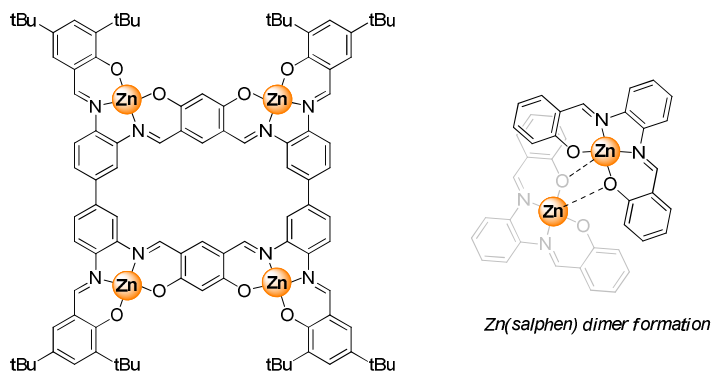


**Scheme 1.** Schematic drawing of a salphen ligand showing the  $N_2O_2$  metal binding pocket and the various possibilities for substitution thereof.

It should also be noted that the rigid geometry around the metal centre, dictated by the salphen ligand, can be used to manipulate properties such as the Lewis acid character of the metal and therefore it can be effectively applied to increase the reactivity, substrate binding properties and self-assembly behaviour of the resulting complex. Thus, the

work reported in this thesis has principally focused on the study of novel self-assembly features and patterns, and on the development of other new application of Zn(salphen) complexes.

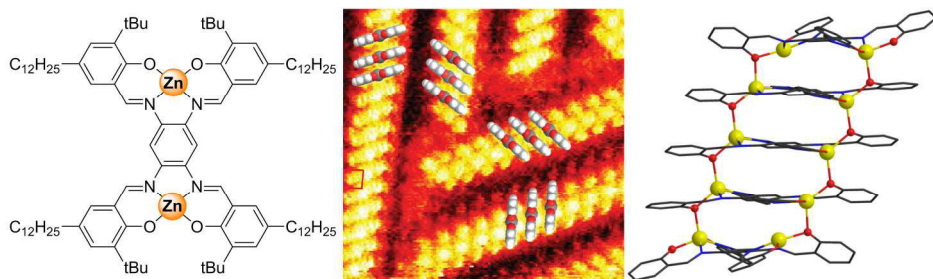
The first two chapters (2 and 3) present detailed studies on the self-assembly of different multinuclear Zn(salphen)s focusing on the type and the strength of the interactions involved. In *Chapter 2* the synthesis and characterization of a *tetra*-Zn(salphen) macrocycle using a metal template approach is described. The macrocyclic Zn complex shows strong self-assembly in comparison to a number of reference/model compounds. The self-assembly process is mediated by the formation of intermolecular dimeric Zn(salphen) units that are held together via  $\mu_2$ -phenoxo bridges (Scheme 2). Competitive UV-Vis/fluorescence titration experiments suggest that a molecular increase of the number of Zn(salphen) units is responsible for the formation of more stable supramolecular aggregates, and de-aggregation is accompanied by a strong hyperchromic effect. The strong self-assembly behaviour of the *tetra*-Zn(salphen) macrocycle was further supported by NMR, mass spectrometry and transmission electron microscopy (TEM) studies.



**Scheme 2.** On the left, line drawing of the *tetra*-Zn(salphen) macrocycle; on the right, a dimeric self-assembled Zn(salphen) complex showing the involved Zn–O coordinative bonds.

*Chapter 3* represents a study on the extremely strong self-assembly of a *bis*-Zn(salphen) complex both in solution as well as at a solid-liquid interface. The *bis*-Zn(salphen) molecules are shown to self-organize into extremely stable, edge-on

orientated oligomeric aggregates (Figure 1), which could not be dissociated by addition of (small amounts of) donating ligands. This behaviour at the liquid-solid interface has demonstrated to be in excellent agreement with solution studies: competitive UV-Vis and fluorescence titrations, dynamic light scattering (DLS) and transmission electron microscopy (TEM) experiments are also in line with a highly increased stability for the assembled state of these *bis*-Zn(salphen)s. DFT analysis carried out for the *bis*-Zn(salphen) shows that an unusual binding mode is operative, and also rationalizes the very high stability of the self-assembled structures provoked by oligomeric  $(\text{Zn-O})_n$  coordination motifs within the (oligomeric) assembly. This coordination mode is strikingly different when compared with mononuclear Zn(salphen) analogues that form dimeric structures having a typical  $\text{Zn}_2\text{O}_2$  central unit (Scheme 2 on the right). The high stability of the multinuclear structure therefore holds great promise for the development of stable self-assembled monolayers (SAMs) with potential for new opto-electronic materials.

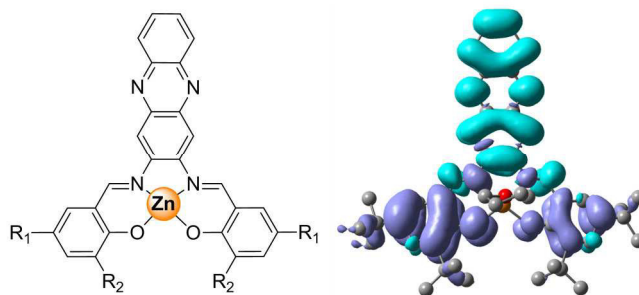


**Figure 1.** On the left, line drawing of the *bis*-Zn(salphen) complexes. In the central part, section of the STM image of an oligomeric aggregate; on the right, the most likely self-assembly mode of a pentameric assembly showing the  $(\text{Zn-O})_n$  oligomeric chains between the individual *bis*-Zn(salphen) units (DFT optimization).

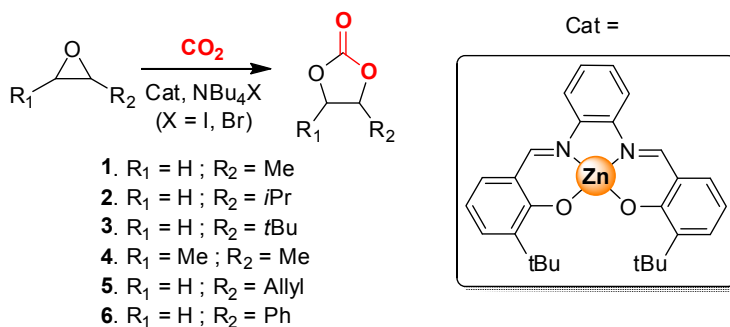
*Chapter 4* reports the synthesis of a new class of Zn(II) Schiff base complex incorporating a phenazine unit in the backbone and is designated as “Zn(salphenazine)”. These Zn(salphenazine) complexes show interesting photophysical properties compared to typical salen and salphen complexes while remaining easily synthesized and tuneable. From the experimental and theoretical UV-Vis data, the absorption bands have been assigned to  $\pi$ - $\pi^*$  transitions which are directly influenced by the type of substituents



present in the salphenazine scaffold (Figure 2). Therefore, by a judicious choice of these groups, it is possible to obtain systems with desired photophysical properties. Zn(salphenazine) complexes have also shown to have potential application in small molecule Organic Solar Cells (smOSCs) due to their high stability and adequate electronic properties against the acceptor C<sub>60</sub>. Even though the efficiency of the device is not competitive yet, Zn(salphenazine)s show the synthetic potential for significant improvement based on the modular construction of these photo-active complexes.



**Figure 2.** Schematic drawing of a Zn(salphenazine) complex (on the left) and a selected  $\pi$ - $\pi^*$  transition represented with electron density difference map EDDM (on the right).



**Scheme 3.** The ring-expansion addition of CO<sub>2</sub> to epoxides (substrates **1-6** used in this investigation) generating five-membered cyclic carbonates using a binary catalyst composed of a Zn(salphen) component (cf., Cat) and NBu<sub>4</sub>X (X = I, Br).

*Chapter 5* reports a detailed DFT study of the reaction mechanism of the ring-expansion addition of CO<sub>2</sub> to epoxides catalyzed by a binary catalyst comprising a Zn(salphen) complex and co-catalytic NBu<sub>4</sub>X (X = Br, I). The catalytic reaction has

been studied in detail describing the three main steps involved: the epoxide ring-opening, the CO<sub>2</sub> insertion step and a final ring-closure step to afford the five-membered cyclic carbonate products. The ring-opening step of the process was examined and the preference for opening at the methylene (C<sub>β</sub>) or methine carbon (C<sub>α</sub>) was established. Also, the CO<sub>2</sub> insertion and the ring-closing steps have been explored for six differently substituted epoxides and proved to be significantly more challenging compared with the ring-opening step. The combined results have helped to explain earlier experimental observations and catalyst limitations, and are useful for improved catalyst design and development.

UNIVERSITAT ROVIRA I VIRGILI

SUPRAMOLECULAR, PHOTOPHYSICAL AND CATALYTIC PROPERTIES OF ZN(SALPHEN) BASED COMPLEXES AND MATERIALS

Giovanni Salassa

Dipòsit Legal: T. 1430-2013

## Acknowledgements

In June 2009 I started my PhD with plenty of doubts and worries. I was not sure that Tarragona and the ICIQ were the appropriate places for me. However, after few weeks in the Kleij group I realized that I had arrived to a good choice. Accordingly I would like to thank the numerous people who have contributed to making my PhD a wonderful experience.

The person to thank first and foremost must be Prof. Dr. Arjan W. Kleij. Under his supervision I learned not just to do experiments for the sake of doing something, but always to ask myself if it will really help me reach my goal. His regular feedback was much appreciated and helped me to successfully accomplish all the projects undertaken. Finally, I am very grateful to him for allowing me to present my results at several international conferences.

During these last four years I have had the possibility to work with many excellent scientists outside of our group and of the ICIQ, which has allowed me to develop my understanding of new and exciting aspects of chemistry. In particular, I thank Dr. Hans Elemans and his collaborators for their outstanding STM studies on the self-assembly of Zn(salphen)s (*Chapter 3*). Quiero igualmente agradecer al Prof. Carles Bo y a Fernando Castro por brindarme la posibilidad de aprender más acerca de la química teórica y los mecanismos de reacción (*Chapter 5*). I would also to express my gratitude to Prof. Dr. Emilio Palomares and Dr. James W. Ryan for the realization of the Organic Solar Cells based on our joint Zn(salphenazine) work (*Chapter 4*). In addition I also appreciate the helpful discussions with Prof. Pau Ballester regarding the modeling studies on the self-assembled bis-Zn(salphen) (*Chapter 3*).

I am really grateful to all the people that over the last four years have been part of the Kleij group. I thank Dr. Ana Maria Castilla for introducing me into the magic world of salphens (*Chapter 2*) and teaching me how a lab must be maintained. I give my thanks to Dr. Sander Wezenberg, working with you was very easy, educational and very successful for both projects in which we have collaborated (the *chirogenesis* work and *Chapter 3*). I am grateful to Dr. Martha V. Escárcega Bobadilla for showing me the Mexican efficiency (another *chirogenesis* collaboration). Dr. Antonello Decortes and

Dr. Daniele Anselmo, the “Italian mafia”, in questi quattro anni è stato un piacere avere un po’ di Italia nel laboratorio, le innumerevoli conversazioni/pettegolezzi/cattiverie rimarranno un ricordo indelebile nella mia memoria. A special acknowledgement must be given to Dr. Christopher J. Whiteoak for his daily English lessons/corrections, for always being available for consulting about chemistry and related things. I am very grateful to all the other people that have been part of the group for all these years: Dr. Robert Haak, Dr. Nicola Kielland, Jonathan Rojas and Margarita Dobrinova. A proper acknowledgement is also required for all the visiting students: Danilo Misseri, Dr. Alessia Coletti, Victor Laserna and the amazing Blerina Gjoka. No me canso de agradecer a Marta Moya y a Ingrid Mateu por hacer mi vida en el ICIQ mucho más fácil, ayudándome con la burocracia que siempre me persigue. A kind acknowledgement is also given to all the ICIQ's Research Support staff, without their help it would not be possible to present all the results in this thesis.

Over the last four years there has not only been hard work and chemistry but also a lot of great parties and social activities. In the first instance I would like to thank the Italian community (*first generation*) who showed and explained to me how to survive in the big jungle of Tarragona. Un sentito grazie a Daniele, Antonello, Moira (la ciociarà), donna Caterina, Margherita, Carlo e gli inseparabili Carlo e Giulia. Secondly, I would like to thank special friends that are still maintaining contact even though they have left Tarragona. Dr. Kian Molawi; a unique party animal in Tarragona with his refined shirts, exotic dance style, and his firm hair cut which will remain legendary. Dr. John (*borrachera*) Clifford, when you decide to party you really do it properly; Kian's PhD party, your wedding and all the other great nights we had are unforgettable memories. Unas gracias especiales al Dr. Sergio Pascual, un amigo leal y honesto, y al Dr. Carlitos Vegas por las noches locas en el Highland. En el medio de mi doctorado tuve la suerte encontrar Ana y pasar un intenso año y medio. Gracias a ella también conocí a un montón de personas extraordinarias como las hermanas Martínez, Vanessa y Judit, a Edu y especialmente a el impresionante (no por su castellano) Dr. Mickael Gicquel (merci pour les soirées a le cinéma). Un agradecimiento especial a Fernando Castro, el hombre de la vaina, gracias por enseñarme tu técnica secreta del pase de la muerte en

bachata, junto con el legendario remolino. During the last two years of my PhD, I had the possibility to hang out with great friends with whom I had epic dinners, trips and parties. I am grateful to Chris (*il ghepardo*) for enriching our boring lives with your English charm. To Asraa, the girl who decides the destiny of every Friday/Saturday night, the first source of information in ICIQ, it was always great fun spending time with you. I would like to thank the dancing queens, Rica and Katya, the 5 hour dancing in Toledo is a record that will not easily be broken. I thank Alice for not breaking any of my wine glasses. Finally, I would like to thank the “most amazing kebab crew” Manuel (la vacca), er baffo Mattia, Dr. John Murphy. Un grazie speciale a colui che ogni sera combatte con me nella Bermuda Time Zone e con cui ho condiviso epiche vittorie e tristi sconfitte sul duro campo di battaglia de “*les golfes*”, Antonio Chutonio (comunemente chiamato Bazzo).

Over these years I have had the pleasure to meet a lot of interesting people with whom I shared coffee breaks, lunches and entertaining moments in ICIQ and in Tarragona. I thank Sonia, Anna, Carla, Imma, Pili, Ondrej, Philipp, Berta, Andrea, Uri, Vijay, Bea, Jordi, Atul, Dina, Pep, Ximo, Dolores, Neyvis, Giuliano, Luca, Kerman, Israel, Maria, Laura and Sofia. The French community: Eddy, Morgane, Anthony, Olivier, Charles and le grand Abel. I also thank all the people that have shared the thesis room with me: Ivan (FB professional), Madeleine (thanks for Fikas), Virginia y Mónica.

I would like to thank all the people that every Thursday evening shared the basketball court with me. First of all, I thank Henrik and Danny for letting this tradition last all these years. Secondly I am grateful to all the present and the former members of the ICIQ team: Enrique, Stephan, Kian, Blaise, Sergio, Jin, Liu, Wang, JR and the native little teenagers.

No puedo no agradecer al mejor equipo de baloncesto de Tarragona, El Club CB San Pedro y San Pablo. Han sido cuatro temporadas memorables y nunca olvidare los grandes jugadores y personas que sois. Gracias Sergi (el presidente), Xavi (gracias por dejarme conocer a estos chavales), Tito, Santi grande, Raul, Joaquin, Oscar, Hector Calvo, Hector Cester, Sergi Millan, Oriol, Abel, Santi pequeño, Carlos (vaya crack), Daniel “questo” De los Mozos y Dani Manudo Guerrero (gracias bro).

Un grazie di cuore a tutti i miei amici rimasti in Canavese (Sapo, Carmen, Ale V., Fabio, Milla, Ale B, Carli, Stefi, Yael, Luca, Mari, Fabiana, Alessando, Massi, Michele ed Enrica) e che in questi anni hanno sempre mantenuto i contatti. Come sempre succede la distanza affievolisce le amicizie, ma nel nostro caso le ha rese più forti. Grazie mille per le visite, i FaceTime, le serate “*usciamo che sta sera c’è Giovo*”, le telefonate, le chat e i mille commenti su FB. Mi avete fatto piangere il cuore (*cit.*). Non posso non ringraziare i migliori maestri al mondo, Carlo e Debora; in questi anni i nostri incontri sono sempre stati fonte di ispirazione.

I must acknowledge the *Stalloni*, two important friends that shared the PhD. adventure on the same explicit social and intellectual level as I did. There are many adjectives and expressions that can describe you, but in my opinion only the legendary sentence of señor Chang can really define the wonderful people you are. I thank Uncle Danny for showing me the Dutch rude and tasteless honesty; your efficiency in taking decisions is very much appreciated. I have to admit that your language skills are remarkable. I thank James *Bitterkas* for being the best wingman over these years, for always being present with your characteristic bitter Irish humor, for keeping me at the “ground state”. I will be missing our classic Friday night with good wine, food and the 5 o’clock Fika.

In fine un sentito grazie dal cuore alla mia famiglia che in questi quattro anni mi ha supportato in questa impresa. Un grazie a mamma e papà per il loro prezioso ed incondizionato aiuto che mi ha permesso sempre di superare ogni ostacolo sin ora. Un ringraziamento speciale a mia sorella Francesca che sempre si preoccupa per la mia salute e la mia felicità. A mio fratello Luca, un semplice ringraziamento non sarebbe sufficiente, il debito nei suoi confronti ormai è incolmabile. Grazie per consigliarmi sempre al meglio in ogni decisione importante.

-Giovanni-

## Curriculum Vitae

Giovanni Salassa was born on November 1 (1984) in Castellamonte Canavese, Italy. In October 2003 he started with his chemistry studies at the University of Turin (Italy). He obtained his BSc degree in February 2007, presenting a thesis entitled “*Hydrogen Bonding: a Solid State NMR Study*”, with this work being carried out under the supervision of Prof. Roberto Gobetto. After obtaining his BSc he started his master studies entitled “*Advanced Chemical Methodologies with Specialization in Reactivity and Catalysis*” at the University of Turin. In March 2009 he obtained his MSc degree with a thesis entitled “*Photoactivation of Ruthenium anticancer complexes*” obtaining the maximum grade (110/110). In June 2009, he moved to the Institute of Chemical Research of Catalonia (ICIQ) in Tarragona (Spain) as a PhD student, and the work described in this thesis was carried out in the group of Prof. Dr. Arjan Kleij. During his PhD, he participated in 6 international conferences with oral (3) and poster (3) contributions, amongst these, the “244<sup>th</sup> ACS National Meeting” in Philadelphia and the “40<sup>th</sup> International Conference on Coordination Chemistry” (ICCC40) in Valencia. Furthermore, he also contributed with an oral communication entitled “*Towards Self-Assembled Functional Materials based on Metallosalens*” at the annual young researcher seminar of the Institute of Chemical Research of Catalonia in December 2012. Giovanni was also selected to present an overview of his research in a scientific discussion group held by the Nobel Prize winner Prof. Ryoji Noyori at the CEICS Nobel Campus “Chemistry for Life” in July 2012. During the “Zing Coordination Chemistry Conference” in December 2011 in Xcaret (Mexico), Giovanni was awarded with a “best poster prize”. Giovanni initially held an ICIQ predoctoral fellowship and at a later stage he was awarded a FPU PhD fellowship from the MINECO. In July 2009 he also assisted in the ICIQ Summer School on homogeneous catalysis.



UNIVERSITAT ROVIRA I VIRGILI

SUPRAMOLECULAR, PHOTOPHYSICAL AND CATALYTIC PROPERTIES OF ZN(SALPHEN) BASED COMPLEXES AND MATERIALS

Giovanni Salassa

Dipòsit Legal: T. 1430-2013

## List of Publications

- **G. Salassa**, J. W. Ryan, E. C. Escudero-Adán, E. Palomares, A. W. Kleij, “*Photophysical Properties of Zn(Salphenazine) Complexes and their Application in Small Molecule Solar Cells*”, *manuscript in preparation*.
- F. Castro-Gómez, **G. Salassa**, A. W. Kleij, C. Bo, “*A DFT Study on the Mechanism for the Cycloaddition Reaction of CO<sub>2</sub> to Epoxides Catalyzed by Zn(salphen) Complexes*”, *Chem. Eur. J.* **2013**, *19*, 6289-6298.
- D. Anselmo, **G. Salassa**, E. C. Escudero-Adán, E. Martin, A. W. Kleij, “*Merging Catalysis and Supramolecular Aggregation Features of Triptycene based Zn(salphen)s*”, *Dalton Trans.* **2013**, *42*, 7962-7970.  
(paper was selected as HOT article by Dalton Transactions)
- D. Anselmo, R. Gramage-Doria, T. Besset, M. V. Escárcega-Bobadilla, **G. Salassa**, E. C. Escudero-Adán, M. M. Belmonte, E. Martin, J. N. H. Reek, A. W. Kleij, “*Supramolecular Bulky Phosphines Comprising of 1,3,5-triaza-7-phosphaadamantane and Zn(salphen)s: Structural Features and Application in Hydrosilylation Catalysis*”, *Dalton Trans.* **2013**, *42*, 7595-7603.
- **G. Salassa**, M. J. J. Coenen, S. J. Wezenberg, B. L. M. Hendriksen, S. Speller, J. A. A. W. Elemans, A. W. Kleij, “*Extremely Strong Self-Assembly of a Bimetallic Salen Complex Visualized at the Single-Molecule Level*”, *J. Am. Chem. Soc.* **2012**, *134*, 7186-7192.
- M. V. Escárcega-Bobadilla, **G. Salassa**, M. Martinez Belmonte, E. C. Escudero-Adán, A. W. Kleij, “*Versatile Switching in Substrate Topicity: Supramolecular Chirality Induction in Di- and Trinuclear Host Complexes*”, *Chem. Eur. J.* **2012**, *18*, 6805-6810.

- C. J. Whiteoak, **G. Salassa**, A. W. Kleij, “Recent advances with  $\pi$ -conjugated salen systems”, *Chem. Soc. Rev.* **2012**, *41*, 622-631.
- E. C. Escudero-Adan, M. Martinez Belmonte, E. Martin, **G. Salassa**, J. Benet-Buchholz, A. W. Kleij. “A Short Desymmetrization Protocol for the Coordination Environment in Bis-Salphen Scaffolds”, *J. Org. Chem.* **2011**, *76*, 5404-5412.
- **G. Salassa**, A. M. Castilla, A. W. Kleij, “Cooperative Self-Assembly of a Macrocyclic Schiff Base Complex”, *Dalton Trans.* **2011**, *40*, 5236–5243.
- S. J. Wezenberg, **G. Salassa**, E. C. Escudero-Adán, J. Benet-Buchholz, A. W. Kleij, “Effective Chirogenesis in a Bis(metallosalphen) Complex through Host-Guest Binding with Carboxylic Acids”, *Angew. Chem. Int. Ed.* **2011**, *50*, 713–716. (paper was highlighted on the Back Cover)
- L. Salassa, D. Gianolio, C. Garino, **G. Salassa**, E. Borfecchia, T. Ruiu, C. Nervi, R. Gobetto, R. Bizzarri, P. J. Sadler, C. Lamberti, “Structure of  $[Ru(bpy)_n(AP)(6-2n)]^{2+}$  homogeneous complexes: DFT calculation vs. EXAFS”, *J. Phys. Conf. Proc.* **2009**, *190*.
- L. Salassa, C. Garino, **G. Salassa**, C. Nervi, R. Gobetto, C. Lamberti, D. Gianolio, R. Bizzarri, P. J. Sadler, “Ligand-Selective Photodissociation from  $[Ru(bpy)(4AP)_4]^{2+}$ : a Spectroscopic and Computational Study”, *Inorg. Chem.* **2009**, *48*, 1469–1481.
- L. Salassa, C. Garino, **G. Salassa**, R. Gobetto, C. Nervi, “Mechanism of Ligand Photodissociation in Photoactivable  $[Ru(bpy)_2L_2]^{2+}$  Complexes: A Density Functional Theory Study”, *J. Am. Chem. Soc.* **2008**, *130*, 9590–9597.